Deciphering the role of host NAD^{+} metabolism in *M. tuberculosis* and *P. falciparum* pathogenesis and designing novel inhibitors against necrotizing toxins

Thesis submitted to Jawaharlal Nehru University
for the award of the degree of

DOCTOR OF PHILOSOPHY

AYUSHI CHAURASIYA

SPECIAL CENTRE FOR MOLECULAR MEDICINE
JAWAHARLAL NEHRU UNIVERSITY
NEW DELHI

2020

CERTIFICATE

The research work in this thesis entitled "Deciphering the role of host NAD$^+$ metabolism in *M. tuberculosis* and *P. falciparum* pathogenesis and designing novel inhibitors against necrotizing toxins" has been carried out by **Ms. Ayushi Chaurasiya** under my guidance at the Special Centre for Molecular Medicine, Jawaharlal Nehru University, New Delhi, India. The work presented here is original and has not been submitted in part or full for any other degree or diploma of any university/institution elsewhere.

Ayushi Chaurasiya
Ayushi Chaurasiya

(Candidate)

Prof. Anand Ranganathan

(Supervisor)

Date: 28-12-2020

Prof. Suman K. Dhar

(Chairperson)

Dedicated to

'Daddy and Mummy'

for their unconditional

Love & Support

ACKNOWLEDGEMENTS

It is a genuine pleasure to express my thanks to all those people who have given invaluable appreciation and support for completion and writing of my thesis work in many ways and made it an unforgettable experience for me.

First and foremost, I would like to express my deepest and heartfelt gratitude to my PhD supervisor Prof. Anand Ranganathan. He has been a wonderful supervisor who encouraged and supported me during difficult times in this journey. His scientific aptitude, enthusiastic motivation and guidance gave me determination and confidence to complete my research work and improved my growth as a researcher. He is a great listener, advisor and always allows his student to think beyond boundaries. It was a privilege for me to work under his supervision and learn from him.

I would also like to thanks Dr. Shailja Singh for her sincere guidance, motivation, and valuable inputs during my thesis work that immensely improved my research and scientific knowledge. I would like to extend my respectful gratitude to Prof. Gobardhan Das for his continued support, scientific inputs and valuable guidance to successfully complete this study. My sincere thanks to Prof. Suman Kumar Dhar, Chairperson SCMM, for his constant support and providing research facilities. I am very grateful to other faculty members of SCMM for their continuous encouragement and improving my scientific skills.

I acknowledge my sincere gratitude to Dr. Neel Sarovar Bhavesh, ICGEB, New Delhi for his valuable suggestions and appropriate evaluation about my thesis work. I would like to thank Dr. Ram Sagar Mishra, BHU, Varanasi for providing compounds (NAD^+ analogues) used in my research work. I am thankful to Dr. Ved Prakash Dwivedi, ICGEB, New Delhi for helping me in conducting *Mycobacterium tuberculosis* related work. I am thankful to Dr. Swati Garg and Dr. Santosh Kumar for their help in experimental work.

I would like to convey my sincere thanks to Dr. Jhalak for her tremendous encouragement and support during this journey. I am really thankful to her for being there in difficult times, teaching me experimental work, giving scientific inputs and

caring like a family member. My sincere thanks to Dr. Amandeep, Dr. Mala, Dr. Pooja, Dr. Sunita and Dr. Neha for their motivation.

My deep and sincere appreciation to my seniors, Dr. Prem, Dr. Niharika, Ms. Shikha and Mr. Sushil, for their precious support and help to complete my thesis work. My sincere thanks to my seniors from SCMM, Dr. Sudhir, Ms. Kirti, and Ms. Pragya, who have always been so helpful for conducting my research work. I would also like to thank my batchmate, Zill e Anam, for her continued encouragement.

A special thanks to my friends Malabika and Jyoti for their continuous support and help in my hard time. I also want to thank my friends Varsha, Pragya, Ragini, Imran, and Tarkeshwar for sharing a great time together. I am grateful to other members from my lab, Pallavi, Manisha, and Mukesh for providing me positive working environment.

I would like to express my sincere thanks to SCMM office staff Mr. Nand Kumar, Mrs. Niti, and Ms. Priyanshu for their help in administrative work. Special thanks to our lab assistant Mr. Ajay for taking care of things required for experiments.

I greatly acknowledge Department of Biotechnology (DBT), New Delhi, India for providing me financial support.

I bestow my deep sense of respect and gratitude to my parents, Late Dr. Bhanu Prakash Chaurasiya and Mrs. Jyoti Chaurasiya, and my siblings, Dr. Pranjal and Dr. Smriti, whose love, blessings, prayers, sacrifices and support helped me to reach this milestone. Special thanks to my brother-in-law, Dr. Nilay, for his guidance, continuous encouragement, endless support and confidence in me. I am immensely grateful for having a great teacher and advisor like him for a long time that helped me to pursue my dreams. I would like to extend my heartfelt thanks and sincere appreciation to my sister-in-law, Dr. Jaya, for her enthusiastic encouragement and support during the time.

I am really thankful to GOD that I am a daughter of Late Dr. B. P. Chaurasiya whose kind personality, teachings, high moral values, patience, hard work, and service to others will always have a special place in my heart to enlighten my path for being a better person and achieving even higher goals. I owe a deep sense of debt and

gratitude for whatever I am today is just because of strong foundation led by him in my upbringing and childhood education. He always stood by me like a pillar during all the ups and downs in my life. Without his unending inspiration, moral support, guidance and believe in me, I could not have complete this journey.

Above all, I am very grateful to almightly for the blessings and providing me enough patience and perseverance.

Ayushi Chaurasiya

TABLE OF CONTENTS

LIST OF FIGURES

4.5 Effect of NAD$^+$ modulation on human erythrocyte survival and *P. falciparum* pathogenesis

4.6 To study effect of selected NAD$^+$ analogues on intracellular pathogenesis

LIST OF TABLES

Chapter 1

Review of Literature

1 REVIEW OF LITERATURE

1.1 Tuberculosis: Overview

With the ambitious dream of "to end tuberculosis epidemic" by 2030 in 2014, WHA (World Health Assembly) decided "ending the tuberculosis epidemic" among the WHO (World Health Organization) targets under the health-related Sustainable Development Goals (SDG) 3 in September 2015. To intensify the effectiveness of this program, WHO set additional 2035 target that with comparison to baseline of 2015, called for reduction in deaths by 95% and decline in tuberculosis incidence by 90% [1, 2]. Tuberculosis, the main causative agent *Mycobacterium tuberculosis*, is a communicable disease that could be pulmonary and extrapulmonary based on the site of infection. "The End tuberculosis strategy" under WHO target has effectively reduced annual tuberculosis incidence to 2% during 2017 and 2018, which is indubitably the highest annual decline in the previous 18 years [3]. Despite this, the disease still remains as a global health burden that accounts for the leading cause of mortality from an infectious disease, leaving behind HIV/AIDS. In 2018 alone, around 10.0 million new cases and 1.451 million deaths including 0.251 million deaths of HIV associated tuberculosis were reported. In 2018, about half a million new cases are estimated to be infected with rifampicin-resistant tuberculosis including 78% cases of multidrug resistance [3]. Emergence of resistance against first line treatments and raise in cases of HIV-tuberculosis comorbidity highlight the pressing need for development of multi-dimensional approach through novel research and chemotherapeutics innovation along with public health efforts to achieve the goal of ending tuberculosis.

Tuberculosis is a worldwide disease with major contribution (44%) from South-East Asia followed by 24% cases from Africa in 2018. The major global burden (two-thirds) of tuberculosis is attributed to eight countries; among them India has highest contribution of 27% [3]. Major contributors are socioeconomic status of country, more importantly, uneven distribution of wealth, poverty, poor health facility, lack of awareness in public; in addition various health risk factors like HIV co-infection, immunosuppression due to other diseases or their curable drugs [4-6].

WHO has initiated programs and strategies to cure and eradicate tuberculosis, most importantly for multidrug resistant (MDR) tuberculosis treatment, in 1993 DOTS program (Directly Observed Treatment Short-Course) and in 1998 DOTS-plus program. For treatment of intensive phase of the disease, four first-line drugs are recommended for drug-susceptible tuberculosis patients: isoniazid, ethambutol, pyrazinamide, and rifampicin for two months and further continuation for four months with rifampicin and isoniazid [7]. WHO has updated and revised guidelines for drug-resistant tuberculosis [8]. Efforts to control tuberculosis have been made but to accomplish the aim of completely eradicating tuberculosis, a better understanding of the disease and future research are required for development of novel therapeutics.

1.1.1 Global epidemiology: Incidence, Mortality, and Prevalence

Tuberculosis is present worldwide and almost one-fourth of the world's population carries tuberculosis infection, with 10 million cases of infection in 2018 [3]. By region in 2018, highest contribution is from South-East Asia (44%) [3]. Other regions accounts for major numbers of cases are Western Pacific (18%) and Africa (24%). Number of cases are significantly less but present in the regions of Eastern Mediterranean (8.1%), America (2.9%), and Europe (2.6%). Highest tuberculosis burden with major contribution for new cases (87%) was found in 30 countries in 2018. Among these countries eight are responsible for two-thirds of new cases of tuberculosis, where India is leading with 27% contribution in new cases [3]. India, the Russian Federation, and China have also been responsible for highest number of drug-resistant tuberculosis cases. Globally in 2018, reported new cases were 0.5 million for rifampicin-resistant tuberculosis. Among rifampicin-resistant tuberculosis cases, 78% patients also reportedly had multidrug-resistant tuberculosis [3].

During the 2000-2018 period, the tuberculosis incidence rate declined at the average rate of 1.6% per year and highest reduction of 2% was reported between 2017 and 2018. In comparison to set goal of 20% decline in tuberculosis incidence rate till 2020 of 'End tuberculosis Strategy', the cumulative decline was only 6.3% between 2015 and 2018 [3].

Mortality from tuberculosis dominates among various infectious diseases contributing highest in number of deaths since 2007. HIV-tuberculosis coinfection is a serious

health threat and major risk factor associated with tuberculosis. In 2018, tuberculosis among HIV negative people was responsible for approximately 1.2 million deaths; additionally 0.25 million deaths were reported in HIV positive individuals. Africa and South-East Asia accounted for 85% of total deaths from tuberculosis globally. Around 30% of global tuberculosis deaths is contributed by India. Tuberculosis mortality rate was reported to be 20 globally in 2018, including deaths of HIV positive individuals. Total number of deaths from tuberculosis was reduced by 11% globally between 2015 and 2018, which is far from achieving the 'End tuberculosis strategy' goal of 35% reduction in deaths till 2020 (Figure 1.1) [3].
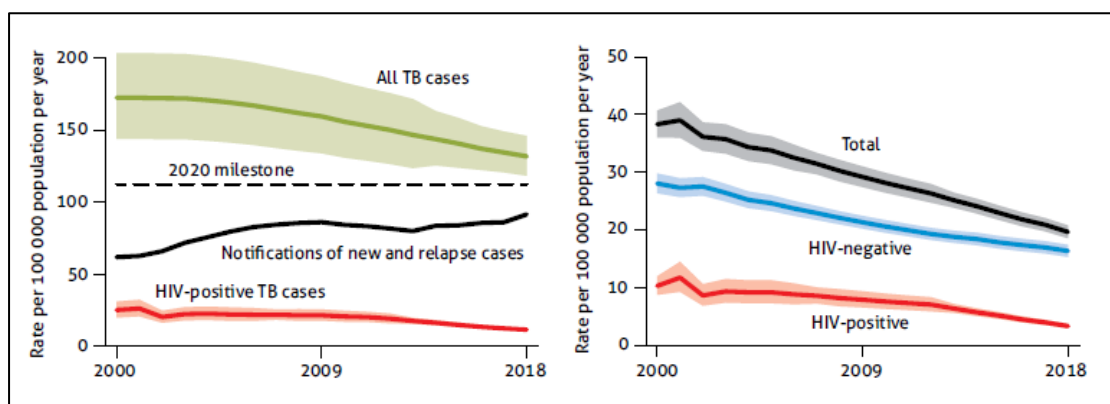
Figure 1.1 Global trends during time period of 2000-2018 in the incidence rate (left) and the mortality rate (right) (Adapted from World Health Organization 2019). Uncertainty intervals are represented by shaded areas [3].

An increase from 6.4 million tuberculosis-positive cases (64% incident tuberculosis) in 2017 to 7.0 million cases in 2018 (70% incident tuberculosis) has been observed. Percentage increase for receiving anti-tuberculosis treatment was from 64% in 2017 to 69% in 2018 of incident tuberculosis patients [3]. Figure 1.2 shows global incidence rates of tuberculosis.
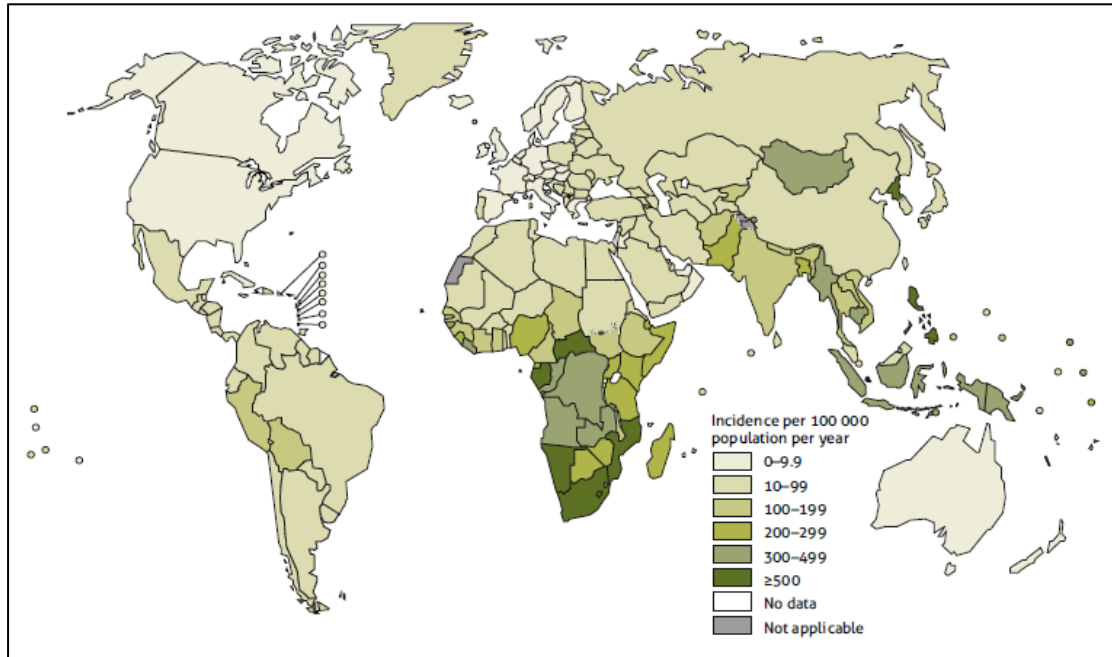
Figure 1.2 Estimated tuberculosis incidence rates worldwide in 2018 (Adapted from World Health Organization 2019) [3].

1.1.2 History

1.1.2.1 General history and discovery of *M. tuberculosis*

Tuberculosis is an ancient disease with the postulated origin of genus mycobacterium, causative agent of tuberculosis, to be more than 150 million years old [9]. According to a study, in East Africa, around 3 million years ago, early progenitor ancestor of *M. tuberculosis* was present and early hominids located in that region might have been infected by this ancestor [10]. From this single ancestor (*M. prototuberculosis*) all modern species/strains of *M. tuberculosis* complex (MTBC) have been suggested to evolve about 20,000 to 15,000 years ago [10, 11]. Evidence of tuberculosis was revealed in 2400 BC old Egyptian mummies and also in early Egyptian art, showing typical characteristics of tuberculosis such as pott's deformities along with other skeletal abnormalities [12-14].

Written documents on tuberculosis were first reported in India and China about 3300 years ago and 2300 years ago, repectively [13, 15]. Biblical books of Deuteronomy and Leviticus also described tuberculosis as schachepheth, an ancient Hebrew word [16].

In ancient Greek literature tuberculosis was well known and called as 'Phthisis' [17, 18]. Tuberculosis was also known as 'consumption', translation of a word from Sanskrit manuscript, defining a wasting disease from around 1000 BC [19]. Hippocrates described symptoms and conditions of tuberculosis accurately, and coined the term Phthisis (decaying), in *Book I, Of the Epidemics* [17]. However, tuberculosis was considered as a hereditary disease [19]. He also discovered tissue tubercles (phymata) in sheep, cattle, and pigs but could not relate it to consumption disease. Aristotle (384-322 BC) had observed and described 'scrofula' on the skin of a pig suffering from phthisis and believed in the contagious nature of disease [20]. Galen (131-201) was the first who suggested contagious nature of phthisis and warned against close contact with phthisic people [20].

During middle ages in Europe, England and France, scrofula (tuberculosis cervical lymph node scar, also called king's evil [19]) was treated with royal touch by monarchs, the sentence meaning 'the King touches you, God cures you' [21, 22]. Francis Sylvius, in his '*Opera Medica'* of 1679, describes tubercles formation in the lungs and other organs of consumptive patients, their progression to abscesses, cavities and empyema [20, 23]. After 10 years of Sylvius discovery, Richard Morton (1637-1698) had noted relation between phthisis and scrofula, and suggested combination syndrome, having 3 stages of the disease: initial inflammation leading to formation of tubercle, progression to ulcer, and finally to phthisis [20]. In 1699, Italian health law Republic of Lucca suspected infectious nature of phthisis and released first official reference specifying disinfection measures [23].

Several studies started indicating the infectious nature of phthisis. First study came up in 1720 by Benjamin Martin reported in his book '*A new Theory of Consumption*' and hypothesized that a small living creature might be responsible for phthisis [19, 20, 22]. In 1779, Sir Percivall Pott defined 'Potts disease' as spinal cord paralysis by tuberculosis infection [23]. Matthew Baille, a Scottish pathologist, in 1793 observed and named caseous necrosis as 'tubercles' [19, 23].

In 1819 Laennec, inventor of the stethoscope, described the concept of tuberculosis as being pulmonary or extrapulmonary in his book '*D'Auscultation Mediate'* [17]. During this time, death rate in parts of Europe London, Stockholm, and Hamburg

reached 800-1000/100,000/ year, similar death rates were observed in America [17]. At this time, tubeculosis had become an epidemic in Western Europe. Mostly young people were infected and died of the disease; tuberculosis was therefore called as 'the robber of youth' [23]. Patients of tuberculosis also showed severe anaemia associated with pallor of body which gave tuberculosis a new term "white plague" [23]. Tuberculosis was also termed as "Captain of All These Men of Death" when tuberculosis epidemic was originated in North America and Europe [23].

Since 17th and 18th centuries, phthisis and consumption terms were used to define tuberculosis. In 1834, Johann Lukas Schönlein observed disease affliction with tubercle and coined the term 'tuberculosis' without knowing scrofula and phthisis are associated with tubercle formation [20, 23]. For treatment and cure of tuberculosis, introduction of Sanatorium was first reported in the doctoral dissertation of Hermann Brehmer 'Tuberculosis is a curable disease' in 1854. He was a botany student who himself suffered from tuberculosis and was cured by visiting the Himalaya Mountains [23].

First strong proof of the infectious nature of tuberculosis was found through Jean-Antoine Villemin's experiments; he infected healthy rabbit with purulent material from a tuberculous tissue of an infected individual. After autopsy, the infected rabbit showed extensive tuberculosis [17]. In 1882, a remarkable discovery of the etiology of tuberculosis was presented by Hermann Heinrich Robert Koch at Berlin Physiological Society in his extraordinary presentation, '*Die Aetiologie der Tuberculose*'. He demonstrated the so-called Koch-Henle postulates that changed the history of tuberculosis and other infectious diseases. In his study, he identified the tubercle bacillus by methylene blue staining, isolated, and cultured the bacillus, and successfully reproduced the disease into laboratory animals by inoculating the bacillus. In 1905, for his incredible contribution in recognising the etiology of tuberculosis, he was awarded with the Noble Prize [17].

Discovery of the causative agent of tuberculosis, *Mycobacterium tuberculosis*, opened new ways for treatment of this deadly disease and introduced a new era and opportunities of research for antibiotic development.

1.1.2.2 Development of tuberculosis treatment

In 1890, Koch proposed tuberculin, a glycerin extract of tubercle bacilli, as treatment for tuberculosis, however, this therapeutic approch failed but tuberculin skin test was later developed as an effective dignostic tool by Clemens Von Pirquet and Charles Montoux during 1907-1908 [21, 24]. Wilhelm Konrad Roentgen in 1895 discovered X-rays and developed the radiograph that become a standard diagnostic tool to monitor severity of tuberculosis progression [20, 21].

Several approches had been used to treat tuberculosis till that time, such as better nutrition, introduction of sanitorium, thoracic tuberculin surgery: pnemothorax and thoracoplasty [19, 21]. The next successful approach was Bacille Calmette Guerin (BCG) vaccine development by Albert Calmette and Camilo Guerin in 1908 using more than 10 years sub-cultured *Mycobacterium bovis* strain for attenuation following the principles of Louis Pasteur. However, efficacy of BCG, first used in humans in 1921, was found to be variable [19, 25]. Currently, a totally effective vaccine against tuberculosis is not available [19].

Continuous efforts were initiated to find chemical compounds effective against tuberculosis. Jorgen Lehmann in 1943 and Gerhard Domagk in 1945 discovered the first therapeutic agents, para-amino salicylic acid (PAS) and thiosemicarbazone, respectively, for treatment of tuberculosis. Both compounds showed efficacy but were found to be bacteriostatic in nature [17, 26]. In 1944, Selman A Waksman and Albert I Schatz reported the isolation of bactericidal agent streptomycin from *Streptomyces griseus*. Streptomycin was the first antibiotic that was effective against *M. tuberculosis* and also bactericidal in nature [22, 26, 27]. In 1948 streptomycin and PAS combination was found to be more potent in treating tuberculosis along with lower chances of development of streptomycin resistance [21].

The next major discovery was the antitubecular activity of the first oral mycobactericidal drug isoniazid [17, 21]. Three different and independent researchers (Squibb, Bayer, and Hoffmann La Roche) in 1951 uncovered isonicotinyl hydrazine's antitubercular activity, a molecule that was first synthesized in 1912 by Hans Meyer and Josef Mally [28]. Addition of isoniazid with other two drugs streptomycin and PAS further reduced mycobacterium survival and rate of drug resistance (triple

therapy recommended for 24 months) [29]. In the United States, Lederle laboratories discovered a new drug, ethambutol, that replaced PAS in 1961 (18 months course duration) [30].

During same time period, in 1957 *Streptomyces mediterranei* (or *Amycolatopsis mediterranei*, a new streptomyces species) was identified that produced, 'rifamycin', a large family of structurally related compounds having antimicrobial activity on several pathogens [21, 31]. In 1965 semisynthetic rifamycin derivative rifampicin (rifampin USAN) synthesized in Milan, was found to be most effective among other derivatives with better oral absorption property and prolonged blood level [21]. Rifampicin was included in tuberculosis therapy with isoniazid and ethambutol (9 months course duration) [21, 32].

The next major achievement was the rediscovery of pyrazinamide in 1972, a nicotinamide analog, as an antituberculosis therapeutic drug [32, 33]. Dalmer and Walter had first synthesized pyrazinamide in 1936. Combination treatment of pyrazinamide with isoniazid and rifampicin increased efficacy and reduced duration of treatment to 6 months [21]. During this time, other drugs were developed: cycloserine, kanamycin, ethionamide, capreomycin and more recently, clofazimine, viomycin and ciprofloxacin, for treatment of drug-resistant tuberculosis [20, 32].

1.1.2.3 Tuberculosis control strategies

Discovery of effective therapeutic agents against tuberculosis translates into control of tuberculosis from treatment to cure. Successful introduction of chemotherapy for treatment of tuberculosis reduced the number of cases, until in late 1980s and early 1990s when two major threat AIDS epidemics and multidrug resistance strains of tuberculosis dramatically increased number of tuberculosis cases. Problem of drug resistance in treatment of tuberculosis was previously solved by drug combination therapies in 1950-1960s. Unfortunately during the 1990s, it reappeared as multidrug-resistant tuberculosis, with resistance to rifampicin and isoniazid [21, 34]. In 1993, tuberculosis was declared as a global emergency by WHO. In 1995, 'Directly Observed Therapy' (DOT) and 'Directly Observed Treatment, Short-course' (DOTS) strategies were recommended and adopted by WHO. These strategies were developed by Karel Styblo in the 1970s with 'the International Union Against Tuberculosis and

Lung Disease', to fight against drug-resistant tuberculosis [23, 34]. For treatment of HIV-tuberculosis coinfection a new strategy and improved medication is needed with less side effects. Recently bedaquiline, delamanid, linezolid, and pretomanid are new therapeutic drugs under study for treatment of drug-resistant tuberculosis [32]. Complete genome sequence of *M. tuberculosis* (H37Rv strain) was reported in 1998 and paved the way for the development of better therapeutics and vaccines to control tuberculosis [35].

DOTS strategy has shown major success in treatment of tuberculosis; since 2000, incidence of tuberculosis has reduced every year by an average of 1.5% and the mortality rate has fallen by around 22% from 2000 to 2015 [23].

In 2015, WHO achieved the set goal to halt and reverse the tuberculosis incidence. Millennium Development Goals (MDGs), established by the United Nations in 2000, led to decrease in death rates and tuberculosis prevalence by 50% compared to 1990 (Stop tuberculosis Partnership targets) [3, 36]. Sustainable Development Goals (SDGs) were adopted by the United Nations in 2015, to take the place of MDGs in 2016 for the period 2016-30 [37]. For post-2015, the 'End tuberculosis Strategy' was developed by WHO during 2012-2014 and adopted by all Member states of WHO for the period 2016-35 as a part of the newly adopted SDGs [1, 37, 38].

The 'End tuberculosis Strategy' proposed new ambitious goals for 2035 with an aim to reduce new cases and tuberculosis deaths by 90% and 95% respectively [1]. During 2018, approximately 10 million incident cases of tuberculosis occurred and tuberculosis related death and annual incident rate reduced by 5% and 2%, respectively from 2017 to 2018 [3]. These data are encouraging but not satisfactory to achieve the proposed goal of tuberculosis eradication by 2035. Even during 1990, decrease in incidence rate was higher. The annual decline in tuberculosis incidence rate should increase as estimated 5% upto 2020 and thereafter acceleration to 10% till 2035 to accomplish set target [39, 40]. Socioeconomic status, HIV-tuberculosis coinfection, and drug-resistant strains of tuberculosis were the main factors responsible for challenges in treatment of tuberculosis. Further extensively drug-resistant (XDR) tuberculosis strains emerged that worsened the situation [39]. XDR isolates are resistant to rifampicin, isoniazid, any fluoroquinolones (levofloxacin or

moxifloxacin), and in addition at least one second-line drug (kanamycin, amikacin, or capreomycin) [41]. Currently available treatment options for tuberculosis need to be improved to eradicate tuberculosis over the coming decades.

1.1.3 Airborne transmission and Clinical manifestation

Even after the remarkable discovery of the causative agent of tuberculosis isolated by Koch [23] its infectious nature remained unrevealed for a long time [42]. Flugge demonstrated development of infection in guinea pig through proximity to be coughing of a tuberculosis patient [43]. His interpretation of airborne transmission of tuberculosis through small respiratory droplet was first confirmed by Richard Riley [44] and later reproduced by Escombe *et al* [45]. Tuberculosis is mainly transmitted through small infectious aerosol particles of size 1 to 5 μm containing microorganisms produced by a person having pulmonary or laryngeal tuberculosis [46]. It has been found that after contact with surface, it is very difficult to re-aerosolize droplets into respirable particles [47]. When inhaled by the person in contact, it infects the upper respiratory tract, bronchi, and further alveoli of the lungs. Development of infection depends on factors like infectiousness of source, susceptibility of the exposed person, exposure time and environment such as ventilation rate, and air circulation of the space [48]. Most of the time, the infected person's immune system inhibits the growth of the bacteria (dormant stage), resulting in latent tuberculosis that is an asymptomatic non-infectious condition present in immunocompetent individuals [49]. In immunocompromised state, latent infections can develop into active tuberculosis [50].

Tuberculosis has two types of clinical manifestations, described as pulmonary tuberculosis: infection of lungs, and extra-pulmonary tuberculosis, in which infection occurs in pleura, joints and bones, lymph nodes, meninges abdomen, genitourinary tract, or skin. Clinical symptoms of tuberculosis vary depending on the type of tuberculosis and the site of infection. Symptoms of pulmonary tuberculosis include chronic cough, fever, weight loss, night sweat, blood-tinged sputum production, and inflammation of the pleura membrane (pleurisy) [51]. Symptoms of extrapulmonary tuberculosis are variable [52, 53] as described in Table 1.1.

Site of infection	Symptoms
Tuberculosis lymphadenitis	Mainly affects cervical chain lymph node, painless swelling of lymph node
Pleural tuberculosis	Asymptomatic or symptoms similar to pulmonary tuberculosis
Central nervous system tuberculosis	Tuberculosis meningitis have symptoms of fever, headache, focal neurological deficits, and meningism, tuberculosis brain abscesses have signs of increased intracranial pressure and headache
Skeletal tuberculosis	Peripheral osteoarticular tuberculosis: localised pain. Spinal tuberculosis: spinal deformity, localised pain
Tuberculosis peritonitis	Weight loss, fever, and abdominal pain
Genitourinary tuberculosis	Pelvic inflammatory disease, flank pain, dysuria, haematuria, and epidydimal masses
Tuberculosis pericarditis	Cough, chest pain, and dyspnoea

Table 1.1 Symptoms of extrapulmonary tuberculosis [52, 53].

Most common site of infection is lymph node followed by pleural effusion. Diagnosis of extrapulmonary tuberculosis can be difficult because of its typical, variable and nonspecific symptoms. However, pulmonary tuberculosis can be easily diagnosed by sputum examination or chest X-ray.

1.1.4 Control of tuberculosis: Treatment with anti-mycobacterial drugs and vaccines

Treatment along with early diagnosis are two main factors involved in control of tuberculosis. Treatment of tuberculosis depends on various factors such as active or dormant state of infection, drug resistance, or site of infection. Majorly used diagnostic tools for the latent tuberculosis infection detection include tuberculin skin test (TST) and interferon-gamma release assays (IGRAs) [49]. Drug-resistant tuberculosis is detected by Xpert/RIF MTB assay, a nucleic acid amplification test (NAAT), that has been adopted by the WHO along with molecular line probe assays (LPAs) and phenotypic drug susceptibility tests (DST) for diagnosis [53-55].

Moreover, development of new simple and faster diagnostic tools are required to detect accurately drug-sensitive and resistant strains of tuberculosis.

Tuberculosis treatment involves use of a combination of drugs in two phases, intensive initial phage of two months followed by a continuation phase of 4 to 6 months. For the treatment of **drug-sensitive tuberculosis,** main antitubercular drugs are isoniazid, rifampin, and pyrazinamide, with either ethambutol or streptomycin added. Depending on the severity of disease, the duration of treatment could be 6-8 months or may extend for 12 months. Based on susceptibility of infection, drugs ethambutol or streptomycin can be discontinued. After two months of treatment, drug pyrazinamide can also be discontinued according to response and susceptibility of infection [51].

Drug-resistant tuberculosis treatment is critical and needs second-line drugs with longer duration of treatment and severe side effect profiles. The DOTS-plus program was initiated by the WHO as a treatment strategy to control resistance against isoniazid and rifampicin, and is defined as **multidrug-resistant tuberculosis (MDR-tuberculosis)**. **Extensive drug-resistant tuberculosis (XDR-tuberculosis)** is defined as MDR-tuberculosis having resistance to any fluoroquinolone in addition to second-line injectable drugs [56].

Medicines for treatment can be categorised as follows (Table 1.2) [56]:

Groups	Medicines	
1	Isoniazid, rifamycins, pyrazinamide, ethambutol	**First-line oral drugs**
2	Aminoglycosides, amikacin, kanamycin, streptomycin, capreomycin (polypeptides)	**Injectable drugs**
3	Moxifloxacin, levofloxacin	**Fluoroquinolones**
4	Cycloserine, thiamides, prothionamide, ethionamide, PAS	**Oral bacteriostatic drugs**
5	Linezolid, bedaquiline, imipenem or cilastatin, meropenem, amoxicillin, clofazimine (for safety profile and efficacy limited data is available)	**New drugs**

Table 1.2 Groups of medicines for treatment of tuberculosis (Modified from Seung et al., 2015) [56].

Two types of drug regimen are mainly followed for MDR-tuberculosis treatment.

Longer MDR-tuberculosis regimen: At least five effective drugs are used for treatment against MDR-tuberculosis usually for 18-20 months. Available medicines are re-grouped according to their safety profile and effectiveness into three categories (Table 1.3) [8, 57].

Groups	Medicines
A	Linezolid, bedaquiline, moxifloxacin or levofloxacin
B	Terizidone or cycloserine, clofazimine
C	Ethambutol, prothionamide or ethionamide, streptomycin or amikacin, meropenem or imipenem–cilastatin, PAS, pyrazinamide, delamanid

Table 1.3 Groups of medicines for longer MDR-tuberculosis regimen [8, 57].

Group A medicines should be included in the regimen along with group B medicines. If Group A and B medicines cannot be used then group C medicines are recommended to be included in the regimen [8].

Shorter MDR-tuberculosis regimen

Duration of this regimen is 9 to 12 months. In this regimen, 4 to 6 months treatment with pyrazinamide, prothionamide (ethionamide), moxifloxacin, kanamycin, clofazamine, ethambutol, and isoniazid (high dose) is followed by five months treatment with moxifloxacin, clofazamine, pyrazinamide, and ethambutol [8, 57].

Vaccine BCG is used for the protection against tuberculosis in children usually meningeal and military tuberculosis. However, it provides short-term immunity and is not effective in adults [58, 59]. Development of novel vaccines is necessary to end tuberculosis. Studies to find new efficacious vaccine candidate for tuberculosis are in progress.

1.2 *Mycobacterium tuberculosis*

Mycobacterium genus consists of more than 170 species that can be divided into rapid-growing microorganisms and slow-growing microorganisms [60]. Three important human pathogens are grouped as slow-growers, that is, *M. ulcerans*, *M. leprae*, and members of the *mycobacterium tuberculosis* complex (MTBC) [61, 62].

Mycobacterium tuberculosis is the most widely spread human pathogen and the main causative agent of human tuberculosis. *M. tuberculosis* and its closely related members causing tuberculosis are grouped in MTBC [61].

1.2.1 The *mycobacterium tuberculosis* complex (MTBC)

Mycobacterium species groups that are genetically related (nearly identical nucleotide sequences), and isolated from different hosts or ecosytems having identical 16s rRNA sequences, are included in MTBC complex [11, 63, 64]. These species comprise pathogens that infect humans: *M. tuberculosis*, *M. africanum*, *M. canettii*; or sheep and goats: *M. caprae*; or rodent: *M. microti*; while *M. bovis* can infect a larger spectrum of host species including bovids and humans. *M. pinnipedi* infects seals and sea lions; recently, *M. mungi*, a new member of MTBC, was isolated from mongoose [65, 66].

M. canettii is a smooth colony-forming bacteria largely different from other tuberculosis bacteria in epidemiology and is specifically present in the Horn of Africa [67]. The *M. canettii* strain was first isolated in the 1960s by Georges Canetti at the Institute Pasteur in Paris and is named after him [68]. Genome-based studies have shown close resemblance of *M. canettii* with the putative common ancestor of MTBC member species [67, 69].

Phylogeny: Main causative agents of human tuberculosis are *M. tuberculosis* and *M. africanum*. Comparative genome analysis has revealed presence of some specific genomic regions, or 'regions of difference', among mycobacterium species. Based on deletion of these regions across the *M. tuberculosis* complex organisms, phylogenies of MTBC members were derived in which *M. tuberculosis* (larger genome) is placed at more ancestral position while *M. bovis* (smaller genome) is placed at a more derived position [70]. Studies have suggested that MTBC has originated in Africa [61]. Members of MTBC showed limited diversity and are assumed to be evolved from clonal expansion of its ancestral causative agent. This clonal group of MTBC members is now represented by 7 lineages that include lineage L1-L4 and L7 (closely related to *M. tuberculosis*), and L5-L6 (closely related to *M. africanum*) and also a branch next to L6 that represents animal-adapted strains [71]. These lineages are linked with different regions of the world [71-73]. *M. tuberculosis* strains are

categorised on the basis of whether *M. tuberculosis* specific deletion (TbD1) is present (TbD1$^+$) or absent (TbD1$^-$), into ancestral (1, 5, 6, 7 and animal lineages) and modern lineages (2, 3, and 4) [70, 71].

1.2.2 *Mycobacterium tuberculosis*: The organism

Tuberculosis, mainly caused by *M. tuberculosis*, is a highly infectious disease with high mortality rate. *Mycobacterium tuberculosis* belongs to the genus *Mycobacterium*, and family *Mycobacteriaceae* (order: *Actinomycetales*; class: *Actinobacteria*) [74, 75]. It is a nonmotile, rod-shaped, aerobic, acid fast bacillus of length 2 to 4 µm and width 0.2 to 0.5 µm. *M. tuberculosis* division is a slow process taking around 15-20 hours' time period. When stained with gram staining mycobacteria resist decolorization with acid alcohol due to presence of a lipid rich cell wall with mycolic acids. For this reason, therefore, it is known as acid fast bacteria [76]. Ziehl-Neelsen staining is widely used to stain acid-fast bacteria [77].

1.2.2.1 The mycobacterial cell envelope

Presence of a unique cell wall structure of *M. tuberculosis* is responsible for providing resistance against several drugs, by forming an effective permeability barriers, one that contains multiple efflux pumps, and has a significant impact on the pathogenesis [78, 79]. Cell wall is an important component to define and categorise bacteria into Gram-negative, Gram-positive, and acid-fast bacillus on the basis of retention of stain and peptidoglycan thickness. Studies have suggested the importance of peptidoglycan as a drug target due to its presence in almost all bacteria [80, 81]. Vitreous sections analysis by Cryo-electron tomography provides an insight into the structure of the outer cell membrane of mycobacteria, also termed as mycomembrane [82, 83]. Despite substantial research, structural composition of mycobacterial cell envelope is not fully elucidated and studies have suggested different models to understand its exact composition [76, 82-87]. According to the most recent model, the mycobacterial cell envelope comprises cell wall, cytoplasmic membrane, and a capsule, an outermost layer, containing proteins and polysaccharide (a loose matrix of glucan, arabinomannan, and mannan) [76, 84, 88]. Mycobacterial capsule and its components play an important role in mycobacterium pathogenesis [89]. The cell wall is composed of peptidoglycan, arabinogalactan, and mycomembrane. Mycomembrane is

a bilayer structure of around 7-8 nm thickness [82, 83], where inner leaflet consists of mycolic acid (long chain fatty acids) linked to arabinogalactan (cell wall polysaccharide) which in turn is covalently bound to peptidoglycan, also called as the mycoloyl-arabinogalactan-peptidoglycan complex, with the outer leaflet made up of free lipids including trehalose dimycolate [76, 86, 88]. The cell wall is separated from conventional plasma membrane by presence of periplasmic space [83]. Mycobacterial cell envelope shares similarity with envelopes of both Gram-negative and Gram-positive bacteria because of the presence of a waxy outer layer and thick peptidoglycan layer, respectively [76, 82]. Various components of mycobacterial cell envelope are involved in the pathogenesis and virulence; this suggests their therapeutic potential as a target for drug development [90, 91]. A number of anti-tuberculosis drugs target mycobacterial cell wall synthesis, including isoniazid and ethambutol, that target mycolic acids and arabinogalactan synthesis, respectively [92, 93].

1.2.2.2 Genomic organization

Substantial progress has been achieved in tuberculosis research due to complete genome sequencing of H37Rv strain of *M.* tuberculosis in 1998 by Stewart Cole and colleagues from the Sanger centre and Pasteur Institute [35, 94]. It has provided a new powerful research tool for understanding the biology, evolution and other aspects of *M. tuberculosis*. The H37Rv reference strain used for *M. tuberculosis* experimental work, is a laboratory derived strain from H37 which is the original strain isolated from a patient in the United States in 1905 [95]. Genome-based studies have a tremendous implication in drug and vaccine development, and also in the study of *M. tuberculosis* molecular epidemiology, phylogeny, and mutations related to drug-resistance [96-101]. In comparison to sequencing techniques (shotgun sequencing) used in 1998, current sequencing techniques are less time-consuming, less costly and do not require a cloning step [102]. First high-throughput technique (next-generation sequencing) was introduced in 2005 with the discovery of pyrosequencing [103]. In bacterial genomics sequencing domain, the most widely used technique currently is the Illumina sequencing platform [104].

TubercuList (tuberculist.epfl.ch) is a public database that incorporates genome sequence annotation data of *M. tuberculosis* reference strain H37Rv [105]. The

TubercuList database is continuously updated by incorporation of new annotation data [106]. The *M. tuberculosis* reference genome (H37Rv strain) is composed of 4,411,529 base pairs (bp) and comprises approximately 4000 protein genes (potential coding capacity approximately 91%) with 65.6% of average G+C content (while at some areas > 80% of high G+C content has been detected), and 50 functional RNA molecules coding genes [107]. Possible function of protein-coding genes was predicted by comparison of available databases and these genes were further classified into 11 broad groups [107, 108]. Around 40% of protein-coding genes were assigned a precise function; 44% showed similarity with available database, while the remaining 16% may have specific mycobacterial function showing no similarity with known proteins [35]. Annotation data showed an unusual presence of PE and PPE protein families in *M. tuberculosis* genome [35]. Proteins of these families are acidic, glycine-rich, where PE stands for Pro-Glu and PPE for Pro-Pro-Glu sequences [107, 108]. Approximately 51% of *M. tuberculosis* proteome has arisen from gene duplication with lack of a following divergence event, which supports the hypothesis of the recent origin of *M. tuberculosis* decendents [11, 35]. *M. tuberculosis* H37Rv genome sequences were re-annotated in 2002 [105]. This study reanalysed the annotation of the coding sequences and changes were incorporated in the functional categories of predicted protein as a significant change from 606 to 272 and 910 to 1051 was observed in the number of unknown proteins and conserved hypothetical proteins respectively [105]. Several approaches have been used to predict the possible function of hypothetical proteins of *M. tuberculosis* [109, 110].

1.3 Pathogenesis of *M. tuberculosis*

1.3.1 Life cycle: Overview

The establishment of tuberculosis infection involves a pattern of events (Figure 1.3) [111] and these events/stages during infection progression can be studied from the cellular and molecular viewpoint of host and bacteria interaction [108, 112, 113].
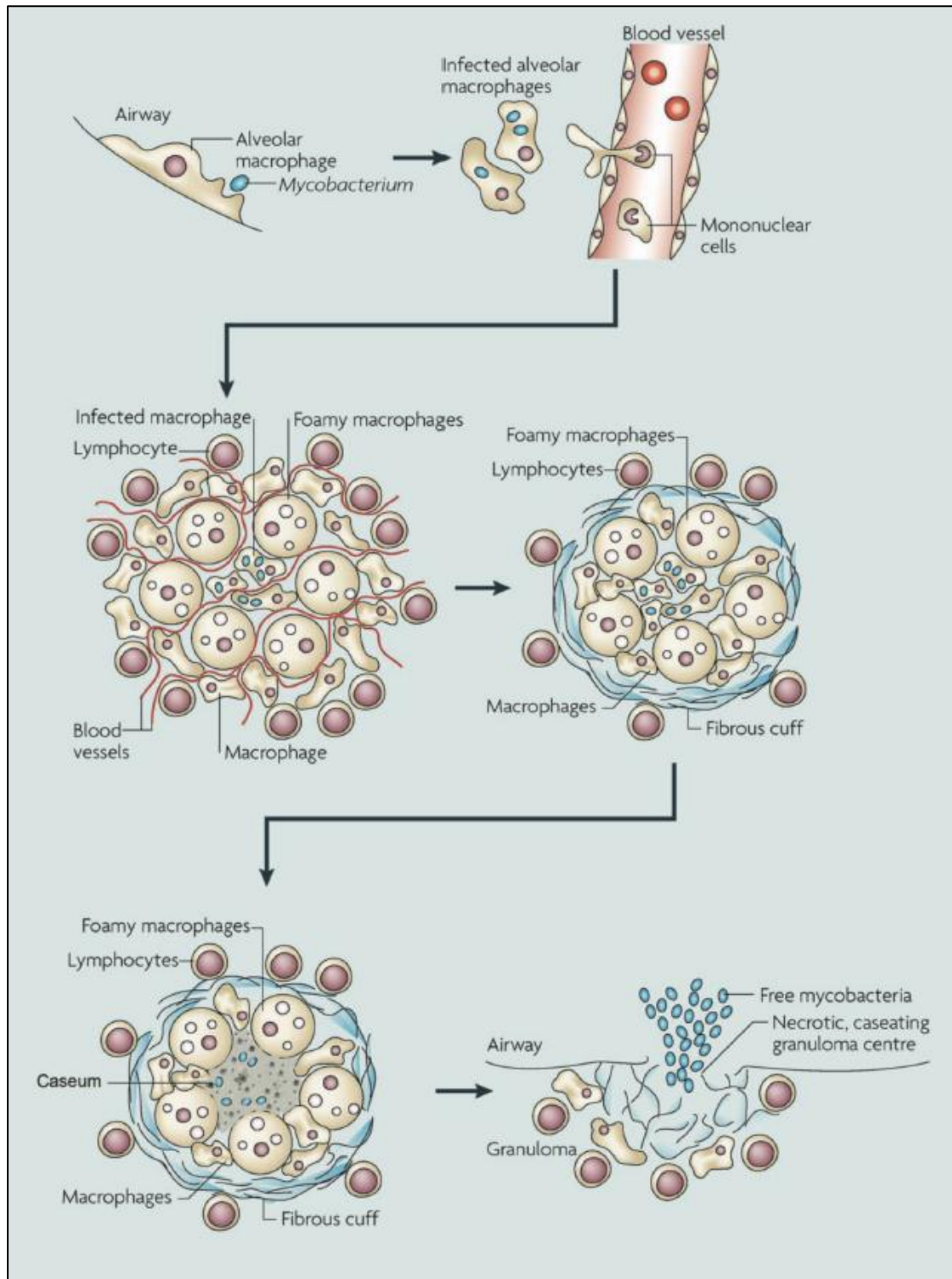
Figure 1.3 The life cycle of *M. tuberculosis* (Adapted from Russell et al., 2010). The infection starts when resident alveolar macrophages phagocytosed the *M. tuberculosis* containing droplets. This followed by recruitment of monocytes and formation of granulomas. In granuloma center, increased necrosis and caseum accumulation finally leads to release of infectious bacilli into the airways [111].

1.3.1.1 Early events during infection

Early events during infection include *M. tuberculosis* entry, infection of the immune cells and initiation of immune response against infection. *M. tuberculosis* spreads through aerosol droplets of size range 0.65-0.7 μm [114], when droplets containing bacteria enters the alveolar passages, *M. tuberculosis* is ingested primarily by alveolar macrophages [115], in addition by dendritic cells [116], epithelial cells [117, 118], and neutrophils [113, 119]. Alveolar epithelial cells type I and II are present in alveoli [120]. Studies have suggested that Type II alveolar epithelial cells can be infected by *M. tuberculosis* and provide a niche for its replication [117, 121, 122]. The innate immune response can be initiated by type II alveolar epithelial cells through secretion of antimicrobial peptides, chemokines, and proinflammatory cytokines that further initiate adaptive immune response [120, 123]. If the first line of defence comprising alveolar epithelial cells and professional phagocytes (monocytes, neutrophils, and dendritic cells) succeed in killing *M. tuberculosis*, the infection is eliminated. On the other hand, if *M. tuberculosis* survive and replicate inside phagocytes, the infection persists causing a clinical manifestation [124]. Interaction between the host and bacteria further determines the infection progression, and whether active or latent tuberculosis infection will develop. Cells of the innate immune system form an effective barrier to clear infection. However, *M. tuberculosis* evades innate immune responses by utilizing various strategies such as induction of anti-inflammatory response, production of reactive oxygen and nitrogen intermediates, inhibition of oxidative stress, blocking maturation and acidification of the phagolysosomes containing *M. tuberculosis* [112, 125, 126].

1.3.1.2 Later events during infection

Later events define survival of *M. tuberculosis* during infection in the lung. They include induction of cell-mediated immunity and granuloma formation. Bacterial replication and further destruction of alveolar macrophages results in inflammatory cells recruitment, mainly blood monocytes and neutrophils, to the site of the infection. Infected monocytes differentiate into dendritic cells and macrophages and phagocytose *M. tuberculosis* to kill the bacteria [127]. Antigen presenting dendritic cells transport *M. tuberculosis* to local lymph nodes and prime CD4^{+} T cells after 6-8 weeks of infection [128, 129]. Initial encounter with *M. tuberculosis* through antigen

presentation by phagocytes activates T cells that enter the site of infection to proliferate granuloma formation [130]. Granuloma formation is the hallmark of tuberculosis, where mononuclear cells serve as building blocks of granuloma. Early stage granuloma is made up of macrophages, neutrophils, monocytes, dendritic cells, and differentiated macrophages cells such as multinucleated giant cells, foamy macrophages, and epithelioid macrophages. Arrival of lymphocytes and initiation of cell mediated immune response leads to formation of more organized, stratified structure within granuloma where the infected macrophage at center becomes enclosed by foamy macrophages, mononuclear phagocytes and a mantle of lymphocytes, further surrounded within a fibrous cuff of collagen that marks the periphery of the structure. At this time of infection, 'containment' phase (latency), granuloma contains the *M. tuberculosis* and spread of infection occurs at additional tissue sites within the host and to other host cell is limited [130, 131].

The final stage is the reactivation of *M. tuberculosis* infection where disease progresses to active state and spread of infection occurs through respiratory droplets. Reactivation of the disease is associated with a weakened immune system due to genetic or environmental factors or defect in signaling of immune system including poor nutrition, or HIV infection [112]. Immunological basis of reactivation involves two mechanisms for development of active tuberculosis: $CD4^+$ T cell defect and TNF neutralization [113]. At this stage, cell death leads to formation of necrotic granuloma and further progression caseates the granuloma, followed by a rupture that leads to spread of infectious bacilli through aerosol [131, 132]. Infection can spread and develop into active pulmonary tuberculosis or initiate infection at other tissue sites as extrapulmonary tuberculosis (miliary tuberculosis). Initiation of active pulmonary tuberculosis results in production of cough and further transmission occurs through spread of aerosol containing infectious bacilli [111, 131].

1.3.2 Intracellular pathogenesis: The host-pathogen interplay

M. tuberculosis infects various host cells, mainly alveolar macrophages. In order to establish infection, *M. tuberculosis* needs to survive within host alveolar macrophages. The host initiates innate immune responses by recognising bacteria via multiple pathways of recognition to protect host cells and clear infection. If innate immune response is not sufficiently able to protect host from infection, then adaptive

immune response is generated which usually contains the bacteria and results in latent infection. However, an immuno-compromised condition and other factors lead to active tuberculosis. Under these conditions, bacteria evades the immune system by various strategies targeting different host defence mechanisms [133]. The interaction of host immune responses with bacterial defense mechanism has an important role in determination of control of infection or its establishment. This interplay between host and *M. tuberculosis* with detailed study of immune responses and how bacteria escape these processes and responses to survive and progress infection is described in the following sections.

1.3.2.1 Innate immune response

Innate immune responses generate at the earliest encounter with *M. tuberculosis*, of the host, and may be responsible for an early clearance of *M. tuberculosis* [134]. The primary role of innate immune system against *M. tuberculosis* infection is in (a) the bacterium recognition, (b) priming and initiation of adaptive immune responses, (c) inflammation regulation [133].

(a) The bacterium recognition

M. tuberculosis and other microbes express pathogen associated molecular patterns (PAMPs) that are recognised by various pattern recognition receptors (PRRs), such as toll-like receptors (TLRs), NOD-like receptors (NLRs), C-type lectin receptors (CLRs), DC-SIGN, and mannose receptors [135, 136]. Cytosolic sensors such as cGAS and STING detect bacterial secondary messengers and bacterial DNA [137, 138]. The mycobacterial components such as peptidoglycan, lipoproteins, phosphatidyl-inositol mannosides, mannose-capped lipoarabinomannan, CpG-containing DNA are recognized by these receptors [133]. The PRRs associated signaling pathways play a crucial role in defence mechanism against *M. tuberculosis*.

The TLRs such as TLR2, TLR4, TLR9 contribute to recognising variety of mycobacterial components as ligands [139]. Studies of myeloid differentiation factor 88 (MyD88), a common TLR adaptor protein, deficient mice has indicated to the significance of TLR signaling pathway in host immune responses against mycobacterium [140]. MyD88 signaling integrates with interleukin-1 (IL-1) receptors and TLR signaling by IRAKs (IL-1-receptor-associated kinases) binding and further

activates various pathways, importantly mitogen activated protein kinases (MAPK) and NF-kB, activator protein 1 (AP1) [133].

M. tuberculosis can evade innate immune response generated by PRRs. These strategies include expression of cell envelope component by specific strains, for example, the strain HN878 (W-Beijing lineage strain) expresses an additional component polyketide synthase-derived phenolic glycolipids (PGLs) [141], or expression of immune-inhibitory lipid components such as W-Beijing strain GC1237-expressed tetraacylated sulfoglycolipids that bind to TLR2 [142], or by enzymatic means to modify cell wall components as the tuberculosis serine-hydrolase, Hip1 (hydrolase important for pathogenesis 1), acts on multimeric GroEL2 (chaperone-like protein of *M. tuberculosis*) and cleaves it into a monomeric secreted form [143]. These *M. tuberculosis* strategies are found to impair innate immune responses [133].

Macrophage defense mechanism in tuberculosis

After recognition by PAMPs receptors, innate immune cells initiate a series of cellular responses to clear and eliminate *M. tuberculosis* infection. The main cellular events include phagocytosis, autophagy, inflammasome activation and apoptosis.

Phagocytosis: *M. tuberculosis* recognition by the macrophage results in phagocytosis and subsequent fusion of the phagosome-sequestered bacterium with lysosomes forming phagolysosome. Further acidification of the phagolysosome leads to killing of bacteria within the phagocytes. In addition, macrophages also produce ROS and nitrogen intermediates that aid clearance of intracellular *M. tuberculosis* [144]. *M. tuberculosis* inhibits phagolysosome maturation using various mechanisms. It secretes proteins of the ESX system, such as ESAT-6 and homologues of SecA ATPase, termed as SecA1 and SecA2, that affect phagosome maturation [145, 146]. *M. tuberculosis* has the ability to escape from phagosome to enter the cytosol for replication using effector proteins of ESX-1 secretion system, mainly ESAT-6. However, recently ESAT-independent mechanism of bacterial escape has also been reported [147-149]. Other *M. tuberculosis* secreted proteins that interfere with maturation of phagosomes include serine/threonine kinases (PknG) and phosphatases

(SapM and PtpA) [150-152]. Secreted PknG also prevents phagosome-lysosome fusion [150, 153].

An important virulence factor, the glycolipid lipoarabinomannan, prevents PI3P production and supresses phagolysosome biosynthesis [154]. Acidification of the phagosome (pH below or equal to 5) is an essential feature of phagosome maturation that is targeted by *M. tuberculosis*. Infection of *M. tuberculosis* inhibits phagosomes acidification, resulting in a minimum pH of 6.4, further preventing phagosome-lysosome fusion. The V-ATPases are required for acidifying the phagosomes but are excluded from the phagosome membrane during *M. tuberculosis* infection [155-157]. Thus, *M. tuberculosis* evades the phagosomal defense of macrophages by preventing phagosomes maturation, phagosomes acidification, and phagosome-lysosome fusion through various mechanisms.

Autophagy: Autophagy promotes bacterial killing and the activation of immune response through antigen presentation. Cytoplasmic components like protein aggregates, damaged organelles, and more importantly, intracellular microbes are captured and degraded by autophagosomes, a process termed as macroautophagy. The autophagosomes with cellular content then fuse with lysosomal organelles and mature into autolysosomes. Inside the cytosol, ubiquitnation of the bacteria that escaped from phagosome occurs and the ubiqutinilated bacteria are further captured by autophagosomes and mature into autolysosome. The protein-protein (Atg5/Atg12) and protein-lipid conjugation (Atg8/LC3) systems are involved in autophagosome formation [136]. However, the role of autophagy in *M. tuberculosis* elimination is not completely understood in active tuberculosis patients and human cells although several studies have been performed in a mouse model [120]. Autophagy is induced by rapamycin, starvation or immune mediators like IFN-γ, toll-like receptors (TLR4 and TLR7), and vitamin D that shows antimicrobial effects [158-161]. Increased risk of development of active tuberculosis has been shown linked with vitamin D deficiency [162]. Studies have reported IFN-γ-mediated induction of autophagy during active tuberculosis [163] but IFN-γ mediated immune response has also been found to be inhibited by *M. tuberculosis* factors such as ESAT-6, and *M. tuberculosis* outer surface sulfatides or lipoarabinomannan [120, 164].

Apoptosis: The mode of host cell death is an important factor to determine the fate of the infection. Apoptosis of infected cell benefits the host as it can control bacterial replication and present bacterial antigens that can elicit T-cell immunity against *M. tuberculosis* infection. However, necrosis of infected cells favours bacterial replication and dissemination [165]. *M. tuberculosis* manipulates host cell death, inhibits apoptosis and induces necrosis, by various mechanisms to evade the innate host defense [120, 166].

Inflammasome activation: Inflammasomes are multiprotein signaling complexes that detect pathogens and lead to caspase-1 activation that converts pro-IL-18 and pro-IL-1β (pro-inflammatory cytokines) into their active forms. The caspase-1 protease with NLRs and adaptor protein (ASC/PYCARD) assemble into an inflammasome. NLRs (cytosolic PRRs) detect stress and pathogens through the recognition of PAMPs and DAMPs. NLRs are activated by a different stimuli, including the AIM2 inflammasome and NLRP3 inflammasome, which detect cytosolic DNA and a variety of cellular stress signals, respectively [167, 168]. During *M. tuberculosis* infection, NLRP3 inflammasome are activated in macrophages [169]. Studies have also reported mycobacterial ESX-1 secretion system-dependent inhibition of AIM2 inflammasome [170].

(b) Priming and initiation of adaptive immune responses

For generating host response against *M. tuberculosis*, the priming of adaptive immune response is a key step. Initiation of adaptive immune response primarily involves dendritic cells (DCs). DCs present *M. tuberculosis* antigens through major histocompatibility complex (MHC), known as professional antigen presenting cells. After the antigen uptake, migration of DCs begins to the draining secondary lymphoid organ (lung draining lymph nodes) and the DCs maturation occurs along with their migration [133, 171]. The dendritic cell migration requires cytokine IL-12, produced by myeloid cells, and is also reported to depend on the chemokines CCL19 and CCL21, and their receptor CCR7 [133, 172]. However, *M. tuberculosis* evolves strategies to inhibit initiation of adaptive response by impairing macrophages antigen presentation through MHC II or impairing human dendritic cell maturation and antigen presentation [173, 174].

1.3.2.2 Adaptive immune response

In order to control *M. tuberculosis* infection and replication, initiation of adaptive immune response is required. Adaptive immunity in tuberculosis involves antigen-specific T-lymphocytes antimicrobial actions and secreted cytokines as main features. Along with this, antibodies, B cells, CD1-restricted T cells, and γδ T cells have also been reported to play a crucial role in adaptive immune response [133]. During *M. tuberculosis* infection, initiation of antigen-specific CD4$^+$ T-cell responses is delayed in mice, human and nonhuman primates, compared to other pathogenic infections. It allows *M. tuberculosis* to evade host immunity and establishes a persistent infection [128, 175, 176].

Peptide antigens-bound MHC/HLA class II molecules are recognised by CD4$^+$ T cells that induces protective immunity against *M. tuberculosis* [136]. The stimulation of CD4$^+$ T cells and antigen presentation is also reported to be inhibited by *M. tuberculosis* [174]. Subsets of the CD4$^+$ T helper (Th) cell include Th1, Th2, Th17 and Treg cells. Notably, the cytokine IFN-γ is produced by Th1 cells, that can also secreted by CD8$^+$ T cells and innate T cells, with Th1 cells showing stronger IFN-γ response compared to CD8$^+$ T cells [177]. The other cytokines secreted by Th1 cells are IL-2, TNF-α, some CCL chemokines, and lymphotoxin. The Th2 cells secrete cytokines including IL-4, IL-5, IL-10 and IL-13. The Th17 cells mediate inflammation at the site of infection and produce cytokines IL-17, IL-17F, IL-21 and IL-22. The exact role of Th17 cells in *M. tuberculosis* infection control is still being defined [136, 178]. A type of T-helper cells subset is FoxP3$^+$, defined as T-regulatory cells (T-regs); it can control activity of other T lymphocytes and impair T-cell responses against *M. tuberculosis* [133, 179].

MHC/HLA class Ia molecule-bound peptide antigens are recognized by classically restricted CD8$^+$ T cells. Additionally, the class Ib molecule HLA-E bound peptide antigen can also be recognized by human CD8$^+$ T cells [180]. During *M. tuberculosis* infection, studies suggest a significant role of CD8$^+$ T cells in the immune defense mechanism. *M. tuberculosis*-infected mice with abrogated MHC class I antigen presentation pathway or with depleted CD8$^+$ T cells live longer than CD4$^+$ T cells deficient or with disrupted MHC class II pathway infected mice, but succumb earlier compared to wild-type controls [181]. Mice infected with *M. tuberculosis* having

impaired CD8^{+} T-cell responses due to lack of TAP-1 antigen presentation molecules succumb more rapidly compared to wild-type *M. tuberculosis*-infected controls [182]. The CD8^{+} T cell-mediated immune response against *M. tuberculosis* includes cytokines secretion (IFN-γ and TNF-α) along with cytolytic action through perforin and granulysin [183]. Evidence for cytokine TNF-α in protective immunity has been found in rheumatoid arthritis patients through use of anti-TNF-α antibodies that deplete a subset of CD8^{+} T cells and lead to latent to active tuberculosis progression [184].

The γδ T cells recognize non-peptide antigens and can be found at mucosal surfaces. These cells proliferate following exposure to *M. tuberculosis*-infected monocytes [133, 185]. Studies have also suggested a role of humoral adaptive immunity in tuberculosis. B-cell deficient mice infected with *M. tuberculosis* showed enhanced recruitment of neutrophils and exacerbated lung immunopathology. Studies indicate role of elevated IL-17 responses in mice lacking B-cells are responsible for this [186, 187].

1.4 Modulation of host cell death by *M. tuberculosis*

Intracellular pathogens use several strategies to modulate host cell processes in order to establish infection and spread. Cell death, the key process to maintain cellular homeostasis, is an important protective immune response against intracellular pathogen infection. However, pathogens evade and manipulate host defense mechanisms including host cell death and use it as virulence strategies for their survival, replication and dissemination [188]. *M. tuberculosis* modulates host cell death pathways along with other strategies to overcome host immune mechanisms [189-191]. Apoptosis can control the *M. tuberculosis* infection and is considered as a protective immune response and a pro-host pathway of host cell death, while necrosis favours the bacterial infection. *M. tuberculosis* infection inhibits apoptosis of infected host cells and induces programmed necrosis [166, 192]. Due to emerging resistance against first line anti-tubercular drugs, host-directed therapies have been identified as a promising approach for novel therapeutics development and *M. tuberculosis* infection control. Host-pathogen interacting partners that are involved in the pathogenesis of disease serve as potential targets. Additionally, crucial host cell processes that are manipulated by pathogens such as host cell death can be targeted to

combat *M. tuberculosis*. In response to *M. tuberculosis* infection, the host cell undergoes various death modalities that either favour the host to clear the infection, or aid the pathogen to establish infection [189, 191].

1.4.1 Apoptosis

Apoptosis, or programmed cell death, is morphologically defined by nuclear fragmentation and condensation, cell body shrinkage, plasma membrane blebbing, and apoptotic bodies formation that are rapidly taken up by phagocytes. The phagocytic clearance of apoptotic cells is defined by a process known as efferocytosis [188, 191]. Apoptosis signaling is regulated by the intrinsic and extrinsic pathways based on an intracellular or an extracellular trigger. *M. tuberculosis* infection modulates host protein associated with apoptosis. The intrinsic pathways are triggered by mycobacterial factors, mainly lipoarabinomannan, and the extrinsic pathways are activated via binding of death receptor ligands (TNF-α or FasL/CD95) to their receptors. The extrinsic pathway results in activation of caspase-8 and further downstream effector caspases 3, 6, and 7. On the other hand, an apoptosis response triggered through the intrinsic pathway initiates activation of tBid that results in cytochrome C release, apoptosome formation, and finally apoptosis [188, 189]. Apoptosis is considered as a innate macrophage defense mechanism against *M. tuberculosis* infection. Apoptosis through cross-priming can stimulate subsets of T-cell such as CD8$^+$ T cells and induce a better T-cell immunity [166].

Upon *M. tuberculosis* infection, several host proteins are induced either by host to control the infection, or by the pathogen to establish infection [189, 190]. TLR2 and TLR4 are the specific TLRs involved in *M. tuberculosis* infection. TLR2 induces apoptosis via the p38 MAPK pathway while TLR4 regulates induction of apoptosis and necrosis [193]. Absence of TLR4 promotes necrosis over apoptosis. Studies have reported that, not *M. bovis* BCG but the virulent *M. tuberculosis* escapes from the phagolysosome by interfering with the TLR2/MyD88 pathway [194]. *M. tuberculosis* infection up-regulates the anti-apoptotic genes, mainly bim, bcl2, mcl-1, and bcl-W and down-regulates the pro-apoptotic genes like bax and bad [195]. Cytokines like IL-10 and TNF-α play a crucial role in *M. tuberculosis* infection progression. IL-10 inhibits INF-γ and lipopolysaccharide-induced apoptosis. Determination of the type of

cell death of infected cells, either through necrosis or apoptosis, is also dependent on the relative levels of TNF-α and IL-10 [196, 197].

Several mycobacterial proteins have a key role in apoptosis regulation. Major *M. tuberculosis* factors regulating host apoptosis involve secreted proteins like P19 and ESAT-6, surface protein PE_PGRS-33, surface glycolipids lipomannan and lipoarabinomannan, and other mycobacterial factors like LpqT, MptpB, Rv0426c, Rv3033, PE31 (Rv3477) [189, 190]. *M. tuberculosis* secretes mycobacterial factors that interfere with the ROS and RNS-mediated apoptosis, by acting as free-radical scavengers. Major Mycobacterial factors that target ROS or RNS to inhibit apoptosis include mycobacterial glycolipids, proteins such as mycobacterial catalase-peroxidase (KatG), NADH dehydrogenase (NuoG), and superoxide dismutase (SodA) [198-201]. Apoptosis could be protective to host when induced as an early response; however, at later stages of infection, induction of apoptosis can favour mycobacterial infection and dissemination [189].

1.4.2 Necrosis

Necrosis is morphologically defined by loss of plasma membrane integrity. It was previously considered as a random uncontrolled process that results from accidental cell death and one that does not involve cellular signaling. However, evidence from recent studies indicates that necrosis is a programmed process regulated by a cascade of signaling pathways [188, 202]. Cell-death types include Regulated Cell Death (RCD) and Accidental Cell Death (ACD) [203]. NCCD-2018 has updated the classification of different mode of cell deaths in which two main categories of necrosis are described as MPT-driven necrosis and necroptosis that is defined as a form of RCD [189, 204]. Necrosis can be triggered by TNF-α receptor, through PRR activation, Ca^+ overload and extensive DNA damage, and is regulated by several factors like MPT (MPT-driven necrosis), RIPK1/RIPK3, MLKL (necroptosis), caspase 11 (pyroptosis), cathepsin B, caspase-1 (pyronecrosis). Along with this, parthanatos, oxytosis, ferroptosis, and ETosis are also included as form of regulated necrosis by the NCCD-2018 [189, 204, 205].

Mycobacterial infection promotes necrosis at higher multiplicities of infection. Granuloma formation is considered as a host defense mechanism to contain and

restrict mycobacteria. However, studies suggest that mycobacterium exploits this host defense mechanism to multiply within the host [206]. Host cell necrosis helps in bacterial dissemination during *M. tuberculosis* infection [207, 208]. *M. tuberculosis* prevents plasma membrane repair that leads to induction of necrosis and subsequent extracellular release of mycobacterium [208]. Necrotic macrophages favour bacterial replication by providing an ideal niche for multiplication of *M. tuberculosis* [165]. *M. tuberculosis* infection also induces necrosis of infected neutrophils [209]. Induction of apoptosis or necrosis is also reported to be regulated through eicosanoids production, prostaglandin E2 (PGE2) versus lipoxin A4 (LXA4), in host cells [210]. Mice that cannot produce LXA4 or PGE2 are more resistant or more susceptible to *M. tuberculosis* infection, respectively [191, 208, 211]. *M. tuberculosis* induces production of LXA4 leading to inhibition of cyclooxygenase 2 (COX2) enzyme expression which is involved in PGE2 synthesis pathway [212, 213]. At higher levels, PGE2 prevents mitochondrial membrane damage and further inhibits induction of necrosis [210, 212]. Leukotriene A4 hydrolase (LTA4H) also plays a role in host necrosis and *M. tuberculosis* infection [214]. Necrosis is induced in both conditions: absence of LTA4H (high LXA4/no LTB4) or during LTA4H overexpression (high LTB4/no LXA4). The absence of LTA4H results in decreased TNF-α levels and bacterial virulence, while LTA4H overexpression leads to increased TNF-α levels and host susceptibility to mycobacterial infection [190, 215]. This suggests a regulation of bacterial burden through TNF-α levels [207, 215]. Necrosis is preferred during *M. tuberculosis* infection over other modes of cell death that have anti-mycobacterial effect. Therefore, induction of necrosis is beneficial for *M. tuberculosis* infection [165, 189].

1.4.3 Necroptosis

Necroptosis, best characterised as a form of regulated necrosis, is initiated by sensing specific signals through various death receptors like FAS receptor, TNF receptor, and pathogen recognition receptors (TLR3, and TLR4). At the molecular level, induction of necroptosis requires activation of RIPK3 that further phosphorylates and activates MLKL. MLKL phosphorylation leads to MLKL oligomerization and membrane translocation that in turn triggers plasma membrane permeabilization. The TNFR1 mediated necroptosis involves activation of RIPK3 by RIPK1 and is reported to be

inhibited by RIPK1 inhibitors such as necrostatin-1 (Nec-1/Nec-1s) [204]. Cell death and inflammation can be linked through necroptosis [216]. Studies have identified the role of ESCRT-III in regulation of necroptosis, where it acts downstream of MLKL [217, 218]. The ESCRT-III mediated plasma membrane repair antagonizes necroptotic cell death [217-219]. Recently, a study has reported the inhibition of ESCRT-III by mycobacterial effectors EsxG/EsxH, both secreted by the ESX-3 type VII secretion system. However, their role in host cell death still needs to be defined [190, 220]. The TNF-α levels have been suggested to regulate cell death mode where higher levels can induce necroptosis [207]; whereas lower levels promote apoptosis [221]. The other host factor, caspase-8, in its active form, inhibits necroptosis while its inactive form favours necroptosis [222].

M. tuberculosis modulates the mode of host cell death and induces necrosis through various mycobacterial factors. The mycobacterial protein ESAT-6 activates NLRP3 inflammasome and induces necrotic cell death of human macrophages [223, 224]. The other mycobacterial factors that induce necrosis include PE_PGRS33, PE25/PPE41, PPE68, and Rv2626c [190].

The exact molecular mechanism of necrosis induction by *M. tuberculosis* still needs to be explored [225]. During infection, pathogenic bacteria secrete toxins to kill the host cells [226]. In case of *M. tuberculosis*, secreted virulence factors that possess strong host cell toxicity have not been well defined [90, 227, 228]. A recent study has identified a channel protein with necrosis-inducing toxin (CpnT) as the main cytotoxicity factor that comprises C-terminal secreted toxin and N-terminal channel domain [229]. *M. tuberculosis* secretes this toxin called tuberculosis necrotizing toxin (TNT) in the host cytosol [229, 230]. TNT possesses NAD^+-glycohydrolase activity and depletes host NAD^+ pool [230]. *M. tuberculosis* produces IFT (immunity factor for TNT) that acts as an anti-toxin for TNT to protect itself from TNT-mediated toxicity [230, 231]. Depletion of host intracellular NAD^+ levels through TNT activates key mediators of necroptosis RIPK3 and MLKL, that results in induction of macrophage necroptosis [192]. TNT-mediated necroptosis does not require the TNF-α and RIPK1. Study suggests that secreted TNT is the main inducer of *M. tuberculosis*-infected host macrophage necroptosis. Interestingly, NAD^+ depletion alone can activate RIPK3 and MLKL pathway leading to necroptosis induction. Furthermore,

lack of RIPK3 or MLKL, or their inhibition, or both, prevent TNT-induced necroptosis of *M. tuberculosis*-infected macrophage [192]. In the infected macrophage, TNT induces ROS production, that further leads to cell death and favours mycobacterial replication [232]. The induced ROS production by TNT is both through necroptosis activation and also in a necroptosis-independent manner. Further, replenishment of NAD^+ and ROS scavenging protects *M. tuberculosis*-infected cells from cell death [232]. These studies suggest importance of host-directed therapies for treatment of tuberculosis [192, 232]. Inhibition of necroptosis or NAD^+ replenishment strategies could be used to prevent macrophage cell death. Targeting TNT could protect macrophage from *M. tuberculosis*-mediated necroptosis and further limit mycobacterial survival inside macrophage.

1.5 Malaria: Overview

To achieve the ultimate target of malaria eradication, WHO established the definition and certification criteria for malaria elimination in the 1960s [233]. During 2000-2015, a significant reduction in mortality and morbidity from malaria, with more than 75 percent decrease in incidence rate, were achieved [234, 235]. A world free of malaria has been the vision of WHO and the global malaria community. To accomplish this, ambitious global targets for 2030 along with milestones for 2020 and 2025 to measure progress were set by WHO in 2015 under the Global Technical Strategy for malaria 2016–2030 [234, 236].

Malaria remains global health threat leading to approximately 228 million cases and 0.4 million deaths in 2018 [236]. The causative agent of malaria is a protozoan parasite belonging to phylum *Apicomplexa* and genus *Plasmodium*. Among all the human infecting *Plasmodium* species, *Plasmodium falciparum* is responsible for more deaths while *Plasmodium vivax* is the most widespread and a major cause of illness globally [237]. The greatest global burden of disease (almost 85%) is present in countries of sub-Saharan Africa and India. Among these countries the largest absolute reduction in malaria cases was reported in India during 2018 compared to 2017 [236]. Incidence rate of malaria has been slowed down dramatically from 2014-2018. Since 2016, reduction in malaria mortality rate has also slowed. Despite the positive progress achieved in malaria elimination programmes, an accelerated change is required to accomplish the goals of Global Technical Strategy for malaria 2016-2030

for complete eradication [236]. The major challenges in achieving malaria elimination include development of insecticide resistance, emergence of resistance against effective anti-malarial drugs and various socio-cultural factors [238]. There is a pressing need to develop effective prevention strategies, treatment regimes, and new effective drugs to combat malaria.

The emerging resistance against effective anti-malarial drugs such as chloroquine leads to high mortality [239-241]. To overcome the problem of drug resistance, combination therapy was employed and approved by WHO instead of monotherapy. A new class of potent antimalarials represented by artemisinins derived from natural products, came up. Artemisinin-based combination therapy (ACT) has been recommended by WHO for the treatment of uncomplicated *P. falciparum* malaria. ACT achieves clearance of parasites through, a fast-acting artemisinin derivative, and clears residual parasitemia, with a slow-acting partner drug [241, 242]. Recent studies have reported development of resistance to the artemisinin and artemisinin-based combination therapy as well, causing ACT failure and an urgent need to discover new antimalarials for treatment of drug-resistant malaria [243].

1.5.1 Global epidemiology

The two *Plasmodium* species, *P. falciparum* and *P. vivax*, are responsible for the majority of human malaria cases worldwide. In 2018, 228 million cases of malaria were reported globally [236]. Most cases occur in the WHO region of Africa (93%), while 2.1% and 3.4% cases were present in the Eastern Mediterranean region and South-East Asian region, respectively. *P. falciparum* is the most prevalent species in these regions. The largest malaria burden, almost 85%, is carried by 19 countries: 18 African countries and India [236]. *P. vivax* is responsible for 3.3% of all estimated malaria cases with the region of South-East Asia having 53% of the total *P. vivax* burden, and 47% being carried by India. In the WHO region of the Americas, *P. vivax* predominates with 75% of malaria cases [236]. The global malaria incidence rate decreased to 57 in 2018 compared to 71 in 2010, with the highest reduction reported in the WHO South-East Asia region, mainly in India, Indonesia and the Greater Mekong subregion (GMS) countries [236]. However, the rate of change was found to be similar during the period 2014 to 2018. The estimated number of death declined to 405,000 in 2018, from 416,000 in 2017 and 585,000 in 2010. Compared with 2010, a

notable reduction in malaria deaths by 2018 was reported in the region of South-East Asia and Africa. In the period 2016-2018, the rate of reduction of malaria mortality has also slowed [236].

1.5.2 History

Malaria (originated from the Italian word "*malaria*" meaning bad air) was first documented in ancient Chinese medical writings of 2700 BC and in the Ebers Papyrus 1200 years later [244, 245]. In the fourth century BC, Hippocrates described malaria as a disease [246]. The parasitic nature of infection was first observed by Laveran, a French military surgeon, in the blood of malaria patients in 1880. For this discovery, Laveran was awarded the Nobel Prize in 1907 [247]. In 1897, Ronald Ross elucidated the whole transmission cycle of the parasite for avian malaria and identified mosquitoes as the vectors. Camillo Golgi and others in 1898 demonstrated that *Anopheles* mosquitoes also transmit human malaria [248].

In China, during the second century BC, *Artemisia annua*, a sweet sagewort plant known as Qinghai, was used to treat malaria [249]. In the 16th century, malaria was treated with the Cinchona tree (*Cinchona succirubra*) bark. Pierre Joseph Pelletier and Joseph Caventou in 1820 extracted and isolated quinine from Cinchona bark, and purified quinine became the new standard treatment of malaria [250]. In 1934, Hans Andersag discovered chloroquine and named it resochin [251]. Later, in 1971, artemisinin, a potent antimalarial, was isolated by Youyou Tu from the plant *Artemisia annua*. The Nobel Prize was awarded to Youyou Tu in 2015 for this discovery [244]. WHO has approved the use of ACTs to reduce development of drug-resistance against the commonly used drugs chloroquine, amodiaquine, and sulfadoxine-pyrimethamine [252].

In 1874, dichlorodiphenyltrichloroethane (DDT) was synthesised by the German chemist Othmer Zeidler during his Ph.D. However, Paul Muller discovered its insecticidal property in 1939. DDT was used to control malaria by attacking the vector at the end of the Second World War [244]. For detection of malaria, in early 1990s, a polymerase chain reaction (PCR) based assay was developed [253]. Rapid diagnostic tests (RDT) for detection of parasite-specific antigens in blood were

subsequently developed and the first RDT was approved by FDA in 2007 for malaria detection [244]. Attempts to develop an effective antimalarial vaccine are underway.

1.5.3 Transmission and Clinical presentation

Plasmodium parasites complete its life cycle in female *Anopheles* mosquito and the human host. Developed blood stage sexual parasites, called gametocytes, can only be transmitted to the mosquito vector. During the blood feed of an infected female *Anopheles* mosquito, *Plasmodium* sporozoites are transmitted to humans. Blood-borne transmission as well as congenital transmission can spread the malaria infection. Environmental suitability for local vectors determines the disease incidence. The environmental factors affect parasite development in the mosquito vector, that further sets transmission limits [237, 254].

Malaria can be categorised into two disease presentations: uncomplicated and severe. The clinical manifestations are affected by host immunity and previous exposure to malaria and are primarily produced due to schizont rupture and erythrocyte destruction leading to release of erythrocyte material and parasites into circulation. Uncomplicated malaria presents non-specific symptoms that resemble a flu-like illness. These can include fever, chills, headache, body-aches, diarrhoea, and cough. Once malaria is suspected, a confirmatory laboratory testing should be performed [254, 255].

Severe malaria complication is mainly associated with falciparum malaria progresses rapidly, making it a potentially fatal disease. For rapid clinical assessment of severe malaria, presence of clinical features need to be evaluated. These include prostration, fast deep breathing, and impaired consciousness. The most common manifestations are acute renal failure, respiratory failure, cerebral malaria, and/or severe anaemia [254, 255].

1.5.4 Control of Malaria: Treatment and anti-malarial drugs

Diagnostic test for malaria

Examination of stained-blood smear using light microscopy remains the gold standard for malaria diagnosis. The thick smears provide sensitivity and thin smears allow quantitation and speciation [254]. In blood, parasite-specific antigens are detected by

RDTs and in all malaria-endemic areas RDTs are now used as the first choice of tests recommended by the WHO. Confirmation of all RDT test results should be carried out by microscopic blood analysis [244]. RDT test commonly incorporates targeting of two antigens: parasite-specific lactate dehydrogenase or *P. falciparum* histidine-rich protein-2 [254].

Vector control

Vector control is an important intervention to control malaria transmission. Vector control strategies include indoor residual spraying (IRS), insecticide-treated nets (ITNs), and long-lasting ITNs (LLINs). Development of insecticide resistance is a major concern in the control of the malaria vector. The classes of insecticides that are approved for IRS include organochlorines (DDT), carbamates, pyrethroids, and organophosphates. However, for ITNs only pyrethroids are approved [256, 257].

Vaccines

It is difficult to develop a vaccine for malaria due to the complex life cycle of malaria parasite that can evade the immune system. Malaria vaccines are divided into three categories according to their primary effect: transmission-blocking vaccines (IBVs), pre-erythrocytic vaccines, and blood-stage vaccines. Studies are underway to develop an effective antimalarial vaccine [244].

Anti-malarial drugs

Antimalarial agents are classified on the basis of their antiplasmodial activity and chemical structure. Five classes of antimalarial agents are classified according to antiplasmodial activity: gametocidal, prophylaxis, sporontocides, blood schizonticides, and tissue schizonticides. According to their structure, anti-malarials are classified into: 4-aminoquinolines, 8-aminoquinolines, hydroxynaphthoquinones, diaminopyrimidines, artemisinin derivatives, quinolines-based cinchona, 4-quinolinemethanols, sulphonamides, and biguanides [252].

Due to emerging resistance against effective anti-malarial drugs chloroquine, sulfadoxine-pyrimethamine (SP), and mefloquine, WHO recommended ACTs for uncomplicated malaria treatment. The most commonly used combination for ACTs are artesunate–mefloquine, artesunate–amodiaquine, DHA–piperaquine, artemether–

lumefantrine, and artesunate–sulfadoxine–pyrimethamine. Development of artemisinin resistant parasites and reported cases of failure of ACTs in some areas represent a global health threat. Until new medicines are available, triple artemisinin-based combination therapies are being evaluated for their potential to fight against drug-resistant malaria [258]. ACT is not recommended during the first trimester of pregnancy. A course of quinine and clindamycin for 7 days is used for treatment of the first trimester uncomplicated falciparum malaria infection [254].

1.6 Pathogenesis of malaria parasite

1.6.1 Life Cycle: Overview

Malaria is caused by *Plasmodium* species. Human infection can occur by five species: *P. falciparum*, *P. vivax*, *P. ovale*, *P. malariae*, and *P. knowlesi* [244]. The *Plasmodium* parasite completes its life cycle in two hosts, a vertebrate and the mosquito, and is divided into two phases, sexual and asexual. Female *Anopheles* mosquitos inoculate sporozoites into human blood after a bite. The sporozoites enter the hepatocytes and through asexual multiplication develop into merozoites. These merozoites invade erythrocytes and multiply. Inside erythrocytes, merozoites develop into trophozoite and schizont stages. Schizont rupture releases merozoites that invade other erythrocytes. Some merozoites develop into female and male gametocytes, sexual forms, and are ingested by the female mosquito. Male gametocytes exflagellate and the fusion of male and female gamete occurs to form a zygote in the midgut that develops later into ookinete. The sporozoites from the oocyst move to the salivary glands of the mosquito and during a blood feed are inoculated into the human host to restart the *Plasmodium* life cycle (Figure 1.4) [254, 259].
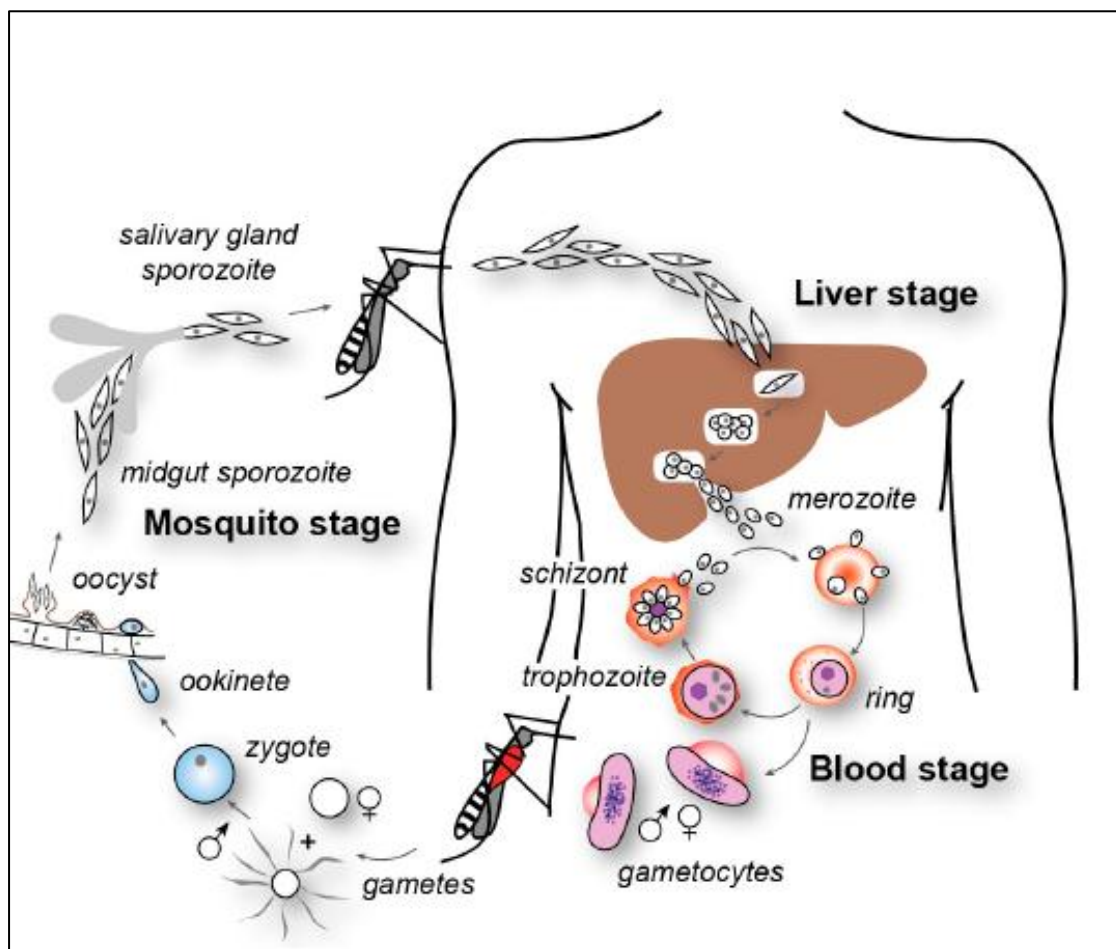
Figure 1.4 The life cycle of *P. falciparum* (Adapted from Cowman et al., 2012). Figure showing stages of *P. falciparum* infection in *Anopheles* mosquito vector and the human host [259].

1.6.2 Invasion process of malaria parasite into erythrocytes

1.6.2.1 Erythrocyte invasion of malaria parasite: General overview

The merozoite invasion is a key step for parasite infection. To exit infected erythrocytes, a process of parasite egress from cells is initiated, one that involves rupture of parasitophorous vacuole and erythrocyte membrane. The process of egress involves increase in intracellular pressure and cell cytoskeleton destabilization followed by rupture of erythrocyte host leading to dispersion of non-motile merozoites. After release from host cell, merozoites take around 60 sec to invade new erythrocytes after recognition and attachment to them [259, 260]**.** Figure 1.5 shows overview of merozoite invasion process [259].
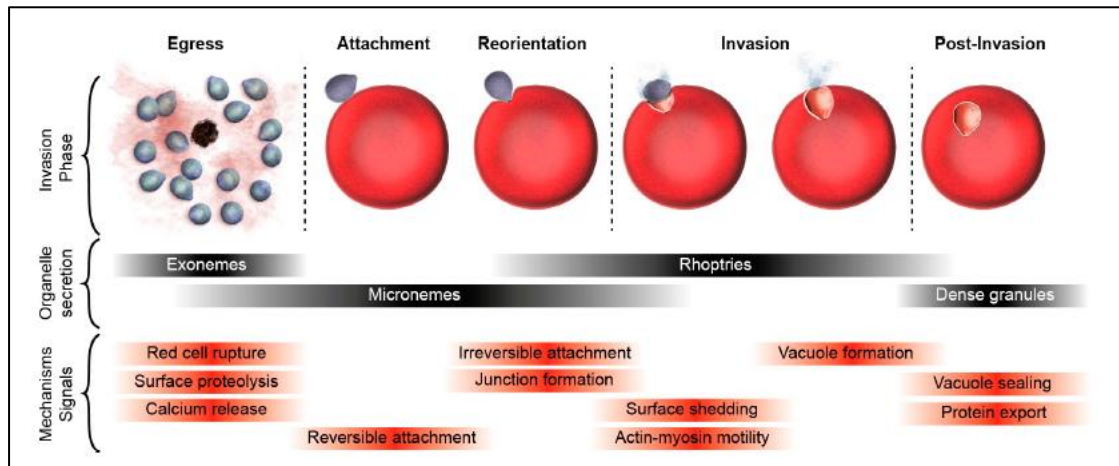
Figure 1.5 Overview of invasion process (Adapted from Cowman et al., 2012). Cellular overview of merozoite invasion from egress to postinvasion with signaling steps [259].

For the initial contact of merozoite with erythrocyte, the first step of invasion involves "long- distance" recognition and primary attachment which is followed by wrapping the erythrocyte surface around the merozoite, a reorientation process that brings apical end adjacent to the erythrocytes [260]. Next, between the host membrane and the parasite, a tight junction forms. Tight junction moves from the apical to the posterior pole of the merozoite. The merozoite surface coating is removed by a serine protease (SUB2) at the moving junction. When tight junction reaches the posterior pole, proteolytic removal of the adhesive protein at the junction occurs, that may involve a serine protease of the rhomboid family. By this process, parasite creates a parasitophorous vacuole and enters into host cell [237, 259, 260].

1.6.2.2 Molecular mechanism of erythrocyte invasion

The process of erythrocyte invasion by free merozoites completes within 2 min, which is fast, dynamic and involves three steps: pre-invasion, active invasion, and echinocytosis (Figure 1.6) [237, 261].
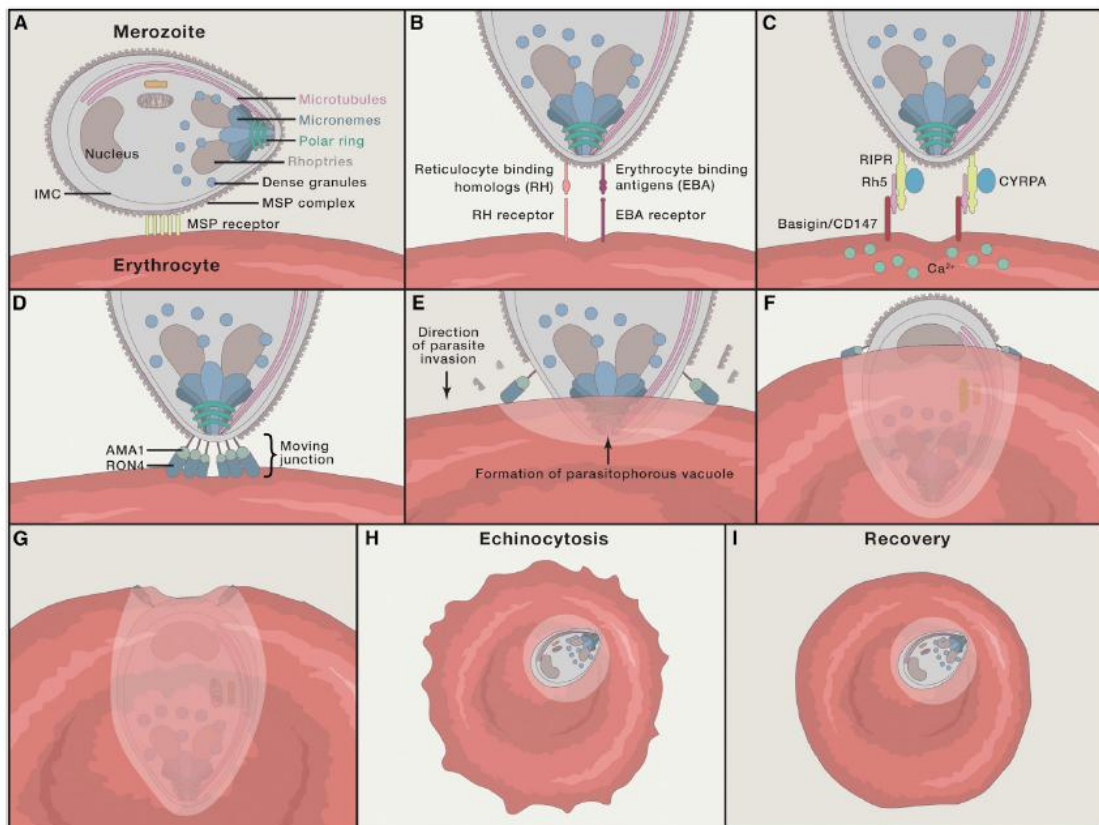
Figure 1.6 Molecular mechanism of erythrocyte invasion (Adapted from Cowman et al., 2016). Figure showing steps of erythrocytes invasion by *Plasmodium* parasite [237].

Initial interaction of merozoites with erythrocytes is known as pre-invasion [237]. The entire free parasite is coated by merozoite surface proteins (MSPs) family which most likely support the primary merozoite attachment to the surface of erythrocyte [262]. MSP1, major merozoite surface glycophosphatidylinositol (GPI)-anchored protein, is the largest and most abundant among these proteins [237]. MSP1 forms a platform for the assembly of different extrinsic proteins containing large complexes that bind erythrocytes [237]. The robust interaction during pre-invasion between the merozoite and erythrocyte leads to deformation of erythrocyte driven by actomyosin motor of the parasite [261]. The parasite proteins secreted from the apical organelles, the rhoptries and micronemes, are involve in the next steps of pre-invasion. Merozoite invasion can be governed by two major classes of proteins: adhesins and invasins. Main identified adhesins belong to the protein ligand families of erythrocytes binding-like (EBL) and binding-like homologues (PfRh) proteins, hailing from micronemes and rhoptries, respectively [263]. These proteins interact with specific receptors such as complement receptor 1 (CR1) and glycophorin A, B, and C, and also has role in

signaling activation [237]. The EBA175 and PfRh4 interact with glycophorin A and CR1, respectively [237]. These parasite-host interactions associated with erythrocyte membrane deformation. Erythrocytes deformation appears to followed by apical reorientation of merozoite which involves PfRh5 protein [263].

The tight junction formation leads to irreversible merozoites attachment to erythrocytes [237]. Apical membrane antigen-1 (AMA-1, micronemal protein) is an important invasin that interacts with the rhoptry neck proteins (RON) complex at the tight junction. The core of tight junction forms of AMA1 and RON2, a part of RON complex spanning the host membrane [259]. The actin-myosin motor generates force and by using it the merozoite enters the erythrocytes into a parasitophorous vacuole [237]. Subsequently, merozoite fusion with the membrane occurs at the posterior end. This step is followed by echinocytosis leading to erythrocyte shrinkage and formation of spiky protrusions [237]. Studies have suggested that the PfRh5 complex and basigin interaction-mediated intra-erythrocytic calcium ion influx may be responsible for this [261].

1.6.3 Merozoite egress from erythrocytes during blood stage replication

After the infection is established, blood-stage parasites undergo schizogony to produce 16-32 daughter merozoites. These merozoites initiate a process called egress and release from the infected erythrocyte to invade new host cells a process that involves parasitophorous vacuole membrane rupture and destruction of erythrocyte membrane [237, 264]. Egress of merozoites is a tightly regulated and coordinated process and regulated by various protein kinases [237]. One of the critical protein kinases for egress is the plant-like calcium-dependent protein kinase (PfCDPK5). The PfCDPK5 deficient parasites show normal maturation of invasion ligands and egress proteases, but are found to be arrested as mature schizonts without disruption of membranes [265]. Another important protein kinase for merozoite egress regulation is cGMP-dependent protein kinase (PfPKG) which is required for discharge of a parasite subtilisin-like serine protease (PfSUB1) into the parasitophorous vacuole [266]. The PfSUB1 has a role in rupture of parasitophorous vacuole membrane and cleaves a number of proteins such as serine repeat antigen (SERA) family of proteins including SERA6 [267, 268]. In addition, SUB1 cleaves MSP1 that appears to promote egress through interaction with the erythrocyte cytoskeleton protein spectrin [269].

1.7 Eryptosis

1.7.1 Eryptosis: Overview

The enucleated reticulocytes formed in the bone marrow from erythrocyte progenitors maturation enter the blood stream and mature into erythrocytes that lack nucleus and mitochondria [270]. After 100-120 days, the mature erythrocytes undergo senescence and subsequently are removed from circulation [271-273]. In the senescence, erythrocytes binding of hemichromes to anion exchanger 1 (AE1) or also known as band 3 protein leads to band 3 clustering that enhances complement C3 fragments deposition and binding of antiband 3 immunoglobulins [270, 272, 274].

Erythrocytes can undergo eryptosis or suicidal death if they experience injury, causing cellular integrity loss prior to senescence [275]. Although erythrocytes lack mitochondria and nuclei, they undergo programmed cell death (eryptosis) that has similarity with apoptosis. Eryptosis shares several physiological characteristics of apoptosis that include cell shrinkage, membrane ruffling and blebbing, cell surface exposure of phosphatidylserine, and elevated intracellular calcium levels [275-277].

1.7.2 Triggers and inhibitors of eryptosis

Eryptosis can be triggered by many xenobiotics such as amiodarone, amphotericin B, anandamide, aurothiomalate, azathioprine, chlorpromazine, cyclosporine, paclitaxel, and dimethylfumarate [270]. Other inducers of eryptosis include factors such as energy depletion [278], osmotic shock [279], oxidative stress [280, 281], or increase in temperature [282].

Eryptosis can be inhibited by many substances, some of which are amitriptyline [283], flufenamic acid [284], catecolamines [285], resveratrol [286], nitric oxide [287], and erythropoietin [288, 289].

1.7.3 Mechanism of eryptosis

Eryptosis is mainly induced through entry of extracellular calcium into cells, that results in increased cytosolic calcium ion (Ca^{2+}) activity [279]. This leads to cell surface exposure of phosphatidylserine, cell shrinkage or decrease in cell volume, and membrane blebbing (Figure 1.7) [270, 279].
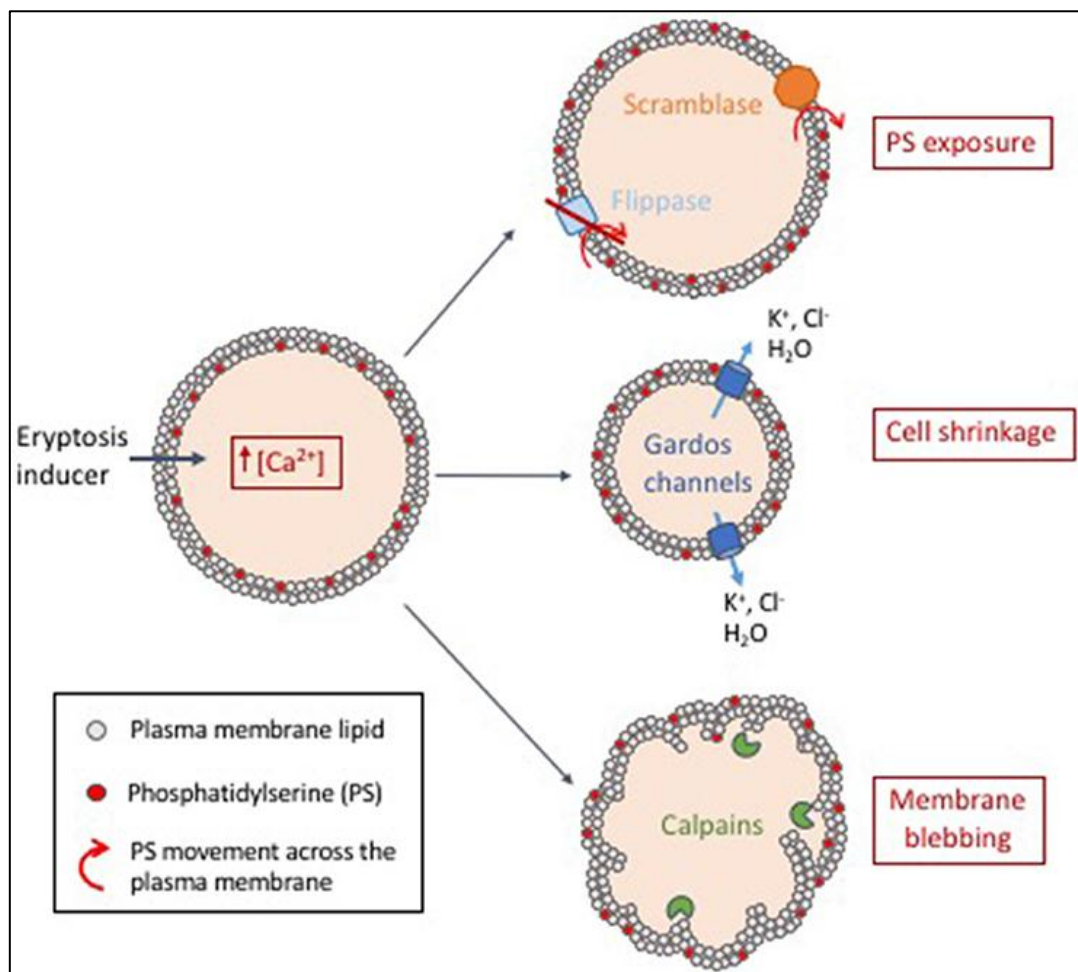
Figure 1.7 Model of proposed mechanism of eryptosis (Adapted from Boulet et al., 2018). Figure showing proposed mechanism of phosphatidylserine exposure, cell shrinkage, and membrane blebbing [270].

1.7.3.1 Phosphatidylserine exposure or changes of cell membrane asymmetry

Elevation in intracellular calcium levels in eryptotic cells inactivates flippases that leads to membrane asymmetry rupture with outer surface exposure of phosphatidylserine on the erythrocyte membrane [276, 290]. In addition, scramblases, another family of membrane proteins, activate due to increased intracellular calcium concentration and bidirectionally transport phospholipid by an ATP-independent process [290]. In case of eryptosis, the exact proteins involved in phosphatidylserine exposure need to be explored. To define enzymatic activities of lipid-transport, the generic term 'flippase' and 'scrumblase' were used [270].

1.7.3.2 Cell shrinkage

The calcium-activated potassium channels, also known as Gardos channels, allow potassium ion (K^+) exit in response to elevated cytosolic calcium levels [291-293]. The plasma membrane hyper-polarise due to intracellular K^+ loss that drives chlorine ions (Cl^-) exit from the cell. Following this, osmosis occurs that results in cell shrinkage due to loss of water [293]. Activation of phospholipase A due to hyperosmotic cell shrinkage leads to production of platelet-activating factor (PAF) [294]. Further PAF-mediated activation of sphingomyelinase cleaves membrane sphingolipid, known as sphingomyelin, and forms ceramide [294, 295]. The important role of ceramide has been identified in induction of apoptosis [296, 297] as well as in eryptosis [298].

1.7.3.3 Calpain activation and membrane blebbing

Calpains, a calcium-dependent cysteine protease family, are activated by autoproteolysis in response to elevated calcium levels [299]. Different amounts of calcium is required for activation of calpains I (or μ-calpains) and calpain II (or M-calpains), which is in micromolar and millimolar, respectively [300]. The spectrin and band 3/AE1, the erythrocyte cytoskeleton proteins, are the important targets of activated calpains [301]. Breakdown of these proteins results in erythrocyte membrane blebbing [302].

Activation of eryptotic pathway depends on a type of trigger for induction of eryptosis. Molecular events leading to eryptosis have not yet been fully elucidated. Eryptosis has been shown regulated by various kinases. Eryptosis stimulators include casein kinase 1 (CK1), protein kinase C (PKC), p38 MAPK, and janus kinase 3 (JAK3). Eryptosis inhibitors include AMP-activated kinase (AMPK), c-GMP-dependent protein kinase I (cGKI), p21-activated kinase 2 (PAK2), rapid accelerated fibrosarcoma (Raf kinase), and mitogen and stress activated kinase 1 and 2 (MSK1and MSK2) [270].

1.8 Eryptosis in malaria

1.8.1 Interplay between *Plasmodium* parasite and host cell death

Intracellular pathogens-mediated manipulation of apoptotic cell death pathway for their survival is well reported [192, 303-305]. In *P. falciparum* infection modulation of apoptotic cell death during liver stage has been well studied [306, 307]. However, during the blood stage cycle these processes have yet to be fully explored. Studies have suggested that the parasite manipulates host cell death pathway during erythrocyte infection (Figure 1.8) [270]**.**
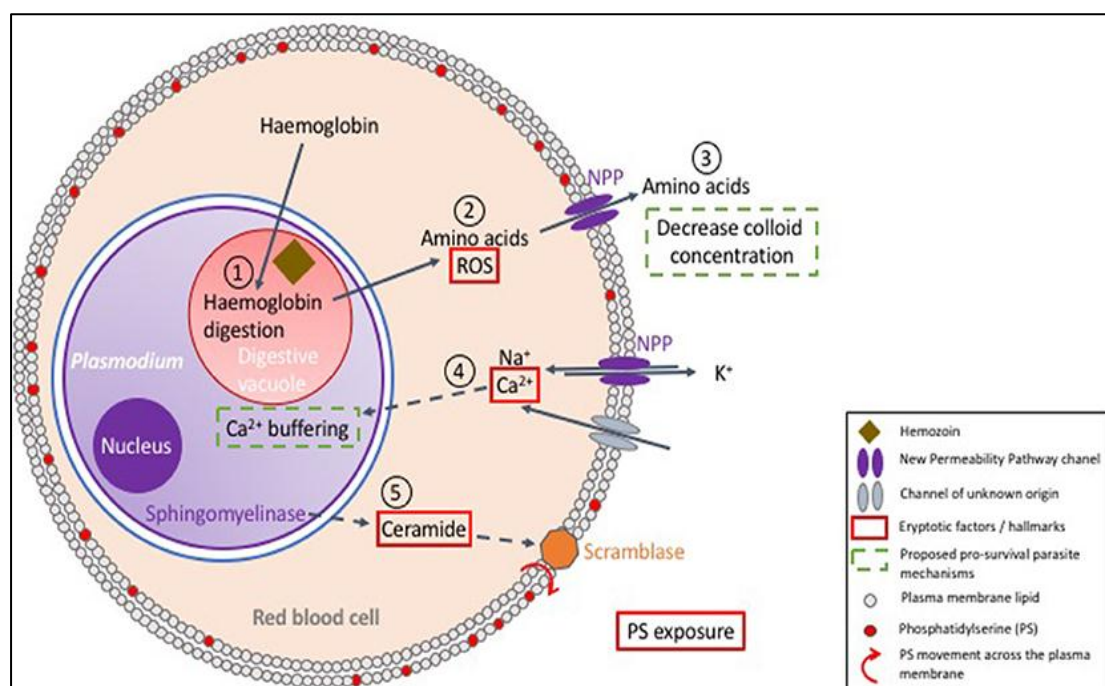
Figure 1.8 Proposed model depicting host erythrocytes and *Plasmodium* parasite interaction (Adapted from Boulet et al., 2018). Hemoglobin digestion involves a process of heme detoxification leading to formation and secretion of amino acids to the erythrocyte cytosol for host cell survival by decreasing colloid concentration (1, 2). ROS production during haemoglobin digestion triggers eryptosis (3). Ca^{2+}, key regulator of eryptosis, enters through NPPs into erythrocytes cytosol that is proposed to sequester by parasite in its own cytosol to inhibit host cell death (4). Ceramide formation by parasite leads to phosphatidylserine exposure and clearance by macrophages (5) [270].

P. falciparum activates ion channels to obtain required nutrients, and Ca^{2+} and sodium ions (Na^+) [308]. During infection, increase in intra-erythrocytic calcium content has been reported [308]. Intracellular calcium is required for parasite development and invasion and suggested to play a key role in parasite signaling pathways [309, 310].

Parasite keeps the free Ca^{2+} level low in host cell by accumulating Ca^{2+} in its own cytosol [311, 312]. Parasite, through Ca^{2+} sequestering, appears to inhibit eryptosis and thus enables erythrocytes to survive longer.

The New Permeability Pathway (NPP) transporters are exported by *Plasmodium* parasite to the erythrocyte membrane to increase the host plasma membrane permeability [308, 313]. The increase in cytosolic Na^+ levels during trophozoite development can induce cell swelling and hemolysis. To maintain the osmotic stability and prevent hemolysis, parasite digests more haemoglobin and secretes unused amino acids using NPP transporter [308, 314].

Studies suggest Ca^{2+} sequestering takes place in order to maintain intracellular calcium concentration and export of excess amino acids as the first sign of parasite-mediated manipulation of eryptosis [270, 308, 311, 312].

Intra-erythrocytic development of *P. falciparum* requires human kinases including p21 activated kinase (PAK) [315]. It has been reported that PAK kinases can act as eryptotic inhibitors in energy depleted conditions [316]. In addition, pathogen-mediated subversion of PAK kinase has been shown for manipulation of apoptosis along with other cellular functions [317]. However, no direct evidence is available that associates PAK activation with eryptosis manipulation [270].

1.8.2 Role of eryptosis in *Plasmodium* infection

The role of eryptosis in *P. falciparum* infection is controversial and debated. Phosphatidylserine exposure favors the host by clearing infected erythrocytes [318, 319]. However, its role has also been suggested in immune evasion of parasite and malaria pathogenesis [320, 321]. Along with inducing exposure of phosphatidylserine, during intracellular development, the parasite accelerates normal erythrocytes senescence and ages the host erythrocyte, leading to infected cell clearance [319, 322]. This contributes in giving partial resistance against malaria in pathological conditions of glucose-6-phosphate dehydrogenase (G6PD)-deficiency, sickle-cell trait, beta-thalassemia-trait, and homozygous hemoglobin-C, by enhancing ring-stage-infected erythrocyte clearance [272, 282, 318, 323, 324]. In malaria infection, preferential parasite invasion of non-eryptotic erythrocytes and increased eryptosis of uninfected erythrocytes has been shown to represent a host defense mechanism

against malaria [270, 325, 326]. These studies suggest induction of eryptosis can reduce malaria parasite burden.

1.8.3 Eryptosis for malaria therapeutic interventions

Inducing eryptosis has also been suggested as a novel anti-malarial strategy to fight against malaria. Many eryptotic inducers affect parasite viability, in which those compounds that do not modulate eryptosis of uninfected erythrocytes can be used for anti-malarial treatment [270]. In addition, it has been shown that some effective antimalarial medicines like mefloquine, quinine, and artesunate induce eryptosis, thus suggesting that eryptosis induction might have a role in their antimalarial effect [327-329]. Studies have shown that parasite interferes with erythrocyte death and appears to inhibit eryptosis [308, 311, 312]. Thus, a novel approach for antimalarial treatment could be preventing *Plasmodium* induced eryptosis inhibition [270].

1.8.4 Energy depletion and eryptosis

Energy depletion is a known trigger of eryptosis [278]. Erythrocytes lack mitochondria and, devoid of *de novo* protein synthesis capacity, depend on glycolysis for ATP production and maintain the existing pool of proteins. Severe phosphate depletion that induces eryptosis may be due to impaired ATP production [330, 331]. It has been suggested that ATP depletion elicits eryptosis [332]. Nicotinamide adenine dinucleotide (NAD^+), a vital cofactor, plays a key role in various energy metabolism pathways including glycolysis [333, 334]. Pathogens modulate intracellular NAD^+ content to manipulate host cell death for successful infection, where NAD^+ depletion induces cell death [335]. *P. falciparum* is also known to modulate intraerythrocytic NAD^+ content during infection. Studies have reported increased NAD^+ content in *P. falciparum* infected erythrocytes compared to uninfected cells [336]. However, role of increased NAD^+ levels in parasite infection is not known. In addition, role of NAD^+ in erythrocyte cell death is also unexplored.

The specific molecular mechanism of eryptosis is not fully elucidated and little is known about host-parasite interaction in this context. Thus, research in this area is needed to understand these processes and use the knowledge gained for therapeutic interventions. Targeting pathogen-mediated manipulation of host cell pathway has been identified as a novel host-directed approach to fight against pathogenic infections. Host-directed therapy could be an effective approach to combat the emerging resistance against antimalarial medicines.

1.9 Role of NAD$^+$ in host-pathogen interaction

1.9.1 NAD$^+$ overview

Nicotinamide adenine dinucleotide (NAD) was identified as a cofactor in fermentation by Sir Arthur Harden more than 100 years ago [337, 338]. Importance of NAD in redox reactions was first showed by Warburg in 1936, who also described the nomenclature, where uncharged chemical backbone refers to 'NAD'. The oxidized and reduced forms are called 'NAD$^+$' and 'NADH' respectively (Figure 1.9) [338]. Significance of NAD$^+$ in health was established in 1937 by discovery that NAD$^+$ precursor (nicotinic acid) was the factor responsible to cure pellagra [339]. NAD$^+$ plays an important role in energy metabolism, signal transduction, and many cellular functions [333]. NAD$^+$ is involved in major energy production pathways where it functions as a coenzyme in redox reactions [334]. NAD$^+$ also acts as a co-substrate for various NAD$^+$-consuming enzymes like PARPs (poly ADP-ribose polymerases), sirtuins, and CD38 [339, 340]. NAD$^+$ deficiency contributes to many disorders including ageing and neurodegeneration, cancers, metabolic disorders and infections [340]. Inadequate NAD$^+$ homeostasis due to changes in the activity of NAD$^+$-dependent enzymes and NAD$^+$ abundance leads to these metabolic diseases. These NAD$^+$-dependent processes are tightly regulated to conserve cellular NAD$^+$ content [339, 341].
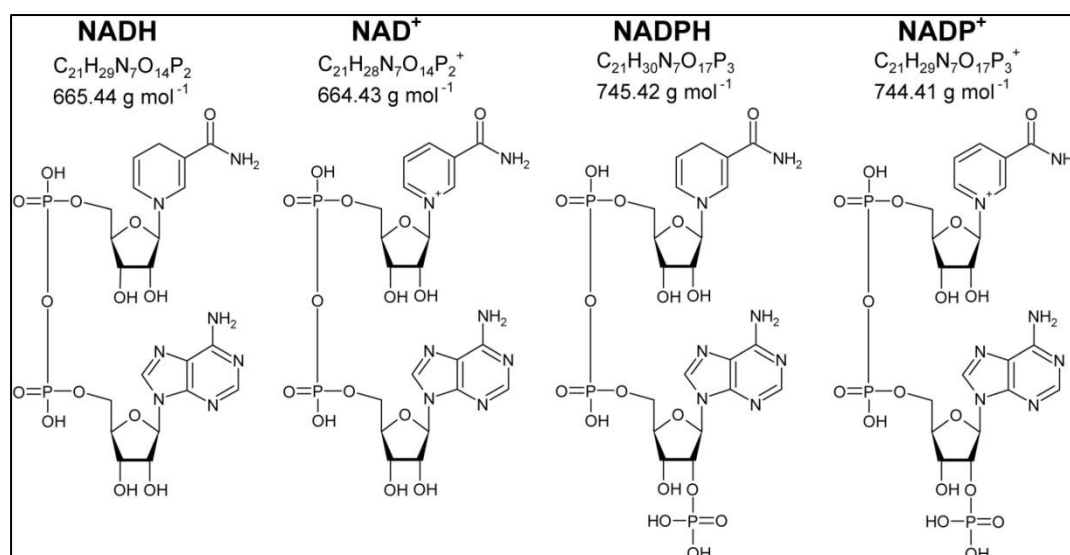
Figure 1.9 Nicotinamide adenine dinucleotide (NAD) cofactors (Adapted from Wang et al., 2017). Molecular structure of oxidised (NAD$^+$) and reduced (NADH) forms of NAD. NADPH refers to phosphorylated form of NADH which is oxidised to NADP$^+$ [342].

1.9.2 Modulation of host NAD$^+$ levels in intracellular pathogen infections

Intracellular NAD$^+$ levels are determined by its biosynthesis (Salvage and/or *de novo* pathway) or degradation (as co-substrate and coenzyme). The role of NAD$^+$ has been identified in the regulation of immune responses and functions during infection. In host-pathogen interactions, the important role of NAD$^+$ metabolism has also been indicated [343, 344]. Intracellular pathogen-mediated modulation of host NAD$^+$ levels has been reported in several diseases [343]. Pathogens utilise NAD$^+$-consuming enzymes to deplete host intracellular NAD$^+$ levels. These secreted enzymes are reported in *Streptococcus pyogenes* and recently in *M. tuberculosis* [230, 345]. Hydrolysis reaction of β-NAD$^+$-degrading enzymes results in two reaction products: 1) nicotinamide, 2) ADP-ribose (strict β-NAD$^+$ glycohydrolases) or cyclic ADP-ribose (ADP-ribosyl cyclases) based on the underlying hydrolysis mechanism involved. ADP-ribose can be transferred to its specific substrate by ADP-glycosyltransferase enzyme (Figure 1.10) [230, 346].
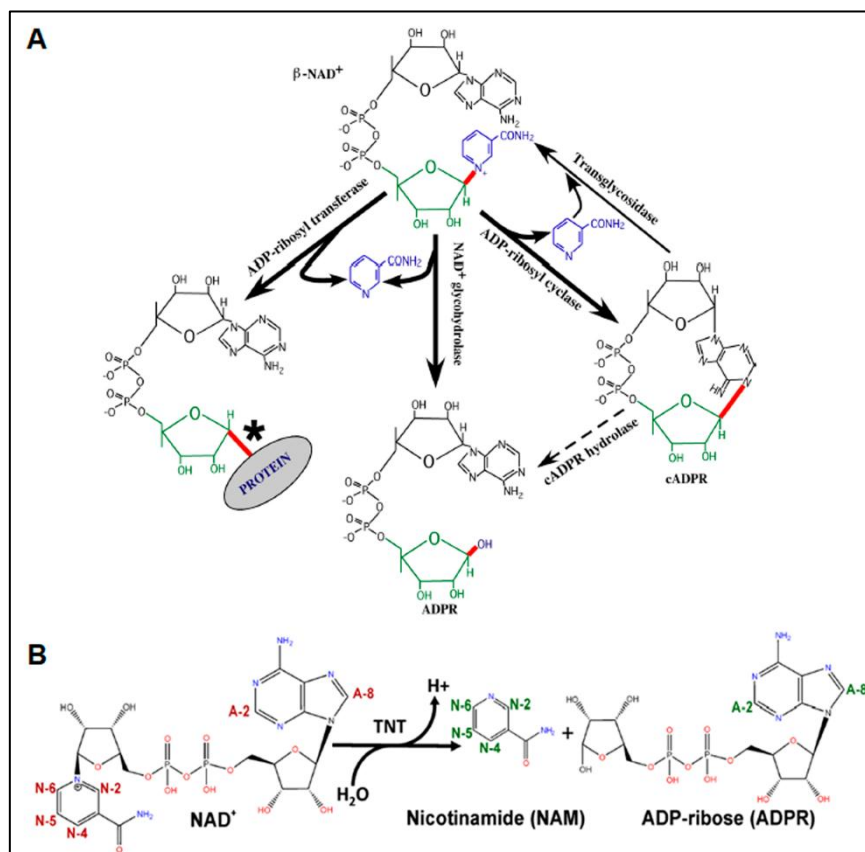
Figure 1.10: Hydrolysis of β-NAD$^+$. (A) Different classes of β-NAD$^+$ degrading enzymes that include strict β-NAD$^+$ glycohydrolase, ADP-ribosyl cyclases, ADP-glycosyltransferase (Adapted from Ghosh et al., 2010) These are classified based on additional bonds (red line) formation they can catalyse. Other reactions catalysed by ADP-ribosyl cyclases indicated by thin lines [346]. (B) Hydrolysis of β-NAD$^+$ by TNT (Adapted from Tak et al., 2019). ^{1}HNMR study to follow resonance of NAD$^+$ protons and the resonance increase of ADP-ribose and nicotinamide protons is shown [231].

The NAD$^+$ glycohydrolase of *Streptococcus pyogenes* produces ADP-ribose that is converted into cyclic ADP-ribose inside the host cell [343, 345, 347]. This results in intracellular NAD$^+$ depletion of the infected host cell leading to, growth arrest and host cell death [335, 343]. Secreted NAD$^+$ glycohydrolase (TNT) of *M. tuberculosis* hydrolyses NAD$^+$ into ADP-ribose and nicotinamide [230]. TNT-induced NAD$^+$ depletion triggers necroptosis via MLKL and RIPK3 dependent pathway [192]. Depletion of intracellular NAD$^+$ levels has also been observed during HIV infection in peripheral blood lymphocytes of patients [348]. On the other hand, *Plasmodium*-infected erythrocytes show increased NAD$^+$ levels compared to uninfected erythrocytes [336]. Modulation of intracellular NAD$^+$ levels appears to be involved in infection progression and establishment. Targeting these could lead to future therapies that might limit infection of intracellular pathogens.

Chapter 2

Introduction

2 INTRODUCTION

2.1 Background

Infectious diseases can be categorized on the basis of how pathogens proliferate inside the host environment. In this context, extracellular pathogens are those that do not invade cells and grow and survive in the extracellular environment of tissues enriched with body fluid or sometimes only adheres to host cells. On the other hand, intracellular pathogens are adapted to complete part of their lifecycle inside host cells. Intracellular pathogens can reproduce and survive inside cells of the host defense system especially mononuclear phagocytes (macrophages and dendritic cells) [349, 350]. These microorganisms alternatively reside and multiply inside the endosomal compartment or the cytosol of various host cells like neutrophils, epithelial cells, or sometimes fibroblasts and erythrocytes [349, 351]. These extraordinary habitats aid intracellular pathogens to gain access to restricted nutrient sources and protect them from competition with other infectious microbes and action of antibiotics along with defense mechanism of host [349]. To spread infection, pathogens disseminate to infect new host cell to initiate a new cycle of infection. Pathogen dissemination plays a crucial role in pathogenesis and establishment of infection. Intracellular pathogens modulate host cell processes to facilitate progression of infection and spread. To evade host immune system pathogens have evolved various survival strategies including manipulation of host cell death pathways [352]. Targeting host cell processes that are involved in the pathogenesis and spread of infection pave the way for development of novel therapeutics. Manipulation of host NAD^+ metabolism has been observed in various diseases; however its significance in the pathogenesis of microbial infections still remains underexplored [343].

NAD^+ metabolism has gained enormous attention for its role in development of various diseases that are associated with imbalance in NAD^+ homeostasis [334]. NAD^+ is an important metabolite that acts as a redox factor or coenzyme and plays a crucial role in regulation of numerous cellular physiological and metabolic pathways [339, 353, 354]. More specifically NAD^+-dependent processes are mediated by "NAD^+–dependent" enzymes that utilized NAD^+ as a substrate. These processes need to be tightly regulated to maintain cellular NAD^+ homeostasis. Change in NAD^+ levels or alteration in NAD^+ homeostasis has been found to be associated with a

number of different diseases [334, 355, 356]. Studies have suggested significance of NAD^+ metabolism in infectious diseases and modulation of infected host NAD^+ levels during pathogen infections [343]. Pathogen secretes NAD^+ utilizing enzymes as virulence factors to modulate host NAD^+ homeostasis such as NADase in *Streptococcus pyogenes* [357, 358] and more recently have also been identified in *M. tuberculosis* [192, 229, 230]. Increase in NAD^+ levels of *P. falciparum*-infected erythrocytes has also been reported [336]. However, significance of pathogen mediated modulation of host NAD^+ homeostasis in the pathogenesis of tuberculosis and malaria and its targeting for development of novel therapeutics still remains unexplored.

Despite the advancement of modern medicine or discovery of novel effective antibiotics, intracellular infections continue to pose a serious global health threat. Intracellular microbe *M. tuberculosis* utilizes diverse strategies to disrupt macrophage activation and microbicidal effector responses [167]. *M. tuberculosis* is the main causative agent of highly infectious airborne disease Tuberculosis that primarily affects lungs and can invade all organs. With an estimated 0.44 million deaths in 2019, tuberculosis is the leading cause of death globally from an infectious disease [3]. Tuberculosis was declared as a global public health emergency in 1993 [359] and strategies were developed to cure tuberculosis with other disease controlling programs, such as DOTS, including in 1998 a DOTS-plus program to combat MDR tuberculosis [360, 361]. WHO set a goal to end tuberculosis epidemic by 2030, and 95% reduction in tuberculosis deaths and 90% decline in the tuberculosis incidence by 2035 [1, 2]. In the years during 2000-2018, incidence of tuberculosis has continuously declined at the rate of 1.6 percent per year with 2% decline in 2017 to 2018, showing substantial progress in controlling the disease [3]. However, emerging cases of HIV-tuberculosis co-infection, latent survival and drug resistance still represent a challenge for treatment and cure of tuberculosis. Most of the cases of tuberculosis (approximately 95%) are present in developing countries that are associated with risk factors namely poverty, malnutrition, and immunosuppression [3]. Increased incidence of drug resistance tuberculosis mainly develops in individuals from high burden countries that have been previously treated with first line drugs, history of exposure to drug resistant patients, inadequate treatment, poor adherence to the treatment regimen, and pre-existing resistance [56]. To decrease the incidence of and

finally eradicate tuberculosis, research efforts are required for discovery of new antimicrobial drugs and better conceptual understanding of disease.

M. tuberculosis can survive and proliferate within alveolar macrophages and dendritic cells, protecting itself from primary innate immune response along with delaying the adaptive immune response by several strategies, for example, releasing virulence factors of ESX-1 type VII secretion system to prevent phagolysosomal fusion and induce host cell death [147, 362, 363]. *M. tuberculosis* is also capable of infecting monocytes, dendritic cells and alveolar epithelial cells [118, 364, 365]. *M. tuberculosis* interacts with phagocytic cells primarily through surface receptors TLR2, TLR4 with other PRRs co-receptors dectin-1, DC-SIGN, mannose receptor and cytoplasmic receptors TLR9 including NOD-2 [366]. These interactions lead to a pro-inflammatory response to clear infection, with induction of IL-10, IL-4 and further expression of TNF-α, and IFN-γ [367]. Host defense mechanism fights against infection by several mechanisms [120] such as accelerated phagolysosome maturation, ROS production [368], autophagy induction [369] and host apoptosis induction [166]. Host immune response also involves secretion of several cytokines and interferon to clear infection such as IL-12, IL-17, IL-23 [370, 371]. However, *M. tuberculosis* evades these host responses and manipulates host cells according to its own benefit. Host defense mechanisms form granuloma to constrain the infection, that initiates with clustering of infected macrophages, followed by arrival of monocytes and T cells to the site of infection [372, 373]. Although granuloma formation can control the infection but changes in granulomas, like central necrosis, formation of cavity, development of caseum supports bacterial spread and growth [372-374]. Initiation of single macrophage death may result in serial killing of remaining macrophages and lead to severe infection [375].

M. tuberculosis infection induces different forms of cell death during disease progression, mainly classified into necrosis and apoptosis [204]. Classical necrosis is characterized by cell swelling, burst and release of cellular content into surrounding tissue, thus eliciting an acute inflammatory response. If necrosis is regulated then it further classified as necroptosis, also known as programed necrosis [376, 377]. Programmed cell death or apoptosis cell death progresses with cell shrinkage, DNA fragmentation, cytoskeleton collapse, disassemble of nuclear envelope and finally

release of apoptotic bodies containing cellular debris [378]. Host cell apoptosis has been reported to serve as direct innate immune response that has bactericidal effect and further initiates T lymphocytes-mediated adaptive immunity to protect against *M. tuberculosis* infection [166, 379]. *M. tuberculosis* is known to manipulate apoptosis pathway and promote necrosis to avoid apoptosis [166, 380]. To inhibit apoptosis, *M. tuberculosis* uses several mechanisms such as over expression of anti-apoptotic proteins Bfl-1 [381] or Mcl-1 of Bcl-2 family [382], inhibition of TNF signaling [383], reduction of Fas expression to prevent T-cell-mediated killing [384], and suppression of FasL mediated signaling [385]. Signal specific necrosis of cells is categorized as programmed necrosis or necroptosis [377]. The mechanism involves initiation through receptors, TLR families and tumor necrosis factor receptor (TNFR), or other mediators like interferon, intracellular RNA and DNA sensors, and further activation of RIPK1 protein kinase and RIPK3 mediated death signals that result in phosphorylation of MLKL and induction of cell necroptosis [216]. Induction of necroptosis or apoptosis is largely dependent on soluble TNF-α level during *M. tuberculosis* infection where higher level elicits necroptosis. On the other hand, a lower level promotes activation of apoptosis [207]. Several studies report *M. tuberculosis*-mediated induction of host cell necrosis. They suggest importance of ESX-1 system protein EsxA in pore formation through the phagosomal membrane and simultaneous induction of host cell necrosis that subsequently aids *M. tuberculosis* escape [386]. Another report suggests *M. tuberculosis*-induced inhibition of Caspase-8 activation that leads to autophosphorylation of RIPK1 and RIPK3 and further RIPK3 mediated induction of necroptosis through MLKL pathway [387, 388]. Virulent *M. tuberculosis* leads to up-regulation of the LXA4 production that results in inhibition of COX2 expression and decreased PGE2 levels. Higher PGE2 levels serve as a central inhibitor of host necroptosis [212].

Although, there are several reports on inhibition of apoptosis and activation of necrosis by *M. tuberculosis*, the exact molecular mechanism behind necroptosis is still not clear. It is well known that since the discovery of the role of diphtheria toxin in pathogenesis of disease, more than 300 bacterial toxins are utilized by pathogens to modify host cell processes to damage host cell, with some classified even as classical virulent factors [226]. However, in the case of *M. tuberculosis*, there was no known secreted toxin reported [90, 227] till a study suggested that the C-terminal domain of

CpnT protein secrets as toxin into host cytoplasm that induces host cell necroptosis [192, 229, 230]. This secreted toxin TNT has NAD^+-glycohydrolase activity and activates host necroptosis through NAD^+ depletion [230]. A previous report has also identified uncharacterized NAD^+-glycohydrolase activity in *M. tuberculosis* lysate [389]. Kinetic studies determined Km (614 ± 43 μM) of TNT is in the range of human cells' physiological NAD^+ concentration (~500–600 μM), where one TNT molecule converts 16 NAD^+ molecules into nicotinamide and ADP-ribose [231, 390]. Along with this, TNT exhibited maximum activity at 6.5 pH and has minimal activity at pH 5.5. This indicated that inside phagolysosomes (pH 5.2) TNT is not active, hence it can not induce toxicity [230, 391]. NAD^+ binding domain of TNT predicted through mutational analysis showed differences in binding site from already known NADases [230, 231]. The NAD^+-glycohydrolase activity of TNT is itself toxic for *M. tuberculosis*. Inside *M. tuberculosis* an antitoxin for TNT i.e. IFT forms a complex with TNT to neutralize its NAD^+-glycohydrolase activity [230]. TNT mediated NAD^+ depletion was found to be sufficient to activate necroptosis via RIPK3 and MLKL dependent pathways. However, this process does not depend on TNF-α or RIPK1 [192]. TNT activity also induces mitochondrial damage, represented by mitochondrial membrane potential loss, ATP depletion, and cytochrome c release. RIPK3 and MLKL inhibition protects cells from TNT mediated necroptosis [192]. *M. tuberculosis* modulates timing of macrophage cell death using TNT induced necroptosis and is suggested to facilitate bacterial dissemination. Additionally, TNT activates ROS production in infected cells and promotes *M. tuberculosis* replication through necroptosis dependent and necroptosis independent pathways [232]. Studies have established the role of TNT in macrophage cell death and suggested its significance in pathogenesis of *M. tuberculosis* especially in bacterial replication and dissemination that suggests TNT NAD^+-glycohydrolase activity can serve as a potential drug target. Studies are required to establish the role of TNT in *M. tuberculosis* pathogenesis and further its targeting to control infection through novel therapeutics.

Another example of obligate intracellular pathogens is represented by Apicomplexans parasites that also utilize several strategies for manipulation of host cells [392]. *Plasmodium falciparum* is a most extensively studied apicomplexan parasite known for remodeling of host erythrocytes [393]. *Plasmodium falciparum* is the main

causative agent of vector-borne and infectious life-threatening disease malaria that presents a serious global health threat with an estimated 0.4 million deaths and 228 million cases globally in 2018 [236]. At a global level, most of the cases of malaria are present in the African Region (93%) and South-East Asia Region (3.4%), where sub-Saharan Africa countries and India account for 85% of global burden [236]. The WHO Global Technical Strategy for Malaria 2016-2030 was adopted in 2015 with an aim to reduce mortality and incidence rate by 90% till 2030 [394]. For anti-malarial therapy, two most effective and crucial medicines are obtained from plants: artemisinin (Qunghao, Artemisia annua) and quinine (Cinchona) [237, 244]. Due to emerging resistance against first-line anti-malarial drugs, WHO has recommended ACT for treatment of malaria [236]. However, an encouraging decrease in the number of deaths has been observed since 2010, but current treatment strategies are not sufficient to accomplish the goal of malaria elimination [236]. Development of new promising anti-malarial drugs is urgently needed, one that should have benefits of being inexpensive, well tolerated, and able to overcome the problem of drug resistance.

Malaria parasite infects two hosts, the female *Anopheles* mosquito (vector) and the human, to complete its life cycle. In the human host, infection starts with the release of sporozoite into human bloodstream through the bite of the mosquito (liver stage cycle). Sporozoite invade liver hepatocytes cells where they replicate into merozoites and the consequent rupture of hepatocytes releases merozoites into the blood stream where they infect host erythrocytes (blood stage cycle). Merozoites complete their multiplication cycle within 48 hours through ring, trophozoite and schizont stages to form daughter merozoites. Daughter merozoites release into the blood stream through the rupturing of erythrocytes, a process known as egress, and infect healthy erythrocytes to start a new cycle of infection. Some of the infected erythrocytes enter into a sexual cycle and develop into gametocytes that further infect female *anopheles* mosquito when it bites an infected human host. Development of merozoite, rupture of infected erythrocytes and re-infection into healthy erythrocytes is a critical process for progression of infection [237]. Malaria parasite resides inside host cells hepatocytes and erythrocytes during infection to replicate and evade host cell response. Preerythrocytic-stage parasites activate secretion of IFN-γ and type I IFNs by CD8^{+} T, γδT, NK, and NKT cells to eliminate intrahepatic parasites. During blood stage,

role of CD4^{+} T helper cells are more important than CD8^{+} T cells as they activates macrophages. Natural killer cells produce IFN-γ, granzyme and perforin to kill infected erythrocytes [395].

During intra-erythrocytic infection cycle, the malaria parasite modulates various host processes to facilitate propagation of infection. To complete its replication cycle malaria parasite needs to inhibit host cell death. In the liver stage cycle, interference with apoptosis of hepatocytes is well studied [306, 307]. However, in the blood stage cycle these processes remain unexplored. Similar to apoptosis, erythrocytes undergo suicidal programmed cell death or eryptosis, characterized by erythrocyte surface exposure of phosphatidylserine, decrease in forward scatter representing erythrocyte shrinkage, and increase in intracellular calcium concentration [276, 277, 396]. Eryptosis has been reported to be triggered by various factors related to cell stress, like oxidative stress, energy depletion, osmotic shock, and xenobiotics [277, 397]. The role of eryptosis in the pathogenesis of malaria is not fully elucidated that eryptosis is beneficial for progression of malaria infection or favors host cell against infection, is also a point of debate. It has been suggested that *P. falciparum* modulates eryptosis to establish and progress infection [270]. Studies have indicated that *P. falciparum* might delay eryptosis by calcium sequestering. The parasite secretes unused amino acids and maintains intra-erythocytic calcium levels during invasion that have been suggested as first sign of parasite mediated manipulation of the host cell death [311, 312]. Parasite mediated modulation of host cell kinases has also been found to be involved in inhibiting eryptosis [398]. Some studies have suggested that eryptotic erythrocytes do not support parasite infection [282, 325]. Similarly, various diseases associated with increased eryptosis such as sickle cell anaemia, and glucose-6-phosphate dehydrogenase deficiency have shown protection against malaria infection [270, 323, 324]. These observations are linked to studies proposing phosphatidylserine exposure leading to parasite clearance at an early stage of infection [282]. Eryptosis-inducing molecules showed antimalarial potential by accelerating clearance of *P. falciparum* infected erythrocytes. Targeting erythrocyte cell death or eryptosis has therapeutic potential for malaria treatment [399].

Like other intracellular pathogens, *P. falciparum* also modulates intra-erythrocytic NAD^{+} levels. *P. falciparum* infected erythrocytes showed increased NAD^{+} levels

compared to uninfected erythrocytes [336]. Previous studies suggested increased NAD^+ levels favors parasite infection [400]. However, its role in pathogenesis of malaria infection is still not clear. Previous studies reported, in brainstems of patient with fatal *Plasmodium falciparum* malaria PARP-1 activation, apoptosis, DNA damage and reversible cellular injury [401]. PARP-1 activation is linked to NAD^+ depletion and further induction of host cell death [402]. It might be possible that NAD^+ depletion elicit eryptosis of erythrocytes as it induces necrosis in other cells [192, 357, 402]. However, studies have not been conducted to determine the role of host NAD^+ modulation in eryptosis. In addition, the precise role of eryptosis and intra-erythrocytic NAD^+ levels in malaria pathogenesis still remains unclear. Furthermore, role of intra-erythrocytic NAD^+ levels in malaria pathogenesis also needs to be established.

Previous studies have indicated importance of host NAD^+ levels and subsequent involvement of host cell death in the pathogenesis of tuberculosis and malaria. Discovering their role in pathogenesis and targeting these pathways and host cell processes that aid intracellular pathogen survival could help in development of novel therapeutics.

2.2 Aims and Objectives

The present study aims to establish the significance of host NAD^+ metabolism in the regulation of infection, propagation, and dissemination of *M. tuberculosis* and *P. falciparum*. *M. tuberculosis*-mediated TNT induced NAD^+ depletion leads to necroptosis of infected macrophage and facilitates mycobacterium survival [192, 230]. Targeting TNT through its natural inhibitor IFT or with designed small molecules can control the infection. In the first part of study, effect of TNT expression and its reversion by IFT in bacterial system would be determined. Further characterization of NAD^+-glycohydrolase activity of purified recombinant TNT (rTNT) and its inhibition through recombinant IFT (rIFT) would be performed. Next, we would investigate whether targeting TNT through IFT can rescue macrophage from TNT-mediated cell death and consequently examine the effect of IFT expression on intracellular mycobacterium growth. To find potent inhibitors against TNT, designed NAD^+ analogues and other selected compounds or drugs would be screened against NAD^+-glycohydrolase activity of rTNT. In the next part of study, the role of

host NAD$^+$ metabolism in the pathogenesis of *P. falciparum* would be studied using rTNT to modulate intra-erythrocytic NAD$^+$ levels. To achieve this, effect of NAD$^+$ depletion on erythrocytic survival and *P. falciparum* growth would be determined. Finally, selected small molecules would be used to target NAD$^+$ homeostasis of infected host cells and screen for their therapeutic potential for blocking infection of *M. tuberculosis* and *P. falciparum*.

The following experimental steps have been performed in this study:

1. Study the effect of TNT expression or IFT-TNT co-expression on bacterial growth and propagation.

2. Expression and purification of recombinant proteins IFT (rIFT), TNT (rTNT), or IFT with TNT (IFT-TNT) complex.

3. Determination of NAD$^+$-glycohydrolase activity of rTNT.

4. Evaluation of inhibitors against NAD$^+$-glycohydrolase activity of rTNT.

5. Performing *in vitro* interaction studies of proteins rTNT with rIFT.

6. Study the effect of TNT-mediated NAD$^+$ depletion on macrophage survival and its targeting through IFT.

7. Targeting TNT through IFT to determine the role of NAD$^+$ modulation and its therapeutic potential in inhibiting *M. tuberculosis* infection and growth.

8. Study the effect of NAD$^+$ modulation on erythrocyte survival and *P. falciparum* infection and growth using rTNT as an endogenous tool.

9. Study the effect of most potent inhibitors of rTNT on *M. tuberculosis* growth and survival.

10. Study the effect of selected NAD$^+$ analogues on *P. falciparum* infection and growth.

Chapter 3
Materials and Methods

3 MATERIALS AND METHODS

3.1 Materials

3.1.1 General materials

In Table 3.1, list of experimental materials and their sources is given. Throughout the section, wherever required details of purchase source of other fine chemicals, enzymes, kits are mentioned.

Material	Source
Fine chemicals	Purchased sources include Sigma, USA; Amresco, USA; Qiagen, Germany; BD Biosciences, USA; GE Heathcare, USA; Cayman Chemical, USA; GenScript, USA
Enzymes	Thermo Scientific, USA; Invitrogen, USA; NEB, USA
Bacteriomatch™ Two-Hybrid System Reporter Kit (the plasmids, and cloning and reporter strains)	Stratagene, USA
Human lung cDNA library (pTRG vector)	Stratagene, USA
Plasmid mini prep, midi prep, gel elution kit	Qiagen, Germany
FITC Annexin-V Apoptosis detection kit with PI	Biolegend, USA
EnzyFluo NAD/NADH Assay Kit	Bioassay Systems, USA

Table 3.1 List of experimental materials and their purchase sources.

3.1.2 Bacterial strains

In the present study, following bacterial strains were used as presented in Table 3.2.

Bacterial strains	Source
E. coli DH5α	Invitrogen Life Technologies, USA. Used in routine cloning experiments.
E. coli XL1-Blue (Bacterial two-hybrid cloning strain)	Stratagene, USA. MRF':Kan^r, Contains *lacI^q* gene Used to propagate pBT, pTRG, and recombinant bacterial-two hybrid plasmids.
E. coli R1 (Bacterial two-hybrid reporter strain)	Stratagene, USA. In the experiments of bacterial two-hybrid assay used as reporter stain for co-transformations.
E. coli BL21 (DE3)	Novagen, Germany. Used for protein expression in bacterial cells.
E. coli C43 (DE3)	Sigma Aldrich, USA. Used for toxic protein expression in bacterial cells.

Table 3.2 List of bacterial strains and their sources used in present study.

3.1.3 *Plasmodium* strain

P. falciparum 3D7 strain, obtained from Malaria Research and Reference Reagent Resource Center (MR4) [403], was used in the present study. It is a chloroquine sensitive strain.

3.1.4 *M. tuberculosis* strain

M. tuberculosis H37Rv [35] or *M. tuberculosis* H37Rv-GFP [404] was used in the present study.

3.1.5 Primers

The primer pairs and their sequences used in this study given in the Table 3.3. These primers pairs were procured from Eurofins, USA.

Primers	Sequence
pBT For	5'-TGAGAGTTGTTCCGTTGTGGGGAA-3'
pBT Rev	5'-CCACAGGGTAGCCAGCAGCATCCT-3'
pTRG For	5'-CAACTGGAAGCTTTCGTTGACTTACGT-3'
pTRG Rev	5'-TAGAGGATCTCACTAGTTCATTAATTAATTA-3'
pBAD For	5'-TCCATAAGATTAGCGGATCCTACCTGACGC-3'
pET28a Rev	5'-AGCAGCCAACTCAGCTTCCTTTCGGGCTTT-3'
pFLAG For	5'-AGGCGTGTACGGTGGGAGGTCTAT-3'
EGFPC1 For	5'-ACGAGCTGTACAAGTCCGGA-3'
Hairpins (HP)	5'-TTTAAACACGTGGCGGCCGCTCTAGAGGCCCGCGC GGGCCTCTAGAGCGGCCGCCACGTGTTTAAA-3'
HP2P	5'-AGCGGCCGCCACGTGTTTAAA-3' (5'-phosphorylated)
HP2	5'-AGCGGCCGCCACGTGTTTAAA-3'
IFT-For	5'-CAGAATTCTACGTAATGACCATCGGCGTGGACCT-3'
IFT-Rev	5'-CCGAATTCTACGTAGCCCTTGTAATCCTTCCACAGG-3'
TNT-For	5'-CCGAATTCTACGTAGGTTGGCACCGTCTGAGCGA-3'
TNT-Rev	5'-GAGAATTCTACGTACTGACGCAGCACGCCGCGAC-3'
TNT-For (cloning in EGFPC1)	5'-CCGAATTCTACGTACGGTTGGCACCGTCTGAGCGA-3'

Table 3.3 List of primers used in present study.

3.1.6 Expression plasmids

The expression plasmids used in this study given in the Table 3.4.

Plasmids	Source and properties
Bait Plasmid (pBT)	Stratagene, USA Size 3.2 kb, chlamp^r, low-copy *p15A* origin of replication, encodes for the full-length bacterial lambda repressor protein (λcI, 237 amino acids).
Target Plasmid (pTRG)	Stratagene, USA Size 4.4 kb, tet^r, low-copy (10-15 copies) *ColE1* origin of replication, directs transcription of the N-terminal domain of the α-subunit of RNA polymerase (RNAP-alpha, 248 amino acids) through a multiple cloning site (MCS) at the 3'-end of the α-subunit gene.
pMTSA	Modification of the commercially available pGEX4T3 (Amersham, USA) plasmid. Size 4.6 kb, Strep^r, arabinose-inducible expression vector.
*Bla*1 cut pET28	Modification of the commercially available pET28a (Invitrogen, USA) plasmid. Size 5.2 kb, kan^r, IPTG-inducible expression vector.
pFLAGCMV4$_{nn}$	Modification of commercial vector pFLAGCMV4 (Sigma Aldrich, USA). Size 6.2 kb, amp^r, mammalian expression vector.

Table 3.4 List of expression plasmids, their sources and properties.

Figure 3.1 Original bacterial two-hybrid vectors pBT and pTRG and their derivatives pBT$_{nn}$ and pTRG$_{nn}$.
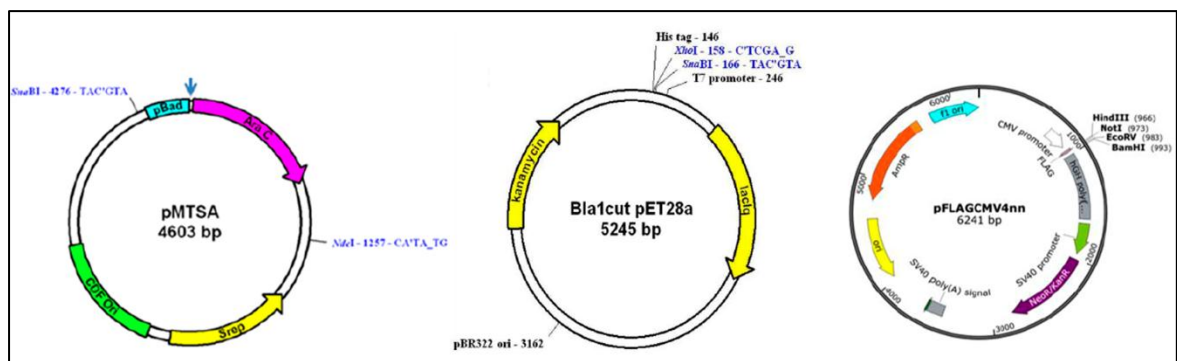
Figure 3.2 Expression vectors used in the present study.

3.1.7 Culture Media

3.1.7.1 Media compositions for *E. coli* culture: List of media composition used in present study is given in the Table 3.5.

Media	Source and composition
LB agar	HiMedia, USA
LB broth	HiMedia, USA
X-Gal indicator plates (per Litre)	Autoclaved LB agar (1 L) was cooled to 55 °C and supplemented with: Chloramphenicol 1 mL of 30 mg/mL Tetracycline 1 mL of 12.5 mg/mL Kanamycin 1 mL of 50 mg/mL X-Gal 1 mL of 80 mg/mL (Sigma) β-galactosidase inhibitor 1 mL of 200 mM (Sigma) IPTG 0.5 mL of 1 M (Sigma)
Arabinose and IPTG containing plates (per Litre)	Autoclaved LB agar (1 L) was cooled to 55 °C and supplemented with: Kanamycin 1 mL of 50 mg/mL Streptomycin 1 mL of 50 mg/mL L-Arabinose 1 mL of 20% stock IPTG 25 µM (Sigma)

Table 3.5 List of media composition for *E. coli* culture.

3.1.7.2 Media compositions for mammalian cell culture: List of media compositions used in present study is given in the Table 3.6.

Media	Source and Composition
DMEM	Gibco, Life Technologies DMEM powder packet was dissolved in 900 mL of autoclaved milli-Q and supplemented with 10 mM HEPES, 2 mM L-glutamine and finally 3.7 g sodium bicarbonate was added (final pH 7.4). Media volume was made up to 1 L and filtered.
RPMI	Gibco, Life Technologies RPMI powder packet was dissolved in 900 mL of autoclaved milli-Q and added with 2.3 g HEPES, 1.46 g L-glutamine and 2 g sodium bicarbonate was added (final pH 7.4). Media volume was made up to 1 L and filtered.

Table 3.6 Media compositions for mammalian cell culture.

3.1.7.3 Media compositions for *P. falciparum* culture

RPMI medium was prepared by dissolving RPMI powder packet in 1 litre of milli-Q. Complete RPMI media contained 5.8 ml of 3.6% sodium bicarbonate and 20 μg of gentamicin along with 10% albumax (Gibco).

3.1.7.3 Media compositions for *M. tuberculosis* culture

Media	Composition
Middlebrook 7H9 broth	4.7 g of 7H9 and Tween 80 (5 mL) was added in 900 mL of water followed by autoclaving and after temperature reach 45 °C, media was supplemented with Middlebrook ADC Enrichment (100 mL).
Middlebrook 7H11 agar	19 g of 7H11 and glycerol (5 mL) added in 900 mL of water followed by autoclaving and after temperature reach 45 °C, media was supplemented with Middlebrook OADC Enrichment (100 mL).

Table 3.7 Media compositions for *M. tuberculosis* culture.

3.1.8 Antibiotics and other stock solutions List of antibiotics and other stock solutions used in present study is given in the Table 3.8

Antibiotics and other stock solutions	Composition
Ampicillin	Stock solution: 100 mg/ml in double-distilled water, working concentration: 100 μg/ml
Kanamycin	Stock solution: 50 mg/ml in double-distilled water, working concentration: 50 μg/ml
Tetracycline	Stock solution:12.5 mg/ml in ethanol/double distilled water (50% v/v), working concentration: 12.5 μg/ml
Streptomycin	Stock solution: 50 mg/ml in double-distilled water, working concentration: 50 μg/ml
Chloramphenicol	Stock solution: 30 mg/ml in 100% ethanol, working concentration: 30 μg/ml
X-Gal	Stock solution: 80 mg/ml in N,N'-dimethyl formamide, working concentration: 80 μg/ml
X-Gal inhibitor (β-galactosidase inhibitor) solution	200 mM in N, N'-dimethyl formamide, working concentration: 200 μM
L-Arabinose	Stock solution: 20% (w/v) in double-distilled water, working concentration: 1% (w/v)
IPTG	Stock solution: 1 M in double-distilled water, working concentration: 25 μM

Table 3.8 List of antibiotics and other stock solutions used in present study.

3.1.9 Antibodies

Following antibodies were used in this study as listed in Table 3.9.

Antibodies	Source
Anti-HMGB1 pAb (rabbit)	Invitrogen (PA1-16926)
Anti-IFT pAb (mouse)	In house
Anti-TNT pAb (mouse)	In house
Alexa Fluor 594 secondary antibody	Thermo Scientific, USA
HRP-conjugated secondary antibody	Thermo Scientific, USA

Table 3.9 List of antibodies used in present study.

3.1.10 Solutions for protein gel electrophoresis and western blotting

3.1.10.1 Solutions for SDS-PAGE gels

The list of required reagents for preparation of 12% and 15% SDS-PAGE gel is given in the Table 3.10.

Component	Resolving		Stacking
	12% gel	**15% gel**	
Distilled water	3.3 mL	2.3 mL	3.1 mL
100% Glycerol	100.0 μL	100.0 μL	50.0 μL
30% Acrylamide	4.0 mL	5.0 mL	650 μL
1.5 M Tris (pH 8.8)	2.5 mL	2.5 mL	-
0.5 M Tris (pH 6.8)	-	-	1.25 mL
10% SDS	100.0 μL	100.0 μL	50.0 μL
40% APS	25.0 μL	25.0 μL	12.0 μL
TEMED	4 μL	4 μL	6 μL

Table 3.10 List of reagents required for preparation12% and 15% SDS-PAGE gel.

30% Acrylamide: Amresco, USA. 30% acrylamide was prepared by dissolving 290 g of acrylamide and 10 g of N,N'-methyl bisacrylamide (bis-acrylamide) in 600 ml of distilled water. The volume was made up and solution was stored at 4 °C in dark bottle.

SDS-PAGE running buffer (10X): 30.2 g of Trisbase, 144 g of Glycine and 10 g of SDS (all reagents from Amresco, USA) was dissolved in 900 ml of distilled water. After adjusting the final pH to 8.3, the volume was made up to 1 L. The stock solution was diluted to 1X before use.

SDS sample-loading buffer (5X): For preparation of SDS sample-loading buffer (5X), 25 ml of 0.5 M Tris, pH 6.8 stock (250 mM), 15 ml of 100% glycerol (30%), 5 g of SDS (10%), 2 ml of 0.5 M EDTA stock (20 mM), 2.5 ml of β-ME (5%), and 10 mg of bromophenol blue were added and volume made up to 50 ml. The sample-loading buffer was diluted to 1X using sample before use.

3.1.10.2 Solutions for western blotting

Phosphate buffered saline (1X) (PBS): 137 mM NaCl, 2.7 mM KCl, 10 mM NaH_2PO_4 and 2 mM K_2HPO_4.

Wash buffer (PBST): 0.05% Tween-20 in PBS.

Transfer buffer: 200 mM glycine, 24 mM Tris base, 20% methanol for 1X working solution. 10X stock buffer was prepared. Stock solution was diluted to 1X before use and 20% methanol added. Chilled buffer was used to transfer proteins on membrane.

Blocking buffer: 5% (w/v) BSA in 0.1% PBST, or 5% (w/v) skimmed milk in 0.05% PBST was used (as per requirement).

3.1.11 Solutions for ELISA

Coating buffer: 0.1 M Bicarbonate buffer, pH 9.6. Solution A: 1 M sodium carbonate stock, to prepare stock, 10.6 g of sodium carbonate was added to 100 ml of distilled water. Solution B: 1M sodium bicarbonate stock, 8.4 g of reagent added to 100 ml of distilled water. Final coating buffer contains 1.6 ml of solution A and 3.4 ml of solution B and final volume made up to 200 ml.

Binding buffer: Binding buffer contains 50 mM HEPES, 5 mM magnesium acetate, and 250 mM potassium acetate, pH 8.0.

Blocking buffer: 3% (w/v) BSA in 0.1% PBST.

Wash buffer (PBST): 0.1% Tween-20 in PBS.

3.1.12 Solutions for Far-western blotting

Denaturation and renaturation buffers:

20 mM Tris (pH 7.6), 100 mM NaCl, 0.5 mM EDTA, 10% glycerol, 0.1% Tween-20, 2% skim milk powder, 1 mM DTT and Guanidine-HCl (variable concentrations).

The composition of reagents is given in Table 3.11.

Concentration of guanidine–HCl (M)	6	3	1	0.1	0
Glycerol (ml)	2.5	2.5	2.5	2.5	2.5
5 M NaCl (ml)	0.5	0.5	0.5	0.5	0.5
1 M Tris, pH 7.5 (ml)	0.5	0.5	0.5	0.5	0.5
0.5 M EDTA (ml)	0.05	0.05	0.05	0.05	0.05
10% Tween-20 (ml)	0.25	0.25	0.25	0.25	0.25
Guanidine–HCl (8 M) (ml)	18.75	9.30	3.13	0.31	0
Milk powder (g)	0.5	0.5	0.5	0.5	0.5
1 M DTT (μl)	25	25	25	25	25
ddH$_2$O (ml)	2.45	12.82	18.07	20.89	21.20
Total volume (ml)	25	25	25	25	25
Time/temperature	30 min/room temperature (RT)	30 min/RT	30 min/RT	30 min/4 °C	1 h overnight/4 °C

Table 3.11 Composition of denaturing and renaturing buffer with varying concentrations of guanidine–HCl used [405].

Protein-binding buffer: 20 mM Tris (pH 7.6), 100 mM NaCl, 0.5 mM EDTA, 10% glycerol, 0.1% Tween-20, 2% skim milk powder and 1 mM DTT. Freshly prepared solution should be used.

3.1.13 Markers and standards

DNA size markers (1 kb DNA ladder) were used in the study, obtained from Thermo Scientific, USA. Molecular weight protein markers (Precision plus protein dual colour standard) for SDS-PAGE gels were obtained from Bio-Rad, USA. PageRuler prestained markers for SDS-PAGE gels were obtained from Fermentas, USA and Genetix Biotech Asia Pvt. Ltc, New Delhi, India. Low molecular weight protein markers for SDS-PAGE gels were procured from GeneDireX, USA.

3.1.14 Miscellaneous Solutions

TE Buffer: 10 mM Tris-HCl (pH 7.5), 1 mM EDTA.

10X TBE Buffer: 890 mM Tris, 890 mM Boric acid, 20 mM EDTA, pH 8.0.

RNAse A: Stock solution of 10 mg/ml; working concentration, 0.2 mg/ml.

3.2 Methods

3.2.1 Construction and cloning of dicodon (DC) libraries

The *de novo* protein/peptide libraries (DC libraries) were synthesized according to the protocol described previously [406, 407]. In this approach, libraries were generated using codon shuffling method where hexamer duplexes of DNA that encode amino acid pairs representing all 20 natural amino acids were assembled (Table 3.12).

Oligonucleotide	Duplex	DC	Oligonucleotide	Duplex	DC
5'-GAGCTC-3'	5'-GAGCTC-3' 3'-CTCGAG-5'	EL	5'-TGCGCA-3'	5'-TGCGCA-3' 3'-ACGCGT-5'	CA
5'-GATATC-3'	5'-GATATC-3' 3'-CTATAG-5'	DI	5'-CCCGGG-3'	5'-CCCGGG-3' 3'-GGGCCC-5'	PG
5'-AAGCTT-3'	5'-AAGCTT-3' 3'-TTCGAA-5'	KL	5'-ATGCAT-3'	5'-ATGCAT-3' 3'-TACGTA-5'	MH
5'-AACGTT-3'	5'-AACGTT-3' 3'-TTGCAA-5'	NV	5'-CAGCTG-3'	5'-CAGCTG-3' 3'-GTCGAC-5'	QL
5'-GGCGCC-3'	5'-GGCGCC-3' 3'-CCGCGG-5'	GA	5'-TACGTA-3'	5'-TACGTA-3' 3'-ATGCAT-5'	YV
5'-AGTACT-3'	5'-AGTACT-3' 3'-TCATGA-5'	ST	5'-TGGCCA-3'	5'-TGGCCA-3' 3'-ACCGGT-5'	WP
5'-TTCGAA-3'	5'-TTCGAA-3' 3'-AAGCTT-5'	FE	5'-CGTACG-3'	5'-CGTACG-3' 3'-GCATGC-5'	RT

Table 3.12 Dicodon sets used for "codon-shuffling" experiments (Adapted from Chopra et al., 2003). Amino acids have been depicted using single-letter codes [406]**.**

The fourteen dicodons in equimolar or in skewed ratios (increasing molar ratios of acidic, basic or hydrophobic dicodons) were ligated for construction of dicodon libraries. The ligated DC mixture was extracted and precipitated using phenol/chloroform/isoamyl alcohol and after resuspension annealed with *Xba*I restriction endonuclease site containing double-stranded hairpins (HP). The HP ligated DC (HPDC) library was digested with *Xba*I enzyme and subsequent PCR amplification of digested HPDC library was carried out using HP2P primer, that acts as both forward and reverse primer. The bacterial two-hybrid vectors, pBT$_{nn}$ and pTRG$_{nn}$, were digested with *Sna*BI enzyme and ligated with amplified *Xba*I-cut HPDC library. The ligation mixture was transformed into XL-1 competent cells and transformed colonies were screened by colony PCR. The transformed colonies were collected by scraping the LB-agar plates and processed to isolate DC plasmid DNA

using protocol (Plasmid Midi-prep, Qiagen, Germany) and stored at -20 °C until further use.

3.2.2 Bacterial two-hybrid studies

In order to identify the binding partner of target proteins, IFT and TNT, the bacterial two-hybrid studies were performed with target proteins and synthesized *de novo* dicodon libraries or human lung cDNA library, pTRG cloned commercially acquired library from Stratagene, USA, cloned in respective bacterial two-hybrid vectors. Equal amount of both plasmids (200-300 ng each) were co-transformed in R1 reporter cells and plated on X-Gal indicator plates. For positive control ESAT6pBT$_{nn}$ and CFP10pTRG$_{nn}$ (a well known protein-protein interaction of *M. tuberculosis*) were co-transformed. The negative control used was co-transformed R1 reporter cells with CFP10pTRG$_{nn}$ DNA and empty pBT$_{nn}$ plasmids. The indicator plates were incubated for 36 hours at 30 ºC. The blue colonies represent positive interactions of proteins. The selected blue colonies harbouring plasmids of interacting partners were verified by plasmid segregation, PCR analysis, and co-transformation in R1 competent cells. The interacting partners were identified by sequencing and BLAST analysis.

3.2.3 Bacterial growth and colony formation

The IFT (Rv3902c) and TNT (C-terminal domain of CpnT Rv3903c, 648-846 amino acids) genes were codon-optimized and synthesized commercially by Genscript (USA). The genes were obtained in pUC57 vector cloned at the unique *Sna*BI restriction site. The *Sna*BI-digested insert of TNT and IFT were cloned into the *Sna*B1-cut dephosphorylated pMTSA and pET28a vectors, respectively. The *E. coli* BL21 (DE3) cells were co-transformed with plasmids carrying IFT and TNT genes. The positive clones were selected by colony PCR, restriction digestion with *Sna*BI enzyme and finally by sequencing. The grown positive co-transformed clones were platted on LB agar plates supplemented with antibiotics streptomycin (100 μg/ml), and kanamycin (50 μg/ml) containing 0.2% arabinose or 25 μM IPTG, or both. TNT and IFT expression was induced with arabinose and IPTG, respectively. The LB agar plates were analysed for determination of the colony formation efficiency after incubation at 37 ˚C for 16 hours.

To study the effect of TNT expression on bacterial growth, the optical density of culture was assessed. For this, secondary culture of positive colonies of co-transformed *E. coli* BL21 (DE3) cells was grown till an OD_{600} of 0.2. Expression of TNT or IFT or both in individual cultures was induced by addition of 0.2% arabinose, or 1 mM IPTG, or both, respectively. Bacterial cultures were grown at 37 ˚C after induction and OD_{600} was measured at different time points.

3.2.4 Cloning, Expression and Purification of proteins

3.2.4.1 Expression and Purification of rTNT protein

The TNT gene was excised using *Sna*B1 enzyme from TNT-pUC57 construct. The eluted TNT insert was ligated into dephosphorylated *Sna*BI-cut pMTSA vector. The cloned *E. coli* C43 (DE3) cells carrying TNT-pMTSA plasmid were grown till mid-log stage in LB medium supplemented with glucose and induced with 0.2% L-arabinose for 10 hours at 25 °C. The induced cell pellet was washed with PBS buffer (4.3 mM Na_2HPO_4, 1.47 mM KH_2PO_4, 150 mM NaCl, 2.7 mM KCl, pH 7.4) and resuspended in lysis buffer for sonication. After sonication, TNT protein was found in the pellet fraction and solubilized in buffer (8M urea containing PBS buffer, pH 8.0) by continuous shaking at 25 °C for 12 hours. The obtained solubilised sample after centrifugation was filtered and allowed to bind with Ni-NTA resin at 25 °C overnight. The bound protein eluted from Ni-NTA resin using imidazole gradient (8M urea in PBS buffer with 20 mM to 500 mM imidazole, pH 8.0) and collected purified fractions were dialysed to gradually remove urea against dialysis buffer (8-0 M urea PBS buffer, pH 8.0). Dialysed protein was analysed on an SDS-PAGE. The purified TNT protein was used to raise anti-TNT antibodies.

3.2.4.2 Expression and Purification of rIFT

The eluted IFT insert digested with *Sna*B1 was cloned into dephosphorylated *Bla*1cut-pET28a vector. The secondary culture of *E. coli* BL21 (DE3) cells carrying IFT-pET28a plasmid was grown till mid-log phase in LB medium containing kanamycin (50 μgml^{-1}) and induced with 1 mM IPTG at 25 °C for 10 hours. The harvested induced cell pellet was resuspended in buffer (2 mM PMSF in PBS buffer, pH 7.4) and sonicated to obtain clear lysate. Sonicated resultant supernatant containing IFT protein was incubated with Ni-NTA resin for binding overnight at 4 °C. The bound IFT protein was eluted from Ni-NTA beads using imidazole gradient (25 mM Tris,

0.3 M NaCl, 50 - 250 mM imidazole, and pH 7.4). The purified fractions were collected and dialysed to remove imidazole. Purified rIFT protein was analysed on an SDS-PAGE and stored at -20°C. To raise anti-IFT antibodies, IFT protein was also purified in PBS buffer.

To produce antibodies against rIFT or rTNT, 50-100μg of protein mixed with Freund's complete adjuvant (Sigma-Aldrich) was used to subcutaneously immunize BALB/c mice followed by three boosters of proteins (rIFT or rTNT) mixed with Freund's incomplete adjuvant (Sigma-Aldrich).

3.2.4.3 Expression and Purification of the IFT-TNT complex

The *E. coli* C43 (DE3) cells were co-transformed with TNT-pMTSA and IFT-pET28a plasmids. The secondary culture *E. coli* C43 (DE3) cells harboring both the plasmids was grown till mid-log phage in LB medium supplemented with glucose containing antibiotics streptomycin (100 μg/ml), kanamycin (50 μg/ml) and for expression of both TNT and IFT proteins, induced with addition of 0.2% L-arabinose and 1 mM IPTG for 12 hours at 25 °C. The induced cell pellet was harvested by centrifugation and washed with Tris-NaCl buffer (20 mM Tris, 0.2 M NaCl, and pH 7.4) followed by resuspension in lysis buffer (2 mM PMSF containing Tris-NaCl buffer). After sonication, the lysate was centrifuged and IFT-TNT complex containing resultant supernatant fraction was allowed to bind with Ni-NTA resin for overnight with constant shaking at 4 °C. The IFT-TNT complex bound resin was first washed with buffer (20 mM imidazole in Tris-NaCl buffer) and then bound proteins were eluted through imidazole gradient (50 - 200 mM imidazole containing 20 mM Tris, 0.2 M NaCl, and pH 7.4). Pooled fractions of eluted proteins were collected and analysed on SDS-PAGE after dialysis against Tris-NaCl buffer to remove imidazole. Purified IFT-TNT complex was quantified by Bradford assay and stored at -20°C.

3.2.4.1 Purification of rTNT from IFT-TNT complex

The rTNT from co-purified IFT-TNT proteins was isolated by heating the IFT-TNT complex (in 20 mM Tris-HCl, 0.2 M NaCl, and pH 7.4) at 55 °C for 20 min thus releasing the free TNT in soluble fraction. The insoluble fraction contained the IFT protein. Purified rTNT protein was analysed on SDS-PAGE to determine the purity of protein.

3.2.5 *In vitro* protein-protein interaction studies

Protein-protein interaction between purified recombinant proteins IFT and TNT was analysed by ELISA and Far-western blotting.

3.2.5.1 Enzyme-linked Immunosorbent Assay (ELISA)

Protein-protein interaction analysis using ELISA was performed according to protocol described previously [408, 409]. Briefly, purified 200 ng rTNT protein was coated on a 96-well microplate (Nunc MaxiSorp ELISA plates) in 100 μl of coating buffer (100 mM sodium carbonate/bicarbonate, pH 9.6). Coated wells were washed and subsequently blocked for 1 hour with blocking buffer (3% BSA in 1xPBS, 0.1% Tween-20) at 37°C. After washing, wells were incubated with varying concentrations (50 ng, 100 ng, 200 ng, 500 ng, 1000 ng) of prey protein IFT in binding buffer (50 mM HEPES, 250 mM potassium acetate and 5 mM magnesium acetate, pH 8.0) for 1 hour at 37˚C. Following incubation, wells were washed and primary antibody (1:15000, anti-IFT antibody mouse polyclonal) was added for 1 hour at 37 °C. After washing, wells were subsequently incubated for 1 hour with secondary antibody (1:5000, anti-mouse HRP conjugated, Thermo Scientific, USA). The wells were thoroughly washed again and HRP substrate TMB was added for 30 min at 37 °C, following which, reaction was stopped using 1N H_2SO_4 solution. The absorbance reading was measured at 450 nm using an ELISA plate reader (TECAN).

3.2.5.2 Far-western blot analysis

The Far-western blotting to analyse *in vitro* protein-protein interaction was performed according to previously described protocol [409]. Briefly, protein TNT (2 μg) purified bait protein rTNT (2μg) was electro-transferred onto the PVDF membrane after separation on 12% SDS-PAGE and subsequently denatured and renatured on the membrane. The membrane with renatured bait protein was blocked with 5% skimmed milk and incubated with prey protein IFT (3 μgml⁻¹) in buffer (2% skimmed milk powder with 20 mM Tris (pH 7.6), 0.5 mM EDTA, 100 mM NaCl, 1 mM DTT, 0.1% Tween-20, 10% glycerol) for 2 hours at room temperature. Prey protein IFT was detected by incubation with primary antibody (1:5000, mouse raised anti-IFT antibody) following secondary antibody (1:5000, HRP-conjugated anti-mouse, Thermo Scientific, USA). The protein was detected by chemiluminescence signal

produced using the Luminol reagent (Bio-Rad). Human protein ETHE1 (raised in-house; unpublished work) was used as negative control.

3.2.6 NAD$^+$-glycohydrolase activity assay

In order to determine the NAD$^+$-glycohydrolase activity of TNT, different methods as described below were used.

The TNT-NADase activity was assessed by NADH fluorescence assay as previously described with minor modifications [230]. To evaluate inhibitory activity of compounds the assay was performed as follows. Briefly, the rTNT (75 nM) was mixed with compounds (10 μM) in assay buffer (20 mM Tris, 0.2 M NaCl, and pH 7.4) and reaction was initiated by adding β-NAD$^+$ (100 μM). After incubation, 5 M NaOH was used to stop the reaction, for this 100 μl of reaction mixture was aliquoted and 70 μl of 5 M NaOH was added in it. Fluorescence signal generated after 1 hour of incubation at 37 ˚C and relative fluorescence was measured using Varioscan multimode microplate reader (Thermo Scientific) at 360 nm excitation and 460 nm emission filter set and compared to a standard NAD$^+$ concentration curve. Relative NAD$^+$ levels were determined with comparison to the control sample.

Next, a highly sensitive fluorescence based enzyme coupled was performed to confirm the inhibitory activity of compounds, as previously described with minor modifications [410]. Briefly, compounds (1 μM) were incubated with TNT (30 nM) in the assay mixture (20 mM Tris, 0.2 M NaCl, and pH 7.4) followed by addition of β-NAD$^+$ (5 μM) to initiate the reaction. The samples were incubated at 37 ˚C and reaction was stopped using 150 mM HCl. Subsequently, sodium phosphate buffer (pH 8) was added to neutralize the reaction and enzyme cycling reaction was conducted to determine the remaining NAD$^+$ content [410]. Fluorescence microplate reader (Fluoroskan Ascent FL, Thermo Scientific) was used to measure the rate of increase in fluorescence at excitation 544 nm and emission 590 nm wavelengths. The relative NAD$^+$ levels were determined by measuring the slope of fluorescent increase in comparison to the control sample. For NAD$^+$ measurement in cell samples, harvested cells were treated with HCl (to extract NAD$^+$) followed by heat incubation and neutralization, and NAD$^+$ levels were determined using fluorescence based coupled enzyme assay [410].

NADase activity of TNT was also determined by EnzyFluo NAD/NADH Assay Kit (Bioassay Systems, USA). Briefly, β-NAD$^+$ (1 μM) was incubated with rTNT (30 nM) in assay buffer (20 mM Tris-HCl, 0.2 M NaCl, and pH 7.4) at 37 °C and manufacturer's protocol was followed to measure the remaining NAD$^+$ content.

All incubations were performed in dark. For all assays, freshly prepared reagents or their fresh aliquots were used. To avoid the freeze-thaw cycle purified rTNT, quantified by Bradford method (Bio-Rad, USA), was stored in aliquots and for every assay a fresh aliquot was used.

3.2.7 Macrophage transfection assay

3.2.7.1 Cloning of IFT and TNT genes into mammalian expression vectors

For expression of IFT and TNT proteins in macrophages, the IFT and TNT genes were cloned into mammalian expression vectors pFLAGCMV4$_{nn}$ and pEGFPC1, respectively. The IFT gene was excised using *Sna*B1 enzyme from IFT-pUC57 construct and eluted IFT insert was ligated into dephosphorylated *Eco*RV-digested pFLAGCMV4$_{nn}$ vector to obtain IFT- pFLAGCMV4$_{nn}$ construct.

For the in-frame cloning of TNT with the EGFP coding sequences, TNT gene with a single nucleotide addition was PCR amplified and insert was prepared after digestion with *Sna*B1 enzyme. Subsequently, TNT insert was ligated into dephosphorylated *Sma*1-digested pEGFPC1 vector to obtain TNT-pEGFPC1 construct.

3.2.7.2 Cell culture and transfection

The RAW 264.7 murine macrophage cell line (ATCC) was cultured in 10% FBS supplemented DMEM medium (Gibco, Life Technologies) with 10 mM HEPES, 2 mM L-glutamine, 100 IUml^{-1} penicillin, 100 μgml^{-1} streptomycin and maintained in 5% CO$_2$ at 37 °C.

For expression analysis, RAW 264.7 cells were transiently transfected with Lipofectamine™ 2000 reagent (Invitrogen, USA) by following the manufacturer's protocol. Seeded cells at approximately 80% confluency were transfected with constructs, TNT-pEGFPC1, or IFT-pCMV4$_{nn}$, or both. Cells transfected with pCMV4$_{nn}$ and pEGFPC1 vectors were taken as control. Respective vectors were used to normalize the single plasmid constructs as for double transfections equal amount of

both plasmids were transfected. Transfected cells were incubated for 48 hours and analysed by confocal microscopy for determination of transfection efficiency and protein expression. To analyse the expression of IFT and TNT proteins, RT-PCR was carried out with gene specific primers and further western blotting was performed with respective antibodies. For this, lysates were prepared using RIPA buffer (G-Biosciences, USA). Cells were incubated in protease inhibitor cocktail (Roche diagnostics) containing lysis buffer and centrifuged at 13,000 rpm for 20 min at 4 ˚C to obtain soluble fractions. Soluble fractions in equal amount were loaded to perform western blot analysis.

3.2.7.3 Confocal microscopy

Seeded RAW macrophages were allowed to adhere on coverslip and cultured for 48 hours post-treatment. After PBS washing, cells were fixed with 4% paraformaldehyde containing PBS buffer for 15 min at RT and again washed with cold PBS. Subsequently, 0.2% Triton X-100 in PBS buffer was used to permeabilise the cells for 10 min at RT. Cells were washed with PBS and incubated with 1% BSA in PBS buffer for blocking. Following PBS washing, cells were incubated with respective primary antibodies (1% BSA in PBS solution) for 1 hour at RT and washed again. Subsequently, cells were stained for 1 hour at RT with respective secondary antibodies and after washing, DAPI antifade solution (Sigma-Aldrich) was used to mount the cells. Stained cells were observed using a confocal microscope (Olympus Corporation, Japan). For IFT expression cells were stained with anti-IFT antibody (1:2500, mouse raised) followed by Alexa Fluor 594 secondary antibody. GFP-expression was observed to detect TNT expression.

3.2.7.4 Western blotting

Transfected cells lysates were quantified by Bradford assay (Bio-Rad, USA) for equal loading of protein samples on 12% SDS-PAGE. Resolved proteins by electrophoresis were transferred from gel to nitrocellulose membrane (Bio-Rad, USA). After blocking with 5% BSA in PBST (1xPBS, 0.05% Tween-20), blots were washed and incubated with anti-IFT or anti-TNT antibodies (1:5000, mouse-raised). Following washing with PBST, HRP-conjugated secondary antibodies (1:5000, Thermo Scientific, USA) were added. The Luminol reagent (Clarity™ western ECL substrate, Bio-Rad) was used to

develop chemiluminescence signal. GAPDH or β-Actin was used as the loading control.

3.2.7.5 RT-PCR analysis

Treated cells were suspended in TRIzol reagent (Invitrogen) and manufacturer's protocol followed to isolate total RNA. Subsequently, synthesis of cDNA was performed with random hexamer primers according to described protocol (RevertAid First Strand cDNA synthesis kit, Thermo Scientific). Synthesised cDNA was amplified for 20-30 cycles at 55–60 °C of annealing temperature using gene specific primers of IFT and TNT or with GAPDH primers (internal control) to normalize the expression. Amplified PCR products were analysed on 1% agarose gel under UV light.

3.2.8 *M. tuberculosis* infection of macrophages

To analyse the effect of IFT expression on intracellular survival of *M. tuberculosis*, RAW 264.7 murine macrophages were transfected with IFT-pCMV4$_{nn}$ construct and incubated for 24 hours. Transfected cells were infected with *M. tuberculosis* strain H37Rv or H37Rv-GFP at a multiplicity of infection of 10 (MOI 10:1) for 4 hours at 37 ˚C. After washing with DMEM (Gibco, USA), infected cells were incubated in complete medium. For further experiments, infected cells were harvested or analysed at respective time points.

3.2.9 Macrophage survival study

Cell death analysis of macrophages expressing TNT compared to control was conducted by MTT assay, propidium iodide (PI) staining, and HMGB1 translocation. *M. tuberculosis*-infected macrophages expressing IFT were analysed by Annexin-V and PI staining, HMGB1 translocation to determine cell survival. Macrophages were treated with selected NAD$^+$ analogues **8, 9, 10** and cell viability was evaluated by MTT assay. For survival study, cells were analysed after 48 hours post-treatment.

3.2.9.1 Cell death analysis by flow cytometry

Transfected RAW macrophages with respective plasmids were stained with PI solution. For cell death analysis of *M. tuberculosis*-infected macrophages, double-staining of control and IFT-expressing macrophages was performed with FITC-

Annexin-V and PI according to the manufacturers' protocol (FITC Annexin-V Apoptosis detection kit with PI, Biolegend, USA). The cell samples were acquired using a flow cytometer (BD LSR Fortessa, Becton Dickinson, USA) and data analysis was performed with FlowJo software (Tree Star Inc, USA).

3.2.9.2 Determination of HMGB1 translocation and release

In the experiments of macrophages transfected with TNT-pEGFPC1 or IFT-pCMV4$_{nn}$ constructs and *M. tuberculosis*-infected macrophages expressing IFT, nuclear to cytoplasmic translocation of HMGB1 protein was analysed by immunofluorescence assay and western blotting. Further, HMGB1 levels in culture supernatant were determined by western blotting to evaluate the HMGB1 release in treated macrophages.

Immunofluorescence assay: After the incubation time, treated cells on glass coverslips were fixed with PBS solution containing 4% formaldehyde for 15 min at RT, followed by permeabilisation with 0.2% Triton X-100 in PBS solution for 10 min at RT. After blocking with 1% BSA in PBS solution, cells were incubated for 1 hour at RT with anti-HMGB1 antibody (0.05 µg/ml, Invitrogen, USA). Following this, a secondary anti-rabbit Alexa Fluor 594 antibody (Thermo Scientific, USA) was added for 1 hour at RT. Cells were washed with PBS between all incubation steps. Cells were mounted with DAPI antifade solution to stain the nuclei and observed under a confocal microscope (Olympus Corporation, Japan).

Nuclear and cytoplasmic extracts preparation: Harvested macrophages, following treatment, were washed with PBS and cytoplasmic extraction buffer (5 mM Tris, pH 7.4, 5 mM KCl, 1.5 mM MgCl$_2$, 2 mM EGTA, 1 mM DTT, 1 mM PMSF) was added to resuspend the cells. The cell samples were incubated for 15 min on ice and vortexed repeatedly during incubation period to lyse cells. The obtained whole cell lysate was centrifuged and after addition with protease inhibitor cocktail (Roche diagnostics), collected supernatant (cytoplasmic fraction) was stored and further assayed for HMGB1 levels. To isolate the nuclear fraction, the pellet obtained after centrifugation was resuspended in nuclear extraction buffer (10 mM Tris, pH 7.4, 5 mM EDTA, 10 mM NaCl, 1% Triton X-100, 1 mM PMSF). The samples were again centrifuged and collected supernatant (nuclear fraction) with protease inhibitor

cocktail (Roche diagnostics) was stored and further analysed to determine HMGB1 levels by western blotting.

To determine the HMGB1 level in culture medium, treated cells were either cultured in minimal volume or harvested culture medium samples were concentrated with the centricon centrifugal filter (Merck Millipore). Protein concentration of samples was quantified by Bradford assay (Bio-Rad, USA) for western blotting.

Western blotting. Samples of cell lysates and culture supernatant were separated by SDS-PAGE and subsequently transferred onto nitrocellulose membrane. The membranes were blocked with 5% BSA in PBST (1xPBS, 0.05% Tween-20) and incubated with anti-HMGB1 antibody (1:2500, Invitrogen, USA) overnight at 4 °C. Following this, HRP-conjugated secondary anti-rabbit antibody (1:5000, Thermo Scientific, USA) was added for 2 hours at RT. Blots were washed with PBST in between incubation steps. Protein bands were visualized using Luminol reagent (Clarity™ western ECL substrate, Bio-Rad) for enhanced chemiluminescence.

3.2.9.3 Cell viability determination by MTT assay

To evaluate effect of TNT-expression on macrophage viability, MTT assay was performed after 48 hours of transfections with TNT-pEGFPC1 and IFT-pCMV4$_{nn}$ constructs. The effect of small molecules **8, 9, 10** on RAW macrophages cell viability was determined by MTT assay, after 48 hours of treatment with varying concentration (1.5 μM, 3 μM, 6 μM, 12 μM, 25 μM) of molecules. Briefly, MTT reagent (0.5 mg/ml in PBS solution) was added to treated cells and incubated for 3 hours at 37 ˚C. Viable cells convert MTT into a product of purple formazan crystal. Following incubation culture medium was removed and to dissolve formazan crystals 100 μl of DMSO was added to each well. The optical density was measured by taking absorbance reading at 570 nm using Varioscan multimode microplate reader (Thermo scientific). The absorbance reading of treated samples was compared with the control to determine percent cell viability.

3.2.10 Intracellular survival of *M. tuberculosis* in macrophages

Treated macrophages were analysed by CFU assay and confocal microscopy to determine *M. tuberculosis* intracellular survival inside macrophages.

3.2.10.1 CFU assay

In IFT-expressing and control RAW macrophages, intracellular growth of *M. tuberculosis* was determined after 24, 48 and 72 hours of infection with *M. tuberculosis* strain H37Rv strain. Post-treatment, infected cells were harvested and 0.05% SDS solution in 7H9 medium (Sigma-Aldrich) was added for cell lysis. The different dilutions of lysates were prepared and subsequently plated on 7H11 agar plates for colony counting. Following incubation of 15 days, plates were analysed and counted for number of *M. tuberculosis* colonies. CFU was calculated by taking into consideration of the dilution factors.

3.2.10.2 Confocal Microscopy

RAW macrophages cultured on coverslip were infected with *M. tuberculosis* H37Rv-GFP (MOI 10:1) and after 48 hours of post-infection fixed with 4% paraformaldehyde solution in PBS. Infected macrophages were mounted with DAPI antifade solution and analysed under a confocal microscope (Olympus Corporation, Japan). Infected macrophages were manually counted and further percentage of infected macrophages was calculated as follows:

Infected macrophages with *M. tuberculosis* (%) = (Number of infected macrophages/Total number of macrophages) *100

3.2.10.3 Effect of small molecules on *M. tuberculosis* intracellular survival

To evaluate the effect of small molecules **8, 9, and 10** on intracellular survival of *M. tuberculosis*, infected peritoneal macrophages were analysed by CFU count after 24, and 48 hours of infection. Briefly, female BALB/c mice (6 to 7 weeks-old) were injected intraperitonealy with 2 ml of thioglycollate solution. All mice were sacrificed on the fifth day of infection and macrophages were collected by *peritoneal* lavage. Isolated murine peritoneal macrophages were seeded in culture plate and incubated for 24 hours. Following incubation, adhered macrophages were infected with *M. tuberculosis* H37Rv (MOI 10:1) for 4h. Infected-macrophages were washed and incubated in small molecules (25 µM) containing complete medium till respective time points and analysed by CFU count.

3.2.11 Protein loading in erythrocytes

Recombinant proteins were loaded in erythrocytes following protocol of previously described method [411]. Briefly, erythrocytes were washed with PBS and resuspended at 50 percent hematocrit in PBS solution supplemented with glucose. Samples were centrifuged and obtained packed erythrocytes were incubated on ice for 5 min followed by lysis with buffer (1 mM ATP, 5mM K_2HPO_4, final pH 7.4) with 1 hour incubation on ice. For erythrocytes loading, PBS (control) or recombinant proteins (5 µg per 50 µl packed erythrocytes in PBS) were added into lysis buffer. After incubation, 25 µl of resealing buffer (237.5 mM KCl, 475 mM KOAc, 25 mM $MgCl_2$, and 25 mM Na_2HPO_4, 1 mM ATP, final pH 7.0) was added for 1 hour at 37˚C to reseal the lysed erythrocytes. Samples were washed thrice with incomplete RPMI medium and analysed for further experiments.

3.2.12 Analysis of eryptosis markers

Flow cytometric assays were performed to analyse the markers of eryptosis by using flow cytometer (BD, LSR Fortessa, Becton Dickinson, USA) and data analysis was conducted through FlowJo software (Tree Star Inc, USA).

3.2.12.1 Evaluation of FITC-dextran loaded erythrocytes

FITC-Dextran 10,000 MW (Sigma-Aldrich) along with BSA or rTNT protein was loaded in erythrocytes. Loaded erythrocytes in PBS-Glucose solution were analysed by flow cytometry (BD, LSR Fortessa) and fluorescence microscopy.

3.2.12.2 Determination of phosphatidylserine exposure and forward scatter

FITC-annexin-V (dilution 1:20, Thermo Scientific) was added to loaded erythrocytes in Annexin-V binding Buffer (10 mM HEPES, 2.5 mM $CaCl_2$, 140 mM NaCl, and pH 7.4) and erythrocytes were incubated for 20 min at RT. Erythrocytes were washed and analysed at 488/530 nm (excitation/emission wavelength) and also measured for forward scatter by flow cytometry (BD, LSR Fortessa). Loaded FITC-annexin-V stained erythrocytes were also analysed using confocal microscope (Nikon, Japan).

3.2.12.3 Quantification of intracellular calcium level

Erythrocytes were incubated with Fluo-4AM (Life Technologies, USA) and analysed at 488/530 nm (excitation/emission wavelength) to measure intracellular Ca^{2+} level by flow cytometry (BD LSR Fortessa).

3.2.12.4 Reactive oxygen species (ROS) measurement

Resealed erythrocytes were incubated for 25 min at 37 °C with 2, 7-Dichlorofluorescein diacetate (DCFDA, Sigma-Aldrich) to determine the ROS generation. After washing, erythrocytes were analysed at 488/530 nm (excitation/emission wavelength) by flow cytometry (BD LSR Fortessa).

3.2.13 *P. falciparum* culture

P. falciparum 3D7 strain was cultured using O^+ erythrocytes in RPMI medium (Gibco,USA) containing 0.5% Albumax II with 2 mM l-glutamine, 25 mM HEPES, 25 mM sodium bicarbonate, 27.2 mgL^{-1} hypoxanthine and final pH 7.4. Culture was maintained at 37 °C in an atmosphere of 90% N_2, 5% O_2, and 5% CO_2. Parasite culture was synchronized through sorbitol treatment. Percoll treatment was performed to purify schizonts. Giemsa stained (Sigma-Aldrich) culture smears were prepared to monitor routine parasitemia and staging.

3.2.14 *P. falciparum* invasion assay

Erythrocytes loaded with recombinant proteins were maintained at 2% hematocrit and 1% parasitemia and infected with schizonts purified using Percoll. Total parasitemia along with numbers of rings and schizonts present in treated samples were evaluated at different time-points by preparing Giemsa-stained thin-blood smears. The counting of number of rings produced per schizont was performed and percent invasion determined as number of rings produced per schizont in treated samples compared to control. After 48 hours of post-infection, final parasitemia of each sample was divided with initial parasitemia to calculate fold change in parasitemia.

3.2.15 *P. falciparum* growth inhibition assay

Synchronized culture of *P. falciparum* at early trophozoite stage was aliquoted in 96-well plates (Nunc, Thermo, USA) at 2% hematocrit and 1% parasitemia. To determine the inhibitory effect of the small molecules, culture was treated with the molecules **8, 9, and 10** (100 nM-20 μM) for 48 hours. At the end of incubation period, parasitemia of samples was calculated by monitoring the Giemsa-stained blood smears. Untreated and DMSO-treated cultures were used as control. Graph pad prism 6.0 (CA, USA) was used to determine IC_{50} values. Percent inhibition of *P. falciparum* growth was determined as follows:

P. falciparum growth Inhibition (%) = (1 − Percent parasitemia of treatment/ Percent parasitemia of Control) ∗ 100.

To determine *P. falciparum* growth, ethidium bromide (10 μM) stained infected erythrocytes were analysed by flow cytometry (BD, LSR Fortessa, Becton Dickinson, USA) using FlowJo software (Tree Star Inc, USA).

3.2.16 *In silico* docking studies

3D protein structure of TNT protein was obtained from Protein databank (PDB ID-4QLP, IFT-TNT complex structure). The protein and ligands structure was optimized using Swiss PDB viewer and chem.Bio Draw ultra 3D software. TNT protein was docked with molecules 8, 9, and 10 using Autodock version 4.2 and Cygwin terminal version 3.1 softwares. For ligand binding, grid was prepared around residues involved in NAD$^+$ Binding and hydrolysis. For further analysis and visualization of docking results, UCSF Chimera version 1.14, Ligplot$^+$ version 2.2, Discovery Studio version 19.1.0 and Pymol version 2.3.2 softwares were used as described previously [412].

3.2.17 Statistical analysis

The results represent mean values of three independent experiments and error bar represented standard deviation of data. Significance of difference was determined through unpaired two-tailed Student's t test to measure *P* values. Calculated P values less than 0.05 were considered as statistically significant. *P* values < 0.05 denotes *, < 0.01 denotes **, and < 0.001 denotes ***.

3.2.18 Ethics Statement

Animal studies were performed following CPCSEA guidelines and approved by Institutional Animal Ethics Committee (IEAC) of JNU. Female BALB/c mice were obtained from Central Laboratory Animal Resources, JNU, New Delhi and maintained under standard conditions and. For experiments, donor blood was obtained from Rotary blood bank (RBB), New Delhi, India.

Chapter 4

Results

4 RESULTS

4.1 Effect of NAD$^+$ modulation on bacterial growth and colony formation unit using TNT-IFT toxin-antitoxin system

Recent studies have identified the presence of the main cytotoxicity factor leading to host cell death during *M. tuberculosis* infection, called as TNT, or tuberculosis necrotizing toxin [229, 230]. TNT is the secreted C-terminal domain of *M. tuberculosis* protein CpnT (channel protein with necrosis inducing-toxin, Rv3903c), that possesses NAD$^+$-glycohydrolase activity [229, 230]. The N-terminal channel domain of CpnT protein forms pores across the outer membrane that enables uptake of nutrients [229]. Further study identified the presence of an antitoxin protein IFT (immunity factor for TNT, Rv3902c) against NADase activity of TNT [230]. Figure 4.1-1 represents the *cpnT–ift* operon and domain structure of *M. tuberculosis* proteins CpnT and IFT. Complete amino acid sequence of proteins TNT and IFT, and protein parameters obtained by the ExPaSy ProtParam tool are presented in Figure 4.1-2 and Table 4.1, respectively.
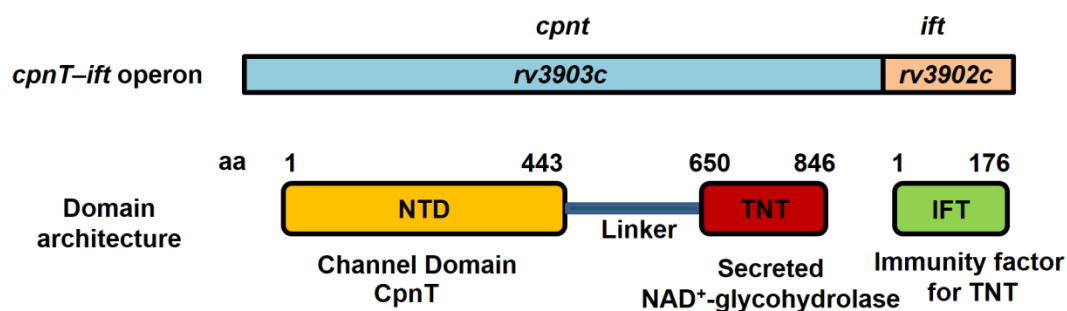
Figure 4.1-1 Schematic representation of the *cpnT–ift* operon and CpnT and IFT protein domain architecture. *M. tuberculosis* CpnT protein (encoded by *rv3903c* gene) consists of two domains, N-terminal channel domain (amino acids 1-443) connected through a linker region (amino acids 443-650) to a secreted C-terminal domain, TNT (amino acids 650-846) (red). The *rv3902c* gene encodes protein IFT, Immunity factor for TNT (green).

>CCP46732.1 Cpnt Rv3903c [Mycobacterium tuberculosis H37Rv]

MAPLAVDPAALDSAGGAVVAAGAGLGAVISSLTAALAGCAGMAGDDPAGAVFGRSYDGSAAALVQAMSVAR
NGLCNLGDGVRMSAHNYSLAEAMSDVAGRAAPLPAPPPSGCVGVGAPPSAVGGGGGAPKGWGWVAPYIGM
IWPNGDSTKLRAAAVAWRSAGTQFALTEIQSTAGPMGVIRAQQLPEAGLIESAFADAYASTTAVVGQCHQLAA
QLDAYAARIDAVHAAVLDLLARICDPLTGIKEVWEFLTDQDEDEIQRIAHDIAVVVDQFSGEVDALAAEITAVVSH
AEAVITAMADHAGKQWDRFLHSNPVGVVIDGTGQQLKGFGEEAFGMAKDSWDLGPLRASIDPFGWYRSWEE
MLTGMAPLAGLGGENAPGVVESWKQFGKSLIHWDEWTTNPNEALGKTVFDAATLALPGGPLSKLGSKGRDIL
AGVRGLKERLEPTTPHLEPPATPPRPGPQPPRIEPPESGHPAPAPAAKPAPVPANGPLPHSPTESKPPPVDRP
AEPVAPSSASAGQPRVSAATTPGTHVPHGLPQPGEHVPAQAPPATTLLGGPPVESAPATAHQPQWATTPAAP
AAAPHSTPGGVHSTESGPHGRSLSAHGSEPTHDGASHGSGHGSGSEPPGLHAPHREQQLAMHSNEPAGEG
WHRLSDEAVDPQYGEPLSRHWDFTDNPADRSRINPVVAQLMEDPNAPFGRDPQGQPYTQERYQERFNSVGP
WGQQYSNFPPNNGAVPGTRIAYTNLEKFLSDYGPQLDRIGGDQGKYLAIMEHGRPASWEQRALHVTSLRDPY
HAYTIDWLPEGWFIEVSEVAPGCGQPGGSIQVRIFDHQNEMRKVEELIRRGVLRQ

>CCP46731.1 Immunity factor for TNT (IFT) Rv3902c [Mycobacterium tuberculosis H37Rv]

MTIGVDLSTDLQDWIRLSGMNMIQGSETNDGRTILWNKGGEVRYFIDRLAGWYVITSSDRMSREGYEFAAASM
SVIEKYLYGYFGGSVRSERELPAIRAPFQPEELMPEYSIGTMTFAGRQRDTLIDSSGTVVAITAADRLVELSHYLD
VSVNVIKDSFLDSEGKPLFTLWKDYKG

Figure 4.1-2 Protein sequences of TNT and IFT. The amino acid sequence of the full length CpnT and IFT proteins are shown. Highlighted region of full length protein CpnT shows protein sequence of TNT used in this study.

Name	Amino acids	M.W. (kDa)	pI	GRAVY
TNT	199	22.80	5.36	-0.863
IFT	176	19.82	4.77	-0.222

Table 4.1 Protein parameters of TNT and IFT proteins. ExPaSy ProtParam tool was used to determine protein parameters of interacting toxin-antitoxin proteins, TNT and IFT.

4.1.1 Cloning of TNT and IFT for co-expression in *E.coli* BL21 cells

To study the effect of NAD^+ modulation on *E.coli* growth and survival, TNT and IFT genes were codon-optimized from Genscript and cloned into expression vectors pMTSA and pET28a, respectively. For cloning *Sna*B1-digested inserts of IFT and TNT, genes were ligated into *Sna*B1-cut expression vectors. Confirmation of positive clones was carried out by colony PCR using gene-specific forward and vector-specific reverse primers, restriction digestion and finally through sequencing (Figure 4.1-3 A and B). Because TNT has NAD^+-glycohydrolase activity, TNT expression would deplete bacterial NAD^+ levels that could be reverted by IFT expression. To express both TNT and IFT proteins, *E.coli* BL21 cells were co-transformed with constructs TNT-pMTSA and IFT-pET28a. Transformation was confirmed by colony PCR with gene specific primers of TNT and IFT (Figure 4.1-3 C).
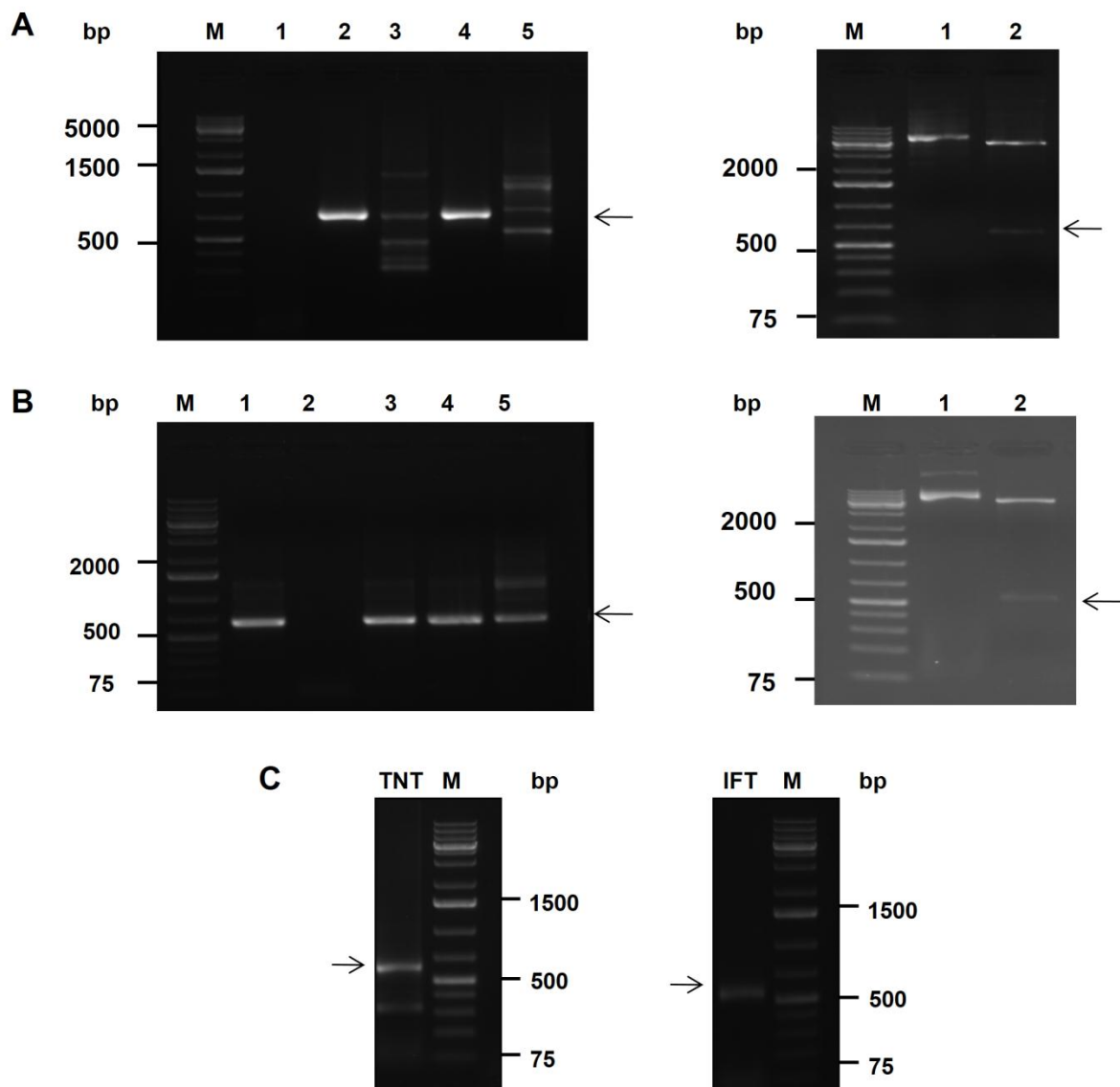
Figure 4.1-3 Cloning of TNT and IFT genes for co-expression in *Ecoli* BL21 cells.

(A) Cloning of TNT into pMTSA expression vector. (B) Cloning of IFT into pET28a expression vector. Colony PCR analysis for screening of positive colonies with gene specific forward and vector specific reverse primers. Lane 1-5 shows PCR analysis of different colonies, Lane M shows 1 kb plus DNA ladder. Confirmation of selected positive clone by restriction digestion with *Sna*B1 enzyme: Lane 1 shows undigested plasmid, Lane 2 shows digested plasmid, Lane M shows 1 kb plus DNA ladder. (C) Confirmation of co-transformed *E.coli* BL21 cells with gene specific primers.

4.1.2 Effect of expression of TNT and IFT proteins on bacterial cell growth and colony formation.

To modulate the intracellular NAD^+ levels of bacterial cells, the co-transformed *E.coli* BL21 cells were induced with arabinose and IPTG to express TNT and IFT proteins, respectively. IFT is a known antitoxin for TNT, hence TNT-mediated NAD^+ depletion can be inhibited by IFT expression. The co-transformed cells were induced with both arabinose and IPTG to study whether IFT expression could revert the effect of TNT. Cells without induction with arabinose or IPTG, and induced with IPTG only, were considered as control. Effect of TNT expression on bacterial growth was determined by measuring optical density of culture at different time points after induction with arabinose, IPTG, or both, that express protein TNT, IFT, or TNT with IFT, respectively. After one hour of post-induction with arabinose, the optical density of bacterial culture did not significantly increased at different time points, which showed that expression of TNT inhibits bacterial growth. Interestingly, bacterial culture induced with both IPTG and arabinose, expressing protein IFT with TNT, showed growth pattern similar to control cultures (Figure 4.1-4 A). This observation confirms the hypothesis that expression of IFT can revert the effect of TNT on bacterial growth. To further evaluate the effect of TNT expression on bacterial colony formation unit, co-transformed cells were plated on agar plates containing arabinose or IPTG or both and only antibiotics supplemented plates were used as control. As mentioned previously, arabinose and IPTG induce expression of TNT and IFT proteins respectively. Co-transformed cells plated on agar plates containing IPTG and IPTG with arabinose were able to form colonies similar to control. In contrast, TNT expression in bacterial cells, plated on agar plates containing arabinose, inhibits bacterial colony formation (Figure 4.1-4 B). The co-transformed cells plated on agar plates without or with arabinose, or IPTG, or both arabinose and IPTG are shown in Figure 4.1-4 C. These results demonstrate a profound impact of TNT expression on bacterial growth and colony formation and reversion of this effect by co-expression of IFT indicates that TNT-mediated NAD^+ depletion could be responsible for inhibition of bacterial growth and colony formation.
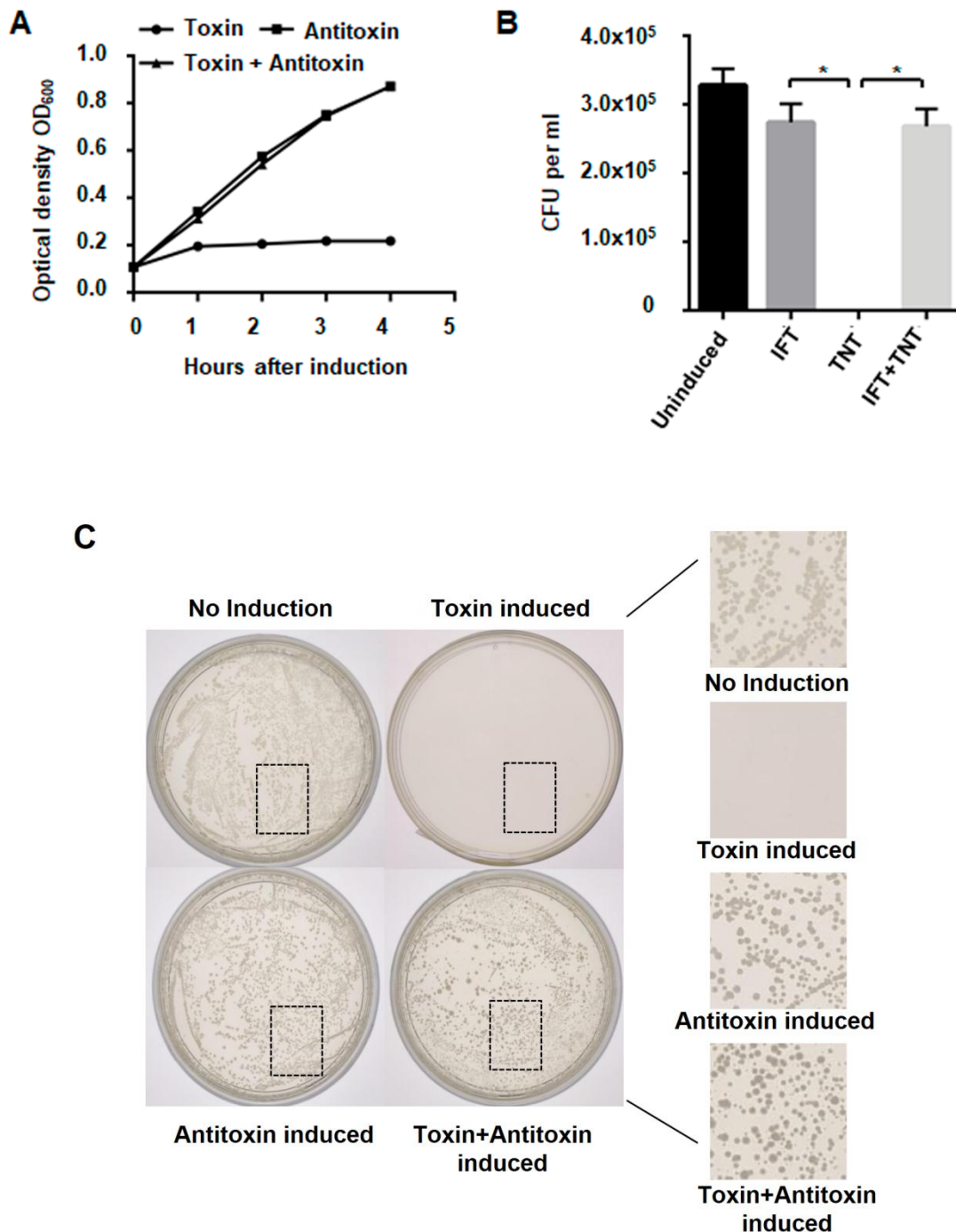
Figure 4.1-4 Effect of expression of TNT and IFT proteins on bacterial cell growth and colony formation. (A) Optical density measured at 600 nm representing bacterial growth. At time zero, bacterial culture was induced with 0.2% arabinose, or 1mM IPTG, or both. (B) CFU count of co-transformed bacterial cells. The cells were incubated at 37°C for 16 hours after plating on 0.2% arabinose, or 25µM IPTG, or both containing agar plates. Co-transformed cells plated on agar plates with appropriate antibiotics only were used as control. (C) Representation of colony formation by co-transformed cells plated on agar plates supplemented with 0.2% arabinose or 25 µM IPTG or both. Significance of difference is calculated using unpaired t-test with Welch correction, *P<0.05.

4.1.3 Determination of intracellular NAD$^+$ level of transformed bacterial cells

In order to determine that TNT-mediated NAD$^+$ depletion is the reason behind toxic effect of TNT expression on bacterial growth and colony formation, the NAD$^+$ levels of co-transformed cells induced with IPTG, or arabinose or both were measured. Equal number of co-transformed cells as calculated by optical density, were used to measure NAD$^+$ levels. Intracellular NAD$^+$ levels of TNT expressing cells were significantly reduced compared to control and IFT expressing cells. Importantly, NAD$^+$ levels of bacterial cells expressing IFT with TNT were significantly increased, which confirmed the reversion of TNT-mediated NAD$^+$ depletion by IFT expression (Figure 4.1-5). These results collectively demonstrate TNT-mediated NAD$^+$ depletion inhibits bacterial growth and colony formation that can be reverted by NAD$^+$ restoration through IFT expression.
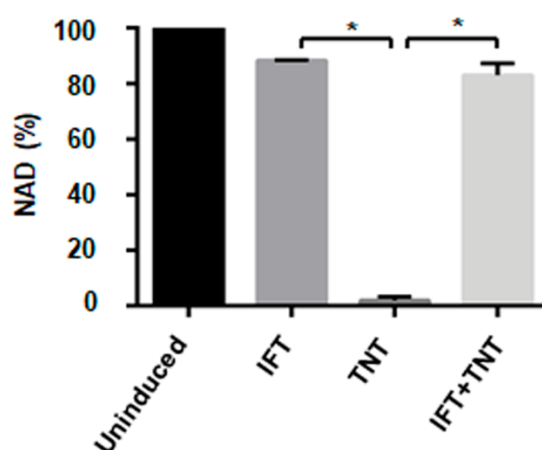
Figure 4.1-5 Determination of NAD$^+$ levels of co-transformed bacterial cells. NAD$^+$ levels of co-transformed bacterial cells were measured using an enzyme-coupling assay. Intracellular NAD$^+$ levels of uninduced bacterial cells were considered as 100%. Statistical significance was determined using unpaired t-test with Welch correction, where *$P<0.05$.

4.2 Cloning, Expression and Purification of recombinant proteins and evaluation of NAD$^+$-glycohydrolase activity of recombinant TNT protein

4.2.1 Cloning, Expression and Purification of recombinant IFT (rIFT) protein

The IFT gene was codon optimized and synthesized by GenScript (USA) and further cloned into expression vector pET28a as described in the previous result section (Figure 4.1-3 B). For purification of IFT protein, *E. coli* BL21 (DE3) cells harboring

IFT-pET28a construct were induced with 1 mM IPTG to express IFT protein tagged with hexa-Histidine at its C-terminal (Figure 4.2-1 A). After induction at 25 °C for 10 hours, rIFT protein was found to be present in both soluble and insoluble fractions (Figure 4.2-1 B). Protein from soluble fraction was purified by Ni-NTA column chromatography using an imidazole gradient. Purified fractions were collected, and dialysed to remove imidazole and run on an SDS-PAGE gel to analyse the integrity of the purified rIFT protein (Figure 4.2-1 C, D). The purified rIFT protein was present at a size approximately 21.6 kDa (IFT-His$_{6x}$) and found to be pure for performing further assays.
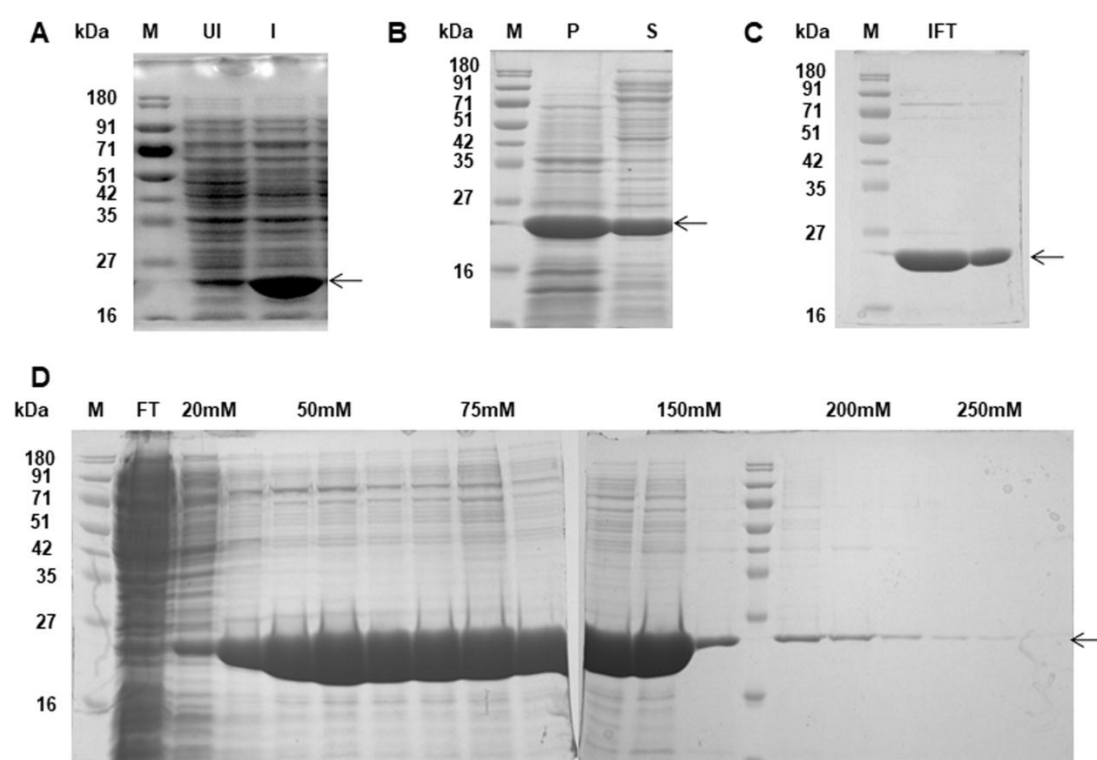
Figure 4.2-1 Expression and Purification of rIFT protein. (A) Expression analysis of rIFT in IFT-pET28a harbouring *E. coli* BL21 (DE3) cells after induction with IPTG. Lane UI and Lane I show Uninduced and induced bacterial cell lysates, respectively. (B) Solubility profile of rIFT. Lane P and Lane S show Pellet fraction (Inclusion bodies) and Soluble fraction after sonication, respectively. (C) Analysis of dialysed purified rIFT on 12% SDS-PAGE. (D) Purification of rIFT using Ni-NTA chromatography through imidazole gradient. Lane M - Puregene prestained protein ladder.

4.2.2 Cloning, Expression and Purification of recombinant TNT (rTNT) protein

The TNT gene was codon optimized and synthesized by GenScript (USA) and further cloned into expression vector pMTSA as described in previous result section (Figure 4.1-3 A). The TNT-pMTSA construct was transformed into *E. coli* C43 (DE3) cells and 0.2% arabinose was added for expression of the C-terminal hexa-Histidine tagged TNT protein. After sonication rTNT protein was found to be present in inclusion bodies (insoluble fraction). It was solubilise with 8M urea for further purification (Figure 4.2-2 A). Protein was purified using Ni-NTA column and dialysed to remove urea (Figure 4.2-2 B). Purified rTNT protein was analysed on 12% SDS-PAGE gel (TNT-His$_{6x}$ ~ 24.6 kDa) and found to be pure (Figure 4.2-2 C).
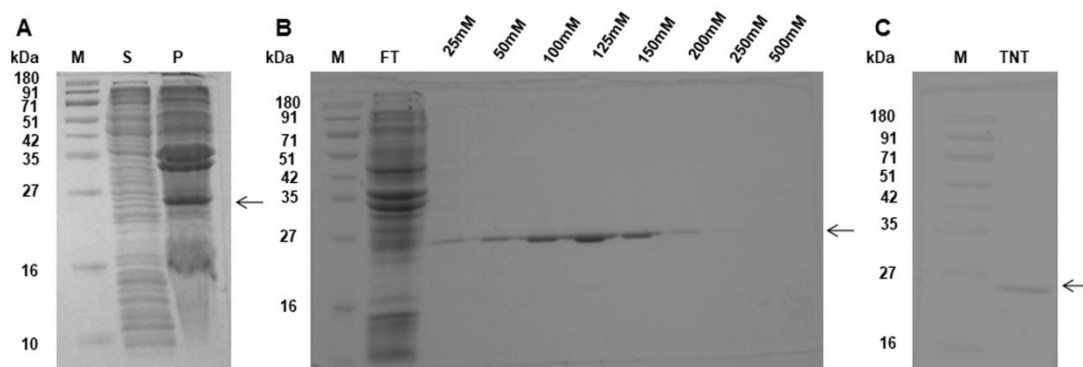
Figure 4.2-2 Expression and Purification of rTNT protein. Expression analysis of rTNT after induction with 0.2% arabinose was performed. (A) Solubility profile of rTNT protein. Lane P and Lane S show Pellet fraction (Inclusion bodies) and Soluble fraction after sonication, respectively. (B) Purification of rTNT using Ni-NTA chromatography. 12% SDS-polyacrylamide gel showing eluted fractions of rTNT protein. (C) Analysis of dialysed purified rTNT on 12% SDS-PAGE. Lane M - Puregene prestained protein ladder.

4.2.3 Co-expression and Purification of IFT and TNT proteins (IFT-TNT complex)

For co-expression of TNT and IFT proteins (IFT-TNT complex), TNT-pMTSA and IFT-pET28a constructs harboring co-transformed cells were grown and the culture was induced with both arabinose and IPTG. Arabinose induces expression of TNT while IPTG induces expression of IFT. After sonication, solubility profile of TNT-IFT complex was analysed and enough amount of protein complex was found in the soluble fraction of the bacterial cell lysate for purification (Figure 4.2-3 A). The TNT-

IFT complex was purified through imidazole gradient using Ni-NTA column and the protein complex was majorly eluted in the imidazole range of 50 mM to 150 mM (Figure 4.2-3 B). Eluted protein fractions of purified TNT-IFT complex were analysed on SDS-polyacrylamide gel.
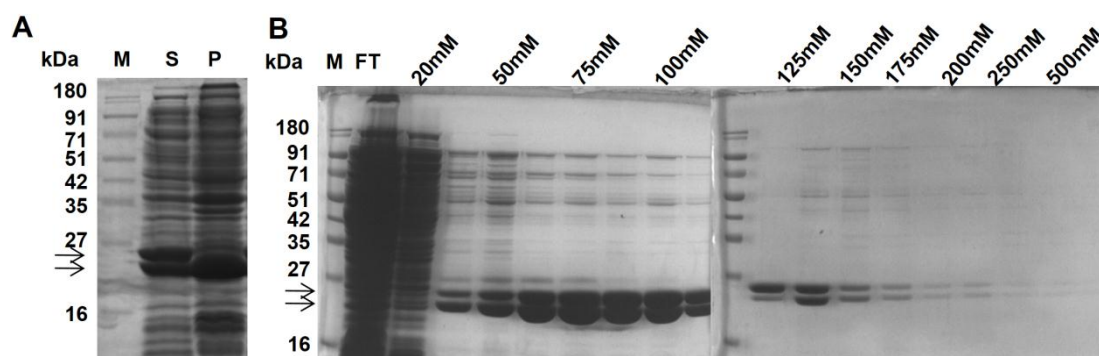
Figure 4.2-3 Co-expression and Purification of IFT-TNT protein complex. (A) Solubility profile of IFT-TNT protein complex. Lane P and Lane S show Pellet fraction (Inclusion bodies) and Soluble fraction, respectively. (B) Purification of IFT-TNT protein complex using Ni-NTA chromatography. Eluted fractions of protein complex were analysed on 12% SDS-polyacrylamide gel. Lane M - Puregene prestained protein ladder.

4.2.4 Purification of rTNT from IFT-TNT complex

The TNT protein was expressed alone and purified from inclusion bodies as the soluble fraction did not contain significant amount of the protein (Figure 4.2-2). The concentration of purified protein from inclusion bodies was less and the protein was refolded to obtain the proper conformation. In order to obtain high quality large amount of rTNT protein for assays, purified IFT-TNT protein complex was heated at 55 °C and rTNT protein was isolated from the soluble fraction. Soluble fraction and insoluble fraction containing purified rTNT and rIFT proteins respectively were analysed on 12% SDS-PAGE gel (Figure 4.2-4). The rTNT protein achieved from IFT-TNT complex was adequate in amount and sufficiently pure to conduct further studies and assays.
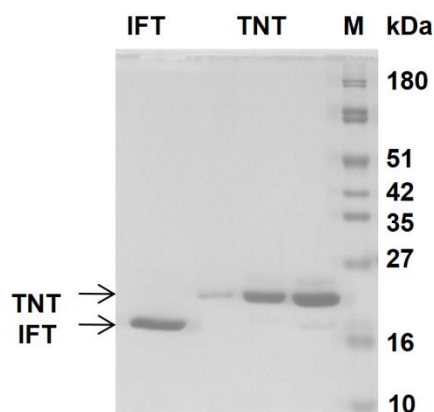
Figure 4.2-4 SDS-PAGE analysis of rTNT purified from IFT-TNT complex. Obtained insoluble (rIFT) and soluble fractions (rTNT) from IFT-TNT complex were analysed on 12% SDS-PAGE gel. Lane M - Puregene prestained protein ladder.

4.2.5 Determination of NAD$^+$-glycohydrolase activity of rTNT

TNT protein is reported to possess β NAD$^+$-glycohydrolase activity [230]. The rTNT protein was purified from inclusion bodies and the IFT-TNT complex. The NADase activity of purified rTNT proteins was determined by an enzyme-coupled assay as described in Methods. Refolded rTNT protein did not exhibit NAD$^+$-glycohydrolase activity while protein purified from IFT-TNT complex showed strong NAD$^+$-glycohydrolase activity (Figure 4.2-5). For enzymatic assays and inhibition studies rTNT protein purified from IFT-TNT complex was used.
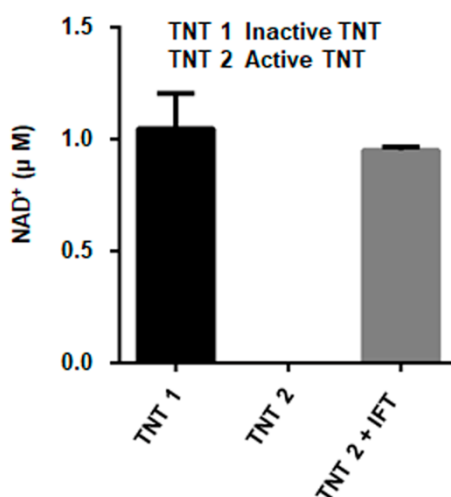
Figure 4.2-5 Evaluation of NAD$^+$-glycohydrolase activity of rTNT.

The rTNT protein (30 nM) purified from inclusion bodies (rTNT 1), or IFT-TNT complex (rTNT2) was incubated with 1 μM NAD$^+$ alone or with IFT. The EnzyFluo NAD/NADH kit was used to measure the remaining NAD$^+$ content.

4.3 Interaction and inhibition studies of TNT protein with IFT and inhibitors

4.3.1 Effect of IFT protein on NADase activity of TNT and its interaction with TNT protein

IFT is a natural inhibitor of TNT activity and acts as an antitoxin for TNT [230]. Interaction studies of purified proteins rIFT and rTNT were performed to confirm the binding of rIFT with rTNT protein. Further, inhibitory potential of rIFT on rTNT NADase activity was evaluated.

### 4.3.1.1 Interaction studies of rIFT and rTNT proteins

In order to study the effect of IFT on TNT NADase activity, *in vitro* interaction studies between rIFT and rTNT proteins were carried out by ELISA and Far-western blotting. To perform ELISA based interaction study, rTNT protein was coated on the ELISA plate and varying concentrations of rIFT protein were overlaid, subsequently detected with specific anti-IFT antibody. The absorbance reading indicated strong interaction between rIFT and rTNT proteins and thus confirmed the interaction (Figure 4.3-1 A). Further confirmation of interaction was carried out by Far-western blotting. The rTNT protein (prey protein) along with control proteins was electrophoresed and transferred onto nitrocellulose membrane. Purified rETHE1 Protein was used as negative control. Transferred proteins were denatured and renatured on the membrane and probed with rIFT protein (bait protein). Subsequent detection with specific anti-IFT antibody found presence of rIFT protein at the position where rTNT protein was located. This finding confirmed that rIFT and rTNT proteins form a complex (Figure 4.3-1 B).
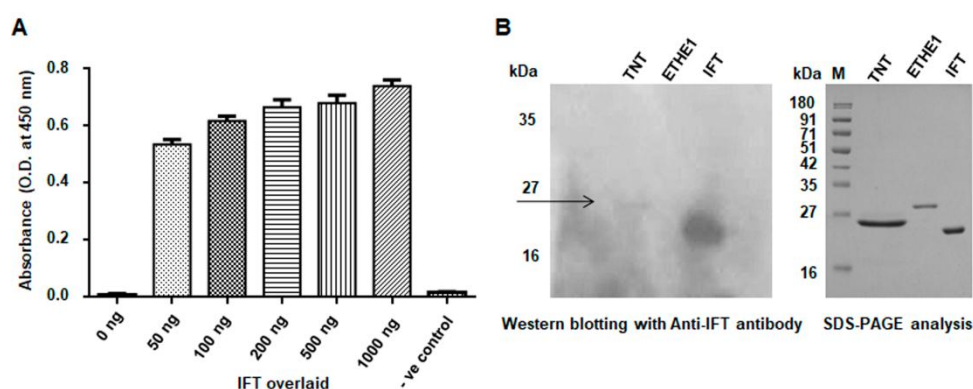
Figure 4.3-1 Protein-protein interaction studies of rIFT and rTNT proteins by ELISA and Far-western blotting. (A) Interaction study between rIFT and rTNT proteins by ELISA. ELISA plates were coated with purified rTNT (200 ng) and rIFT in varying concentration was overlaid. The rIFT was detected by anti-IFT antibody (mouse raised) and anti-mouse HRP conjugated secondary antibody. Buffer alone was taken as control. (B) Far-western blot analysis showing rIFT and rTNT proteins interaction. For negative control rETHE1 protein was used.

4.3.1.2 Determination of inhibitory potential of rIFT protein against rTNT NADase activity

After confirmation of interaction between rIFT and rTNT proteins, the study proceeded to evaluate effect of rIFT on rTNT NADase activity. SDS-PAGE analysis of purified rIFT, rTNT and IFT-TNT protein complex is shown in Figure 4.3-2 A. The reaction to determine NADase activity was conducted in the presence and absence of rIFT protein and remaining NAD^+ content was determined after incubation. The NAD^+ content of reaction containing rTNT protein was reduced to around 20 percent while presence of rIFT with rTNT protein significantly increased the NAD^+ levels similar to controls. The reactions without rTNT and containing NAD^+ only, and NAD^+ along with rIFT protein, were used as control (Figure 4.3-2 B). These results confirm the inhibition of NADase activity of TNT by IFT and suggested IFT can be used as a natural inhibitor of TNT for further studies.
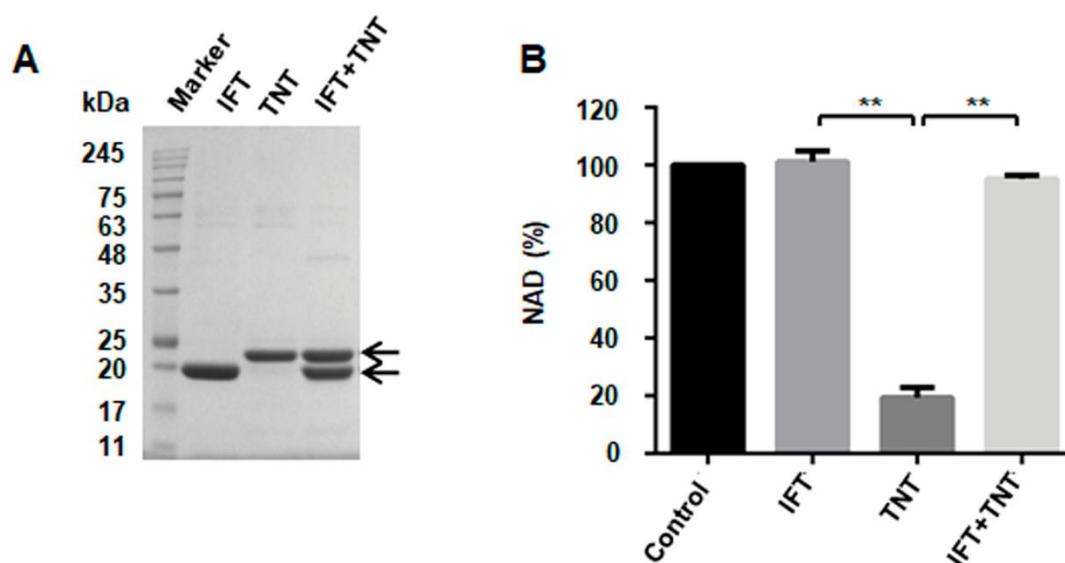
Figure 4.3-2 Effect of rIFT on NAD^+-glycohydrolase activity of rTNT. (A) SDS-PAGE analysis of purified rIFT, rTNT and IFT-TNT protein complex. Lane M - Prestained protein ladder. (B) rTNT protein (75 nM) was incubated with 200 μM final concentration of NAD^+ in the presence and absence of rIFT and remaining NAD^+ levels was determined by the NADH fluorescence assay. The NAD^+ level of control reaction (without rTNT) was considered as 100%. The *P* values calculated using the unpaired t-test with Welch correction,**$P<0.01$.

4.3.2 Designing *de novo* peptide inhibitors against IFT and TNT proteins

Previous studies have reported significance of IFT-TNT protein-protein interaction for survival of *M. tuberculosis*. Expression of TNT itself has been found toxic for *M. tuberculosis* and TNT neutralisation through IFT is crucial for its survival [230]. Therefore, targeting IFT through designing inhibitors against it could have significant impact on *M. tuberculosis* growth and survival. Along with this, secreted TNT is involved in mediating host cell death and has important role in *M. tuberculosis* pathogenesis. Recent studies have suggested TNT as an important factor involved in *M. tuberculosis* virulence but its targeting has not been reported. Therefore, proteins IFT, TNT, and IFT-TNT complex were identified as potential therapeutic targets and *de novo* libraries were screened to isolate potent inhibitors against them.

4.3.2.1 Construction and cloning of *de novo* dicodon libraries and amplification of human lung cDNA library

To find charge-based small peptide or protein binders against target protein, our lab has developed a method for construction of *de novo* dicodon libraries [407]. In the first step, dicodons were HP ligated and after *Xba*I digestion, PCR amplification with HP2P primers was performed. Amplified PCR product was electrophoresed on agarose gel to select members of size less than 1000 base pairs and further cloning was carried out into bacterial two-hybrid expression vectors pBT_{nn} and $pTRG_{nn}$. Confirmation of positive clones was performed by colony PCR, and showed around 60-70% positive clones (Figure 4.3-3 A). On the basis of the presence of positively or negatively charged amino acids, developed libraries were positively charged (KLRT), or negatively charged (DIEL), or neutral (equimolar library). As calculated from ProtParam tool, both IFT and TNT proteins are negatively charged with pI value of 4.77 and 5.36, respectively. Based on electrostatic interactions these proteins should bind preferably with positively charged binders, therefore KLRT library was used to screen binders against IFT and TNT proteins. Along with this, for bacterial two-hybrid studies a commercially constructed human lung cDNA library in pTRG (Stratagene, USA) was also used that was further amplified and checked by PCR (Figure 4.3-3 B).
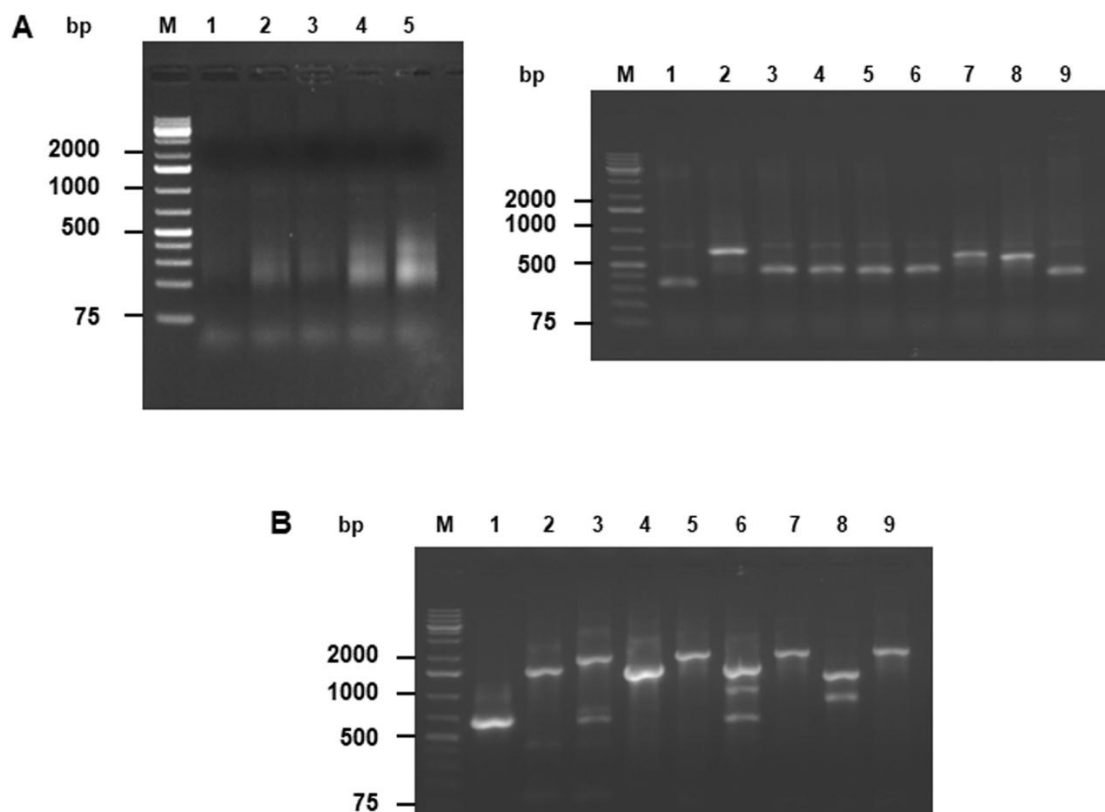
Figure 4.3-3 Construction of dicodon libraries and colony PCR of cloned peptide or protein libraries (A) Eluted dicodon inserts run on 1% agarose gel. Lane 1- Equimolar; Lane 2 - KLRT3*; Lane 3 - KLRT5*; Lane 4 - DIEL3*; Lane 5 - DIEL5*. Colony PCR of cloned colonies of KLRT library with pTRG$_{nn}$ primers. Lane M-1 kb plus DNA marker. (B) Colony PCR of various clones of human lung cDNA library with pTRG primers. Lane M -1 kb plus DNA marker.

4.3.2.2 Identification of inhibitors against IFT.

Bacterial two-hybrid studies were performed to find binders against the IFT protein. The codon optimised IFT gene was cloned into bacterial two-hybrid expression vectors, pBT$_{nn}$ and pTRG$_{nn}$. The positive clones were selected by colony PCR analysis with IFT forward and vector reverse primers, restriction digestion analysis with *Sna*BI, and finally by sequencing (Figure 4.3-4 A, B). The cloned IFT was co-transformed with libraries: *de novo* library or human lung cDNA library, and blue colonies were selected as hits. All selected hits were further segregated, and retransformed on X-gal plates to confirm interaction. Selected hits with consistent results of interaction were sequenced. This approach yielded binders against IFT protein, but even after several attempts one could not find a strong binder. One binder that displayed consistent interaction was identified but the strength of interaction was

moderate and not well enough to perform culture-based studies. Results of bacterial two-hybrid studies of IFT with its binder are presented in Figure 4.3-5. Analysis of physical parameters of identified binder, IH2, using ProtParam tool is shown in Table 4.2.
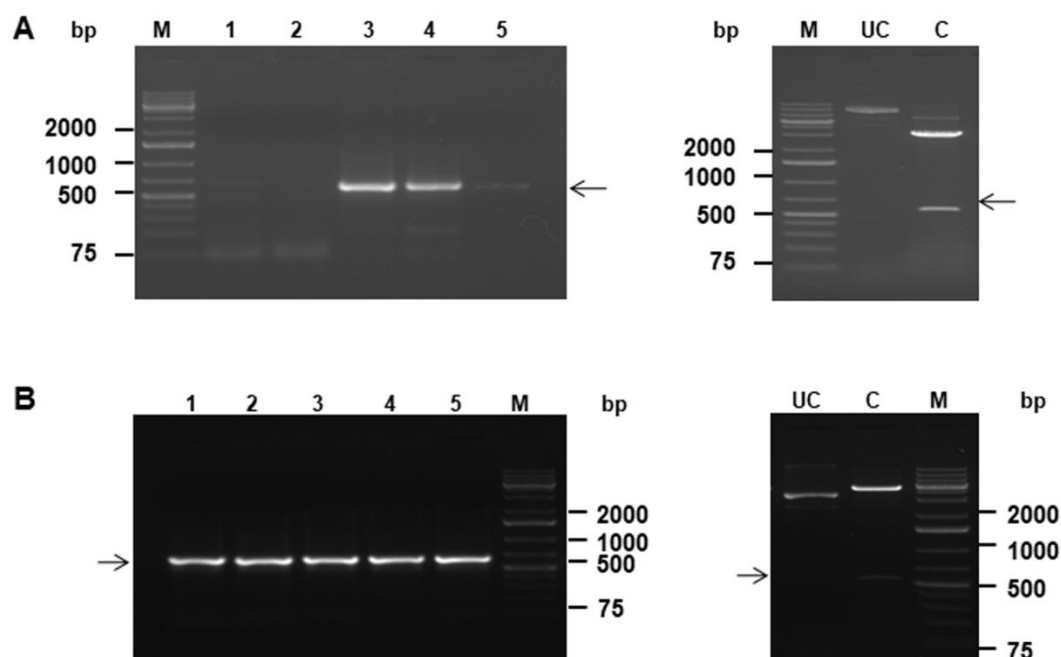
Figure 4.3-4 Cloning of IFT gene into pBT$_{nn}$ and pTRG$_{nn}$ vectors. (A) Cloning of IFT gene into pBT$_{nn}$ vector. (B) Cloning of IFT gene into pTRG$_{nn}$ vector. Colony PCR analysis of cloned colonies with IFT forward and vector reverse primers (left panel). Lane 1-5 show various clones of IFT cloned into vectors. Restriction digestion analysis of selected colony (right panel). Lane UC shows undigested plasmid, Lane C shows digested plasmid. Lane M - 1 kb plus DNA marker.
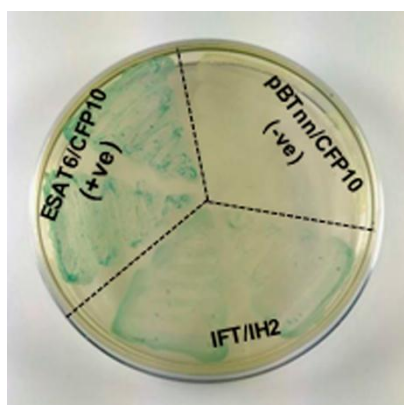

Figure 4.3-5 Identification of binders against IFT. Bacterial two-hybrid study of IFT-pBT$_{nn}$ with human lung cDNA library was performed. Liquid patch analysis of identified binder IH2 with IFT on X-gal indicator plate where colony streaks denote gene cloned in respective vectors pBT$_{nn}$ and pTRG$_{nn}$.

Gene	Protein Sequence	Amino acids	M.W. (kDa)	pI	GRAVY
IH2	VVLPQRPVHRHLPGLPPGAQPTPAPHPPAGP AAEEAGPACPPLLLHHTPESSMLRHTAARPR GYRKGLRRRL	72	7.74	11.71	-0.649

Table 4.2 Protein parameters of the identified binder IH2 were determined using ProtParam tool from the ExPASy server.

4.3.2.3 Identification of inhibitors against TNT

In order to perform bacterial two-hybrid studies to find *de novo* protein or peptide inhibitors against TNT, the first step was to clone TNT gene into pBT$_{nn}$ and pTRG$_{nn}$ vectors. For this, *Sna*B1-digested insert of TNT was ligated into dephosphorylated *Sna*BI-cut pBT$_{nn}$ and pTRG$_{nn}$ plasmids. In blunt-end cloning, incorporation of insert could be in both orientations, so it was required to confirm that insert is cloned in the right orientation. Ligated colonies were screened with gene-specific primers and around 70-80 percent colonies were found positive for presence of TNT insert; surprisingly not even a single colony was in the right orientation when screened with vector specific forward and gene specific reverse primers (Figure 4.3-6). The reason behind this could be the toxic nature of TNT and that even small amount of TNT that is expressed from the leaky expression of bacterial two-hybrid vectors leads to bacterial cell death or inhibition of colony formation. With these unexpected results, the idea to find a peptide or protein inhibitors using bacterial two-hybrid system was abandoned and we looked at the enzymatic property of TNT as an alternative strategy to find novel inhibitors against TNT protein.
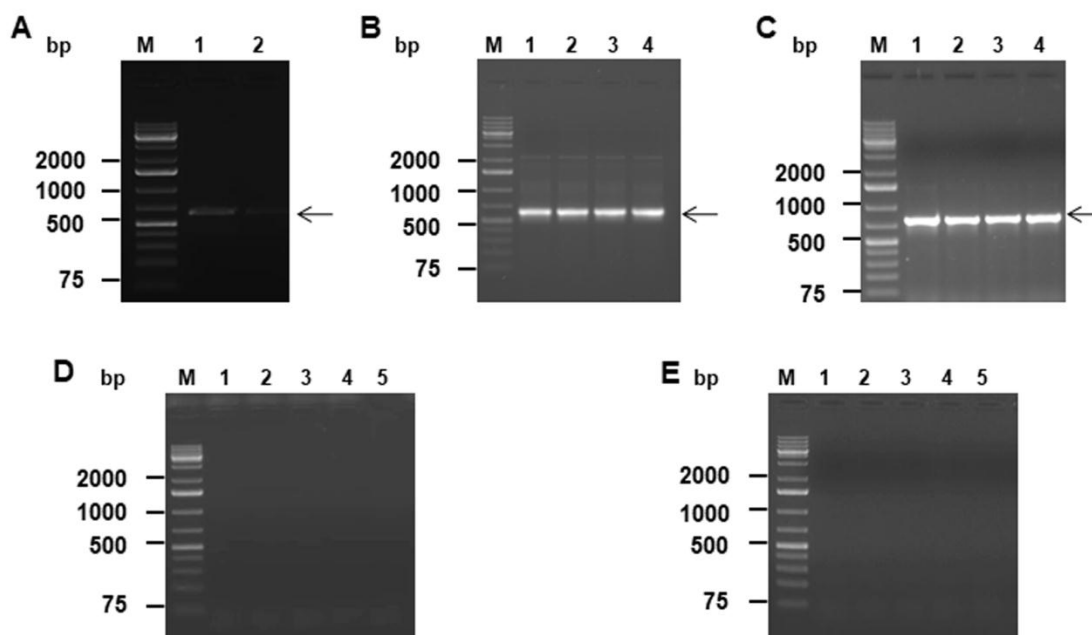
Figure 4.3-6 Cloning of TNT gene into pBT$_{nn}$ and pTRG$_{nn}$ vectors. (A) Eluted TNT insert digested with *Sna*B1. (B) Colony PCR of cloned colonies with gene specific TNT primers. (C) Colony PCR of cloned colonies with vector specific primers. (D) Colony PCR analysis of ligated insert orientation with TNT forward and pBT$_{nn}$ reverse primers. (E) Colony PCR analysis of ligated insert orientation with TNT forward and pTRG$_{nn}$ reverse primers. Lanes show various clones of TNT cloned into respective vectors. Lane M - 1 kb plus DNA marker.

4.3.3 Determination of inhibitory effect of selected drugs and compounds on NADase activity of TNT

TNT is a NAD$^+$-glycohydrolase of *M. tuberculosis* origin that like other NADases possesses a NAD$^+$ binding site [230]. TNT hydrolyses substrate NAD$^+$ into ADP-ribose and nicotinamide. For inhibition of NADase activity of TNT, these considerations were kept in mind to select drugs and compounds for further study. Decrease in NAD$^+$ content represents NADase activity. Nicotinamide is an end product of TNT-mediated NADase reaction and so its inhibitory potential on NAD$^+$-glycohydrolase activity of rTNT was evaluated. Results showed nicotinamide inhibits only 20% of rTNT NADase activity (Figure 4.3-7 A). As reported previously, the drug Pyrazinamide, a first line anti-tubercular drug, is a pyrazine analogue of nicotinamide while Ribavirin is a nucleoside analogue [413]. The NAD$^+$-glycohydrolase activity of *Streptomyces griseus* culture is known to be inhibited by

APBA (3-Aminophenylboronic acid) [414]. Based on these reports, drugs Pyrazinamide and Ribavirin, and compound APBA were selected and their inhibitory potential against rTNT NADase activity was determined. The presence of drugs Ribavirin and Pyrazinamide did not affect rTNT activity and significant reduction in NAD$^+$-glycohydrolase activity was not observed (Figure 4.3-7 A, B). In addition, around 40% reduction in NADase activity of rTNT was found in presence of APBA (Figure 4.3-7 C). Thus, our study was further extended to find potent inhibitors against TNT.
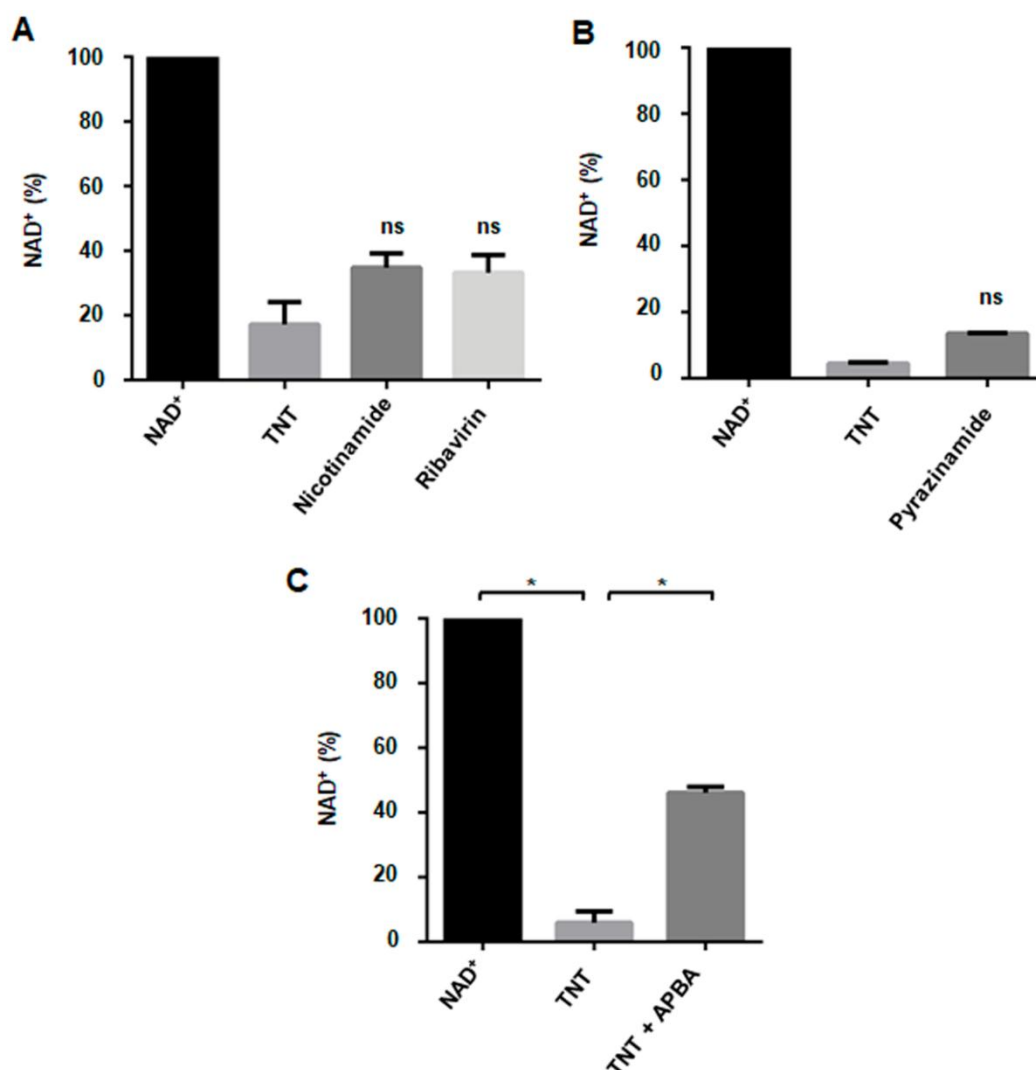
Figure 4.3-7 Evaluation of inhibitory potential of drugs and compounds against rTNT NADase activity. The NAD$^+$-glycohydrolase activity is calculated from percent decrease in NAD$^+$ content relative to control. **(A, B)** Relative NAD$^+$ levels were measured using NADH fluorescence method in the presence of drugs or compounds (100 μM) with purified TNT (75 nM) and 200 μM NAD$^+$. **(C)** Purified rTNT NADase activity measured in the presence of 1 μM APBA using enzyme coupling method where TNT (30 nM) incubated with APBA (1 μM) and 5 μM NAD$^+$ was added to start the reaction. *P* values calculated using the unpaired t-test, *$P < 0.05$.

4.3.4 Evaluation of inhibitory potential of designed NAD$^+$ analogues against TNT NADase activity

Selected drugs and compound were screened against NADase activity of TNT but only APBA exhibited around 40% reduction in TNT activity. In order to find potent inhibitors against TNT, NAD$^+$ analogues were designed and synthesized (Figure 4.3-8, Chapter 8 Reference 1). The NAD$^+$-dependent enzymes utilise NAD$^+$ as a cofactor that suggests therapeutic potential of NAD$^+$ analogues. These analogues can bind to the NAD$^+$ binding pocket of TNT, a NAD$^+$ utilizing enzyme, to inhibit its NADase activity.
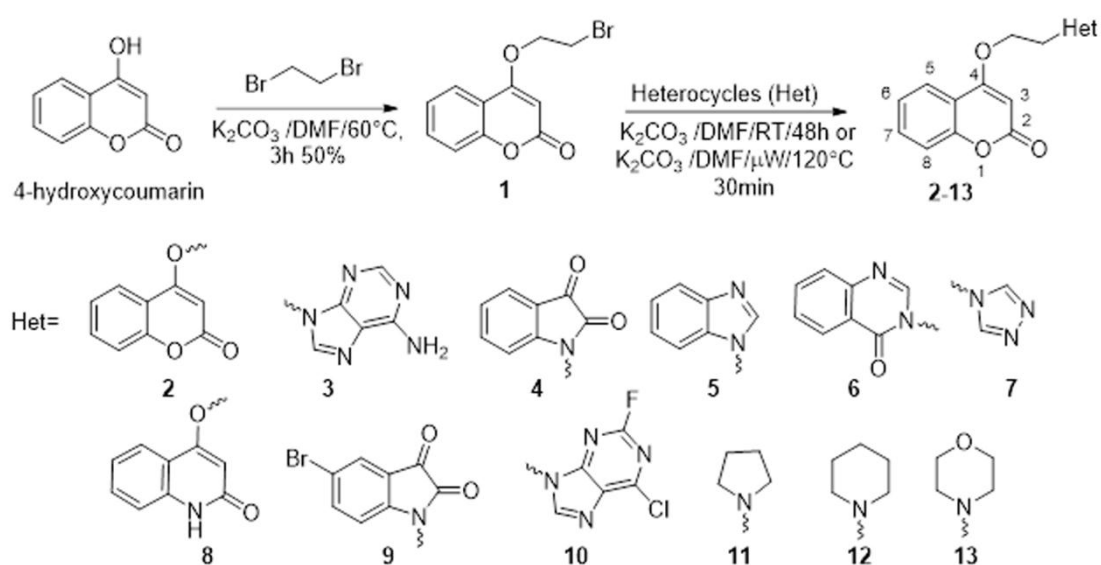
Figure 4.3-8 Scheme showing synthesis of diverse hybrid molecules (Reference 1 from Chapter 8).

4.3.4.1 Effect of designed NAD$^+$ analogues on NADase activity of rTNT

To determine the inhibitory potential of the NAD$^+$ analogues on NADase activity of TNT, the analogues were incubated with rTNT and the remaining NAD$^+$ levels were evaluated by the NADH fluorescence method. Decrease in the NAD$^+$ content represents NADase activity. Results showed molecules **1, 3, 4, 5** as moderate inhibitors, while **2, 6, 7, 11, 12, 13, 14** as weak inhibitors of rTNT NADase activity. Molecules **8, 9, and 10** were found to be the most efficient inhibitors with strong inhibitory activities (Figure 4.3-9 A). To further confirm these results a highly sensitive fluorescence based enzyme coupled assay was performed as described in Methods. Assay results further confirmed molecules **8, 9, 10** as strong inhibitors of

NADase activity of rTNT (Figure 4.3-9 B). Comparison of inhibitory potential of drugs, compounds, and synthesized NAD$^+$ analogues is presented in Figure 4.3-10. Chemical properties of compounds (Chapter 8 Reference 1) with their inhibitory potential are given in Table 4.3.
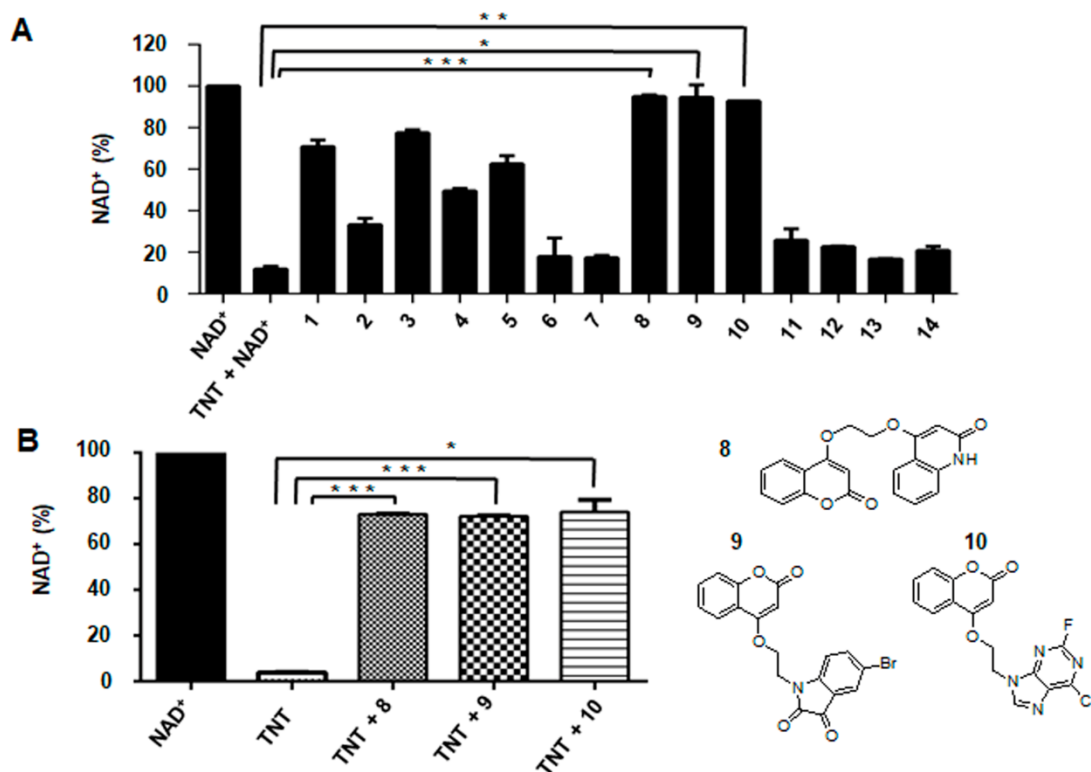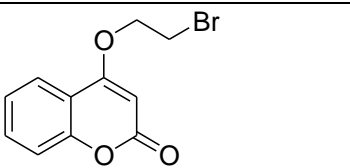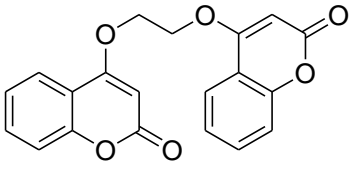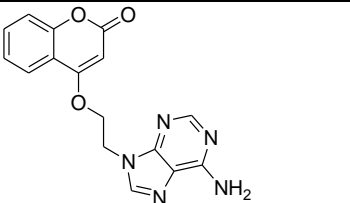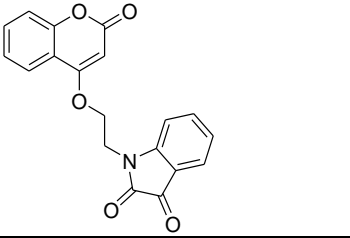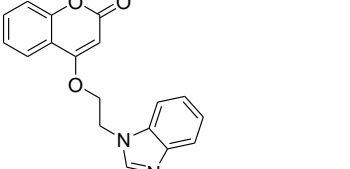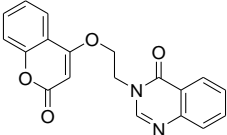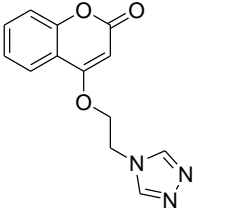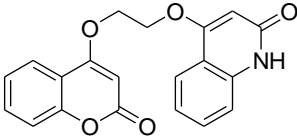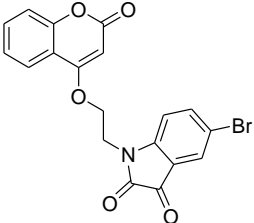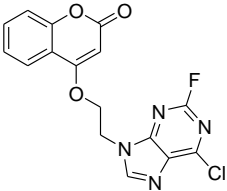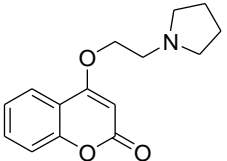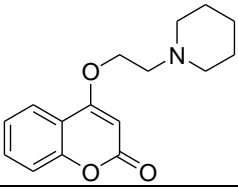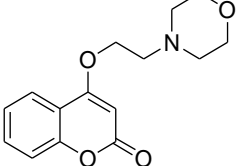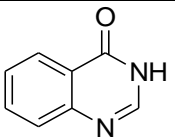
Figure 4.3-9 Effect of designed NAD$^+$ analogues on NADase activity of rTNT.

(A) Evaluation of inhibitory potential of compounds against rTNT NADase activity through NADH fluorescence assay. rTNT (75 nM) was incubated with small molecules (10 μM), following this 100 μM NAD$^+$ was added and remaining NAD$^+$ content was determined. NAD$^+$ content of control reaction without rTNT was considered as 100%. The NAD$^+$-glycohydrolase activity is calculated from percent decrease in NAD$^+$ amount. **(B)** Enzyme-coupling assay to determine the inhibitory potential of small molecules **8, 9, 10** against rTNT NADase activity. rTNT (30 nM) was incubated with 1 μM of small molecules and 5 μM NAD$^+$ and remaining NAD$^+$ levels determined. *P* values were calculated using unpaired t-test with Welch's correction, *$P<0.05$, **$P<0.01$, ***$P<0.001$.
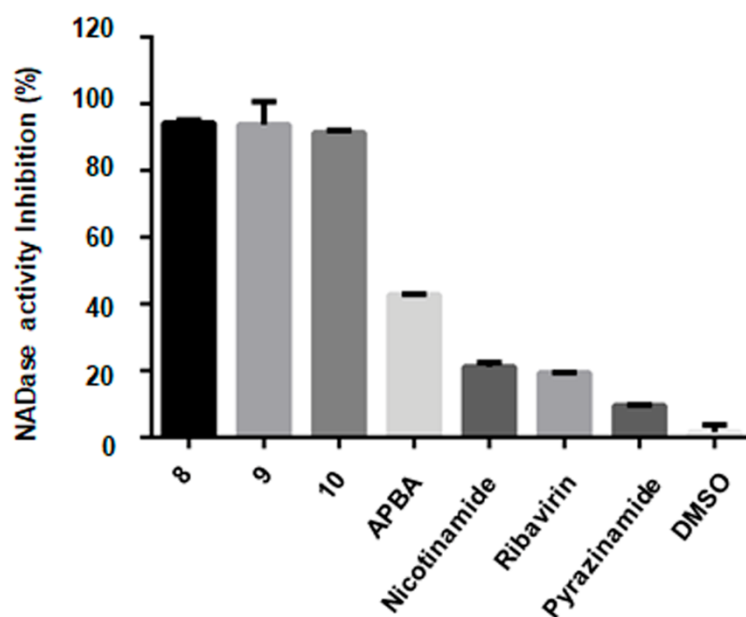
Figure 4.3-10 Percent inhibition in TNT NAD^+-glycohydrolase activity by drugs, compounds, and synthesized NAD^+ analogues.

Compounds	Compound Structure	Molecular Formula	Molecular Weight	Remaining NAD^+ %	Percent Inhibition
1		$C_{11}H_9BrO_3$	267.97	70.83	66.53
2		$C_{20}H_{14}O_6$	350.07	33.30	23.43
3		$C_{16}H_{13}N_5O_3$	323.10	77.47	74.14
4		$C_{19}H_{13}NO_5$	335.07	49.50	42.04
5		$C_{18}H_{14}N_2O_3$	306.10	62.59	57.07

6		$C_{19}H_{14}N_2O_4$	334.09	17.96	5.85
7		$C_{13}H_{11}N_3O_3$	257.08	17.38	5.16
8		$C_{20}H_{15}NO_5$	349.09	95.02	94.28
9		$C_{19}H_{12}BrNO_5$	412.98	94.53	93.71
10		$C_{16}H_{10}ClFN_4O_3$	360.04	92.88	91.82
11		$C_{15}H_{17}NO_3$	259.12	25.84	14.86
12		$C_{16}H_{19}NO_3$	273.13	22.73	11.30
13		$C_{15}H_{17}NO_4$	275.11	16.79	4.49
14		$C_8H_6N_2O$	146.04	20.92	9.23
Without inhibitor	-	-	-	12.88	-

Table 4.3 Chemical properties of hybrid small molecules and their effect on the TNT NADase activity.

4.3.4.2 Interaction study of selected NAD⁺ analogues with TNT protein

To study the interaction of small molecules **8, 9, 10** with TNT protein *in silico* studies were performed. For this, available structural information of protein complex IFT-TNT (PDB code: 4QLP) was used to prepare a homology model for the TNT protein. Small molecules were docked against TNT protein and results indicated strong binding of small molecules with NAD⁺ binding pocket of TNT (Figure 4.3-11). The interaction was mainly through hydrogen bonds (polar contacts). The strength of interaction was determined through binding affinity where small molecules **8 and 9** showed similar binding affinity and strong interaction with TNT. Small molecules 10 showed lower binding affinity and relatively weak interaction compared to these molecules (Table 4.4).

Minimum binding energy of TNT-**8**, TNT-**9**, and TNT-**10** complex was determined by Ligplot analysis and Hydrogen-bonding analysis and found to be -8.92 kcal/mol, -8.43 kcal/mol, and -7.33 kcal/mol, respectively.

TNT-8 COMPLEX

Index	Residue	AA	Distance H-A	Distance D-A	Donor Angle	Donor Atom	Acceptor Atom
1	731B	ASN	2.33	3.02	138.13	861 [Nam]	2083 [O2]
2	764B	LYS	2.06	2.85	156.34	1193 [N3]	2098 [O2]
3	764B	LYS	2.52	3.02	110.1	1192 [N3]	2102 [O2]
4	765B	TYR	3.29	3.97	137.27	1218 [N3]	2102 [O2]
5	822B	GLN	3.47	3.93	116.17	1801 [Nam]	2082 [1]
6	822B	GLN	1.65	2.63	165.83	2082 [1]	1800 [O2]
7	824B	ARG	3.55	4.07	121.99	1822 [Ng+]	2083 [O2]

TNT-9 COMPLEX

Index	Residue	AA	Distance H-A	Distance D-A	Donor Angle	Donor Atom	Acceptor Atom
1	765B	TYR	1.86	2.69	167.32	1166 [O3]	1995 [O3]

TNT-10 COMPLEX

Index	Residue	AA	Distance H-A	Distance D-A	Donor Angle	Donor Atom	Acceptor Atom
1	764B	LYS	2.1	2.9	153.46	1142 [Nam]	1992 [O2]

Table 4.4 Hydrogen bond analysis of complex TNT-8, TNT-9, TNT-10.
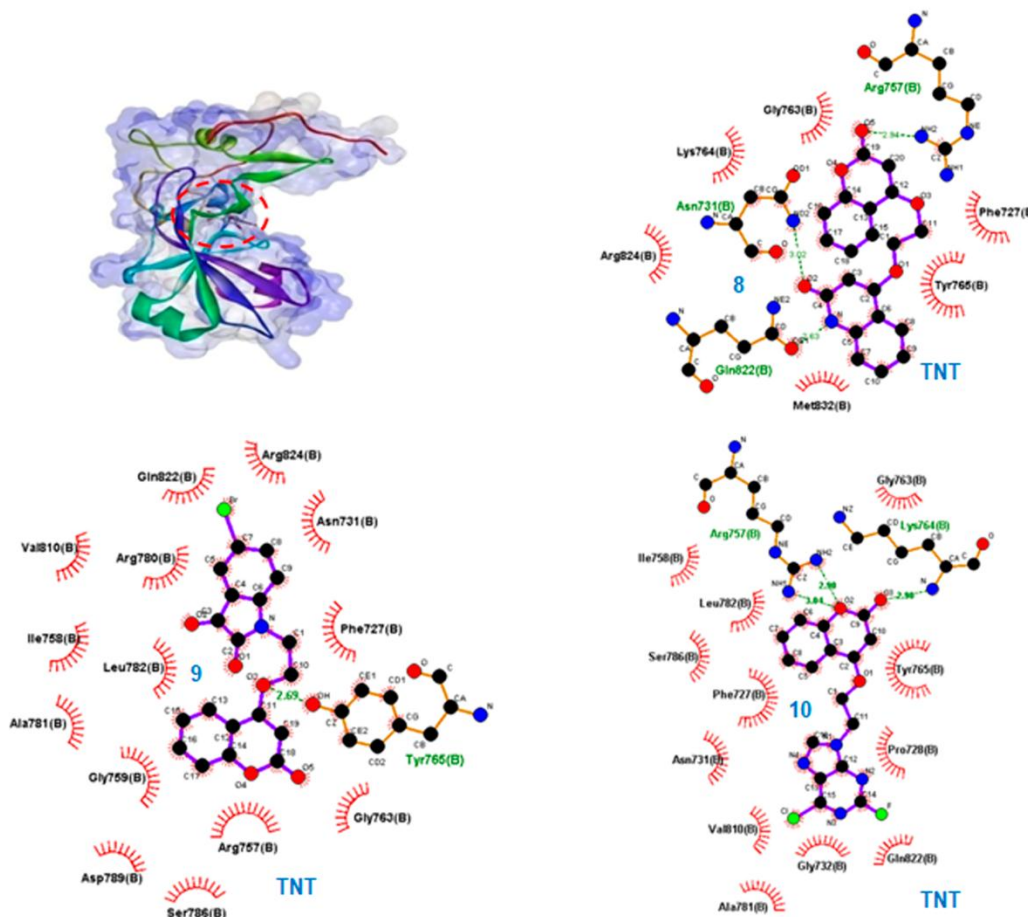
Figure 4.3-11 3D surface model of TNT-**8**, TNT-**9**, and TNT-**10** complex.

4.4 Effect of NAD$^+$ modulation on macrophage survival and *M. tuberculosis* pathogenesis

4.4.1 Effect of NAD$^+$ modulation on macrophage survival

M. tuberculosis secretes TNT into infected macrophage cytoplasm that subsequently leads to macrophage cell death by depleting intracellular NAD$^+$ levels [192, 230]. Restoration of intracellular NAD$^+$ levels could inhibit host cell death. As reported and shown in previous experiments, IFT inhibits TNT activity; therefore, it can rescue macrophages from TNT-mediated host cell death through restoration of intracellular NAD$^+$ levels.

4.4.1.1 Cloning of IFT and TNT genes in mammalian expression vectors

To study this hypothesis, TNT and IFT genes were cloned into pEGFPC1 and pCMV4$_{nn}$ vectors for expression of proteins in macrophage cells. For this, the *Sna*B1-digested IFT insert from IFT-pUC57 construct was subcloned into *Eco*Rv-cut pFLAG-CMV4$_{nn}$ vector. Screening of positive clones was performed first with colony

PCR using IFT forward and vector reverse primers followed by gene specific primers. Subsequently double digestion of positive clones was performed with restriction enzymes *Sna*B1 and *Pvu*1 (Figure 4.4-1 A). Further confirmation was carried out through sequencing. The PCR amplified *Sna*B1-digested TNT insert was ligated to *Sma*1-cut pEGFPC1 vector as described in methods. Confirmation of clones was carried out by colony PCR with gene forward and vector reverse primers followed by gene specific primers and finally through sequencing (Figure 4.4-1 B).
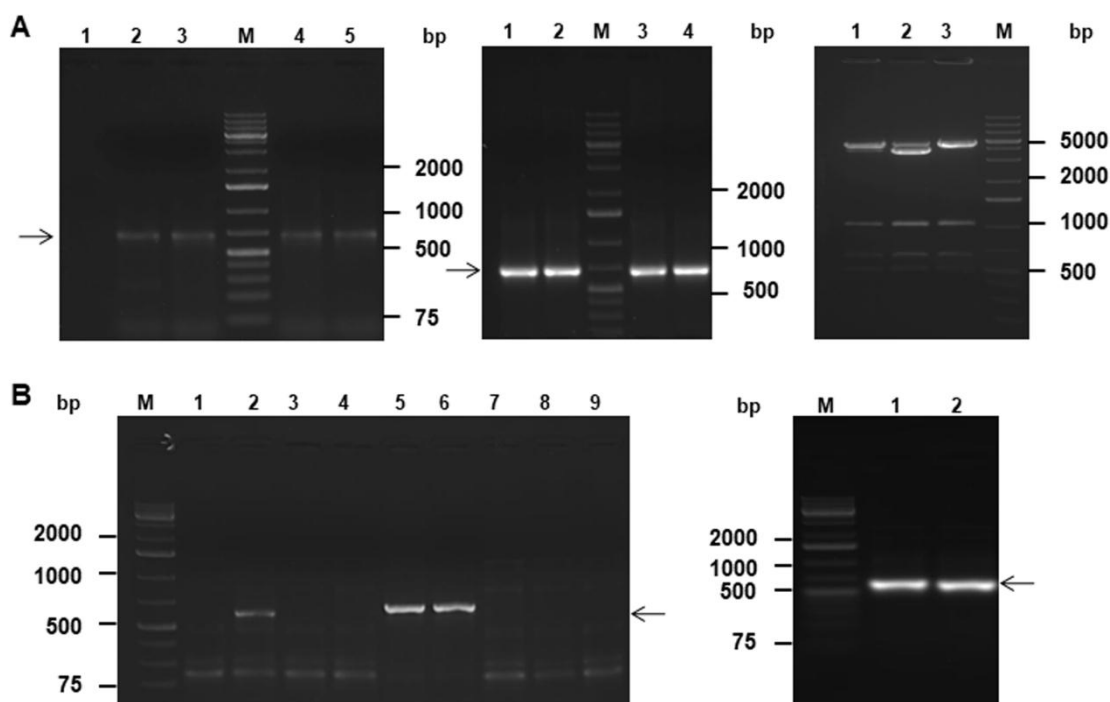
Figure 4.4-1 Cloning of IFT and TNT genes in mammalian expression vectors. (A) Cloning of IFT insert into pCMV4$_{nn}$ vector; Confirmation by colony PCR with vector forward and IFT reverse primers (left), with gene-specific primers (middle), and double digestion of positive clones with restriction enzymes *Sna*B1 and *Pvu*1. Restriction digestion of clones having insert in right orientation produces fragments of 632, 490, 4608, 1095 base pairs length. (B) Cloning of TNT insert into pEGFPC1 vector; Confirmation by colony PCR with TNT forward and vector reverse primers (left), with gene-specific primers (right).

4.4.1.2 Expression of IFT and TNT genes in macrophage cells

RAW 264.7 mouse macrophages were transfected with TNT-pEGFPC1 construct alone to deplete intracellular NAD^+ levels, or both TNT-pEGFPC1 and IFT-pCMV4$_{nn}$ constructs, to rescue NAD^+ depletion. The macrophage cells transfected with IFT-pCMV4$_{nn}$ construct and with pEGFPC1 and pCMV4$_{nn}$ vectors were used as controls. After 48 hours post-transfection, the macrophages were analysed for expression of

proteins IFT and TNT with respective gene specific primers by RT-PCR (Figure 4.4-2 A). Further confirmation of expression of proteins IFT and TNT was performed through confocal microscopic studies and western blotting using IFT and TNT specific antibodies raised against purified proteins (Figure 4.4-2 B). The TNT-pEGFPC1 construct expressed GFP-tagged TNT protein, and therefore the green fluorescence of GFP was assessed to analyse TNT expression, while to analyse IFT expression macrophages were stained with primary anti-IFT antibody and secondary Alexa Fluor 594 antibody. These results exhibited successful transfection and expression of IFT and TNT proteins in respective transfected cells.
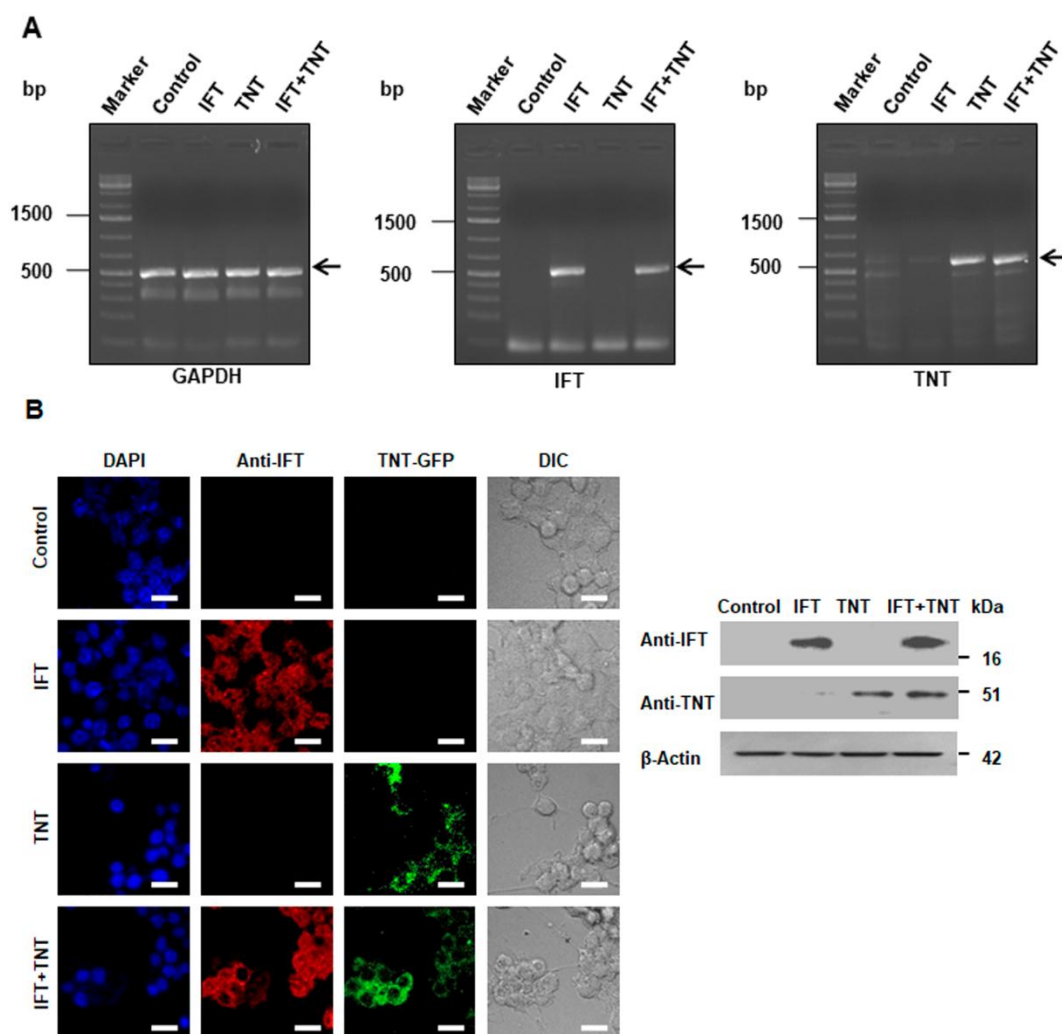
Figure 4.4-2 Expression of IFT and TNT proteins in macrophage cells after 48 hours post-transfection. (A) RT-PCR analysis of IFT and TNT transfected cells with gene-specific primers. GAPDH was used as control. (B) Macrophage cells transfected with IFT-pCMV4$_{nn}$, or TNT-pEGFPC1, or both constructs analysed by confocal microscopy (left panel) and western blotting (right panel). For confocal microscopic studies, cells were stained with anti-IFT antibody or GFP expression was analysed to detect expression of IFT and TNT proteins, respectively. Respective antibodies raised against rIFT or rTNT were used for western blot analysis. β-Actin was used as loading control. Scale bar 25 μm, enlarged 10 μm.

4.4.1.3 Impact of NAD$^+$ modulation through TNT on macrophage cells survival and its reversion by IFT expression

To study the effect of TNT-mediated NAD$^+$ modulation on macrophage cell death, transfected cells expressing TNT, or IFT, or both proteins, were cultured for 48 hours after transfection and MTT assay was conducted to analyse cell viability. Macrophage cells transfected with TNT-pEGFPC1, expressing TNT, showed increased cell death as determined though MTT assay. In contrast, cell viability significantly increased when IFT was expressed with TNT in macrophages, which indicated that expression of IFT restored host intracellular NAD$^+$ levels and further rescued macrophage cells from TNT-mediated cell death (Figure 4.4-3 A). In addition, TNT expressing macrophages showed higher number of PI positive cells compared to other groups of transfected macrophages which further confirms effect of expression of TNT and IFT on macrophage cell death (Figure 4.4-3 B). These results were validated by determination of NAD$^+$ levels of transfected macrophages where NAD$^+$ levels of TNT expressing macrophages were found significantly low but increased in the presence of IFT with TNT. The NAD$^+$ levels of IFT expressing macrophages were found similar to control macrophages, transfected with vectors only (Figure 4.4-3 C). These results demonstrated the role of intracellular NAD$^+$ levels in host cell survival.

HMGB1 secretion is a known marker for programmed necrosis. In healthy or apoptotic cells HMGB1, a chromatin binding protein, primarily localizes in the nucleus. However, in necroptotic cells, it is distributed throughout the cytoplasm and finally secreted into extracellular environment [415]. The transfected cells were analysed for the HMGB1 localisation using confocal microscopy and western blotting (Figure 4.4-3 D). Confocal microscopic studies showed that in the control and IFT expressing macrophages, HMGB1 was localised in the nucleus similar to healthy cells. In contrast, analysis of TNT expressing macrophages showed a nucleus to cytoplasmic translocation and distribution of HMGB1 throughout the cytoplasm. Importantly, HMGB1 was retained in the macrophage nucleus, expressing both TNT and IFT proteins (Figure 4.4-3 D, left panel). Western blot analysis of nucleus and cytoplasmic fractions of different groups of transfected macrophages confirm these findings. These results were corroborated by HMGB1 level determination in the culture supernatant through western blotting. The level of HMGB1 protein in the culture supernatant of TNT expressing macrophages was significantly higher than the

other controls and much decreased in TNT and IFT co-expressing macrophages (Figure 4.4-3 D, right panel). These results confirm that TNT-mediated NAD$^+$ depletion leads to programmed necrosis of macrophages which could be reverted by restoration of NAD$^+$ levels by IFT.
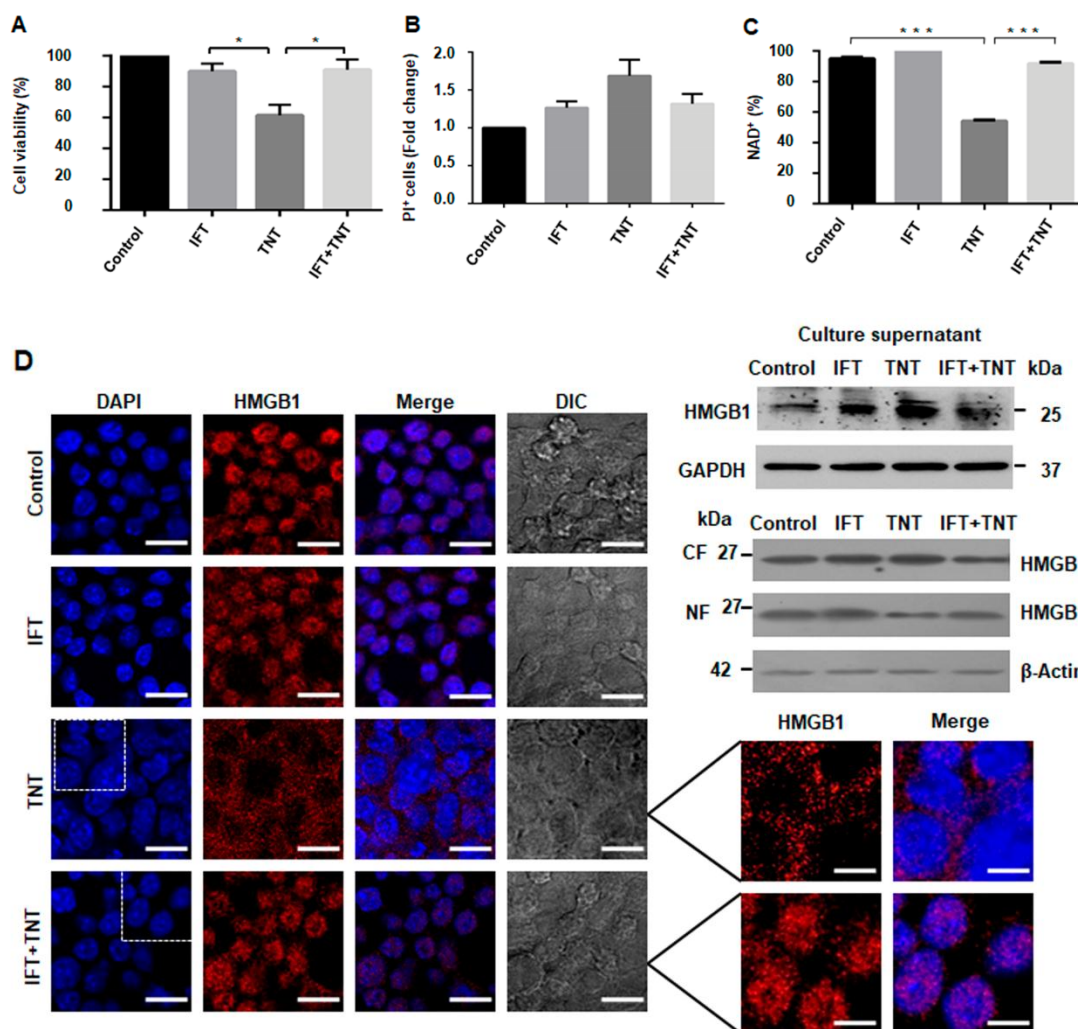
Figure 4.4-3 Effect of TNT expression on macrophage cells survival and its reversion by IFT. (A) Determination of cell viability by MTT assay in different sets of transfected macrophages. (B) Cell death analysis by PI staining of transfected macrophages using flow cytometry. (C) Evaluation of intracellular NAD$^+$ levels of transfected macrophages. (D) Analysis of nucleus to cytoplasmic translocation of HMGB1 through confocal microscopy (left panel). Determination of HMGB1 levels by western blotting in the culture supernatant (right upper panel) and in the nuclear and cytoplasmic fractions of transfected macrophages (right lower panel). β-Actin or GAPDH was used as loading control. *P* values measured using unpaired t-test, *P<0.05, **P<0.01, ***P< 0.001. Insets show magnifications of cells. Scale bar 25 μm, enlarged 10 μm.

4.4.2 Effect of host intracellular NAD$^+$ levels on *M. tuberculosis* pathogenesis

M. tuberculosis promotes necrosis of infected macrophages to facilitate its intracellular growth and evasion from host defense system [166, 192]. Recent studies have shown TNT-mediated NAD$^+$ depletion as a major cytotoxicity factor for the induction of necroptosis of infected macrophages [192, 230]. Previous results of *E.coli* and macrophage experiments have shown reversion of toxic effect of TNT by NAD$^+$ restoration through IFT expression (Figure 4.1-3, 4.4-3). The IFT-mediated NAD$^+$ restoration of *M. tuberculosis*-infected macrophages could also inhibit host cell death and intracellular mycobacterium growth. Therefore, IFT expressing macrophages were examined for the intracellular growth of *M. tuberculosis* and infected macrophage survival.

4.4.2.1 Analysis of intracellular *M. tuberculosis* growth inside IFT expressing macrophage

To study whether intracellular NAD$^+$ modulation has an impact on growth and survival of *M. tuberculosis*, the IFT-pCMV4$_{nn}$ construct was transfected in RAW264.7 murine macrophages and cells were further infected with *M. tuberculosis*. Macrophages were examined for the intracellular growth of *M. tuberculosis* through confocal microscopic studies; results showed IFT expression in macrophages leads to significant reduction in the percentage of *M. tuberculosis* H37Rv-GFP infected macrophages compared to control macrophages, transfected with pCMV4$_{nn}$ vector only (Figure 4.4-4 A). In addition, intracellular growth of *M. tuberculosis* was also determined through CFU count. The CFU count of *M. tuberculosis* H37Rv in IFT expressing macrophages was found significantly low after 72 hours of infection compared to control (Figure 4.4-4 B). In order to validate the association of intracellular NAD$^+$ levels with survival of *M. tuberculosis* inside the transfected macrophages, the intracellular NAD$^+$ levels were evaluated. The result revealed significant reduction in the NAD$^+$ levels of *M. tuberculosis*-infected macrophages that were increased with IFT expression in infected cells compared to uninfected control (Figure 4.4-4 C). These findings indicated the significance of intracellular NAD$^+$ restoration through IFT in control of *M. tuberculosis* infection and suggested therapeutic potential of NAD$^+$ restoration in treatment of tuberculosis.
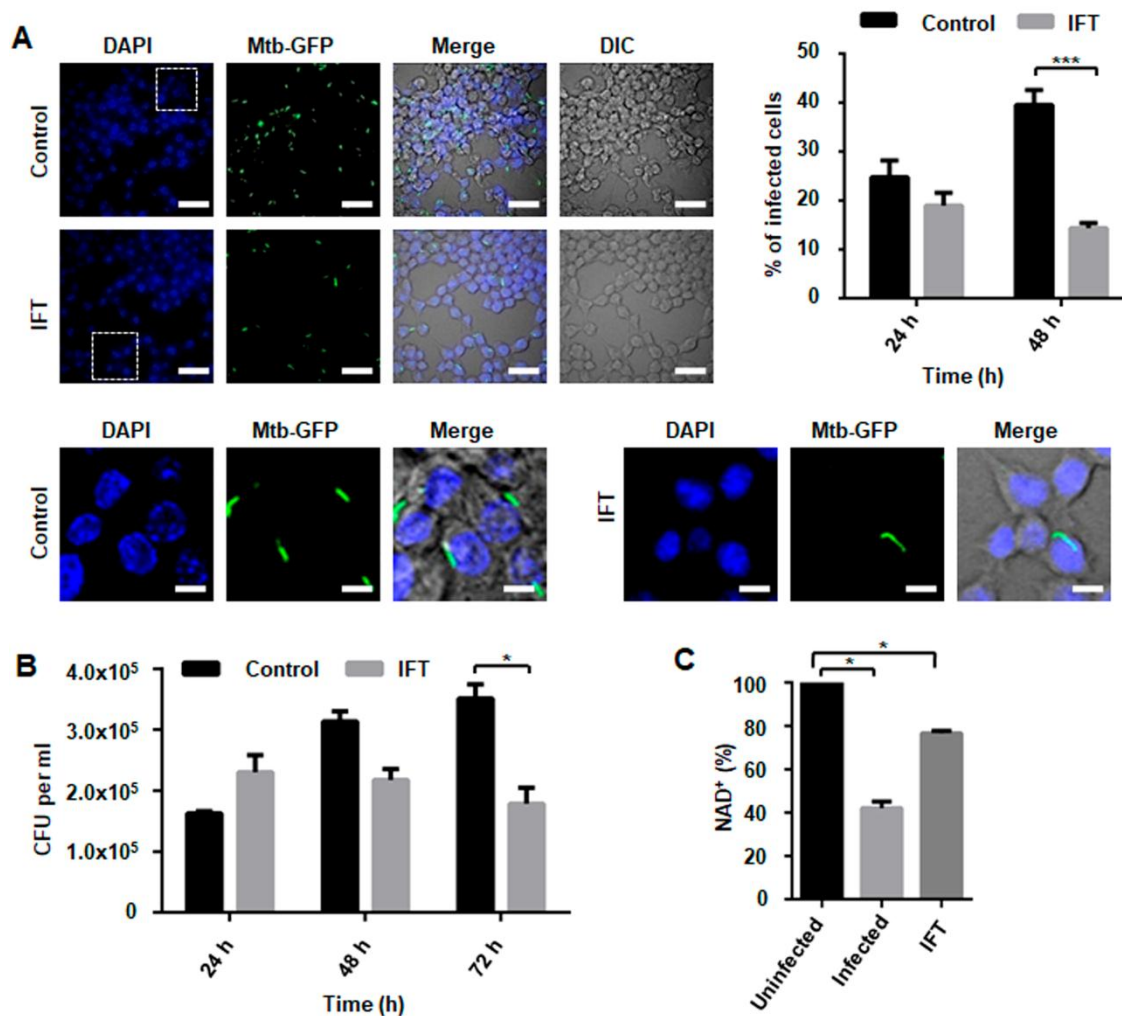
Figure 4.4-4 Determination of *M. tuberculosis* viability in IFT-expressing macrophages. The control and IFT-expressing RAW 264.7 macrophage cells were infected at 10:1 MOI with *M. tuberculosis* H37Rv or H37Rv-GFP strain and *M. tuberculosis* viability was determined at different time points. (A) Confocal microscopic study showing infection pattern of *M. tuberculosis* H37Rv-GFP in RAW 264.7 cells. DAPI was used to stain nuclei. (B) Analysis of colony forming units (CFUs) per milliliter of intracellular *M. tuberculosis* at different time points after infection. (C) Intracellular NAD^+ content of uninfected, *M. tuberculosis* H37Rv-infected control and IFT transfected infected macrophages measured using enzyme-coupling assay. The NAD^+ level of uninfected cell was considered as 100%. Unpaired t-tests with Welch's correction was used to calculate significance of difference. $*P < 0.05$, $***P < 0.001$. Scale bar 50 μm, enlarged image 10 μm.

4.4.2.2 Effect of NAD^+ restoration on *M. tuberculosis*-infected macrophage survival

Previous experiments on *M. tuberculosis*-infected macrophages have shown that maintaining NAD^+ homeostasis through IFT expression significantly reduces *M. tuberculosis* viability. To further evaluate whether maintaining NAD^+ levels of

infected macrophage is associated with macrophage survival that leads to reduction in *M. tuberculosis* viability, macrophage cell death was analysed by Annexin-V and PI staining and HMGB1 translocation. Significant reduction in number of Annexin-V and PI positive cells was observed in IFT-expressing infected macrophages compared to the control infected macrophages (Figure 4.4-5).
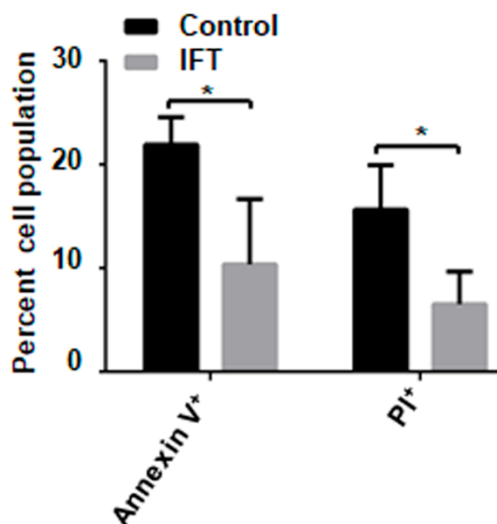
Figure 4.4-5 Cell death analysis of *M. tuberculosis*-infected macrophages expressing IFT through flow cytometry. Annexin-V and PI stained infected macrophages transfected with IFT construct or with vector only were analysed after 48 hours of transfections. Statistical significance was determined using unpaired t-test, *$P<0.05$.

Next, HMGB1 levels of different groups were determined. Confocal microscopic studies were conducted to examine the nuclear to cytoplasmic translocation of HMGB1 protein. The results showed translocation of HMGB1 protein from nucleus to cytoplasm in control infected macrophages. However, it was retained in the nucleus of uninfected and IFT-expressing infected macrophages (Figure 4.4-6 A). Translocation of HMGB1 was further confirmed through western blot analysis of nucleus and cytoplasmic fractions of *M. tuberculosis*-infected, IFT-transfected and control macrophages (Figure 4.4-6 B, left panel). In addition, HMGB1 levels in culture supernatant of different groups of macrophages were also analysed using western blotting. Increased level of HMGB1 protein was detected in the culture supernatant of *M. tuberculosis*-infected macrophages, which was reduced by expression of IFT (Figure 4.4-6 B, right panel). Secretion of HMGB1 into culture supernatant or its cytoplasmic translocation is an important marker of necrotic cell death. More importantly, macrophages expressing IFT showed retention of HMGB1

in nucleus and significant reduction in HMGB1 levels in culture supernatant that suggests cells did not undergo necrotic cell death and activation of host defense mechanism could be the reason behind decrease in *M. tuberculosis* viability.
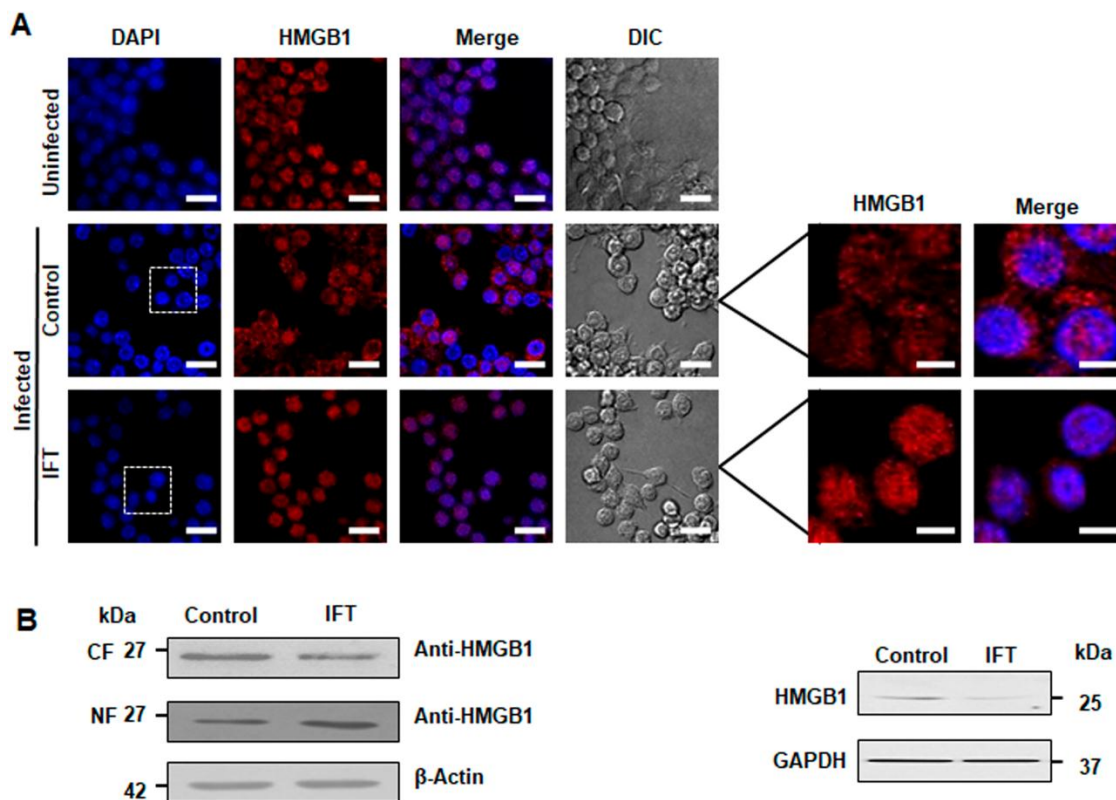
Figure 4.4-6 Analysis of HMGB1 translocation in *M. tuberculosis*- infected macrophages expressing IFT. Infected macrophages expressing IFT were analysed compared to controls infected cells and uninfected cells after 48 hours post-transfection. (A) Confocal microscopic images showing translocation of HMGB1 protein from nucleus to cytoplasm. Scale bar 25 µm. Enlarged image 10 µm. (B) Western blotting to analyse HMGB1 levels in the nuclear and cytoplasmic fractions (left panel), and culture supernatant (right panel) of different sets of macrophages. β-Actin or GAPDH was used as loading control.

4.5 Effect of NAD$^+$ modulation on human erythrocyte survival and *P. falciparum* pathogenesis

Depletion of intracellular NAD$^+$ levels induces host cell death in different cell types [192, 357, 402]. Eryptosis of erythrocytes is reported to play an important role in the intra-erythrocytic survival of *P. falciparum* [270, 396]. Studies have suggested increased intra-erythrocytic NAD$^+$ levels of infected erythrocytes facilitate *P.*

falciparum infection [336, 400]. However, significance of NAD$^+$ modulation in the eryptosis of erythrocytes and *P. falciparum* infection has not been explored. Here, TNT, a NAD$^+$-glycohydrolase of *M. tuberculosis* origin, was used to modulate the intra-erythrocytic NAD$^+$ levels and further studies were performed to determine its role in erythrocyte survival and *P. falciparum* pathogenesis.

4.5.1 Effect of NAD$^+$ modulation on erythrocyte survival

4.5.1.1 Loading of erythrocytes with recombinant proteins

To modulate intra-erythrocytic NAD$^+$ levels, erythrocytes were loaded with rTNT and rIFT proteins. The erythrocyte loading was performed using hypotonic pre-swelling method as described previously, by preparing erythrocyte ghosts and further encapsulation of recombinant proteins [411]. Studies have reported various drugs and proteins could be loaded efficiently in the erythrocyte ghosts [411, 416, 417]. The FITC-dextran (70 kDa) was encapsulated with rTNT protein or control protein BSA to determine loading efficiency. The results of FACS analysis and confocal microscopic studies showed homogenous and efficient loading of erythrocytes. Loaded erythrocytes with proteins rTNT, or rIFT, or both, were evaluated by specific antibodies against these proteins through western blotting, that confirmed the efficient and specific loading of erythrocytes (Figure 4.5-1). Collectively, these data show efficient loading and retention of cargo protein in loaded erythrocytes.
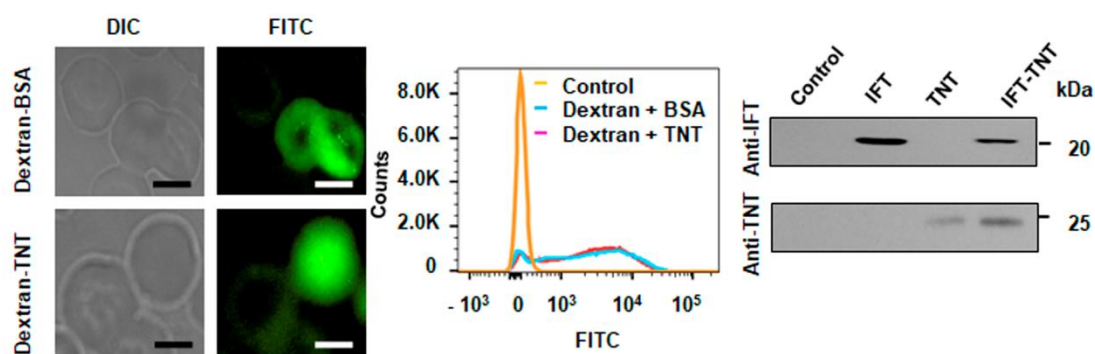
Figure 4.5-1 Evaluation of loading efficiency of recombinant proteins in human erythrocytes by microscopic studies and western blot analysis. Dextran-FITC with BSA or Dextran-FITC with rTNT loaded erythrocytes were analysed by microscopic imaging (left), and flow cytometry (middle); western blot analysis of recombinant proteins loaded erythrocytes with anti-IFT or anti-TNT antibody (right). Scale bar 5 μm.

4.5.1.2 Effect of intra-erythrocytic NAD$^+$ levels on induction of eryptosis

Next, effect of NAD$^+$ modulation through loaded recombinant proteins was evaluated on the eryptosis induction by determining markers of eryptosis, such as phosphatidylserine exposure on the cell surface, cell shrinkage, increased ROS levels and elevation in cytosolic calcium ion levels (Figure 4.5-2, 4.5-3) [277].

Loaded erythrocytes were incubated at 37 °C for 48 hours and evaluated for cell surface exposure of phosphatidylserine by staining with FITC-labeled Annexin-V. The stained erythrocytes were analysed through confocal microscopy and flow cytometry. The confocal microscopic studies showed Annexin-V binding on the surface of erythrocytes loaded with rTNT protein (Figure 4.5-2 A, left). Erythrocytes were examined in parallel by flow cytometric analysis that showed increased percentage of Annexin-V positive erythrocytes compared to other controls, thus corroborated with results of confocal studies (Figure 4.5-2 A, right, 4.5-3 A). Simultaneously, erythrocytes shrinkage reflected by forward scatter was determined through FACS analysis. The rTNT-loaded erythrocytes exhibited significant decrease in forward scatter reflecting erythrocyte shrinkage compared to recombinant IFT-loaded and control erythrocytes (Figure 4.5-2 B, left, 4.5-3 B). These results indicated induction of eryptosis of rTNT-loaded erythrocytes, and for further confirmation additional markers of eryptosis were analysed. For this, the reactive oxygen species formation was determined by using 2',7'-dichlorodihydrofluorescein diacetate (DCFDA). The rTNT-loaded erythrocytes exhibited increased ROS generation represented by increased DCFDA fluorescence compared to control and rIFT-loaded erythrocytes (Figure 4.5-2 B, middle, 4.5-3 C). Further experiments to evaluate cytosolic Ca^{2+} activity by determining Fluo-4AM fluorescence was performed. The elevation in cytosolic Ca^{2+} activity was detected in rTNT-loaded erythrocytes (Figure 4.5-2 B, right, 4.5-3 D). Analysis of eryptosis markers suggested induction of eryptosis in erythrocytes loaded with rTNT. To further study whether the NAD$^+$ depletion through rTNT is associated with induction of eryptosis, the intra-erythrocytic NAD$^+$ levels of loaded erythrocytes were determined. As expected, after incubation of 48 hours NAD$^+$ levels of erythrocytes loaded with rTNT significantly decreased, approximately 80 percent, while they remained similar to control erythrocytes in the presence of rIFT with rTNT (Figure 4.5-4). Altogether, these

results suggested significant role of intra-erythrocytic NAD$^+$ levels in eryptosis induction.
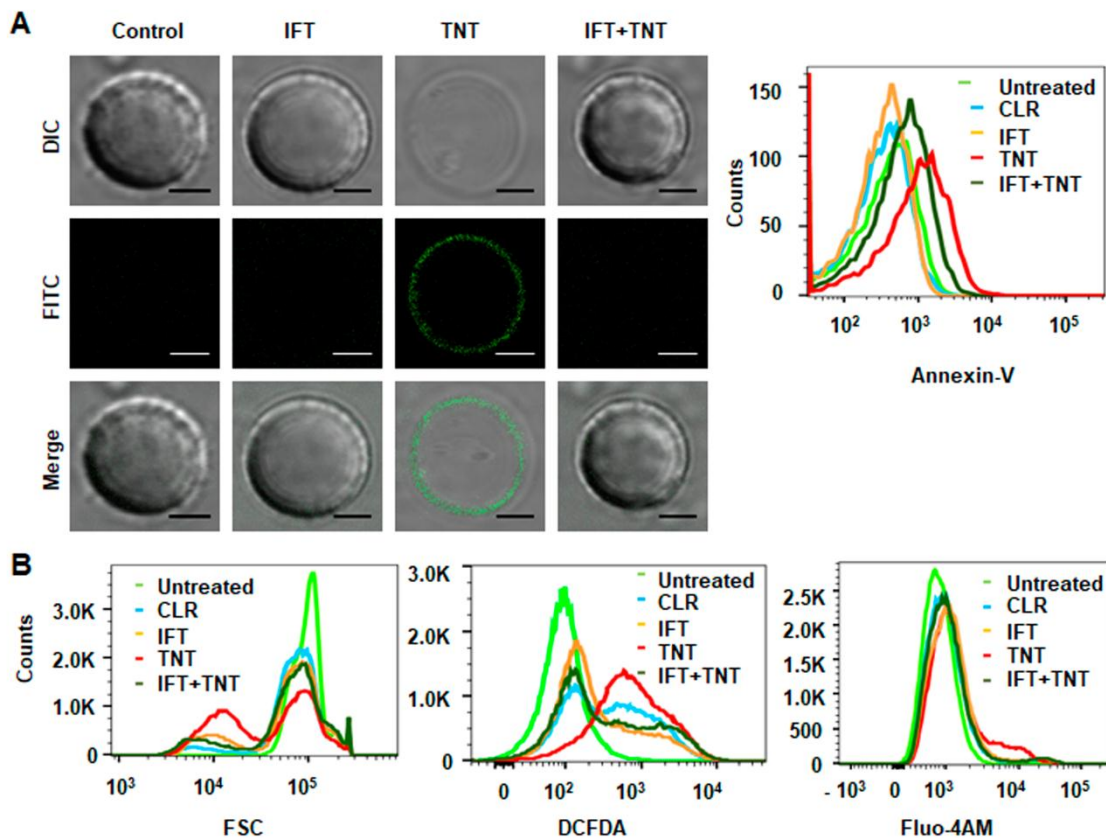
Figure 4.5-2 Evaluation of eryptosis induction in recombinant protein loaded erythrocytes. (A) Confocal microscopic analysis of recombinant protein loaded-erythrocytes for Annexin-V binding (left), Histogram showing Annexin-V binding on erythrocyte surface representing phosphatidylserine exposure at cell surface (right). (B) Histogram showing other eryptosis markers cell shrinkage, ROS formation, and cytosolic Ca^{2+} activity through determination of forward scatter (left), DCFDA (middle), and Fluo-4AM fluorescence (right), respectively. Scale bar 4 μm.
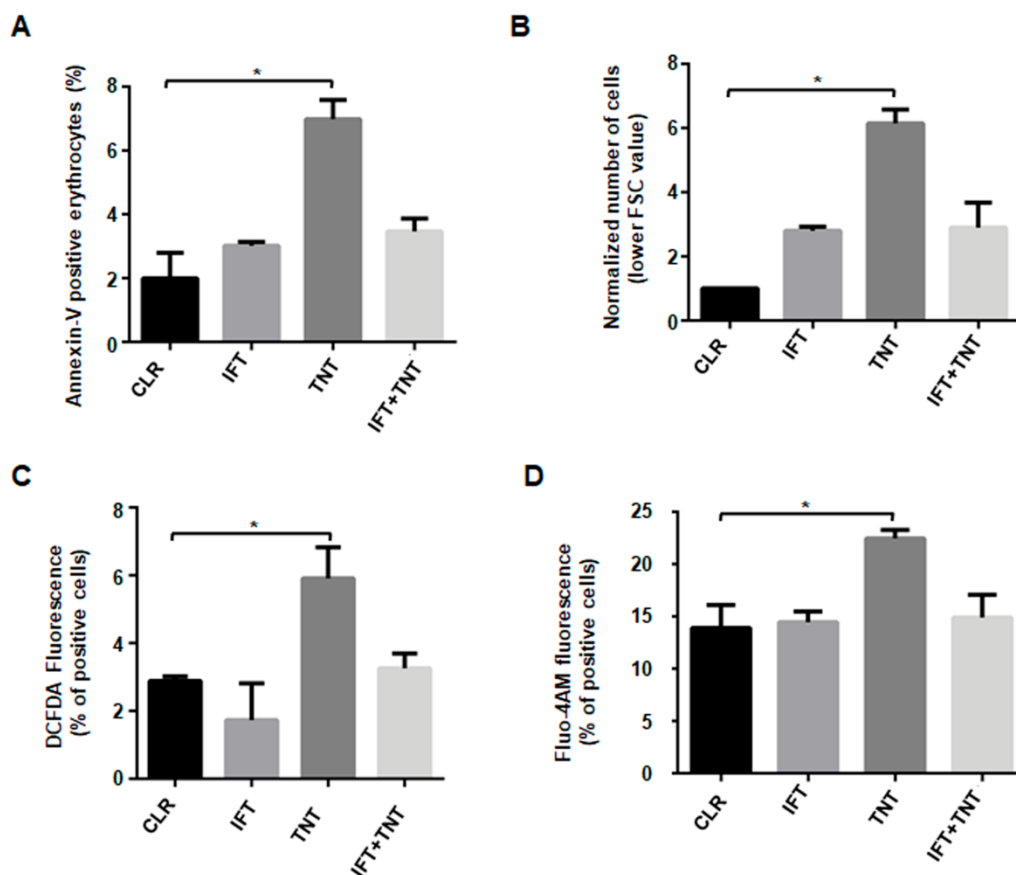
Figure 4.5-3 Percentage analysis of eryptotic erythrocytes loaded with recombinant proteins. Loaded-erythrocytes were evaluated after 48 hours of incubation at 37 °C. (A) Percentage of Annexin-V positive erythrocytes. (B) Analysis of Forward scatter. Decreased forward scatter reflecting cell shrinkage observed in TNT-loaded erythrocytes compared to control. Normalised number of erythrocytes with decreased forward scatter compared to control is shown. (C) Percentage of erythrocytes showing DCFDA fluorescence. (D) Percentage of Fluo-4AM fluorescence positive erythrocytes. Statistical significance of data was calculated from student t-test, $*P<0.05$.
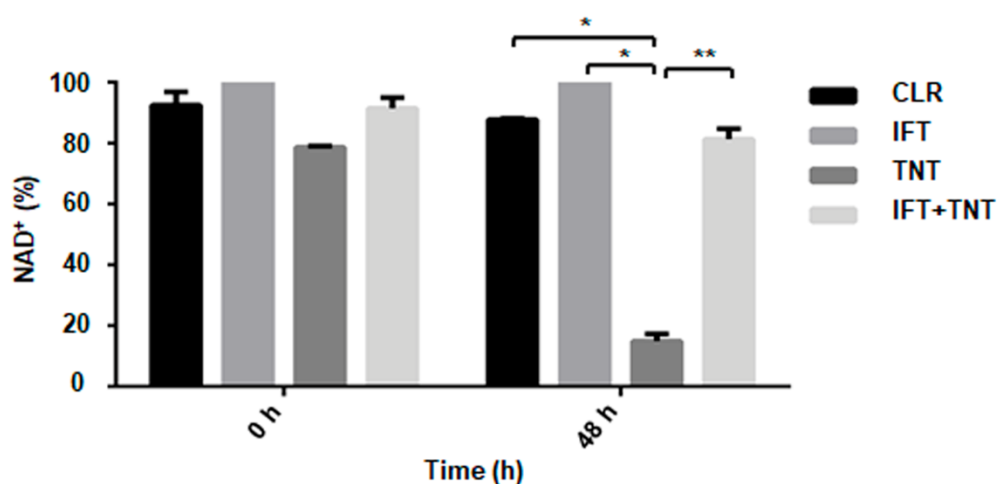
Figure 4.5-4 Determination of NAD$^+$ levels of erythrocytes loaded with recombinant proteins. Control erythrocytes and rIFT, or rTNT, or both loaded erythrocytes were analysed at initial time point and after 48 hours of incubation. *P* values were calculated from student t-test with Welch's correction, $*P<0.05$, $**P<0.01$, $***P< 0.001$.

4.5.2 Effect of NAD$^+$ modulation on *P. falciparum* pathogenesis

In order to determine the significance of intra-erythrocytic NAD$^+$ levels on growth and infection progression of *P. falciparum*, the control and respective proteins, rTNT or rIFT or both, loaded erythrocytes were infected with schizont stage parasites. The parasite growth was examined by analysing Giemsa stained culture smears at different time points that showed significant decrease in *P. falciparum* amplification in rTNT-loaded erythrocytes compared to other controls. Microscopic imaging results indicated invasion defect as number of attached merozoites on erythrocytes surface were increased with decreased ring formation in rTNT-loaded erythrocytes after 56 hours of infection (Figure 4.5-5 A). The results exhibited the parasitemia of erythrocytes loaded with rTNT was decreased by 2.5 folds compared to control. In contrast, parasitemia was increased compared to control when rIFT was loaded with rTNT. The rIFT-loaded erythrocytes showed parasitemia comparable to control and rIFT with rTNT loaded erythrocytes (Figure 4.5-5 B). To further analyse the invasion defect, counting of number of rings produced from a single schizont was performed for different sets of loaded erythrocytes during second cycle of infection. The presence of rTNT drastically decreased the number of ring-stage parasites; interestingly, the effect was reverted by rIFT when loaded with rTNT (Figure 4.5-5 C). The previous results of rTNT-loaded erythrocytes showed that decrease in intra-erythrocytic NAD$^+$ content elicits eryptosis of erythrocytes. This could be the possible reason that induction of premature eryptosis due to decrease in intra-erythrocytic NAD$^+$ levels leads to formation of unhealthy merozoites and further invasion defects with decreased parasitemia. Previous reports suggesting requirement of higher NAD$^+$ levels for *P. falciparum* infection are supported by these results. These results represent a novel finding in the pathogenesis of *P. falciparum*, where intra-erythrocytic NAD$^+$ depletion leads to eryptosis that further decelerates *P. falciparum* growth.
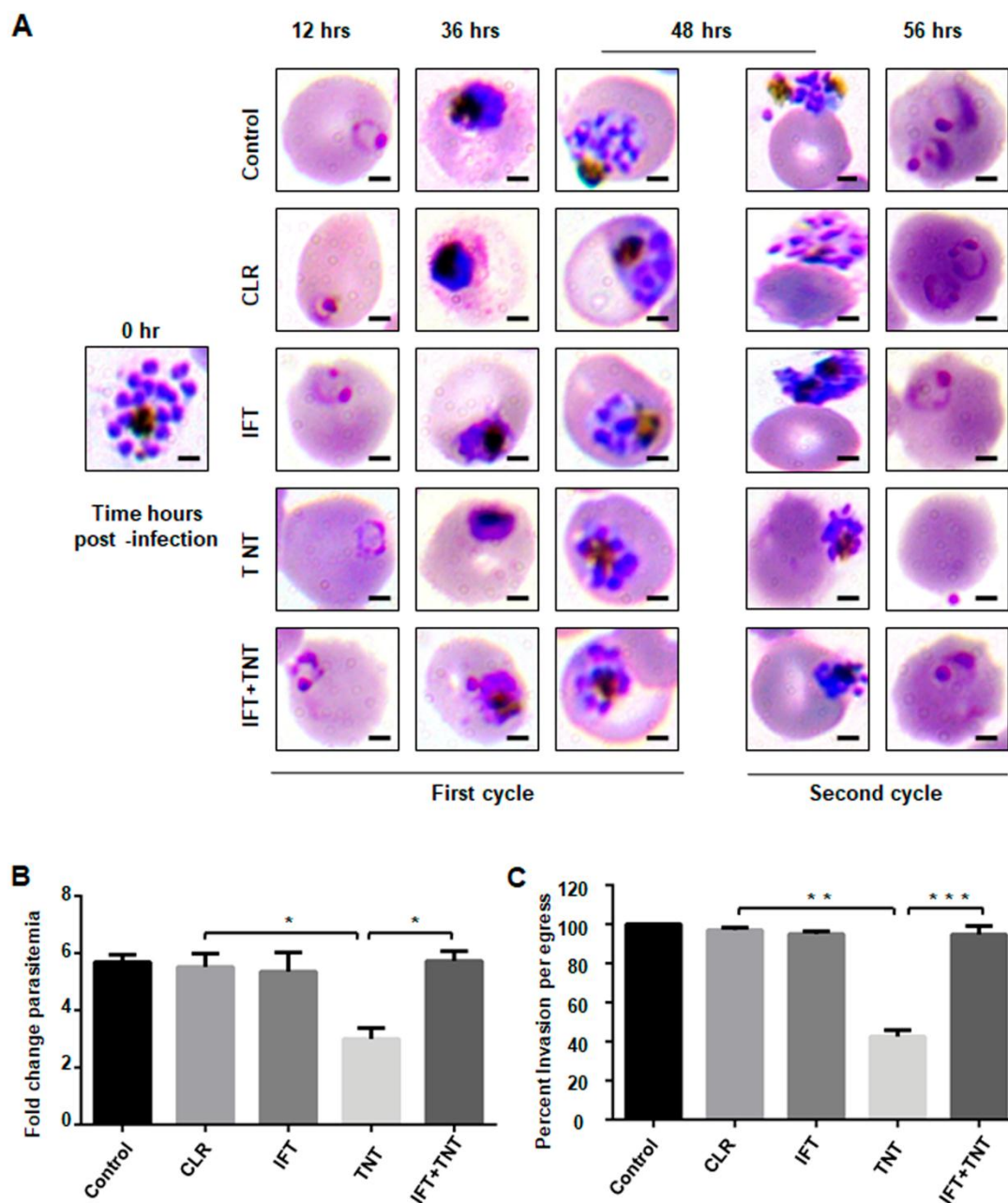
Figure 4.5-5 Effect of NAD⁺ modulation on *P. falciparum* pathogenesis. Erythrocytes loaded with recombinant proteins were infected with schizont stage *P. falciparum* parasites and analysed at different time points. (A) Giemsa-stained culture smears were analysed at different time points after infection using Light microscopic imaging. Scale bar 2 μm. (B) Fold change in parasitemia after 48 hours of infection compared to control at the time of infection, and (C) Percent invasion determined after 56 hours of *P. falciparum* infection. *P* values were calculated from student t-test with Welch's correction, *$P<0.05$, **$P<0.01$, ***$P< 0.001$.

4.6 To study effect of selected NAD$^+$ analogues on intracellular pathogenesis

M. tuberculosis secretes TNT, a NAD$^+$ glycohydrolase, to modulate host NAD$^+$ homeostasis by depleting intracellular NAD$^+$ pool [230]. NAD$^+$ modulation through TNT has significant role as it induces host necroptosis and facilitates *M. tuberculosis* survival [192]. As results depicted in Figure 4.4-4 show, inhibition of TNT by IFT has therapeutic potential for *M. tuberculosis* treatment. Results also showed a novel finding that intra-erythrocytic NAD$^+$ depletion elicits eryptosis of human erythrocytes (Figure 4.5-2, 4.5-3, 4.5-4). More importantly, depletion of intra-erythrocytic NAD$^+$ levels affects parasite invasion and *P. falciparum* growth (Figure 4.5-5). As discussed previously, NAD$^+$ analogues have been designed and molecules **8, 9, 10** showed strong inhibitory potential against NADase activity of rTNT protein (Figure 4.3-9). The results indicated these are the most potential mimic of NAD$^+$; therefore further studies were conducted to evaluate the effect of these small molecules on *M. tuberculosis* and *P. falciparum* infection and growth.

4.6.1 Effect of NAD$^+$ analogues on *M. tuberculosis* growth and intracellular survival

To determine the anti-tubercular activity of small molecules, peritoneal macrophages were infected with *M. tuberculosis* H37Rv followed by treatment with small molecules **8, 9, and 10**. The intracellular survival of *M. tuberculosis* inside macrophage was evaluated after 24 and 48 hours of infection by CFU count. The result exhibited molecules **8 and 9** significantly reduce bacterial load after 48 hours of infection while molecule **10** showed moderate reduction compared to untreated control. These data represent molecules **8 and 9** as potent anti-tubercular agents (Figure 4.6-1).
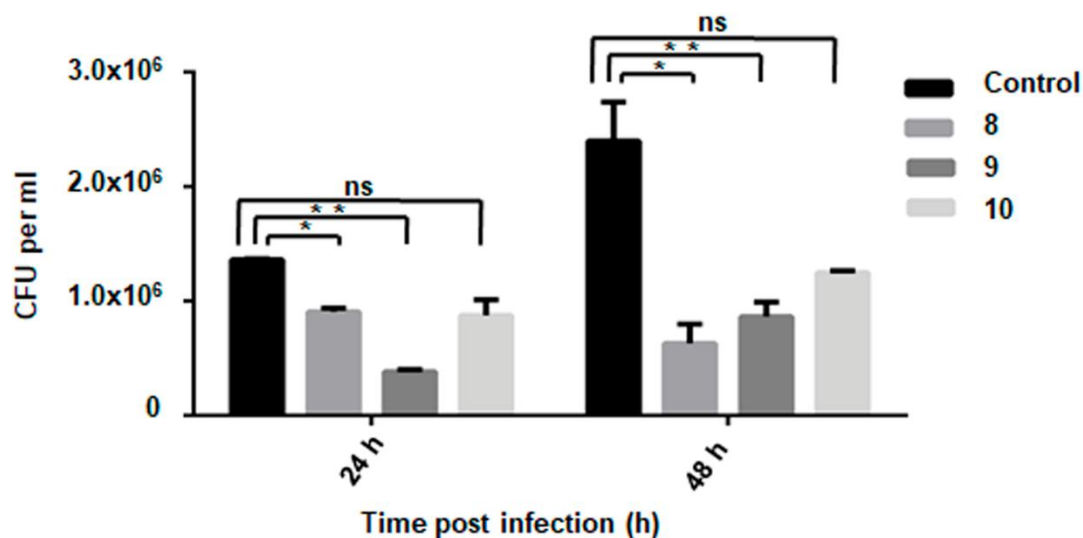
Figure 4.6-1 Effect of small molecules on intracellular survival of *M. tuberculosis*. Intracellular viability of *M. tuberculosis* was analysed after 24 and 48 hours of post-infection in cultures treated with small molecules **8, 9, 10** by CFU count. *P* values were calculated from student t-test with Welch's correction (*$P<0.05$, **$P<0.01$).

4.6.2 Effect of NAD$^+$ analogues on *P. falciparum* growth and infection

To determine the anti-malarial potential of small molecules **8, 9, and 10**, the erythrocytes were infected with trophozoite stage of *P. falciparum* 3D7 parasite culture and treated with different concentration of small molecules to perform growth inhibition assay. After 48 hours of post-treatment, parasite viability was determined by preparing Giemsa-stained blood smear for each set of parasite culture. The stained smears were counted for number of infected erythrocytes and the parasitemia was determined. The percent parasite viability was calculated compared to control and the IC$_{50}$ values were determined. The small molecules **8, 9 and 10** were found to have IC$_{50}$ values of 657.1 nM, 367.5 nM, and 1.516 μM, respectively. Molecule **9** emerged as the most potent anti-malarial agent among them (Figure 4.6-2 A). The effect of molecules on *P. falciparum* growth was further confirmed by flow cytometry analysis of treated and control erythrocytes stained with ethidium bromide which showed inhibition of *P. falciparum* growth by molecule **9** most effectively (Figure 4.6-2 B).
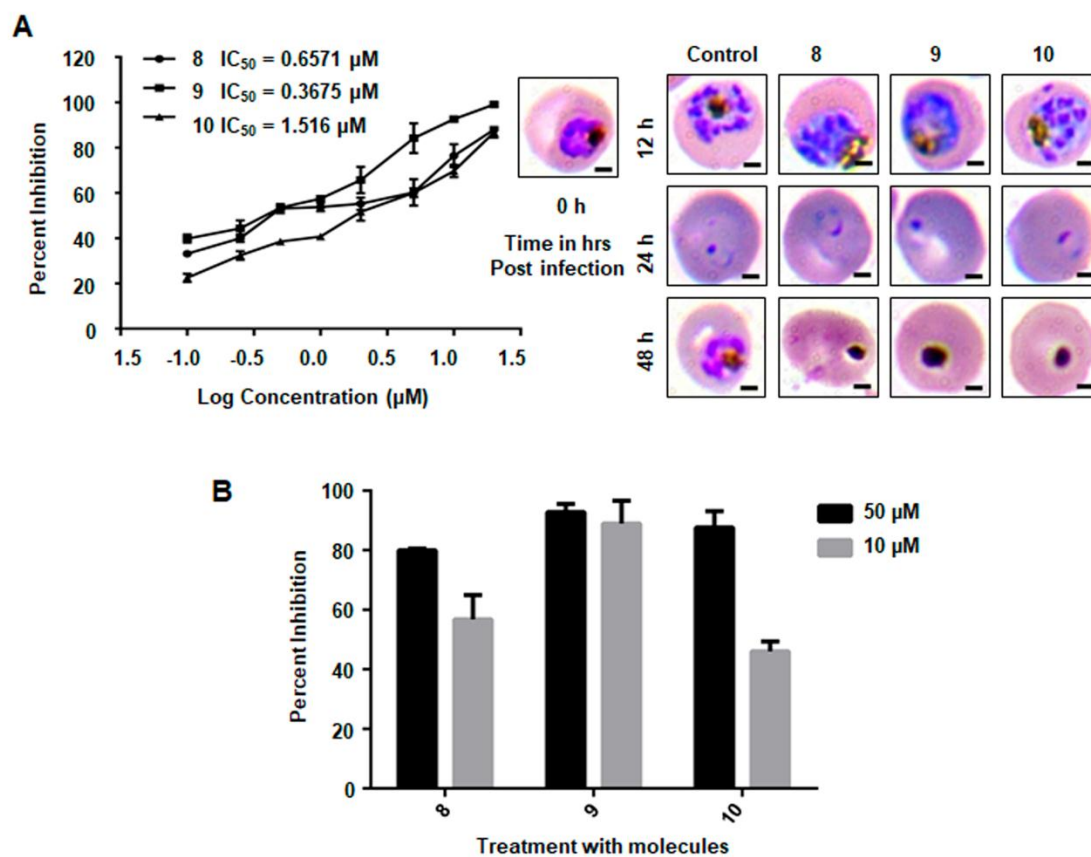
Figure 4.6-2 Effect of small molecules on *P. falciparum* growth. (A) Growth inhibition assay of *P. falciparum* 3D7 strain after treatment of parasite culture with small molecules **8, 9 and 10** after 48 hours post-infection. The non-linear regression analysis of plotted graph was performed using graph pad prism 6 software to calculate IC$_{50}$ values of small molecules (left panel), Giemsa analysis of culture smears at different time points after infection (right panel). Scale bar represents 2 μm. (B) Flow cytometry analysis of control and molecules treated erythrocytes for determination of parasite growth.

4.6.3 Effect of NAD$^+$ analogues on host macrophages and human erythrocytes

In order to study the drug potential of the aforementioned compounds, their effect on host cell viability was evaluated. To investigate the cytotoxic effect of selected small molecules, RAW 264.7 macrophages were treated with different concentrations of molecules for 48 hours and cell viability compared to control was determined. The results showed no significant difference in viability of treated macrophage cells in comparison to untreated control, thus indicating these molecules are not cytotoxic in nature (Figure 4.6-3 A). In order to confirm these molecules do not affect host erythrocytes NAD$^+$ levels without *P. falciparum* infection, the intra-erythrocytic NAD$^+$ levels of molecules treated erythrocytes were determined. The result confirmed

that NAD$^+$ levels were not affected by molecules treatment and found similar to untreated control (Figure 4.6-3 B).
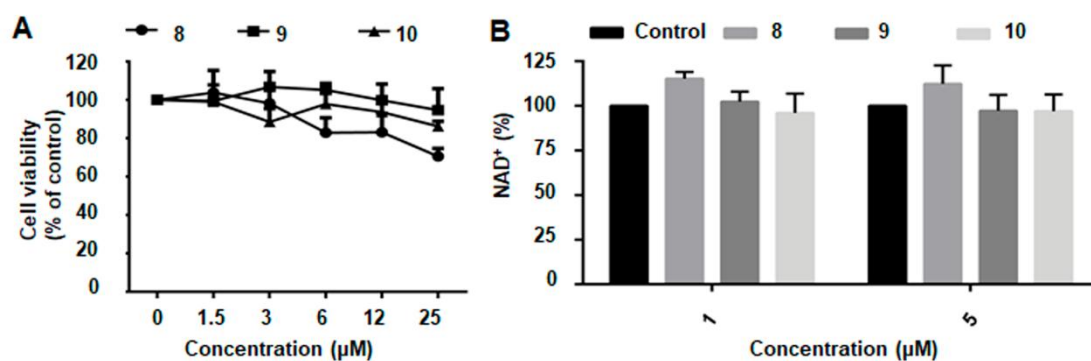
Figure 4.6-3 Evaluation of effect of small molecules on host macrophages and human erythrocytes. (A) Determination of host cell viability in order to evaluate cytotoxicity of small molecules. MTT assay was performed to evaluate the viability of RAW macrophage cells treated with different concentration of molecules as shown in figure. (B) Intra-erythrocytic NAD$^+$ levels of small molecules-treated erythrocytes compared to untreated control were determined. NAD$^+$ level of control untreated erythrocytes was considered as 100%.

Collectively, these data represent small molecules **8 and 9** as novel therapeutic agents for treatment of tuberculosis and malaria. These results also represent NAD$^+$ mimicking molecules as novel class of compounds having drug potential for diseases involving NAD$^+$ in their pathogenesis.

Chapter 5

Discussion

5 DISCUSSION

5.1 Overview of the findings

Intracellular pathogens manipulate host cell pathways for infection propagation and dissemination. Targeting or modulating host cell processes involved in pathogenesis can control the pathogen infection. These host cell pathways can be important targets for development of small-molecule inhibitors and novel drugs. NAD^+ metabolism appears to be potential therapeutic target in various diseases. Studies have indicated modulation of NAD^+ metabolism could play a key role in pathogen infection and spread [343]. This study presents the importance of host NAD^+ metabolism in the pathogenesis of *M. tuberculosis* and *P. falciparum* and development of small molecule inhibitors as novel drug candidates targeting modulation of this important pathway. *M. tuberculosis* secretes TNT, a NAD^+-glycohydrolase, in the cytoplasm of infected macrophages to deplete its intracellular NAD^+ levels [229, 230]. To study the impact of host intracellular NAD^+ homeostasis on infection propagation, TNT was targeted through its natural inhibitor and further used as a molecular tool to modulate intra-erythrocytic NAD^+ levels.

NAD^+ metabolism has gained importance due to identification of a set of enzymes as therapeutic targets that are tightly regulated by NAD redox balance. NAD^+-utilizing enzymes act as metabolic regulators in the cells for downstream metabolic pathways. NAD^+, an oxidoreductase cofactor, is involved in maintaining cellular redox status and directly links it with regulation of signaling and transcriptional events [353]. The modulation of NAD^+ homeostasis has been shown associated with development of various diseases such as metabolic disorders, cancers, aging, and neurodegenerative diseases [334, 418, 419]. Studies have suggested NAD^+ metabolism has an important role in host-pathogen interactions [343]. Recent research indicated NAD^+ as an immuno-metabolic circuit modulator that regulates immune responses and functions. The studies suggested an important role of NAD^+ during infection in immune system perturbations indicating its therapeutic potential [344].

Targeting NAD^+ metabolism in host-pathogen interactions could be a potential therapeutic option for treatment of pathogenic infections. Modulation of host intracellular NAD^+ levels has been reported in various types of intracellular infections [343]. Intracellular NAD^+ levels of peripheral blood lymphocytes of HIV-infected

patients found to be decreased could be reverted by exogenous administration of nicotinamide [348]. *Streptococcus pyogenes* depletes infected host cell NAD$^+$ levels through secretion of NAD$^+$ glycohydrolase leading to growth arrest and cell death and disruption of several host innate immune defense processes [335, 343, 345, 420, 421]. However, further studies are required to understand these processes and explore their drug target potential.

Recently, a remarkable example of host intracellular NAD$^+$ level modulation has been found to be represented in *M. tuberculosis*, the causative agent of tuberculosis. *M. tuberculosis* infection induces macrophage necrosis that facilitates mycobacterial replication and dissemination [192, 230]. Virulent *M. tuberculosis* inhibits host cell apoptosis and promotes necrosis to evade host immune response [166, 210]. The *M. tuberculosis* secreted toxin, TNT (tuberculosis necrotizing toxin), has been identified as major cytotoxicity factor in macrophage. TNT is a NAD$^+$-glycohydrolase that hydrolyses host intracellular NAD$^+$ pool leading to host cell death. *M. tuberculosis* also produces IFT protein, a natural inhibitor of TNT activity [230]. The decreased NAD$^+$ levels through TNT induces necroptosis by RIPK3 and MLKL pathways. Further, NAD$^+$ depletion was itself reported sufficient for induction of necroptosis [192]. Furthermore, TNT induces ROS production leading to host cell death and promotes mycobacterial replication [232]. These studies suggested TNT as a potential target for drug development against *M. tuberculosis* infection. The role of TNT in mycobacterial infection has been shown but its specific targeting for anti-tubercular drug development is remained unexplored.

Here, we first determined the effect of TNT expression in bacterial system and further investigated whether IFT, the natural inhibitor of TNT, could revert this effect. TNT expression inhibits bacterial growth and colony formation. TNT is a NAD$^+$-glycohydrolase, thus bacterial cells expressing TNT show significant depletion of NAD$^+$ levels. Co-expression of IFT with TNT elevates NAD$^+$ levels that then protects bacterial cells from toxic effect of TNT. These results suggested a requirement of adequate NAD$^+$ levels for bacterial growth and colony formation. This also indicated a universal role of NAD$^+$ in cell survival and growth, not only in eukaryotic system but also for prokaryotic system.

The proteins rIFT and rTNT were purified for *in vitro* interaction studies. TNT expression was found toxic for bacterial cells. To obtain adequate amount of rTNT,

the IFT-TNT protein complex was purified and rTNT was isolated from this complex. The purified rTNT protein was found active showing NAD^+ hydrolysis in the reaction mixture. The *in vitro* interaction studies of rIFT and rTNT proteins through ELISA and Far-western blotting confirmed the interaction of IFT and TNT proteins. Further, rIFT was found to inhibit NADase activity of TNT as reported in previous study [230]. Inhibition of TNT activity through IFT in bacterial system and *in vitro* assays confirms the efficiency of IFT-TNT system for further use in determination of the effect of NAD^+ modulation on macrophage and erythrocyte cell survival.

In order to find *de novo* peptide or protein inhibitors against TNT using the bacterial two-hybrid system from protein or peptide libraries, we first tried to clone TNT into bacterial two-hybrid system vectors. However, TNT could not be cloned into these vectors because of its inherent toxicity due to leaky expression of the inserted gene. We next looked for inhibitors against the NADase activity of TNT. TNT is a NAD^+ consuming enzyme and cleaves its substrate NAD^+ into nicotinamide and ADP-ribose [230]. Like other NADases, TNT also possesses a NAD^+ binding pocket. On the basis of these properties of TNT, we screened Nicotinamide (an end product of NADase reaction), Pyrazinamide (pyrazine analogue of nicotinamide), Ribavirin (nucleoside analogue), and APBA (reported NADase inhibitor) and found only APBA significantly inhibited around 40 percent of NADase activity of TNT. In order to develop potent novel inhibitors against TNT, NAD^+ analogues were designed and synthesized that could bind to the NAD^+ binding pocket of TNT. After screening small molecules, **8, 9, and 10** showed remarkable inhibitory potencies. *In silico* studies confirmed strong binding of these small molecules at the NAD^+-binding pocket of TNT. These NAD^+ analogues represent a novel class of inhibitors for treatment of tuberculosis by targeting TNT. Several studies have also identified NAD^+ analogues as enzyme inhibitors with anticancer or antimicrobial therapeutic potential. These analogues target NAD^+ dependent enzymes such as NAD^+ glycohydrolase CD38, Sirtuins, and ADP ribosyltransferases [422].

Previous reports have shown TNT depletes macrophage NAD^+ pool thus leading to necrosis [230]. We next studied the effect of targeting TNT through its natural inhibitor IFT in macrophages. Results showed NAD^+ restoration by IFT inhibits macrophage cell death. These results suggest NAD^+ replenishment could be an effective therapy for treatment of tuberculosis by preventing macrophage death. In

this experiment, TNT and IFT proteins were expressed in macrophages and macrophage cell death was analysed by MTT assay, PI staining, and HMGB1 translocation. Macrophages expressing TNT demonstrated increased macrophage death and decreased NAD^+ levels that was reverted by co-expression of IFT with TNT. The HMGB1 secretion has been identified as primary necrosis cell death marker [415]. HMGB1 also acts as pro-inflammatory mediator protein. TNT expression leads to HMGB1 release. Similar pattern of HMGB1 release by *S. pyogenes* NAD^+ glycohydrolase (SPN) with NADase activity in infected cells has also been shown [420] with suggested role in infection. Thus indicated TNT mediated HMGB1 release could also be involved in infection but the mechanism might be different.

The results of macrophage experiment indicate targeting TNT with IFT in *M. tuberculosis*-infected macrophages could affect viability of mycobacteria. We found that NAD^+ restoration through IFT inhibits infected macrophage cell death that further limits *M. tuberculosis* intracellular survival. These results indicated NAD^+ replenishment could be used as a potential therapeutic strategy for treatment of tuberculosis. Since IFT specifically targets TNT, these results also suggested inhibitors targeting TNT could be a promising drug candidate. These results are in line with previous findings where NAD^+ replenishment by nicotinamide reduces TNT-induced ROS levels and *M. tuberculosis* mediated host cell death [232]. We have identified potent small molecules inhibitors **8, 9, and 10** against TNT NADase activity in *in vitro* assays. We tested inhibitory potential of these molecules against *M. tuberculosis* intracellular viability. The selected potent small molecule inhibitors **8 and 9** reduce intracellular mycobacterial survival that suggested their candidature for therapeutic interventions.

Previous studies have reported induction of host cell death through NAD^+ depletion in different types of cells [192, 357, 402]. Mature erythrocytes undergo a form of programmed cell death known as eryptosis. *Plasmodium* parasites also known to manipulate host cell processes including programmed cell death pathway like other intracellular pathogens [270, 396]. During *P. falciparum* infection elevation in NAD^+ levels of infected erythrocytes have been observed. These increased intra-erythrocytic NAD^+ levels might have a role in *P. falciparum* infection [336, 400]. To study the significance of NAD^+ modulation in eryptosis and *P. falciparum* infection, we have

used TNT as molecular tool and manipulated intra-erythrocytic NAD^+ levels. The rIFT and rTNT proteins were loaded using hypotonic pre-swelling method and prepared erythrocyte ghosts were encapsulated with recombinant proteins. The results of FITC-dextran loading and western blotting confirmed efficient loading and retention of recombinant proteins, IFT and TNT. The efficient loading of various drugs and proteins have been shown in erythrocyte ghosts previously [411, 416, 417].

These efficiently loaded erythrocytes were analysed for induction of eryptosis markers to study the effect of NAD^+ modulation. The markers of eryptosis include phosphatidylserine exposure, cell shrinkage, elevated intracellular Ca^{2+} levels, and increased ROS levels [277]. The erythrocytes loaded with rTNT exhibited increased Annexin-V binding on the erythrocyte surface, decrease in forward scatter reflected by erythrocyte shrinkage, increased ROS generation, and elevation in cytosolic Ca^{2+} activity compared to control and rIFT-loaded erythrocytes. These results showed induction of eryptosis in TNT-loaded erythrocytes. Subsequently, the decreased NAD^+ levels of recombinant TNT-loaded erythrocytes further confirm TNT-mediated NAD^+ depletion is responsible for eryptosis induction. Altogether, these results demonstrate a novel finding that depletion of intra-erythrocytic NAD^+ levels leads to induction of eryptosis. Induction of eryptosis has been shown to be elicited by various stimulators such as energy depletion, oxidative stress, osmotic shock and specific xenobiotics [270, 277, 397]. NAD^+ depletion triggers cell death in different types of cells, however, the cell-death patterns are according to specific cell type. Intra-erythrocytic NAD^+ depletion may lead to metabolic collapse or initiate other molecular mechanism that results in induction of eryptosis, the precise cause of eryptosis remains unclear yet. Reduced NAD^+ levels of erythrocytes could inhibit glycolysis pathway leading to pyruvate and ATP deprivation in cells. Previous studies have shown ATP depletion triggers eryptosis and reduces parasite entry [332, 423].

Intracellular pathogens are known to manipulate host cell death pathway to survive inside cells. In case of malaria infection these studies have been performed during liver cell infection. However, little is known at the erythrocyte stage infection [270]. The role of eryptosis on parasite infection also remains unclear. To better understand the interplay of *Plasmodium* parasite with host erythrocytes, the effect of eryptosis on parasite progression was investigated. For this, rIFT and rTNT-loaded erythrocytes were examined during parasite infection. Parasite amplification was found reduced in

rTNT-loaded erythrocytes compared to other groups. The rTNT-loaded erythrocytes demonstrated resistance to invasion with increased number of free merozoites. Erythrocytes loading with rTNT leads to depletion of intra-erythrocytic NAD^+ levels and induction of eryptosis. Therefore, invasion defect in rTNT-loaded eryptotic erythrocytes may be due to impaired merozoites formation as a result of premature eryptosis induction. This is supported by studies that reported accelerated eryptosis in many clinical disorders such as beta-thalassemia, sickle-cell anemia, glucose-6-phosphate dehydrogenase (G6PD)-deficiency along with resistance to *P. falciparum* infection [270, 324]. In addition, a wide range of eryptosis inducing xenobiotics like paclitaxel, cyclosporine, chlorpromazine, PGE2, curcumin, and ionomycin confer resistance against malaria infection [282, 325].

Host cell factors reported to be involved during malaria merozoite entry include cytoskeleton proteins of erythrocytes such as spectrin and actin [424]. Studies have suggested reduced expression of erythrocyte cytoskeleton proteins may account for defect in parasite entry in eryptotic or ATP depleted erythrocytes [423-425]. It has been reported that reduced erythrocytic ATP levels impair merozoite invasion [423]. Along with it, the current study demonstrates the significance of intra-erythrocytic NAD^+ levels in parasite invasion process. The *P. falciparum* infected erythrocytes have shown increased NAD^+ levels in comparison with uninfected erythrocytes. However, in this context the role of parasite mediated elevation in NAD^+ levels remains unclear [336, 400]. Here, the findings indicate these elevated NAD^+ levels are important to prevent the premature eryptosis and favour *P. falciparum* propagation. Thus, targeting the parasite NAD^+ pathways can be used as a strategy for drug development against malaria.

For the therapeutic implication of study, the NAD^+ analogues were designed and synthesized. These NAD^+ analogues were screened against TNT for their specificity. The selected analogues bind to the NAD^+ binding pocket of TNT as suggested in *in silico* studies. These small molecules have resemblance with NAD^+, that suggested they can serve as therapeutic agents against both malaria and tuberculosis infection. To target NAD^+ modulation in *P. falciparum* and *M. tuberculosis* infection, the selected analogues were tested for their inhibitory potential against these pathogens. The results identified molecules **8 and 9** as potent anti-tubercular agents. These small molecules **8, 9, and 10** were also found effective against *P. falciparum* growth with

the IC_{50} values of 657.1 nM, 367.5 nM, and 1.516 μM respectively. Thus, molecule **9** has identified as the most potent anti-malarial agent. Even though these results represent NAD^+ analogues as novel candidates for treatment of these diseases, it was necessary to confirm their specificity and nontoxicity toward host cells. The possibility of non-specific cross reactivity of NAD^+ analogues with numerous host NAD^+ dependent enzymes may limit their therapeutic potential. To eliminate the possibility of this limitation, the cytotoxicity of these molecules towards host macrophages was determined. These molecules not only don't exhibit cytotoxicity, they also do not affect intra-erythrocytic NAD^+ levels of host erythrocytes, suggesting pathogenic factors being responsible for their inhibitory effect. These results further confirm their therapeutic potential. These NAD^+ analogues possess anti-tubercular activity and also show strong anti-malarial activity. However, this study could not reveal the possible mechanisms behind the strong anti-malarial nature of these compounds but suggested presence of a pathogenic factor. The study could be extended in this direction to identify the exact possible mechanism of action. In addition, these NAD^+ analogues could also have significance in treatment of diseases where NAD^+ modulation is a pathological factor.

In conclusion, the present study establishes the role of modulation of host NAD^+ levels in the regulation of *M. tuberculosis* and *P. falciparum* infection propagation and dissemination. It is well reported that *M. tuberculosis* secreted toxin TNT depletes host intracellular NAD^+ levels leading to death of infected macrophages. The current study represents therapeutic implication of these findings by targeting TNT through its natural inhibitor IFT that control mycobacterial growth by allowing macrophage survival with suggested significance of NAD^+ replenishment therapy in tuberculosis treatment. The specific targeting of TNT by designed NAD^+ analogues also limits mycobacterial growth. Next, our TNT study reveals a novel finding that depletion of intra-erythrocytic NAD^+ levels leads to induction of eryptosis that results in reduction of parasite propagation in these erythrocytes. Importantly, designed NAD^+ analogues show potent anti-tubercular and anti-malarial activity thus paving the way for drug-intervention for the treatment of malaria, and tuberculosis.

Chapter 6

Summary and

Conclusion

6 SUMMARY AND CONCLUSION

6.1 Summary

Intracellular pathogens continue to pose a serious global health threat due to emergence of drug resistance against commonly used antibiotics. To establish successful infection and disseminate to other cells, these pathogens have evolved various survival strategies including manipulation of important host cell processes such as host cell death pathways [352]. Targeting these host cell processes involved in pathogenesis could pave the way for development of novel therapeutics. Selected host-directed therapies with minimum side effects have an advantage as it reduces the risk of development of drug resistance. The significance of host NAD^+ metabolism has been observed in various diseases; however its role in the pathogenesis of intracellular infections still remains underexplored [343]. Intracellular microbe *M. tuberculosis*, causative agent of tuberculosis, depletes host intracellular NAD^+ levels by secreting TNT into cytosol, thus inducing host cell death to facilitate dissemination. Another intracellular pathogen *P. falciparum*, causative agent of malaria, also modulates intra-erythrocytic NAD^+ levels during infection. In addition, progression of *P. falciparum* infection also depends on the induction of eryptosis. However, the significance of host NAD^+ metabolism in pathogenesis of *M. tuberculosis* and *P. falciparum* infection and its utilization for drug development are areas as yet underexplored.

The present study tries to explore the significance and therapeutic potential of host NAD^+ metabolism in the regulation of *M. tuberculosis* and *P. falciparum* infection progression. The study discovers a novel finding that intra-erythrocytic NAD^+ depletion elicits eryptosis and that the *Plasmodium* parasite could not invade these eryptotic erythrocytes. *M. tuberculosis* toxin, TNT, was also identified as a potential target, and inhibiting its activity shows reduction in *M. tuberculosis* growth. The results suggest NAD^+ replenishment therapies have the potential for treatment of tuberculosis. The selected designed NAD^+ analogues inhibit TNT activity and show no toxicity towards host macrophages. These analogues exhibit inhibitory effect against *M. tuberculosis* and *P. falciparum* growth and represent novel therapeutic agents for treatment of tuberculosis and malaria.

6.2 Conclusion

The following conclusions have been derived from the present study:

i. TNT mediated NAD^+ depletion inhibits bacterial growth and colony formation that could be reverted by expression of its natural inhibitor, IFT.

ii. IFT expression in macrophage inhibits TNT induced host macrophage death by maintaining intracellular NAD^+ levels.

iii. Targeting TNT through expression of IFT in *M. tuberculosis*-infected macrophages limits intracellular survival of *M. tuberculosis* by inhibiting death of infected macrophage.

iv. Intra-erythrocytic NAD^+ depletion triggers eryptosis of erythrocytes.

v. Induction of eryptosis through NAD^+ depletion is represented by an increase in phosphatidylserine exposure, erythrocyte shrinkage, elevation in intracellular Ca^{2+} levels, and increase in ROS generation.

vi. Eryptosis induction through NAD^+ depletion inhibits parasite invasion of erythrocytes.

vii. Screening of designed and synthesised NAD^+ analogues against TNT-NADase activity leads to identification of small molecules **8, 9, and 10** with strong inhibitory activities.

viii. Among Nicotinamide, Pyrazinamide, Ribavirin, and APBA, only APBA inhibits 40 percent of rTNT-NADase activity.

ix. *In silico* studies show strong binding of these small molecules at the NAD^+ binding pocket of TNT.

x. Selected small molecules reduce intracellular survival of *M. tuberculosis* and results show that molecules **8 and 9** are the most potent anti-tubercular agents.

xi. Selected small molecules **8, 9, and 10** exhibit anti-malarial activity with IC_{50} values of 657.1 nM, 367.5 nM, and 1.516 μM, with molecule **9** showing the most potent anti-malarial activity.

Chapter 7

References

REFERENCES

1. Organization WH. The end TB strategy: World Health Organization, **2015**.

2. Organization WH. Implementing the end TB strategy: the essentials: World Health Organization, **2015**.

3. Annabel B, Anna D, Hannah M. Global tuberculosis report 2019. Geneva: World Health Organization **2019**.

4. Lonnroth K, Jaramillo E, Williams BG, Dye C, Raviglione M. Drivers of tuberculosis epidemics: the role of risk factors and social determinants. Social science & medicine **2009**; 68:2240-6.

5. O'Hare B, Makuta I, Chiwaula L, Bar-Zeev N. Income and child mortality in developing countries: a systematic review and meta-analysis. Journal of the Royal Society of Medicine **2013**; 106:408-14.

6. Ward JL, Viner RM. The impact of income inequality and national wealth on child and adolescent mortality in low and middle-income countries. BMC public health **2017**; 17:429.

7. Organization WH, Initiative ST. Treatment of tuberculosis: guidelines. World Health Organization, **2010**.

8. Organization WH. WHO consolidated guidelines on drug-resistant tuberculosis treatment. World Health Organization, **2019**.

9. Hayman J. Mycobacterium ulcerans: an infection from Jurassic time? Lancet **1984**; 2:1015-6.

10. Gutierrez MC, Brisse S, Brosch R, et al. Ancient origin and gene mosaicism of the progenitor of Mycobacterium tuberculosis. PLoS pathogens **2005**; 1:e5.

11. Sreevatsan S, Pan X, Stockbauer KE, et al. Restricted structural gene polymorphism in the Mycobacterium tuberculosis complex indicates evolutionarily recent global dissemination. Proceedings of the National Academy of Sciences of the United States of America **1997**; 94:9869-74.

12. Zimmerman MR. Pulmonary and osseous tuberculosis in an Egyptian mummy. Bulletin of the New York Academy of Medicine **1979**; 55:604-8.

13. Cave A, Demonstrator A. The evidence for the incidence of tuberculosis in ancient Egypt. British Journal of Tuberculosis **1939**; 33:142-52.

14. Morse D, Brothwell DR, Ucko PJ. Tuberculosis in Ancient Egypt. The American review of respiratory disease **1964**; 90:524-41.

15. Brown L. The story of clinical pulmonary tuberculosis: The Radiological Society of North America, **1941**.

16. Daniel VS, Daniel TM. Old Testament biblical references to tuberculosis. Clinical infectious diseases : an official publication of the Infectious Diseases Society of America **1999**; 29:1557-8.

17. Daniel TM. The history of tuberculosis. Respiratory medicine **2006**; 100:1862-70.

18. Meachen GN. A Short History of Tuberculosis. A Short History of Tuberculosis **1936**.

19. Pezzella AT. History of Pulmonary Tuberculosis. Thoracic surgery clinics **2019**; 29:1-17.

20. Herzog H. History of tuberculosis. Respiration; international review of thoracic diseases **1998**; 65:5-15.

21. Riva MA. From milk to rifampicin and back again: history of failures and successes in the treatment for tuberculosis. The Journal of antibiotics **2014**; 67:661-5.

22. Daniel TM. Captain of death: the story of tuberculosis. Boydell & Brewer, **1997**.

23. Barberis I, Bragazzi NL, Galluzzo L, Martini M. The history of tuberculosis: from the first historical records to the isolation of Koch's bacillus. Journal of preventive medicine and hygiene **2017**; 58:E9-E12.

24. Yang H, Kruh-Garcia NA, Dobos KM. Purified protein derivatives of tuberculin--past, present, and future. FEMS immunology and medical microbiology **2012**; 66:273-80.

25. Hawgood BJ. Albert Calmette (1863-1933) and Camille Guerin (1872-1961): the C and G of BCG vaccine. Journal of medical biography **2007**; 15:139-46.

26. Ryan F. The Forgotten Plague: How the Battle Against Tuberculosis Was Won--and Lost. **1993**.

27. Schatz A, Bugie E, Waksman SA. Streptomycin, a substance exhibiting antibiotic activity against gram-positive and gram-negative bacteria. 1944. Clinical orthopaedics and related research **2005**:3-6.

28. McDermott W. The story of INH. The Journal of infectious diseases **1969**; 119:678-83.

29. Fox W. Various Combinations of Isoniazid with Streptomycin or with PAS in the Treatment of Pulmonary Tuberculosis. Group; 1.

30. Doster B, Murray FJ, Newman R, Woolpert SF. Ethambutol in the initial treatment of pulmonary tuberculosis. U.S. Public Health Service tuberculosis therapy trials. The American review of respiratory disease **1973**; 107:177-90.

31. Sensi P. History of the development of rifampin. Reviews of infectious diseases **1983**; 5 Suppl 3:S402-6.

32. Murray JF, Schraufnagel DE, Hopewell PC. Treatment of Tuberculosis. A Historical Perspective. Annals of the American Thoracic Society **2015**; 12:1749-59.

33. Mc KD, Malone L, et al. The effect of nicotinic acid amide on experimental tuberculosis of white mice. The Journal of laboratory and clinical medicine **1948**; 33:1249-53.

34. Bayer R, Wilkinson D. Directly observed therapy for tuberculosis: history of an idea. Lancet **1995**; 345:1545-8.

35. Cole ST, Brosch R, Parkhill J, et al. Deciphering the biology of Mycobacterium tuberculosis from the complete genome sequence. Nature **1998**; 393:537-44.

36. Raviglione MC, Uplekar MW. WHO's new Stop TB Strategy. Lancet **2006**; 367:952-5.

37. Floyd K, Glaziou P, Zumla A, Raviglione M. The global tuberculosis epidemic and progress in care, prevention, and research: an overview in year 3 of the End TB era. The Lancet Respiratory medicine **2018**; 6:299-314.

38. Uplekar M, Weil D, Lonnroth K, et al. WHO's new end TB strategy. Lancet **2015**; 385:1799-801.

39. Chakaya JM, Harries AD, Marks GB. Ending tuberculosis by 2030-Pipe dream or reality? International journal of infectious diseases : IJID : official publication of the International Society for Infectious Diseases **2020**; 92S:S51-S4.

40. Loddenkemper R, Murray JF. Tuberculosis and War: Lessons Learned From World War II. Tuberculosis and War. Vol. 43: Karger Publishers, **2018**:214-28.

41. Shah I, Poojari V, Meshram H. Multi-Drug Resistant and Extensively-Drug Resistant Tuberculosis. Indian journal of pediatrics **2020**; 87:833-9.

42. Fennelly KP. Variability of airborne transmission of Mycobacterium tuberculosis: implications for control of tuberculosis in the HIV era. Clinical infectious diseases : an official publication of the Infectious Diseases Society of America **2007**; 44:1358-60.

43. Flügge C. Die Verbreitung der Phthise durch staubförmiges Sputum und durch beim Husten verspritzte Tröpfchen. Zeitschrift für Hygiene und Infektionskrankheiten **1899**; 30:107-24.

44. Riley RL, Mills CC, Nyka W, et al. Aerial dissemination of pulmonary tuberculosis. A two-year study of contagion in a tuberculosis ward. 1959. American journal of epidemiology **1995**; 142:3-14.

45. Escombe AR, Oeser C, Gilman RH, et al. The detection of airborne transmission of tuberculosis from HIV-infected patients, using an in vivo air sampling model. Clinical infectious diseases : an official publication of the Infectious Diseases Society of America **2007**; 44:1349-57.

46. Riley RL. Airborne infection. The American journal of medicine **1974**; 57:466-75.

47. Ko G, Burge HA, Muilenberg M, Rudnick S, First M. Survival of mycobacteria on HEPA filter material. Journal of the American Biological Safety Association **1998**; 3:65-78.

48. Nardell EA. Transmission and Institutional Infection Control of Tuberculosis. Cold Spring Harbor perspectives in medicine **2015**; 6:a018192.

49. Thillai M, Pollock K, Pareek M, Lalvani A. Interferon-gamma release assays for tuberculosis: current and future applications. Expert review of respiratory medicine **2014**; 8:67-78.

50. Berry MP, Blankley S, Graham CM, Bloom CI, O'Garra A. Systems approaches to studying the immune response in tuberculosis. Current opinion in immunology **2013**; 25:579-87.

51. Fogel N. Tuberculosis: a disease without boundaries. Tuberculosis **2015**; 95:527-31.

52. Golden MP, Vikram HR. Extrapulmonary tuberculosis: an overview. American family physician **2005**; 72:1761-8.

53. Kumar K, Kon OM. Diagnosis and treatment of tuberculosis: latest developments and future priorities. Annals of Research Hospitals **2017**; 1.

54. Steingart KR, Schiller I, Horne DJ, Pai M, Boehme CC, Dendukuri N. Xpert(R) MTB/RIF assay for pulmonary tuberculosis and rifampicin resistance in adults. The Cochrane database of systematic reviews **2014**:CD009593.

55. Nathavitharana RR, Cudahy PG, Schumacher SG, Steingart KR, Pai M, Denkinger CM. Accuracy of line probe assays for the diagnosis of pulmonary and multidrug-resistant tuberculosis: a systematic review and meta-analysis. European Respiratory Journal **2017**; 49.

56. Seung KJ, Keshavjee S, Rich ML. Multidrug-resistant tuberculosis and extensively drug-resistant tuberculosis. Cold Spring Harbor perspectives in medicine **2015**; 5:a017863.

57. Shah I, Poojari V, Meshram H. Multi-Drug Resistant and Extensively-Drug Resistant Tuberculosis. The Indian Journal of Pediatrics **2020**:1-7.

58. Mangtani P, Abubakar I, Ariti C, et al. Protection by BCG vaccine against tuberculosis: a systematic review of randomized controlled trials. Clinical infectious diseases : an official publication of the Infectious Diseases Society of America **2014**; 58:470-80.

59. Sterne JA, Rodrigues LC, Guedes IN. Does the efficacy of BCG decline with time since vaccination? The international journal of tuberculosis and lung disease : the official journal of the International Union against Tuberculosis and Lung Disease **1998**; 2:200-7.

60. Fedrizzi T, Meehan CJ, Grottola A, et al. Genomic characterization of Nontuberculous Mycobacteria. Scientific reports **2017**; 7:45258.

61. Gagneux S. Ecology and evolution of Mycobacterium tuberculosis. Nature reviews Microbiology **2018**; 16:202-13.

62. Rogall T, Wolters J, Flohr T, Bottger EC. Towards a phylogeny and definition of species at the molecular level within the genus Mycobacterium. International journal of systematic bacteriology **1990**; 40:323-30.

63. Imaeda T. Deoxyribonucleic acid relatedness among selected strains of Mycobacterium tuberculosis, Mycobacterium bovis, Mycobacterium bovis BCG, Mycobacterium microti, and Mycobacterium africanum. International Journal of Systematic and Evolutionary Microbiology **1985**; 35:147-50.

64. Brosch R, Pym AS, Gordon SV, Cole ST. The evolution of mycobacterial pathogenicity: clues from comparative genomics. Trends in microbiology **2001**; 9:452-8.

65. Alexander KA, Laver PN, Michel AL, et al. Novel Mycobacterium tuberculosis complex pathogen, M. mungi. Emerging infectious diseases **2010**; 16:1296-9.

66. Smith NH, Kremer K, Inwald J, et al. Ecotypes of the Mycobacterium tuberculosis complex. Journal of theoretical biology **2006**; 239:220-5.

67. Supply P, Marceau M, Mangenot S, et al. Genomic analysis of smooth tubercle bacilli provides insights into ancestry and pathoadaptation of Mycobacterium tuberculosis. Nature genetics **2013**; 45:172-9.

68. van Soolingen D, Hoogenboezem T, de Haas PE, et al. A novel pathogenic taxon of the Mycobacterium tuberculosis complex, Canetti: characterization of an exceptional isolate from Africa. International journal of systematic bacteriology **1997**; 47:1236-45.

69. Supply P, Brosch R. The Biology and Epidemiology of Mycobacterium canettii. Advances in experimental medicine and biology **2017**; 1019:27-41.

70. Brosch R, Gordon SV, Marmiesse M, et al. A new evolutionary scenario for the Mycobacterium tuberculosis complex. Proceedings of the National Academy of Sciences of the United States of America **2002**; 99:3684-9.

71. Orgeur M, Brosch R. Evolution of virulence in the Mycobacterium tuberculosis complex. Current opinion in microbiology **2018**; 41:68-75.

72. Firdessa R, Berg S, Hailu E, et al. Mycobacterial lineages causing pulmonary and extrapulmonary tuberculosis, Ethiopia. Emerging infectious diseases **2013**; 19:460-3.

73. Gagneux S, Small PM. Global phylogeography of Mycobacterium tuberculosis and implications for tuberculosis product development. The Lancet infectious diseases **2007**; 7:328-37.

74. Shinnick TM, Good RC. Mycobacterial taxonomy. European journal of clinical microbiology & infectious diseases : official publication of the European Society of Clinical Microbiology **1994**; 13:884-901.

75. Forbes BA. Mycobacterial Taxonomy. Journal of clinical microbiology **2017**; 55:380-3.

76. Daffe M, Draper P. The envelope layers of mycobacteria with reference to their pathogenicity. Advances in microbial physiology **1998**; 39:131-203.

77. Vilcheze C, Kremer L. Acid-Fast Positive and Acid-Fast Negative Mycobacterium tuberculosis: The Koch Paradox. Microbiology spectrum **2017**; 5.

78. Jarlier V, Nikaido H. Mycobacterial cell wall: structure and role in natural resistance to antibiotics. FEMS microbiology letters **1994**; 123:11-8.

79. Brennan PJ, Nikaido H. The envelope of mycobacteria. Annual review of biochemistry **1995**; 64:29-63.

80. Errington J. L-form bacteria, cell walls and the origins of life. Open biology **2013**; 3:120143.

81. Maitra A, Munshi T, Healy J, et al. Cell wall peptidoglycan in Mycobacterium tuberculosis: An Achilles' heel for the TB-causing pathogen. FEMS microbiology reviews **2019**; 43:548-75.

82. Hoffmann C, Leis A, Niederweis M, Plitzko JM, Engelhardt H. Disclosure of the mycobacterial outer membrane: cryo-electron tomography and vitreous sections reveal the lipid bilayer structure. Proceedings of the National Academy of Sciences of the United States of America **2008**; 105:3963-7.

83. Zuber B, Chami M, Houssin C, Dubochet J, Griffiths G, Daffe M. Direct visualization of the outer membrane of mycobacteria and corynebacteria in their native state. Journal of bacteriology **2008**; 190:5672-80.

84. Chiaradia L, Lefebvre C, Parra J, et al. Dissecting the mycobacterial cell envelope and defining the composition of the native mycomembrane. Scientific reports **2017**; 7:12807.

85. Sani M, Houben EN, Geurtsen J, et al. Direct visualization by cryo-EM of the mycobacterial capsular layer: a labile structure containing ESX-1-secreted proteins. PLoS pathogens **2010**; 6:e1000794.

86. Marrakchi H, Laneelle MA, Daffe M. Mycolic acids: structures, biosynthesis, and beyond. Chemistry & biology **2014**; 21:67-85.

87. Bansal-Mutalik R, Nikaido H. Mycobacterial outer membrane is a lipid bilayer and the inner membrane is unusually rich in diacyl phosphatidylinositol dimannosides. Proceedings of the National Academy of Sciences of the United States of America **2014**; 111:4958-63.

88. Daffé M. QA, Marrakchi H. . Mycolic Acids: From Chemistry to Biology. In: Geiger O. (eds) Biogenesis of Fatty Acids, Lipids and Membranes. Handbook of Hydrocarbon and Lipid Microbiology Springer, Cham, **2017**:1-36.

89. Daffe M, Etienne G. The capsule of Mycobacterium tuberculosis and its implications for pathogenicity. Tubercle and lung disease : the official journal of the International Union against Tuberculosis and Lung Disease **1999**; 79:153-69.

90. Forrellad MA, Klepp LI, Gioffre A, et al. Virulence factors of the Mycobacterium tuberculosis complex. Virulence **2013**; 4:3-66.

91. Becker K, Sander P. Mycobacterium tuberculosis lipoproteins in virulence and immunity - fighting with a double-edged sword. FEBS letters **2016**; 590:3800-19.

92. Vilchèze C. Mycobacterial Cell Wall: A Source of Successful Targets for Old and New Drugs. Applied Sciences **2020**; 10:2278.

93. Jackson M, McNeil MR, Brennan PJ. Progress in targeting cell envelope biogenesis in Mycobacterium tuberculosis. Future microbiology **2013**; 8:855-75.

94. Brosch R, Gordon SV, Billault A, et al. Use of a Mycobacterium tuberculosis H37Rv bacterial artificial chromosome library for genome mapping, sequencing, and comparative genomics. Infection and immunity **1998**; 66:2221-9.

95. Kubica GP, Kim TH, Dunbar FP. Designation of strain H37Rv as the neotype of Mycobacterium tuberculosis. International Journal of Systematic and Evolutionary Microbiology **1972**; 22:99-106.

96. Comas I. Genomic Epidemiology of Tuberculosis. Advances in experimental medicine and biology **2017**; 1019:79-93.

97. Walker TM, Kohl TA, Omar SV, et al. Whole-genome sequencing for prediction of Mycobacterium tuberculosis drug susceptibility and resistance: a retrospective cohort study. The Lancet Infectious diseases **2015**; 15:1193-202.

98. Roetzer A, Diel R, Kohl TA, et al. Whole genome sequencing versus traditional genotyping for investigation of a Mycobacterium tuberculosis outbreak: a longitudinal molecular epidemiological study. PLoS medicine **2013**; 10:e1001387.

99. Mestre O, Luo T, Dos Vultos T, et al. Phylogeny of Mycobacterium tuberculosis Beijing strains constructed from polymorphisms in genes involved in DNA replication, recombination and repair. PloS one **2011**; 6:e16020.

100. O'Toole RF, Gautam SS. Limitations of the Mycobacterium tuberculosis reference genome H37Rv in the detection of virulence-related loci. Genomics **2017**; 109:471-4.

101. Seib KL, Dougan G, Rappuoli R. The key role of genomics in modern vaccine and drug design for emerging infectious diseases. PLoS genetics **2009**; 5:e1000612.

102. Besser J, Carleton HA, Gerner-Smidt P, Lindsey RL, Trees E. Next-generation sequencing technologies and their application to the study and control of bacterial infections. Clinical microbiology and infection : the official publication of the European Society of Clinical Microbiology and Infectious Diseases **2018**; 24:335-41.

103. Margulies M, Egholm M, Altman WE, et al. Genome sequencing in microfabricated high-density picolitre reactors. Nature **2005**; 437:376-80.

104. Sato MP, Ogura Y, Nakamura K, et al. Comparison of the sequencing bias of currently available library preparation kits for Illumina sequencing of bacterial genomes and metagenomes. DNA research : an international journal for rapid publication of reports on genes and genomes **2019**; 26:391-8.

105. Camus JC, Pryor MJ, Medigue C, Cole ST. Re-annotation of the genome sequence of Mycobacterium tuberculosis H37Rv. Microbiology **2002**; 148:2967-73.

106. Lew JM, Mao C, Shukla M, et al. Database resources for the tuberculosis community. Tuberculosis **2013**; 93:12-7.

107. Cole ST. Learning from the genome sequence of Mycobacterium tuberculosis H37Rv. FEBS letters **1999**; 452:7-10.

108. Smith I. Mycobacterium tuberculosis pathogenesis and molecular determinants of virulence. Clinical microbiology reviews **2003**; 16:463-96.

109. Gazi MA, Kibria MG, Mahfuz M, et al. Functional, structural and epitopic prediction of hypothetical proteins of Mycobacterium tuberculosis H37Rv: An in silico approach for prioritizing the targets. Gene **2016**; 591:442-55.

110. Doerks T, van Noort V, Minguez P, Bork P. Annotation of the M. tuberculosis hypothetical orfeome: adding functional information to more than half of the uncharacterized proteins. PloS one **2012**; 7:e34302.

111. Russell DG, Barry CE, 3rd, Flynn JL. Tuberculosis: what we don't know can, and does, hurt us. Science **2010**; 328:852-6.

112. Sasindran SJ, Torrelles JB. Mycobacterium Tuberculosis Infection and Inflammation: what is Beneficial for the Host and for the Bacterium? Frontiers in microbiology **2011**; 2:2.

113. Ernst JD. The immunological life cycle of tuberculosis. Nature reviews Immunology **2012**; 12:581-91.

114. Fennelly KP, Jones-Lopez EC. Quantity and Quality of Inhaled Dose Predicts Immunopathology in Tuberculosis. Frontiers in immunology **2015**; 6:313.

115. Schlesinger LS, Bellinger-Kawahara CG, Payne NR, Horwitz MA. Phagocytosis of Mycobacterium tuberculosis is mediated by human monocyte complement receptors and complement component C3. Journal of immunology **1990**; 144:2771-80.

116. Wolf AJ, Linas B, Trevejo-Nunez GJ, et al. Mycobacterium tuberculosis infects dendritic cells with high frequency and impairs their function in vivo. Journal of immunology **2007**; 179:2509-19.

117. Bermudez LE, Sangari FJ, Kolonoski P, Petrofsky M, Goodman J. The efficiency of the translocation of Mycobacterium tuberculosis across a bilayer of epithelial and endothelial cells as a model of the alveolar wall is a consequence of transport within mononuclear phagocytes and invasion of alveolar epithelial cells. Infection and immunity **2002**; 70:140-6.

118. Bermudez LE, Goodman J. Mycobacterium tuberculosis invades and replicates within type II alveolar cells. Infection and immunity **1996**; 64:1400-6.

119. Eum SY, Kong JH, Hong MS, et al. Neutrophils are the predominant infected phagocytic cells in the airways of patients with active pulmonary TB. Chest **2010**; 137:122-8.

120. Lerner TR, Borel S, Gutierrez MG. The innate immune response in human tuberculosis. Cellular microbiology **2015**; 17:1277-85.

121. Scordo JM, Knoell DL, Torrelles JB. Alveolar Epithelial Cells in Mycobacterium tuberculosis Infection: Active Players or Innocent Bystanders? Journal of innate immunity **2016**; 8:3-14.

122. Dobos KM, Spotts EA, Quinn FD, King CH. Necrosis of lung epithelial cells during infection with Mycobacterium tuberculosis is preceded by cell permeation. Infection and immunity **2000**; 68:6300-10.

123. McCormick TS, Weinberg A. Epithelial cell-derived antimicrobial peptides are multifunctional agents that bridge innate and adaptive immunity. Periodontology 2000 **2010**; 54:195-206.

124. de Martino M, Galli L, Chiappini E. Reflections on the immunology of tuberculosis: will we ever unravel the skein? BMC infectious diseases **2014**; 14 Suppl 1:S1.

125. Flynn JL, Chan J. Immunology of tuberculosis. Annual review of immunology **2001**; 19:93-129.

126. Fenton MJ, Vermeulen MW, Kim S, Burdick M, Strieter RM, Kornfeld H. Induction of gamma interferon production in human alveolar macrophages by Mycobacterium tuberculosis. Infection and immunity **1997**; 65:5149-56.

127. Saha P, Geissmann F. Toward a functional characterization of blood monocytes. Immunology and cell biology **2011**; 89:2-4.

128. Wolf AJ, Desvignes L, Linas B, et al. Initiation of the adaptive immune response to Mycobacterium tuberculosis depends on antigen production in the local lymph node, not the lungs. The Journal of experimental medicine **2008**; 205:105-15.

129. Tian T, Woodworth J, Skold M, Behar SM. In vivo depletion of CD11c+ cells delays the CD4+ T cell response to Mycobacterium tuberculosis and exacerbates the outcome of infection. Journal of immunology **2005**; 175:3268-72.

130. Ulrichs T, Kaufmann SH. New insights into the function of granulomas in human tuberculosis. The Journal of pathology **2006**; 208:261-9.

131. Russell DG. Who puts the tubercle in tuberculosis? Nature reviews Microbiology **2007**; 5:39-47.

132. Kaplan G, Post FA, Moreira AL, et al. Mycobacterium tuberculosis growth at the cavity surface: a microenvironment with failed immunity. Infection and immunity **2003**; 71:7099-108.

133. Sia JK, Rengarajan J. Immunology of Mycobacterium tuberculosis Infections. Microbiology spectrum **2019**; 7.

134. Verrall AJ, Netea MG, Alisjahbana B, Hill PC, van Crevel R. Early clearance of Mycobacterium tuberculosis: a new frontier in prevention. Immunology **2014**; 141:506-13.

135. Janeway CA. Approaching the asymptote? Evolution and revolution in immunology. In: Cold Spring Harbor symposia on quantitative biology. Cold Spring Harbor Laboratory Press:1-13.

136. Philips JA, Ernst JD. Tuberculosis pathogenesis and immunity. Annual review of pathology **2012**; 7:353-84.

137. Collins AC, Cai H, Li T, et al. Cyclic GMP-AMP Synthase Is an Innate Immune DNA Sensor for Mycobacterium tuberculosis. Cell host & microbe **2015**; 17:820-8.

138. Watson RO, Bell SL, MacDuff DA, et al. The Cytosolic Sensor cGAS Detects Mycobacterium tuberculosis DNA to Induce Type I Interferons and Activate Autophagy. Cell host & microbe **2015**; 17:811-9.

139. Jo EK, Yang CS, Choi CH, Harding CV. Intracellular signalling cascades regulating innate immune responses to Mycobacteria: branching out from Toll-like receptors. Cellular microbiology **2007**; 9:1087-98.

140. Fremond CM, Yeremeev V, Nicolle DM, Jacobs M, Quesniaux VF, Ryffel B. Fatal Mycobacterium tuberculosis infection despite adaptive immune response in the absence of MyD88. The Journal of clinical investigation **2004**; 114:1790-9.

141. Reed MB, Domenech P, Manca C, et al. A glycolipid of hypervirulent tuberculosis strains that inhibits the innate immune response. Nature **2004**; 431:84-7.

142. Blanc L, Gilleron M, Prandi J, et al. Mycobacterium tuberculosis inhibits human innate immune responses via the production of TLR2 antagonist glycolipids. Proceedings of the National Academy of Sciences of the United States of America **2017**; 114:11205-10.

143. Naffin-Olivos JL, Georgieva M, Goldfarb N, et al. Mycobacterium tuberculosis Hip1 modulates macrophage responses through proteolysis of GroEL2. PLoS pathogens **2014**; 10:e1004132.

144. Ehrt S, Schnappinger D. Mycobacterial survival strategies in the phagosome: defence against host stresses. Cellular microbiology **2009**; 11:1170-8.

145. Sullivan JT, Young EF, McCann JR, Braunstein M. The Mycobacterium tuberculosis SecA2 system subverts phagosome maturation to promote growth in macrophages. Infection and immunity **2012**; 80:996-1006.

146. Hou JM, D'Lima NG, Rigel NW, et al. ATPase activity of Mycobacterium tuberculosis SecA1 and SecA2 proteins and its importance for SecA2 function in macrophages. Journal of bacteriology **2008**; 190:4880-7.

147. de Jonge MI, Pehau-Arnaudet G, Fretz MM, et al. ESAT-6 from Mycobacterium tuberculosis dissociates from its putative chaperone CFP-10 under acidic conditions and exhibits membrane-lysing activity. Journal of bacteriology **2007**; 189:6028-34.

148. Conrad WH, Osman MM, Shanahan JK, et al. Mycobacterial ESX-1 secretion system mediates host cell lysis through bacterium contact-dependent gross membrane disruptions. Proceedings of the National Academy of Sciences of the United States of America **2017**; 114:1371-6.

149. Houben D, Demangel C, van Ingen J, et al. ESX-1-mediated translocation to the cytosol controls virulence of mycobacteria. Cellular microbiology **2012**; 14:1287-98.

150. Walburger A, Koul A, Ferrari G, et al. Protein kinase G from pathogenic mycobacteria promotes survival within macrophages. Science **2004**; 304:1800-4.

151. Saleh MT, Belisle JT. Secretion of an acid phosphatase (SapM) by Mycobacterium tuberculosis that is similar to eukaryotic acid phosphatases. Journal of bacteriology **2000**; 182:6850-3.

152. Bach H, Papavinasasundaram KG, Wong D, Hmama Z, Av-Gay Y. Mycobacterium tuberculosis virulence is mediated by PtpA dephosphorylation of human vacuolar protein sorting 33B. Cell host & microbe **2008**; 3:316-22.

153. Cowley S, Ko M, Pick N, et al. The Mycobacterium tuberculosis protein serine/threonine kinase PknG is linked to cellular glutamate/glutamine levels and is important for growth in vivo. Molecular microbiology **2004**; 52:1691-702.

154. Fratti RA, Chua J, Vergne I, Deretic V. Mycobacterium tuberculosis glycosylated phosphatidylinositol causes phagosome maturation arrest. Proceedings of the National Academy of Sciences of the United States of America **2003**; 100:5437-42.

155. Deretic V, Singh S, Master S, et al. Mycobacterium tuberculosis inhibition of phagolysosome biogenesis and autophagy as a host defence mechanism. Cellular microbiology **2006**; 8:719-27.

156. Sturgill-Koszycki S, Schlesinger PH, Chakraborty P, et al. Lack of acidification in Mycobacterium phagosomes produced by exclusion of the vesicular proton-ATPase. Science **1994**; 263:678-81.

157. Korb VC, Chuturgoon AA, Moodley D. Mycobacterium tuberculosis: Manipulator of Protective Immunity. International journal of molecular sciences **2016**; 17:131.

158. Yuk J-M, Shin D-M, Lee H-M, et al. Vitamin D3 induces autophagy in human monocytes/macrophages via cathelicidin. Cell host & microbe **2009**; 6:231-43.

159. Delgado MA, Elmaoued RA, Davis AS, Kyei G, Deretic V. Toll-like receptors control autophagy. The EMBO journal **2008**; 27:1110-21.

160. Harris J, De Haro SA, Master SS, et al. T helper 2 cytokines inhibit autophagic control of intracellular Mycobacterium tuberculosis. Immunity **2007**; 27:505-17.

161. Alonso S, Pethe K, Russell DG, Purdy GE. Lysosomal killing of Mycobacterium mediated by ubiquitin-derived peptides is enhanced by autophagy. Proceedings of the National Academy of Sciences of the United States of America **2007**; 104:6031-6.

162. Nnoaham KE, Clarke A. Low serum vitamin D levels and tuberculosis: a systematic review and meta-analysis. International journal of epidemiology **2008**; 37:113-9.

163. Rovetta AI, Pena D, Hernandez Del Pino RE, et al. IFNG-mediated immune responses enhance autophagy against Mycobacterium tuberculosis antigens in patients with active tuberculosis. Autophagy **2014**; 10:2109-21.

164. Wang X, Barnes PF, Dobos-Elder KM, et al. ESAT-6 inhibits production of IFN-gamma by Mycobacterium tuberculosis-responsive human T cells. Journal of immunology **2009**; 182:3668-77.

165. Lerner TR, Borel S, Greenwood DJ, et al. Mycobacterium tuberculosis replicates within necrotic human macrophages. The Journal of cell biology **2017**; 216:583-94.

166. Behar SM, Martin CJ, Booty MG, et al. Apoptosis is an innate defense function of macrophages against Mycobacterium tuberculosis. Mucosal immunology **2011**; 4:279-87.

167. Upadhyay S, Mittal E, Philips JA. Tuberculosis and the art of macrophage manipulation. Pathogens and disease **2018**; 76.

168. Tschopp J, Schroder K. NLRP3 inflammasome activation: The convergence of multiple signalling pathways on ROS production? Nature reviews Immunology **2010**; 10:210-5.

169. McElvania Tekippe E, Allen IC, Hulseberg PD, et al. Granuloma formation and host defense in chronic Mycobacterium tuberculosis infection requires PYCARD/ASC but not NLRP3 or caspase-1. PloS one **2010**; 5:e12320.

170. Shah S, Bohsali A, Ahlbrand SE, et al. Cutting edge: Mycobacterium tuberculosis but not nonvirulent mycobacteria inhibits IFN-beta and AIM2 inflammasome-dependent IL-1beta production via its ESX-1 secretion system. Journal of immunology **2013**; 191:3514-8.

171. Mihret A. The role of dendritic cells in Mycobacterium tuberculosis infection. Virulence **2012**; 3:654-9.

172. Khader SA, Partida-Sanchez S, Bell G, et al. Interleukin 12p40 is required for dendritic cell migration and T cell priming after Mycobacterium tuberculosis infection. The Journal of experimental medicine **2006**; 203:1805-15.

173. Sia JK, Georgieva M, Rengarajan J. Innate Immune Defenses in Human Tuberculosis: An Overview of the Interactions between Mycobacterium tuberculosis and Innate Immune Cells. Journal of immunology research **2015**; 2015:747543.

174. Harding CV, Boom WH. Regulation of antigen presentation by Mycobacterium tuberculosis: a role for Toll-like receptors. Nature reviews Microbiology **2010**; 8:296-307.

175. Lin PL, Pawar S, Myers A, et al. Early events in Mycobacterium tuberculosis infection in cynomolgus macaques. Infection and immunity **2006**; 74:3790-803.

176. Kursar M, Bonhagen K, Kohler A, Kamradt T, Kaufmann SH, Mittrucker HW. Organ-specific CD4+ T cell response during Listeria monocytogenes infection. Journal of immunology **2002**; 168:6382-7.

177. Ngai P, McCormick S, Small C, et al. Gamma interferon responses of CD4 and CD8 T-cell subsets are quantitatively different and independent of each other during pulmonary Mycobacterium bovis BCG infection. Infection and immunity **2007**; 75:2244-52.

178. Dheda K, Schwander SK, Zhu B, van Zyl-Smit RN, Zhang Y. The immunology of tuberculosis: from bench to bedside. Respirology **2010**; 15:433-50.

179. Joosten SA, Ottenhoff TH. Human CD4 and CD8 regulatory T cells in infectious diseases and vaccination. Human immunology **2008**; 69:760-70.

180. Heinzel AS, Grotzke JE, Lines RA, et al. HLA-E-dependent presentation of Mtb-derived antigen to human CD8+ T cells. The Journal of experimental medicine **2002**; 196:1473-81.

181. Mogues T, Goodrich ME, Ryan L, LaCourse R, North RJ. The relative importance of T cell subsets in immunity and immunopathology of airborne Mycobacterium tuberculosis infection in mice. The Journal of experimental medicine **2001**; 193:271-80.

182. Behar SM, Dascher CC, Grusby MJ, Wang CR, Brenner MB. Susceptibility of mice deficient in CD1D or TAP1 to infection with Mycobacterium tuberculosis. The Journal of experimental medicine **1999**; 189:1973-80.

183. Stenger S, Mazzaccaro RJ, Uyemura K, et al. Differential effects of cytolytic T cell subsets on intracellular infection. Science **1997**; 276:1684-7.

184. Bruns H, Meinken C, Schauenberg P, et al. Anti-TNF immunotherapy reduces CD8+ T cell-mediated antimicrobial activity against Mycobacterium tuberculosis in humans. The Journal of clinical investigation **2009**; 119:1167-77.

185. Havlir DV, Ellner JJ, Chervenak KA, Boom WH. Selective expansion of human gamma delta T cells by monocytes infected with live Mycobacterium tuberculosis. The Journal of clinical investigation **1991**; 87:729-33.

186. Kozakiewicz L, Chen Y, Xu J, et al. B cells regulate neutrophilia during Mycobacterium tuberculosis infection and BCG vaccination by modulating the interleukin-17 response. PLoS pathogens **2013**; 9:e1003472.

187. Maglione PJ, Xu J, Chan J. B cells moderate inflammatory progression and enhance bacterial containment upon pulmonary challenge with Mycobacterium tuberculosis. Journal of immunology **2007**; 178:7222-34.

188. Lamkanfi M, Dixit VM. Manipulation of host cell death pathways during microbial infections. Cell host & microbe **2010**; 8:44-54.

189. Mohareer K, Asalla S, Banerjee S. Cell death at the cross roads of host-pathogen interaction in Mycobacterium tuberculosis infection. Tuberculosis **2018**; 113:99-121.

190. Mittal E, Deore S, Kumar M, Krishnasastry M. When to Die Is the Question: Need and Manipulation of Cell Death by Mycobacterium. Current Molecular Biology Reports **2020**; 6:103-15.

191. Srinivasan L, Ahlbrand S, Briken V. Interaction of Mycobacterium tuberculosis with host cell death pathways. Cold Spring Harbor perspectives in medicine **2014**; 4.

192. Pajuelo D, Gonzalez-Juarbe N, Tak U, Sun J, Orihuela CJ, Niederweis M. NAD(+) Depletion Triggers Macrophage Necroptosis, a Cell Death Pathway Exploited by Mycobacterium tuberculosis. Cell reports **2018**; 24:429-40.

193. Sanchez D, Rojas M, Hernandez I, Radzioch D, Garcia LF, Barrera LF. Role of TLR2- and TLR4-mediated signaling in Mycobacterium tuberculosis-induced macrophage death. Cellular immunology **2010**; 260:128-36.

194. Rahman A, Sobia P, Gupta N, Kaer LV, Das G. Mycobacterium tuberculosis subverts the TLR-2-MyD88 pathway to facilitate its translocation into the cytosol. PloS one **2014**; 9:e86886.

195. Danelishvili L, McGarvey J, Li YJ, Bermudez LE. Mycobacterium tuberculosis infection causes different levels of apoptosis and necrosis in human macrophages and alveolar epithelial cells. Cellular microbiology **2003**; 5:649-60.

196. Bingisser R, Stey C, Weller M, Groscurth P, Russi E, Frei K. Apoptosis in human alveolar macrophages is induced by endotoxin and is modulated by cytokines. American journal of respiratory cell and molecular biology **1996**; 15:64-70.

197. Rojas M, Olivier M, Gros P, Barrera LF, Garcia LF. TNF-alpha and IL-10 modulate the induction of apoptosis by virulent Mycobacterium tuberculosis in murine macrophages. Journal of immunology **1999**; 162:6122-31.

198. Li Z, Kelley C, Collins F, Rouse D, Morris S. Expression of katG in Mycobacterium tuberculosis is associated with its growth and persistence in mice and guinea pigs. The Journal of infectious diseases **1998**; 177:1030-5.

199. Hinchey J, Lee S, Jeon BY, et al. Enhanced priming of adaptive immunity by a proapoptotic mutant of Mycobacterium tuberculosis. The Journal of clinical investigation **2007**; 117:2279-88.

200. Chan J, Fan XD, Hunter SW, Brennan PJ, Bloom BR. Lipoarabinomannan, a possible virulence factor involved in persistence of Mycobacterium tuberculosis within macrophages. Infection and immunity **1991**; 59:1755-61.

201. Velmurugan K, Chen B, Miller JL, et al. Mycobacterium tuberculosis nuoG is a virulence gene that inhibits apoptosis of infected host cells. PLoS pathogens **2007**; 3:e110.

202. Kroemer G, Galluzzi L, Vandenabeele P, et al. Classification of cell death: recommendations of the Nomenclature Committee on Cell Death 2009. Cell death and differentiation **2009**; 16:3-11.

203. Galluzzi L, Bravo-San Pedro J, Vitale I, et al. Essential versus accessory aspects of cell death: recommendations of the NCCD 2015. Cell Death & Differentiation **2015**; 22:58-73.

204. Galluzzi L, Vitale I, Aaronson SA, et al. Molecular mechanisms of cell death: recommendations of the Nomenclature Committee on Cell Death 2018. Cell death and differentiation **2018**; 25:486-541.

205. Vanden Berghe T, Linkermann A, Jouan-Lanhouet S, Walczak H, Vandenabeele P. Regulated necrosis: the expanding network of non-apoptotic cell death pathways. Nature reviews Molecular cell biology **2014**; 15:135-47.

206. Davis JM, Ramakrishnan L. The role of the granuloma in expansion and dissemination of early tuberculous infection. Cell **2009**; 136:37-49.

207. Roca FJ, Ramakrishnan L. TNF dually mediates resistance and susceptibility to mycobacteria via mitochondrial reactive oxygen species. Cell **2013**; 153:521-34.

208. Divangahi M, Chen M, Gan H, et al. Mycobacterium tuberculosis evades macrophage defenses by inhibiting plasma membrane repair. Nature immunology **2009**; 10:899-906.

209. Dallenga T, Repnik U, Corleis B, et al. M. tuberculosis-Induced Necrosis of Infected Neutrophils Promotes Bacterial Growth Following Phagocytosis by Macrophages. Cell host & microbe **2017**; 22:519-30 e3.

210. Behar SM, Divangahi M, Remold HG. Evasion of innate immunity by Mycobacterium tuberculosis: is death an exit strategy? Nature reviews Microbiology **2010**; 8:668-74.

211. Bafica A, Scanga CA, Serhan C, et al. Host control of Mycobacterium tuberculosis is regulated by 5-lipoxygenase-dependent lipoxin production. The Journal of clinical investigation **2005**; 115:1601-6.

212. Chen M, Divangahi M, Gan H, et al. Lipid mediators in innate immunity against tuberculosis: opposing roles of PGE2 and LXA4 in the induction of macrophage death. The Journal of experimental medicine **2008**; 205:2791-801.

213. Desai SJ, Prickril B, Rasooly A. Mechanisms of Phytonutrient Modulation of Cyclooxygenase-2 (COX-2) and Inflammation Related to Cancer. Nutrition and cancer **2018**; 70:350-75.

214. Tobin DM, Vary JC, Jr., Ray JP, et al. The lta4h locus modulates susceptibility to mycobacterial infection in zebrafish and humans. Cell **2010**; 140:717-30.

215. Tobin DM, Roca FJ, Oh SF, et al. Host genotype-specific therapies can optimize the inflammatory response to mycobacterial infections. Cell **2012**; 148:434-46.

216. Pasparakis M, Vandenabeele P. Necroptosis and its role in inflammation. Nature **2015**; 517:311-20.

217. Gong YN, Guy C, Olauson H, et al. ESCRT-III Acts Downstream of MLKL to Regulate Necroptotic Cell Death and Its Consequences. Cell **2017**; 169:286-300 e16.

218. Tonnus W, Gembardt F, Hugo C, Linkermann A. Die later with ESCRT! Oncotarget **2017**; 8:41790-1.

219. Jimenez AJ, Maiuri P, Lafaurie-Janvore J, Divoux S, Piel M, Perez F. ESCRT machinery is required for plasma membrane repair. Science **2014**; 343:1247136.

220. Mittal E, Skowyra ML, Uwase G, et al. Mycobacterium tuberculosis Type VII Secretion System Effectors Differentially Impact the ESCRT Endomembrane Damage Response. mBio **2018**; 9.

221. Micheau O, Tschopp J. Induction of TNF receptor I-mediated apoptosis via two sequential signaling complexes. Cell **2003**; 114:181-90.

222. Feltham R, Vince JE, Lawlor KE. Caspase-8: not so silently deadly. Clinical & translational immunology **2017**; 6:e124.

223. Mishra BB, Moura-Alves P, Sonawane A, et al. Mycobacterium tuberculosis protein ESAT-6 is a potent activator of the NLRP3/ASC inflammasome. Cellular microbiology **2010**; 12:1046-63.

224. Wong KW, Jacobs WR, Jr. Critical role for NLRP3 in necrotic death triggered by Mycobacterium tuberculosis. Cellular microbiology **2011**; 13:1371-84.

225. Lee J, Repasy T, Papavinasasundaram K, Sassetti C, Kornfeld H. Mycobacterium tuberculosis induces an atypical cell death mode to escape from infected macrophages. PloS one **2011**; 6:e18367.

226. Henkel JS, Baldwin MR, Barbieri JT. Toxins from bacteria. Exs **2010**; 100:1-29.

227. Gordon SV, Bottai D, Simeone R, Stinear TP, Brosch R. Pathogenicity in the tubercle bacillus: molecular and evolutionary determinants. BioEssays : news and reviews in molecular, cellular and developmental biology **2009**; 31:378-88.

228. Mukhopadhyay S, Nair S, Ghosh S. Pathogenesis in tuberculosis: transcriptomic approaches to unraveling virulence mechanisms and finding new drug targets. FEMS microbiology reviews **2012**; 36:463-85.

229. Danilchanka O, Sun J, Pavlenok M, et al. An outer membrane channel protein of Mycobacterium tuberculosis with exotoxin activity. Proceedings of the National Academy of Sciences of the United States of America **2014**; 111:6750-5.

230. Sun J, Siroy A, Lokareddy RK, et al. The tuberculosis necrotizing toxin kills macrophages by hydrolyzing NAD. Nature structural & molecular biology **2015**; 22:672-8.

231. Tak U, Vlach J, Garza-Garcia A, et al. The tuberculosis necrotizing toxin is an NAD(+) and NADP(+) glycohydrolase with distinct enzymatic properties. The Journal of biological chemistry **2019**; 294:3024-36.

232. Pajuelo D, Gonzalez-Juarbe N, Niederweis M. NAD hydrolysis by the tuberculosis necrotizing toxin induces lethal oxidative stress in macrophages. Cellular microbiology **2020**; 22:e13115.

233. Li XH, Kondrashin A, Greenwood B, Lindblade K, Loku Galappaththy G, Alonso P. A Historical Review of WHO Certification of Malaria Elimination. Trends in parasitology **2019**; 35:163-71.

234. Organization WH. Global technical strategy for malaria 2016-2030. World Health Organization, **2015**.

235. Organization WH. World malaria report 2015. World Health Organization, **2016**.

236. WHO. Global malaria report 2019: World Health Organization Geneva, **2019**.

237. Cowman AF, Healer J, Marapana D, Marsh K. Malaria: biology and disease. Cell **2016**; 167:610-24.

238. Dhiman S. Are malaria elimination efforts on right track? An analysis of gains achieved and challenges ahead. Infectious diseases of poverty **2019**; 8:14.

239. Payne D. Spread of chloroquine resistance in Plasmodium falciparum. Parasitology today **1987**; 3:241-6.

240. Antony HA, Parija SC. Antimalarial drug resistance: An overview. Tropical parasitology **2016**; 6:30-41.

241. Eastman RT, Fidock DA. Artemisinin-based combination therapies: a vital tool in efforts to eliminate malaria. Nature reviews Microbiology **2009**; 7:864-74.

242. Nosten F, White NJ. Artemisinin-based combination treatment of falciparum malaria. The American journal of tropical medicine and hygiene **2007**; 77:181-92.

243. Dondorp AM, Smithuis FM, Woodrow C, Seidlein LV. How to Contain Artemisinin- and Multidrug-Resistant Falciparum Malaria. Trends in parasitology **2017**; 33:353-63.

244. Talapko J, Skrlec I, Alebic T, Jukic M, Vcev A. Malaria: The Past and the Present. Microorganisms **2019**; 7.

245. Gilles HM. Historical outline. Essential malariology **2002**; 4:1-7.

246. Krettli AU, Miller LH. Malaria: a sporozoite runs through it. Current biology : CB **2001**; 11:R409-12.

247. Tan SY, Ahana A. Charles Laveran (1845-1922): Nobel laureate pioneer of malaria. Singapore medical journal **2009**; 50:657-8.

248. Cox FE. History of the discovery of the malaria parasites and their vectors. Parasites & vectors **2010**; 3:1-9.

249. Hsu E. The history of qing hao in the Chinese materia medica. Transactions of the Royal Society of Tropical Medicine and Hygiene **2006**; 100:505-8.

250. Achan J, Talisuna AO, Erhart A, et al. Quinine, an old anti-malarial drug in a modern world: role in the treatment of malaria. Malaria journal **2011**; 10:144.

251. Krafts K, Hempelmann E, Skorska-Stania A. From methylene blue to chloroquine: a brief review of the development of an antimalarial therapy. Parasitology research **2012**; 111:1-6.

252. Alven S, Aderibigbe B. Combination Therapy Strategies for the Treatment of Malaria. Molecules **2019**; 24.

253. Snounou G, Viriyakosol S, Jarra W, Thaithong S, Brown KN. Identification of the four human malaria parasite species in field samples by the polymerase chain reaction and detection of a high prevalence of mixed infections. Molecular and biochemical parasitology **1993**; 58:283-92.

254. Ashley EA, Pyae Phyo A, Woodrow CJ. Malaria. Lancet **2018**; 391:1608-21.

255. Bartoloni A, Zammarchi L. Clinical aspects of uncomplicated and severe malaria. Mediterranean journal of hematology and infectious diseases **2012**; 4.

256. Raghavendra K, Barik TK, Reddy BP, Sharma P, Dash AP. Malaria vector control: from past to future. Parasitology research **2011**; 108:757-79.

257. Organization WH. The technical basis for coordinated action against insecticide resistance: preserving the effectiveness of modern malaria vector control: meeting report. **2011**.

258. Ashley EA, Phyo AP. Drugs in Development for Malaria. Drugs **2018**; 78:861-79.

259. Cowman AF, Berry D, Baum J. The cellular and molecular basis for malaria parasite invasion of the human red blood cell. The Journal of cell biology **2012**; 198:961-71.

260. Cowman AF, Crabb BS. Invasion of red blood cells by malaria parasites. Cell **2006**; 124:755-66.

261. Weiss GE, Gilson PR, Taechalertpaisarn T, et al. Revealing the sequence and resulting cellular morphology of receptor-ligand interactions during Plasmodium falciparum invasion of erythrocytes. PLoS pathogens **2015**; 11:e1004670.

262. Koch M, Baum J. The mechanics of malaria parasite invasion of the human erythrocyte - towards a reassessment of the host cell contribution. Cellular microbiology **2016**; 18:319-29.

263. Tham WH, Healer J, Cowman AF. Erythrocyte and reticulocyte binding-like proteins of Plasmodium falciparum. Trends in parasitology **2012**; 28:23-30.

264. Hale VL, Watermeyer JM, Hackett F, et al. Parasitophorous vacuole poration precedes its rupture and rapid host erythrocyte cytoskeleton collapse in Plasmodium falciparum egress. Proceedings of the National Academy of Sciences of the United States of America **2017**; 114:3439-44.

265. Dvorin JD, Martyn DC, Patel SD, et al. A plant-like kinase in Plasmodium falciparum regulates parasite egress from erythrocytes. Science **2010**; 328:910-2.

266. Collins CR, Hackett F, Strath M, et al. Malaria parasite cGMP-dependent protein kinase regulates blood stage merozoite secretory organelle discharge and egress. PLoS pathogens **2013**; 9:e1003344.

267. Collins CR, Hackett F, Atid J, Tan MSY, Blackman MJ. The Plasmodium falciparum pseudoprotease SERA5 regulates the kinetics and efficiency of malaria parasite egress from host erythrocytes. PLoS pathogens **2017**; 13:e1006453.

268. Thomas JA, Tan MSY, Bisson C, et al. A protease cascade regulates release of the human malaria parasite Plasmodium falciparum from host red blood cells. Nature microbiology **2018**; 3:447-55.

269. Das S, Hertrich N, Perrin AJ, et al. Processing of Plasmodium falciparum Merozoite Surface Protein MSP1 Activates a Spectrin-Binding Function Enabling Parasite Egress from RBCs. Cell host & microbe **2015**; 18:433-44.

270. Boulet C, Doerig CD, Carvalho TG. Manipulating Eryptosis of Human Red Blood Cells: A Novel Antimalarial Strategy? Frontiers in cellular and infection microbiology **2018**; 8:419.

271. Kiefer CR, Snyder LM. Oxidation and erythrocyte senescence. Current opinion in hematology **2000**; 7:113-6.

272. Arese P, Turrini F, Schwarzer E. Band 3/complement-mediated recognition and removal of normally senescent and pathological human erythrocytes. Cellular physiology and biochemistry : international journal of experimental cellular physiology, biochemistry, and pharmacology **2005**; 16:133-46.

273. Bosman GJ, Willekens FL, Werre JM. Erythrocyte aging: a more than superficial resemblance to apoptosis? Cellular physiology and biochemistry : international journal of experimental cellular physiology, biochemistry, and pharmacology **2005**; 16:1-8.

274. Lutz HU. Innate immune and non-immune mediators of erythrocyte clearance. Cellular and molecular biology **2004**; 50:107-16.

275. Lang F, Qadri SM. Mechanisms and significance of eryptosis, the suicidal death of erythrocytes. Blood purification **2012**; 33:125-30.

276. Bratosin D, Estaquier J, Petit F, et al. Programmed cell death in mature erythrocytes: a model for investigating death effector pathways operating in the absence of mitochondria. Cell death and differentiation **2001**; 8:1143-56.

277. Lang KS, Lang PA, Bauer C, et al. Mechanisms of suicidal erythrocyte death. Cellular physiology and biochemistry : international journal of experimental cellular physiology, biochemistry, and pharmacology **2005**; 15:195-202.

278. Klarl BA, Lang PA, Kempe DS, et al. Protein kinase C mediates erythrocyte "programmed cell death" following glucose depletion. American journal of physiology Cell physiology **2006**; 290:C244-53.

279. Lang KS, Duranton C, Poehlmann H, et al. Cation channels trigger apoptotic death of erythrocytes. Cell death and differentiation **2003**; 10:249-56.

280. Lang F, Abed M, Lang E, Foller M. Oxidative stress and suicidal erythrocyte death. Antioxidants & redox signaling **2014**; 21:138-53.

281. Kamp D, Sieberg T, Haest CW. Inhibition and stimulation of phospholipid scrambling activity. Consequences for lipid asymmetry, echinocytosis, and microvesiculation of erythrocytes. Biochemistry **2001**; 40:9438-46.

282. Foller M, Bobbala D, Koka S, Huber SM, Gulbins E, Lang F. Suicide for survival--death of infected erythrocytes as a host mechanism to survive malaria. Cellular physiology and biochemistry : international journal of experimental cellular physiology, biochemistry, and pharmacology **2009**; 24:133-40.

283. Brand V, Koka S, Lang C, et al. Influence of amitriptyline on eryptosis, parasitemia and survival of Plasmodium berghei-infected mice. Cellular physiology and biochemistry : international journal of experimental cellular physiology, biochemistry, and pharmacology **2008**; 22:405-12.

284. Kasinathan RS, Foller M, Koka S, Huber SM, Lang F. Inhibition of eryptosis and intraerythrocytic growth of Plasmodium falciparum by flufenamic acid. Naunyn-Schmiedeberg's archives of pharmacology **2007**; 374:255-64.

285. Lang PA, Kempe DS, Akel A, et al. Inhibition of erythrocyte "apoptosis" by catecholamines. Naunyn-Schmiedeberg's archives of pharmacology **2005**; 372:228-35.

286. Qadri SM, Foller M, Lang F. Inhibition of suicidal erythrocyte death by resveratrol. Life sciences **2009**; 85:33-8.

287. Nicolay JP, Liebig G, Niemoeller OM, et al. Inhibition of suicidal erythrocyte death by nitric oxide. Pflugers Archiv : European journal of physiology **2008**; 456:293-305.

288. Vota DM, Crisp RL, Nesse AB, Vittori DC. Oxidative stress due to aluminum exposure induces eryptosis which is prevented by erythropoietin. Journal of cellular biochemistry **2012**; 113:1581-9.

289. Myssina S, Huber SM, Birka C, et al. Inhibition of erythrocyte cation channels by erythropoietin. Journal of the American Society of Nephrology : JASN **2003**; 14:2750-7.

290. Segawa K, Nagata S. An Apoptotic 'Eat Me' Signal: Phosphatidylserine Exposure. Trends in cell biology **2015**; 25:639-50.

291. Brugnara C, de Franceschi L, Alper SL. Inhibition of Ca(2+)-dependent K+ transport and cell dehydration in sickle erythrocytes by clotrimazole and other imidazole derivatives. The Journal of clinical investigation **1993**; 92:520-6.

292. Bookchin RM, Ortiz OE, Lew VL. Activation of calcium-dependent potassium channels in deoxygenated sickled red cells. Progress in clinical and biological research **1987**; 240:193-200.

293. Lang PA, Kaiser S, Myssina S, Wieder T, Lang F, Huber SM. Role of Ca2+-activated K+ channels in human erythrocyte apoptosis. American journal of physiology Cell physiology **2003**; 285:C1553-60.

294. Lang PA, Kempe DS, Tanneur V, et al. Stimulation of erythrocyte ceramide formation by platelet-activating factor. Journal of cell science **2005**; 118:1233-43.

295. Barenholz Y, Thompson TE. Sphingomyelins in bilayers and biological membranes. Biochimica et biophysica acta **1980**; 604:129-58.

296. Dbaibo GS, Perry DK, Gamard CJ, et al. Cytokine response modifier A (CrmA) inhibits ceramide formation in response to tumor necrosis factor (TNF)-alpha: CrmA and Bcl-2 target distinct components in the apoptotic pathway. The Journal of experimental medicine **1997**; 185:481-90.

297. Birbes H, El Bawab S, Obeid LM, Hannun YA. Mitochondria and ceramide: intertwined roles in regulation of apoptosis. Advances in enzyme regulation **2002**; 42:113-29.

298. Lang KS, Myssina S, Brand V, et al. Involvement of ceramide in hyperosmotic shock-induced death of erythrocytes. Cell death and differentiation **2004**; 11:231-43.

299. Berg CP, Engels IH, Rothbart A, et al. Human mature red blood cells express caspase-3 and caspase-8, but are devoid of mitochondrial regulators of apoptosis. Cell death and differentiation **2001**; 8:1197-206.

300. Perrin BJ, Huttenlocher A. Calpain. The international journal of biochemistry & cell biology **2002**; 34:722-5.

301. Schwarz-Ben Meir N, Glaser T, Kosower NS. Band 3 protein degradation by calpain is enhanced in erythrocytes of old people. The Biochemical journal **1991**; 275 (Pt 1):47-52.

302. Larsen AK, Lametsch R, Elce J, et al. Genetic disruption of calpain correlates with loss of membrane blebbing and differential expression of RhoGDI-1, cofilin and tropomyosin. The Biochemical journal **2008**; 411:657-66.

303. Hay S, Kannourakis G. A time to kill: viral manipulation of the cell death program. The Journal of general virology **2002**; 83:1547-64.

304. James ER, Green DR. Manipulation of apoptosis in the host-parasite interaction. Trends in parasitology **2004**; 20:280-7.

305. Ashida H, Mimuro H, Ogawa M, et al. Cell death and infection: a double-edged sword for host and pathogen survival. The Journal of cell biology **2011**; 195:931-42.

306. Kaushansky A, Metzger PG, Douglass AN, et al. Malaria parasite liver stages render host hepatocytes susceptible to mitochondria-initiated apoptosis. Cell death & disease **2013**; 4:e762.

307. van de Sand C, Horstmann S, Schmidt A, et al. The liver stage of Plasmodium berghei inhibits host cell apoptosis. Molecular microbiology **2005**; 58:731-42.

308. Kirk K. Membrane transport in the malaria-infected erythrocyte. Physiological reviews **2001**; 81:495-537.

309. Wasserman M, Alarcon C, Mendoza PM. Effects of Ca++ depletion on the asexual cell cycle of Plasmodium falciparum. The American journal of tropical medicine and hygiene **1982**; 31:711-7.

310. Enomoto M, Kawazu S, Kawai S, et al. Blockage of spontaneous Ca2+ oscillation causes cell death in intraerythrocitic Plasmodium falciparum. PloS one **2012**; 7:e39499.

311. Adovelande J, Bastide B, Deleze J, Schrevel J. Cytosolic free calcium in Plasmodium falciparum-infected erythrocytes and the effect of verapamil: a cytofluorimetric study. Experimental parasitology **1993**; 76:247-58.

312. Tiffert T, Staines HM, Ellory JC, Lew VL. Functional state of the plasma membrane Ca2+ pump in Plasmodium falciparum-infected human red blood cells. The Journal of physiology **2000**; 525 Pt 1:125-34.

313. Huber SM, Duranton C, Lang F. Patch-clamp analysis of the "new permeability pathways" in malaria-infected erythrocytes. International review of cytology **2005**; 246:59-134.

314. Lew VL, Tiffert T, Ginsburg H. Excess hemoglobin digestion and the osmotic stability of Plasmodium falciparum-infected red blood cells. Blood **2003**; 101:4189-94.

315. Sicard A, Semblat JP, Doerig C, et al. Activation of a PAK-MEK signalling pathway in malaria parasite-infected erythrocytes. Cellular microbiology **2011**; 13:836-45.

316. Zelenak C, Foller M, Velic A, et al. Proteome analysis of erythrocytes lacking AMP-activated protein kinase reveals a role of PAK2 kinase in eryptosis. Journal of proteome research **2011**; 10:1690-7.

317. John Von Freyend S, Kwok-Schuelein T, Netter HJ, Haqshenas G, Semblat JP, Doerig C. Subverting Host Cell P21-Activated Kinase: A Case of Convergent Evolution across Pathogens. Pathogens **2017**; 6.

318. Ayi K, Giribaldi G, Skorokhod A, Schwarzer E, Prendergast PT, Arese P. 16alpha-bromoepiandrosterone, an antimalarial analogue of the hormone dehydroepiandrosterone, enhances phagocytosis of ring stage parasitized erythrocytes: a novel mechanism for antimalarial activity. Antimicrobial agents and chemotherapy **2002**; 46:3180-4.

319. Turrini F, Ginsburg H, Bussolino F, Pescarmona GP, Serra MV, Arese P. Phagocytosis of Plasmodium falciparum-infected human red blood cells by human monocytes: involvement of immune and nonimmune determinants and dependence on parasite developmental stage. Blood **1992**; 80:801-8.

320. Eda S, Sherman IW. Cytoadherence of malaria-infected red blood cells involves exposure of phosphatidylserine. Cellular physiology and biochemistry : international journal of experimental cellular physiology, biochemistry, and pharmacology **2002**; 12:373-84.

321. Sherman IW, Eda S, Winograd E. Cytoadherence and sequestration in Plasmodium falciparum: defining the ties that bind. Microbes and infection **2003**; 5:897-909.

322. Sherman IW, Eda S, Winograd E. Erythrocyte aging and malaria. Cellular and molecular biology **2004**; 50:159-69.

323. Ayi K, Turrini F, Piga A, Arese P. Enhanced phagocytosis of ring-parasitized mutant erythrocytes: a common mechanism that may explain protection against falciparum malaria in sickle trait and beta-thalassemia trait. Blood **2004**; 104:3364-71.

324. Cappadoro M, Giribaldi G, O'Brien E, et al. Early phagocytosis of glucose-6-phosphate dehydrogenase (G6PD)-deficient erythrocytes parasitized by Plasmodium falciparum may explain malaria protection in G6PD deficiency. Blood **1998**; 92:2527-34.

325. Totino PR, Daniel-Ribeiro CT, Ferreira-da-Cruz Mde F. Refractoriness of eryptotic red blood cells to Plasmodium falciparum infection: a putative host defense mechanism limiting parasitaemia. PloS one **2011**; 6:e26575.

326. Totino PR, Magalhaes AD, Silva LA, Banic DM, Daniel-Ribeiro CT, Ferreira-da-Cruz Mde F. Apoptosis of non-parasitized red blood cells in malaria: a putative mechanism involved in the pathogenesis of anaemia. Malaria journal **2010**; 9:350.

327. Bissinger R, Barking S, Alzoubi K, Liu G, Liu G, Lang F. Stimulation of Suicidal Erythrocyte Death by the Antimalarial Drug Mefloquine. Cellular physiology and biochemistry : international journal of experimental cellular physiology, biochemistry, and pharmacology **2015**; 36:1395-405.

328. Alzoubi K, Calabro S, Bissinger R, Abed M, Faggio C, Lang F. Stimulation of suicidal erythrocyte death by artesunate. Cellular physiology and biochemistry : international journal of experimental cellular physiology, biochemistry, and pharmacology **2014**; 34:2232-44.

329. Mischitelli M, Jemaa M, Almasry M, Faggio C, Lang F. Stimulation of Erythrocyte Cell Membrane Scrambling by Quinine. Cellular physiology and biochemistry : international journal of experimental cellular physiology, biochemistry, and pharmacology **2016**; 40:657-67.

330. Birka C, Lang PA, Kempe DS, et al. Enhanced susceptibility to erythrocyte "apoptosis" following phosphate depletion. Pflugers Archiv : European journal of physiology **2004**; 448:471-7.

331. Lang E, Lang F. Triggers, inhibitors, mechanisms, and significance of eryptosis: the suicidal erythrocyte death. BioMed research international **2015**; 2015:513518.

332. Hortle E, Nijagal B, Bauer DC, et al. Adenosine monophosphate deaminase 3 activation shortens erythrocyte half-life and provides malaria resistance in mice. Blood **2016**; 128:1290-301.

333. Okabe K, Yaku K, Tobe K, Nakagawa T. Implications of altered NAD metabolism in metabolic disorders. Journal of biomedical science **2019**; 26:34.

334. Canto C, Menzies KJ, Auwerx J. NAD(+) Metabolism and the Control of Energy Homeostasis: A Balancing Act between Mitochondria and the Nucleus. Cell metabolism **2015**; 22:31-53.

335. Michos A, Gryllos I, Hakansson A, Srivastava A, Kokkotou E, Wessels MR. Enhancement of streptolysin O activity and intrinsic cytotoxic effects of the group A streptococcal toxin, NAD-glycohydrolase. The Journal of biological chemistry **2006**; 281:8216-23.

336. Zerez CR, Roth EF, Jr., Schulman S, Tanaka KR. Increased nicotinamide adenine dinucleotide content and synthesis in Plasmodium falciparum-infected human erythrocytes. Blood **1990**; 75:1705-10.

337. Harden A, Young WJ. The alcoholic ferment of yeast-juice. Part II.—The coferment of yeast-juice. Proceedings of the Royal Society of London Series B, Containing Papers of a Biological Character **1906**; 78:369-75.

338. Rajman L, Chwalek K, Sinclair DA. Therapeutic Potential of NAD-Boosting Molecules: The In Vivo Evidence. Cell metabolism **2018**; 27:529-47.

339. Elhassan YS, Philp AA, Lavery GG. Targeting NAD+ in Metabolic Disease: New Insights Into an Old Molecule. Journal of the Endocrine Society **2017**; 1:816-35.

340. Xie N, Zhang L, Gao W, et al. NAD(+) metabolism: pathophysiologic mechanisms and therapeutic potential. Signal transduction and targeted therapy **2020**; 5:227.

341. Houtkooper RH, Auwerx J. Exploring the therapeutic space around NAD+. The Journal of cell biology **2012**; 199:205-9.

342. Wang X, Saba T, Yiu HH, Howe RF, Anderson JA, Shi J. Cofactor NAD (P) H regeneration inspired by heterogeneous pathways. Chem **2017**; 2:621-54.

343. Mesquita I, Varela P, Belinha A, et al. Exploring NAD+ metabolism in host-pathogen interactions. Cellular and molecular life sciences : CMLS **2016**; 73:1225-36.

344. Singhal A, Cheng CY. Host NAD+ metabolism and infections: therapeutic implications. International immunology **2019**; 31:59-67.

345. Tatsuno I, Isaka M, Minami M, Hasegawa T. NADase as a target molecule of in vivo suppression of the toxicity in the invasive M-1 group A Streptococcal isolates. BMC microbiology **2010**; 10:144.

346. Ghosh J, Anderson PJ, Chandrasekaran S, Caparon MG. Characterization of Streptococcus pyogenes beta-NAD+ glycohydrolase: re-evaluation of enzymatic properties associated with pathogenesis. The Journal of biological chemistry **2010**; 285:5683-94.

347. Karasawa T, Takasawa S, Yamakawa K, Yonekura H, Okamoto H, Nakamura S. NAD(+)-glycohydrolase from Streptococcus pyogenes shows cyclic ADP-ribose forming activity. FEMS microbiology letters **1995**; 130:201-4.

348. Murray MF, Nghiem M, Srinivasan A. HIV infection decreases intracellular nicotinamide adenine dinucleotide [NAD]. Biochemical and biophysical research communications **1995**; 212:126-31.

349. Kaufmann SH. Intracellular pathogens: living in an extreme environment. Immunological reviews **2011**; 240:5-10.

350. Thakur A, Mikkelsen H, Jungersen G. Intracellular Pathogens: Host Immunity and Microbial Persistence Strategies. Journal of immunology research **2019**; 2019:1356540.

351. Cossart P, Helenius A. Endocytosis of viruses and bacteria. Cold Spring Harbor perspectives in biology **2014**; 6.

352. Flieger A, Frischknecht F, Hacker G, Hornef MW, Pradel G. Pathways of host cell exit by intracellular pathogens. Microbial cell **2018**; 5:525-44.

353. Houtkooper RH, Canto C, Wanders RJ, Auwerx J. The secret life of NAD+: an old metabolite controlling new metabolic signaling pathways. Endocrine reviews **2010**; 31:194-223.

354. Katsyuba E, Romani M, Hofer D, Auwerx J. NAD+ homeostasis in health and disease. Nature Metabolism **2020**:1-23.

355. Magni G, Amici A, Emanuelli M, Orsomando G, Raffaelli N, Ruggieri S. Enzymology of NAD+ homeostasis in man. Cellular and molecular life sciences : CMLS **2004**; 61:19-34.

356. Ruggieri S, Orsomando G, Sorci L, Raffaelli N. Regulation of NAD biosynthetic enzymes modulates NAD-sensing processes to shape mammalian cell physiology under varying biological cues. Biochimica et biophysica acta **2015**; 1854:1138-49.

357. Stevens DL, Salmi DB, McIndoo ER, Bryant AE. Molecular epidemiology of nga and NAD glycohydrolase/ADP-ribosyltransferase activity among Streptococcus pyogenes causing streptococcal toxic shock syndrome. The Journal of infectious diseases **2000**; 182:1117-28.

358. Meehl MA, Pinkner JS, Anderson PJ, Hultgren SJ, Caparon MG. A novel endogenous inhibitor of the secreted streptococcal NAD-glycohydrolase. PLoS pathogens **2005**; 1:e35.

359. Organization WH. TB: a global emergency. TB: a global emergency, **1994**:28-.

360. Malin AS, McAdam K. Escalating threat from tuberculosis: the third epidemic. Thorax **1995**; 50:S37.

361. Organization WH. Guidelines for establishing DOTS-Plus pilot projects for the management of multidrug-resistant tuberculosis (MDR-TB): World Health Organization, **2000**.

362. MacGurn JA, Cox JS. A genetic screen for Mycobacterium tuberculosis mutants defective for phagosome maturation arrest identifies components of the ESX-1 secretion system. Infection and immunity **2007**; 75:2668-78.

363. Aguilo JI, Alonso H, Uranga S, et al. ESX-1-induced apoptosis is involved in cell-to-cell spread of Mycobacterium tuberculosis. Cellular microbiology **2013**; 15:1994-2005.

364. Schluger NW, Rom WN. The host immune response to tuberculosis. American journal of respiratory and critical care medicine **1998**; 157:679-91.

365. Henderson RA, Watkins SC, Flynn JL. Activation of human dendritic cells following infection with Mycobacterium tuberculosis. Journal of immunology **1997**; 159:635-43.

366. Mortaz E, Adcock IM, Tabarsi P, et al. Interaction of Pattern Recognition Receptors with Mycobacterium Tuberculosis. Journal of clinical immunology **2015**; 35:1-10.

367. Abebe M, Kim L, Rook G, et al. Modulation of cell death by M. tuberculosis as a strategy for pathogen survival. Clinical & developmental immunology **2011**; 2011:678570.

368. Chan J, Xing Y, Magliozzo RS, Bloom BR. Killing of virulent Mycobacterium tuberculosis by reactive nitrogen intermediates produced by activated murine macrophages. The Journal of experimental medicine **1992**; 175:1111-22.

369. Gutierrez MG, Master SS, Singh SB, Taylor GA, Colombo MI, Deretic V. Autophagy is a defense mechanism inhibiting BCG and Mycobacterium tuberculosis survival in infected macrophages. Cell **2004**; 119:753-66.

370. Khader SA, Cooper AM. IL-23 and IL-17 in tuberculosis. Cytokine **2008**; 41:79-83.

371. Domingo-Gonzalez R, Prince O, Cooper A, Khader SA. Cytokines and chemokines in Mycobacterium tuberculosis infection. Tuberculosis and the Tubercle Bacillus **2017**:33-72.

372. Ramakrishnan L. Revisiting the role of the granuloma in tuberculosis. Nature reviews Immunology **2012**; 12:352-66.

373. Barry CE, 3rd, Boshoff HI, Dartois V, et al. The spectrum of latent tuberculosis: rethinking the biology and intervention strategies. Nature reviews Microbiology **2009**; 7:845-55.

374. Silva Miranda M, Breiman A, Allain S, Deknuydt F, Altare F. The tuberculous granuloma: an unsuccessful host defence mechanism providing a safety shelter for the bacteria? Clinical & developmental immunology **2012**; 2012:139127.

375. Mahamed D, Boulle M, Ganga Y, et al. Intracellular growth of Mycobacterium tuberculosis after macrophage cell death leads to serial killing of host cells. eLife **2017**; 6.

376. Fink SL, Cookson BT. Apoptosis, pyroptosis, and necrosis: mechanistic description of dead and dying eukaryotic cells. Infection and immunity **2005**; 73:1907-16.

377. Vandenabeele P, Galluzzi L, Vanden Berghe T, Kroemer G. Molecular mechanisms of necroptosis: an ordered cellular explosion. Nature reviews Molecular cell biology **2010**; 11:700-14.

378. Taylor RC, Cullen SP, Martin SJ. Apoptosis: controlled demolition at the cellular level. Nature reviews Molecular cell biology **2008**; 9:231-41.

379. Winau F, Weber S, Sad S, et al. Apoptotic vesicles crossprime CD8 T cells and protect against tuberculosis. Immunity **2006**; 24:105-17.

380. Divangahi M, Behar SM, Remold H. Dying to live: how the death modality of the infected macrophage affects immunity to tuberculosis. Advances in experimental medicine and biology **2013**; 783:103-20.

381. Kausalya S, Somogyi R, Orlofsky A, Prystowsky MB. Requirement of A1-a for bacillus Calmette-Guerin-mediated protection of macrophages against nitric oxide-induced apoptosis. Journal of immunology **2001**; 166:4721-7.

382. Sly LM, Hingley-Wilson SM, Reiner NE, McMaster WR. Survival of Mycobacterium tuberculosis in host macrophages involves resistance to apoptosis dependent upon induction of antiapoptotic Bcl-2 family member Mcl-1. Journal of immunology **2003**; 170:430-7.

383. Keane J, Balcewicz-Sablinska MK, Remold HG, et al. Infection by Mycobacterium tuberculosis promotes human alveolar macrophage apoptosis. Infection and immunity **1997**; 65:298-304.

384. Oddo M, Renno T, Attinger A, Bakker T, MacDonald HR, Meylan PR. Fas ligand-induced apoptosis of infected human macrophages reduces the viability of intracellular Mycobacterium tuberculosis. Journal of immunology **1998**; 160:5448-54.

385. Loeuillet C, Martinon F, Perez C, Munoz M, Thome M, Meylan PR. Mycobacterium tuberculosis subverts innate immunity to evade specific effectors. Journal of immunology **2006**; 177:6245-55.

386. Simeone R, Bobard A, Lippmann J, et al. Phagosomal rupture by Mycobacterium tuberculosis results in toxicity and host cell death. PLoS pathogens **2012**; 8:e1002507.

387. Danelishvili L, Yamazaki Y, Selker J, Bermudez LE. Secreted Mycobacterium tuberculosis Rv3654c and Rv3655c proteins participate in the suppression of macrophage apoptosis. PloS one **2010**; 5:e10474.

388. Tummers B, Green DR. Caspase-8: regulating life and death. Immunological reviews **2017**; 277:76-89.

389. Gopinathan KP, Sirsi M, Vaidyanathan CS. Nicotinamide-adenine dinucleotide glycohydrolase of Mycobacterium tuberculosis H37Rv. The Biochemical journal **1964**; 91:277-82.

390. Hara N, Yamada K, Shibata T, Osago H, Hashimoto T, Tsuchiya M. Elevation of cellular NAD levels by nicotinic acid and involvement of nicotinic acid phosphoribosyltransferase in human cells. The Journal of biological chemistry **2007**; 282:24574-82.

391. Russell DG. New ways to arrest phagosome maturation. Nature cell biology **2007**; 9:357-9.

392. Plattner F, Soldati-Favre D. Hijacking of host cellular functions by the Apicomplexa. Annual review of microbiology **2008**; 62:471-87.

393. Spillman NJ, Beck JR, Goldberg DE. Protein export into malaria parasite-infected erythrocytes: mechanisms and functional consequences. Annual review of biochemistry **2015**; 84:813-41.

394. Organization WH. Global Technical Strategy for Malaria 2016–2030. Geneva: World Health Organization; 2015, **2017**.

395. Belachew EB. Immune Response and Evasion Mechanisms of Plasmodium falciparum Parasites. Journal of immunology research **2018**; 2018:6529681.

396. Lang F, Lang PA, Lang KS, et al. Channel-induced apoptosis of infected host cells-the case of malaria. Pflugers Archiv : European journal of physiology **2004**; 448:319-24.

397. Pretorius E, du Plooy JN, Bester J. A Comprehensive Review on Eryptosis. Cellular physiology and biochemistry : international journal of experimental cellular physiology, biochemistry, and pharmacology **2016**; 39:1977-2000.

398. Carvalho TG, Morahan B, John von Freyend S, et al. The ins and outs of phosphosignalling in Plasmodium: Parasite regulation and host cell manipulation. Molecular and biochemical parasitology **2016**; 208:2-15.

399. Lang F, Jilani K, Lang E. Therapeutic potential of manipulating suicidal erythrocyte death. Expert opinion on therapeutic targets **2015**; 19:1219-27.

400. O'Hara JK, Kerwin LJ, Cobbold SA, et al. Targeting NAD+ metabolism in the human malaria parasite Plasmodium falciparum. PloS one **2014**; 9:e94061.

401. Medana IM, Mai NT, Day NP, et al. Cellular stress and injury responses in the brains of adult Vietnamese patients with fatal Plasmodium falciparum malaria. Neuropathology and applied neurobiology **2001**; 27:421-33.

402. Du L, Zhang X, Han YY, et al. Intra-mitochondrial poly(ADP-ribosylation) contributes to NAD+ depletion and cell death induced by oxidative stress. The Journal of biological chemistry **2003**; 278:18426-33.

403. Walliker D, Quakyi IA, Wellems TE, et al. Genetic analysis of the human malaria parasite Plasmodium falciparum. Science **1987**; 236:1661-6.

404. Kumar K, Tharad M, Ganapathy S, et al. Phenylalanine-rich peptides potently bind ESAT6, a virulence determinant of Mycobacterium tuberculosis, and concurrently affect the pathogen's growth. PloS one **2009**; 4:e7615.

405. Wu Y, Li Q, Chen XZ. Detecting protein-protein interactions by Far western blotting. Nature protocols **2007**; 2:3278-84.

406. Chopra S, Ranganathan A. Protein evolution by "codon shuffling": a novel method for generating highly variant mutant libraries by assembly of hexamer DNA duplexes. Chemistry & biology **2003**; 10:917-26.

407. Rao A, Chopra S, Ram G, Gupta A, Ranganathan A. Application of the "codon-shuffling" method. Synthesis and selection of de novo proteins as antibacterials. The Journal of biological chemistry **2005**; 280:23605-14.

408. Bhalla K, Chugh M, Mehrotra S, et al. Host ICAMs play a role in cell invasion by Mycobacterium tuberculosis and Plasmodium falciparum. Nature communications **2015**; 6:6049.

409. Prakash P, Zeeshan M, Saini E, et al. Human Cyclophilin B forms part of a multi-protein complex during erythrocyte invasion by Plasmodium falciparum. Nature communications **2017**; 8:1548.

410. Graeff R, Lee HC. A novel cycling assay for cellular cADP-ribose with nanomolar sensitivity. Biochem J **2002**; 361:379-84.

411. Murphy SC, Harrison T, Hamm HE, Lomasney JW, Mohandas N, Haldar K. Erythrocyte G protein as a novel target for malarial chemotherapy. PLoS medicine **2006**; 3:e528.

412. Anam ZE, Joshi N, Gupta S, et al. A De novo Peptide from a High Throughput Peptide Library Blocks Myosin A -MTIP Complex Formation in Plasmodium falciparum. International journal of molecular sciences **2020**; 21.

413. Gebeyehu G, Marquez VE, Van Cott A, et al. Ribavirin, tiazofurin, and selenazofurin: mononucleotides and nicotinamide adenine dinucleotide analogues. Synthesis, structure, and interactions with IMP dehydrogenase. Journal of medicinal chemistry **1985**; 28:99-105.

414. Penyige A, Deak E, Kalmanczhelyi A, Barabas G. Evidence of a role for NAD+-glycohydrolase and ADP-ribosyltransferase in growth and differentiation of Streptomyces griseus NRRL B-2682: inhibition by m-aminophenylboronic acid. Microbiology **1996**; 142 (Pt 8):1937-44.

415. Scaffidi P, Misteli T, Bianchi ME. Release of chromatin protein HMGB1 by necrotic cells triggers inflammation. Nature **2002**; 418:191-5.

416. Bird J, Best R, Lewis DA. The encapsulation of insulin in erythrocytes. The Journal of pharmacy and pharmacology **1983**; 35:246-7.

417. Bourgeaux V, Lanao JM, Bax BE, Godfrin Y. Drug-loaded erythrocytes: on the road toward marketing approval. Drug design, development and therapy **2016**; 10:665-76.

418. Chiarugi A, Dolle C, Felici R, Ziegler M. The NAD metabolome--a key determinant of cancer cell biology. Nature reviews Cancer **2012**; 12:741-52.

419. Verdin E. NAD(+) in aging, metabolism, and neurodegeneration. Science **2015**; 350:1208-13.

420. Chandrasekaran S, Caparon MG. The Streptococcus pyogenes NAD(+) glycohydrolase modulates epithelial cell PARylation and HMGB1 release. Cellular microbiology **2015**; 17:1376-90.

421. Bastiat-Sempe B, Love JF, Lomayesva N, Wessels MR. Streptolysin O and NAD-glycohydrolase prevent phagolysosome acidification and promote group A Streptococcus survival in macrophages. mBio **2014**; 5:e01690-14.

422. Depaix A, Kowalska J. NAD Analogs in Aid of Chemical Biology and Medicinal Chemistry. Molecules **2019**; 24.

423. Zuccala ES, Satchwell TJ, Angrisano F, et al. Quantitative phospho-proteomics reveals the Plasmodium merozoite triggers pre-invasion host kinase modification of the red cell cytoskeleton. Scientific reports **2016**; 6:19766.

424. Shear HL, Roth EF, Jr., Ng C, Nagel RL. Resistance to malaria in ankyrin and spectrin deficient mice. British journal of haematology **1991**; 78:555-60.

425. Gonzalez V, Combe A, David V, et al. Host cell entry by apicomplexa parasites requires actin polymerization in the host cell. Cell host & microbe **2009**; 5:259-72.

Chapter 8
Publications and Presentations

PUBLICATIONS AND PRESENTATIONS

8.1 Publications

1. **Chaurasiya A**, Garg S, Khanna A, Narayana C, Dwivedi VP, Joshi N, Anam Z, Singh N, Singhal J, Kaushik S, Kahlon AK, Srivastava P, Marothia M, Kumar M, Kumar S, Kumari G, Munjal A, Gupta S, Singh P, Pati S, Das G, Sagar R, Ranganathan A and Singh S. Pathogen induced subversion of NAD^+ metabolism mediating host cell death: a target for development of chemotherapeutics. (Manuscript ID: CDDISCOVERY-20-0997R, Cell Death Discovery, In Press).

2. **Chaurasiya A**, Garg S, Anam Z, Kumari G, Joshi N, Kumari J, Singhal J, Singh N, Kaushik S, Kahlon AK, Dubey N, Srivastava P, Marothia M, Kumar M, Das G, Singh S and Ranganathan A. Repositioning of the anti-Hepatitis C Virus drug Alisporivir against Artemisinin-resistant *Plasmodium falciparum*. (Manuscript under preparation)

3. Anam Z, D.A.B. Rex, Yadav P, Sah R K, Kumari G, **Chaurasiya A**, Singh N, Prasad T.S., Pati S, Singh S and Ranganathan A. Complementary cross-talk between palmitoylation and phosphorylation in regulation of *Plasmodium falciparum* invasion of erythrocytes. (Manuscript under preparation).

4. Anam Z, Joshi N, Gupta S, Yadav P, **Chaurasiya A**, Kahlon AK, Kaushik S, Munde M, Ranganathan A, Singh S. A De novo Peptide from a High Throughput Peptide Library Blocks Myosin A-MTIP Complex Formation in *Plasmodium falciparum*. International journal of molecular sciences. 2020 Jan;21(17):6158.

5. Prakash P, Zeeshan M, Saini E, Muneer A, Khurana S, Chourasia BK, Deshmukh A, Kaur I, Dabral S, Singh N, Anam Z, **Chaurasiya A**, Kaushik S, Dahiya P, Kalamuddin M, Thakur JK, Mohmmed A, Ranganathan A and Malhotra P. Human Cyclophilin B forms part of a multi-protein complex during erythrocyte invasion by Plasmodium falciparum. Nature communications. 2017 Nov 16;8(1):1-2.

8.2 List of Conference attended and Presentations

1. **Ayushi Chaurasiya,** Divyank Mahajan, Tapsya Srivastava, Anand Ranganathan. Peptide/Protein engineering for therapeutic intervention against cancer. Bioengineering Conference 2020, NIT Rourkela, Rourkela, Odisha, India, December 2020 (Oral Presentation).

2. **Ayushi Chaurasiya,** Divyank Mahajan, Tapsya Srivastava, Anand Ranganathan. Identification of novel inhibitors against protein that promotes mitochondrial biogenesis in cancers. Advances in Mitochondrial Medicine and Translational Research, Society of Mitochondria Research and Medicine (SMRM) and Manipal School of Life Sciences, MAHE, Manipal, India, November 2020 (Oral Presentation).

3. **Ayushi Chaurasiya**, Kuhulika Bhalla, Anand Ranganathan. Targeting essential proteins of *P. falciparum* and *M. tuberculosis* through design of novel peptide inhibitors. 7th Symposium on Frontiers in Molecular Medicine-2017, Special Centre for Molecular Medicine, Jawaharlal Nehru University, New Delhi, India, March 2017 (Poster Presentation).

4. **Ayushi Chaurasiya**, Kuhulika Bhalla, Anand Ranganathan. Targeting essential proteins of *P. falciparum* and *M. tuberculosis* through design of novel peptide inhibitors. National Science Day Symposium 2017, Department of Science and Technology and Jawaharlal Nehru University, New Delhi, India, February 2017 (Poster Presentation).

ARTICLE   Open Access

Pathogen induced subversion of NAD$^+$ metabolism mediating host cell death: a target for development of chemotherapeutics

Ayushi Chaurasiya[1], Swati Garg[1], Ashish Khanna[2], Chintam Narayana[2], Vedprakash Dwivedi[3], Nishant Joshi[4], Zill e Anam[1], Niharika Singh[1], Jhalak Singhal[1], Shikha Kaushik[1], Amandeep Kaur[1], Pallavi Srivastava[1], Manisha Marothia[1], Mukesh Kumar[1], Santosh Kumar[3], Geeta Kumari[1], Akshay Munjal, Sonal Gupta[1], Preeti Singh[1], Soumya Pati[4], Gobardhan Das[1], Ram Sagar[2], Anand Ranganathan[1] and Shailja Singh[1]

Abstract
Hijacking of host metabolic status by a pathogen for its regulated dissemination from the host is prerequisite for the propagation of infection. *M. tuberculosis* secretes an NAD$^+$-glycohydrolase, TNT, to induce host necroptosis by hydrolyzing Nicotinamide adenine dinucleotide (NAD$^+$). Herein, we expressed TNT in macrophages and erythrocytes; the host cells for *M. tuberculosis* and the malaria parasite respectively, and found that it reduced the NAD$^+$ levels and thereby induced necroptosis and eryptosis resulting in premature dissemination of pathogen. Targeting TNT in *M. tuberculosis* or induced eryptosis in malaria parasite interferes with pathogen dissemination and reduction in the propagation of infection. Building upon our discovery that inhibition of pathogen-mediated host NAD$^+$ modulation is a way forward for regulation of infection, we synthesized and screened some novel compounds that showed inhibition of NAD$^+$-glycohydrolase activity and pathogen infection in the nanomolar range. Overall this study highlights the fundamental importance of pathogen-mediated modulation of host NAD$^+$ homeostasis for its infection propagation and novel inhibitors as leads for host-targeted therapeutics.

Introduction

Intracellular pathogens have evolved strategies to manipulate host cell pathways for dissemination and infection propagation. Unlike independent organisms, intracellular pathogens depend on the activities of host cell to complete their life cycle. Some of these pathogens have evolved strategies for host manipulation to increase their survival causing detrimental effects to the host,

leading to its death. Because dissemination is an essential aspect of pathogenesis, targeting or modulating host processes involved in pathogenesis can control the infection[1]. Pathogen-mediated changes in host intracellular nicotinamide adenine dinucleotide (NAD$^+$), an essential coenzyme and a redox factor regulating numerous cellular metabolic pathways, levels have been observed in various diseases[2,3]. In particular, host uses NAD$^+$ as a substrate for a group of "NAD$^+$-dependent" enzymes[4,5].

Recently, *Mycobacterium tuberculosis*, the causative agent for tuberculosis, mediated modulation of host NAD$^+$ homeostasis has been presented as one of the most fascinating examples of a pathogen's infection strategy wherein NAD$^+$ depletion through TNT activates necroptosis pathways in order to facilitate growth and spread of *M. tuberculosis*[6–8]. However, the regulation of

Q1–Q4

Correspondence: Ram Sagar (ram.sagar@bhu.ac.in) or
Anand Ranganathan (anand.icgeb@gmail.com) or Shailja Singh (shailja.
jnu@gmail.com)
[1]Special Centre for Molecular Medicine, Jawaharlal Nehru University, New Delhi 110067, India
[2]Department of Chemistry, Institute of Science, Banaras Hindu University, Varanasi 221005 Uttar Pradesh, India
Full list of author information is available at the end of the article
These authors contributed equally: Ayushi Chaurasiya, Swati Garg, Ashish Khanna
Edited by A. Janic

Article

A De novo Peptide from a High Throughput Peptide Library Blocks Myosin A -MTIP Complex Formation in *Plasmodium falciparum*

Zill e Anam [1], Nishant Joshi [2], Sakshi Gupta [3], Preeti Yadav [1], Ayushi Chaurasiya [1], Amandeep Kaur Kahlon [1], Shikha Kaushik [1], Manoj Munde [3], Anand Ranganathan [1,*] and Shailja Singh [1,*]

[1] Special Centre for Molecular Medicine, Jawaharlal Nehru University, New Delhi 110067, India;
    zillzz85@gmail.com (Z.e.A.); preetiyadav.bms@gmail.com (P.Y.); ayushi.chaurasiya01@gmail.com (A.C.);
    amangenomics@gmail.com (A.K.K.); shikhakaushik29@gmail.com (S.K.)
[2] Department of Life Sciences, School of Natural Sciences, Shiv Nadar University, Greater Noida,
    Uttar Pradesh 201304, India; nj633@snu.edu.in
[3] School of Physical Sciences, Jawaharlal Nehru University, New Delhi 110067, India;
    sakshi2027@gmail.com (S.G.); mundemanoj@gmail.com (M.M.)
* Correspondence: anand.icgeb@gmail.com (A.R.); shailja.jnu@gmail.com (S.S.)

check for updates

Abstract: Apicomplexan parasites, through their motor machinery, produce the required propulsive force critical for host cell-entry. The conserved components of this so-called glideosome machinery are myosin A and myosin A Tail Interacting Protein (MTIP). MTIP tethers myosin A to the inner membrane complex of the parasite through 20 amino acid-long C-terminal end of myosin A that makes direct contacts with MTIP, allowing the invasion of *Plasmodium falciparum* in erythrocytes. Here, we discovered through screening a peptide library, a de-novo peptide ZA1 that binds the myosin A tail domain. We demonstrated that ZA1 bound strongly to myosin A tail and was able to disrupt the native myosin A tail MTIP complex both in vitro and in vivo. We then showed that a shortened peptide derived from ZA1, named ZA1S, was able to bind myosin A and block parasite invasion. Overall, our study identified a novel anti-malarial peptide that could be used in combination with other antimalarials for blocking the invasion of *Plasmodium falciparum*.

Keywords: malaria; peptide inhibitor; myosin A; myosin A tail interacting protein (MTIP)

1. Introduction

The burden caused by a malarial parasite—*Plasmodium falciparum*—remains huge despite a recent decline in the number of malaria cases [1]. The non-responsiveness of the parasite to existing therapies calls for an urgent need for discovering new drugs that are parasite-specific. For successful transmission, the parasite must complete its life cycle in each of the sub microenvironments: gut of Anopheles mosquito, hepatocytes, and erythrocytes. Entry in erythrocytes allows asexual reproduction of the parasite, leading to rapid proliferation and an exponential increase in the number of merozoites. It is an essential step in the parasite life cycle and is also an attractive target since the merozoites are in the bloodstream and directly exposed, thereby making them vulnerable to drugs [2].

The encounter of the malarial parasite with host erythrocyte is mediated by sequential and highly dynamic processes involving initial interaction of the egressed merozoite, leading to re-orientation of the apical end, the formation of a tight junction in between the two membranes, followed by the engagement of invasion motor and entry. This is concluded by the shedding of a protein coat, the formation of the parasitophorous vacuole, resealing of red blood cell (RBC) membrane,

ARTICLE

Human Cyclophilin B forms part of a multi-protein complex during erythrocyte invasion by *Plasmodium falciparum*

Prem Prakash[1,2], Mohammad Zeeshan[1], Ekta Saini[1], Azhar Muneer[1], Sachin Khurana[1], Bishwanath Kumar Chourasia[1], Arunaditya Deshmukh[1], Inderjeet Kaur[1], Surabhi Dabral[1], Niharika Singh[1,3], Zille Anam[3], Ayushi Chaurasiya[3], Shikha Kaushik[3], Pradeep Dahiya[4], Md. Kalamuddin[1], Jitendra Kumar Thakur[4], Asif Mohmmed[1], Anand Ranganathan[2,3] & Pawan Malhotra[1]

Invasion of human erythrocytes by *Plasmodium falciparum* merozoites involves multiple interactions between host receptors and their merozoite ligands. Here we report human Cyclophilin B as a receptor for PfRhopH3 during merozoite invasion. Localization and binding studies show that Cyclophilin B is present on the erythrocytes and binds strongly to merozoites. We demonstrate that PfRhopH3 binds to the RBCs and their treatment with Cyclosporin A prevents merozoite invasion. We also show a multi-protein complex involving Cyclophilin B and Basigin, as well as PfRhopH3 and PfRh5 that aids the invasion. Furthermore, we report identification of a de novo peptide CDP3 that binds Cyclophilin B and blocks invasion by up to 80%. Collectively, our data provide evidence of compounded interactions between host receptors and merozoite surface proteins and paves the way for developing peptide and small-molecules that inhibit the protein–protein interactions, individually or in toto, leading to abrogation of the invasion process.

[1] Malaria Biology Group, International Centre for Genetic Engineering and Biotechnology (ICGEB), Aruna Asaf Ali Marg, New Delhi 110067, India. [2] Recombinant Gene Products Group, International Centre for Genetic Engineering and Biotechnology (ICGEB), Aruna Asaf Ali Marg, New Delhi 110067, India. [3] Special Centre for Molecular Medicine, Jawaharlal Nehru University, Aruna Asaf Ali Marg, New Delhi 110067, India. [4] Plant Mediator Lab, National Institute of Plant Genome Research, Aruna Asaf Ali Marg, New Delhi 110067, India. Prem Prakash and Mohammad Zeeshan contributed equally to this work. Correspondence and requests for materials should be addressed to A.R. (email: anand.icgeb@gmail.com) or to P.M. (email: pawanmal@gmail.com)

Appendix

APPENDIX

Symbols and Abbreviations

%	Percent
°C	Degree celsius
ACT	Artemisinin-based combination therapy
ADC	Bovine Albumin, Dextrose, Catalase
AE1	Anion exchanger 1
AIM2	Absent in melanoma-2
AMA1	Apical membrane antigen 1
AMP	Adenosine monophosphate
APBA	3-Aminophenylboronic acid
APS	Ammonium persulfate
ASC/PYCARD	Apoptosis-associated speck-like protein containing a caspase recruiting domain
ATCC	American type culture collection
Atg	Autophagy-related gene
ATP	Adenosine triphosphate
BC	Before Christ
BCG	Bacillus Calmette Guerin
BLAST	Basic local alignment search tool
bp	Base pair
BSA	Bovine serum albumin
Ca^{2+}	Calcium ion
CCL	Chemokine (C-C motif) ligand
CCR	CC-chemokine receptor
CD	Cluster of differentiation
CFU	Colony forming unit
cGAS	Cyclic GMP–AMP synthase
Cl^-	Chlorine ion
CO_2	Carbon dioxide
COX2	Cyclooxygenase 2

CpnT	Channel protein with necrosis-inducing toxin
CR1	Complement receptor 1
DAMP	Danger-associated molecular pattern
DAPI	4′,6-diamidino-2-phenylindole
DC	Dicodon
DCFDA	2, 7-Dichlorofluorescein diacetate
DCs	Dendritic cells
DC-SIGN	Dendritic cell-specific intercellular adhesion molecule (ICAM)-3-grabbing non-integrin
DMEM	Dulbecco's modified eagle's medium
DNA	Deoxyribonucleic Acid
dNTP	Deoxynucleoside triphosphate
DOT	Directly observed therapy
DOTS	Directly observed treatment short-course
DTT	Dithiothreitol
E. coli	*Escherichia coli*
EDTA	Ethylenediamine tetra acetate
ELISA	Enzyme-linked immunosorbent assay
ESAT-6	6-kDa early secretory antigenic target
ESCRT-III	Endosomal sorting complexes required for transport-III
ESX	ESAT-6 secretion system
FACS	Fluorescence-activated cell sorting
FasL	Fas-ligand
FDA	Food and drug administration
Fluo-4AM	Fluo-4-acetoxymethyl
g	Gram
GFP	Green fluorescent protein
GMP	Guanosine monophosphate
His	Histidine
HIV	Human immunodeficiency virus
HLA	Human leukocyte antigen

HMGB1	High-mobility group box 1
HP	Hairpins
HPDC	HP ligated dicodon
HRP	Horseradish Peroxidase
IFN	Interferon
IFT	Immunity factor for TNT
IL	Interleukin
IPTG	Isopropyl β-d-1-thiogalactopyranoside
IRS	Indoor residual spraying
ITNs	Insecticide-treated nets
K$^+$	Potassium ion
kb	Kilobases
kDa	Kilodalton
L	Litre
LB	Luria Bertani (media)
LC3	Microtubule-associated protein 1A/1B light chain 3
LTA4H	Leukotriene A4 hydrolase
LTB4	Leukotriene B4
LXA4	Lipoxin A4
M	Molar
M. tuberculosis	*Mycobacterium tuberculosis*
MAPK	Mitogen activated protein kinases
MCS	Multiple Cloning Site
MDG	Millennium Development Goal
MDR	Multidrug resistant
mg	Milligram
MHC	Major histocompatibility complex
min	Minute
mL	Millilitre
MLKL	Mixed lineage kinase domain like pseudokinase
mM	Millimolar

MOI	Multiplicity of infection
MPT	Mitochondrial permeability transition
MQ	Milli Q (water grade)
MSP	Merozoite surface protein
MTBC	*M. tuberculosis* complex
MTT	3-(4,5-dimethylthiazol-2-yl)-2,5-diphenyltetrazolium bromide
MyD88	Myeloid differentiation factor 88
NAD$^+$	Nicotinamide adenine dinucleotide
NADH	Nicotinamide adenine dinucleotide hydrogen (hydride)
NCCD	Nomenclature committee on cell death
NF-κB	Nuclear factor-κB
ng	Nanogram
Ni-NTA	Ni-nitrilotriacetate
NLR	Nucleotide-binding oligomerization domain-like receptor
NLRP3	NOD-like receptor family, pyrin domain-containing-3
nm	Nanometer
nM	Nanomolar
NPP	New permeability pathway
OADC	Oleic acid, Albumin, Dextrose, Catalase
OD$_{600}$	Optical density (measured at 600 nm)
ORF	Open reading frame
P. falciparum	*Plasmodium falciparum*
PAF	Platelet-activating factor
PAGE	Polyacrylamide gel electrophoresis
PAK2	p21-activated kinase 2
PAMP	Pathogen associated molecular pattern
PARP	Poly ADP ribose polymerase
PAS	Para-amino salicylic acid
PBS	Phosphate buffered saline
PBST	Phosphate buffered saline-tween-20
PCR	Polymerase chain reaction

PGE2	Prostaglandin E2
PI	Propidium iodide
PI3P	Phosphatidylinositol 3-phosphate
PMSF	Phenylmethylsulfonyl fluoride
PRR	Pattern recognition receptor
RCD	Regulated cell death
RDT	Rapid diagnostic test
RIPA	Radioimmunoprecipitation assay
RIPK1	Receptor-interacting protein kinase 1
RNA	Ribonucleic acid
RNase	Ribonuclease
RON	Rhoptry neck proteins
RNS	Reactive nitrogen species
ROS	Reactive oxygen species
rpm	Revolutions per minute
RPMI	Roswell park memorial institute (media)
RT	Room temperature
SDG	Sustainable Development Goal
SDS	Sodium dodecyl sulphate
sec	Seconds
SERA	Serine repeat antigen
STING	Stimulator of IFN genes
TAP-1	Transporter associated with antigen processing 1
TBE	Tris borate EDTA buffer
TE	Tris-EDTA
TEMED	Tetramethylethylenediamine
Th cells	T helper cells
TLR	Toll-like receptor
TMB	Tetramethylbenzidine
TNFR	Tumor necrosis factor receptor
TNF-α	Tumour necrosis factor-α

TNT	Tuberculosis necrotizing toxin
WHA	World Health Assembly
WHO	World Health Organization
XDR	Extremely drug-resistant
X-Gal	5-bromo-4-chloro-3-indolyl-β-d-galactopyranoside
βME	2-mercaptoethanol
µg	Microgram
µL	Microlitre
µm	Micrometer
µM	Micromolar

Ayushi Chaurasiya Thesis 2020

by Ayushi Chaurasiya

Ayushi Chaurasiya Thesis 2020

Publication

7   W. W. Yew, C. Lange, C. C. Leung. "Treatment of tuberculosis: update 2010", European Respiratory Journal, 2010
Publication

     <1%

8   Matthias Eberhard, Michael Föller, Florian Lang. "Effect of Phytic Acid on Suicidal Erythrocyte Death", Journal of Agricultural and Food Chemistry, 2010
Publication

     <1%

9   d-nb.info
Internet Source

     <1%

10   res.mdpi.com
Internet Source

     <1%

11   Saborni Chakraborty, Joseph Gonzalez, Karlie Edwards, Vamsee Mallajosyula et al. "Proinflammatory IgG Fc structures in patients with severe COVID-19", Cold Spring Harbor Laboratory, 2020
Publication

     <1%

12   Mary Jackson, Casey M. Stevens, Lei Zhang, Helen I. Zgurskaya, Michael Niederweis. "Transporters Involved in the Biogenesis and Functionalization of the Mycobacterial Cell Envelope", Chemical Reviews, 2020
Publication

     <1%

13 A. Thomas Pezzella. "History of Pulmonary Tuberculosis", Thoracic Surgery Clinics, 2019
Publication

<1%

14 Krishnaveni Mohareer, Suman Asalla, Sharmistha Banerjee. "Cell death at the cross roads of host-pathogen interaction in Mycobacterium tuberculosis infection", Tuberculosis, 2018
Publication

<1%

15 www.nature.com
Internet Source

<1%

16 ecommons.usask.ca
Internet Source

<1%

17 "ADP-Ribose Transfer Reactions", Springer Nature, 1989
Publication

<1%

18 Yijun Lou, Xiao-Qiang Zhao. "Modelling Malaria Control by Introduction of Larvivorous Fish", Bulletin of Mathematical Biology, 2011
Publication

<1%

19 Marra Jai Aghajani, Tao Yang, Ulf Schmitz, Alexander James et al. "Epithelial-to-mesenchymal transition and its association with PD-L1 and CD8 in thyroid cancer", Endocrine Connections, 2020
Publication

<1%

20   "Eukaryome Impact on Human Intestine Homeostasis and Mucosal Immunology", Springer Science and Business Media LLC, 2020
Publication
   <1%

21   eprints.ru.ac.za
Internet Source
   <1%

22   O. Danilchanka, J. Sun, M. Pavlenok, C. Maueroder et al. "An outer membrane channel protein of Mycobacterium tuberculosis with exotoxin activity", Proceedings of the National Academy of Sciences, 2014
Publication
   <1%

23   David Pajuelo, Norberto Gonzalez-Juarbe, Michael Niederweis. "NAD hydrolysis by the tuberculosis necrotizing toxin induces lethal oxidative stress in macrophages", Cellular Microbiology, 2019
Publication
   <1%

24   research.library.mun.ca
Internet Source
   <1%

25   digitalcommons.wustl.edu
Internet Source
   <1%

26   Claus Belka. "Intracellular mediators of erucylphosphocholine-induced apoptosis", Oncogene, 05/01/2003
   <1%